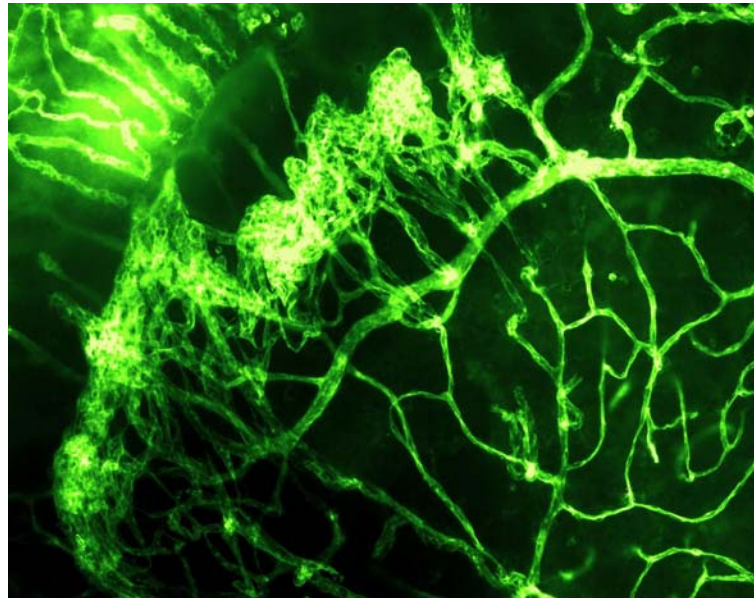# HERITABLE INFLUENCES IN OXYGEN-INDUCED RETINOPATHY

Peter van Wijngaarden

MBBS (Hons)

Thesis submitted for the degree of

Doctor of Philosophy

January 2006

Faculty of Health Sciences

School of Medicine

Flinders University of South Australia

Adelaide, Australia

For Amber

TABLE OF CONTENTS

SUMMARY OF THESIS

Retinopathy of prematurity, a disease characterised by aberrant retinal vascular development in premature neonates, is a leading cause of blindness and visual impairment in childhood. This work sought to examine differences in the susceptibility of inbred rat strains to oxygen-induced retinopathy, a model of human retinopathy of prematurity. The overriding aim was to identify genetic factors in rats that might be generalisable to humans.

Newborn rats of six different strains were exposed to alternating cycles of hyperoxia and relative hypoxia for fourteen days. Rats were removed to room air and killed for analysis immediately, to assess oxygen-induced retinal vascular attenuation, or four days later to evaluate the extent of hypoxia-induced vasoproliferation. Whole flat-mounted retinae were stained with fluorophore conjugated isolectin GS-IB4, and measurement of vascular area was conducted using fluorescence microscopy and video-image analysis. A hierarchy of susceptibility to the inhibitory effects of cyclic hyperoxia and relative hypoxia on postnatal retinal vascularization was identified for the rat strains studied. Susceptibility to vascular attenuation was predictive of the subsequent risk of vascular morphological abnormalities. Cross-breeding experiments between susceptible and resistant strains demonstrated that the susceptible phenotype was dominantly inherited in an autosomal fashion. These studies confirmed an association between ocular pigmentation and retinopathy risk, however the finding of differential susceptibility amongst albino rat strains implicated factors in addition to those associated with ocular pigmentation.

Quantitative real-time reverse transcription-polymerase chain reaction was used to compare the retinal expression of angiogenic factor genes in susceptible and resistant strains with the aim of identifying a genetic basis for the strain difference. Eight angiogenic factor genes were selected for study: vascular endothelial growth factor (VEGF); VEGF receptor 2; angiopoietin 2; Tie2; pigment epithelium-derived factor; erythropoietin; cyclooxygenase-2 and insulin-like growth factor-1. The most notable difference between strains was the expression of vascular endothelial growth factor

(VEGF) during the cyclic hyperoxia exposure period – higher VEGF expression was associated with relative resistance to retinopathy. Other differences in retinal angiogenic factor gene expression between strains, such as higher expression of VEGF receptor 2 and angiopoietin 2 in resistant strains, appeared to be secondary to those in VEGF. Following cyclic hyperoxia, the expression pattern of angiogenic factor genes changed – messenger RNA levels of hypoxia-induced genes, including VEGF, VEGF receptor 2, angiopoietin 2 and erythropoietin, were significantly higher in those strains with larger avascular areas, than in those strains that were relatively resistant to retinopathy. These findings provide firm evidence for hereditary risk factors for oxygen-induced retinopathy in the rat. Differences in the regulatory effects of oxygen on VEGF expression appear to be central to the risk of retinopathy. The potential relevance of these hereditary factors is discussed in the context of the human disease.

PUBLICATIONS ARISING FROM THIS THESIS

1.   van Wijngaarden, P., Coster, D.J. and Williams, K.A, *Inhibitors of Ocular Neovascularization: Promises and Potential Problems.* Journal of the American Medical Association, March 23/30, 2005. **293**(12): p. 1509-1513.

2.   van Wijngaarden, P., Coster, D.J., Brereton, H.M., Gibbins, I.L. and Williams, K.A, *Strain-Dependent Differences in Oxygen-Induced Retinopathy in the Inbred Rat.* Investigative Ophthalmology and Visual Science, April, 2005. **46**(4): p. 1445-1452.

DECLARATION

I certify that this thesis does not incorporate without acknowledgement any material previously submitted for a degree or diploma in any university; and that to the best of my knowledge and belief it does not contain any material previously published or written by another person except where due reference is made in the text.

Signed: _____   Date: _____

Peter van Wijngaarden

ACKNOWLEDGEMENTS

have received such remarkable support!

In a similar vein, I thank all of the members of the Ophthalmology Department at Flinders University for their friendship and assistance. Joyce Moore, Lyn Harding, Kirsty Marshall, Claire Jessup, Paul Badenoch, David Dimasi, Melinda Tea, Marian Turner, Matt Wenham, Alix Farrall, Scott Standfield, Margaret Philpott, Doug Parker, Claude Kauffman and Shiwani Sharma have all been bastions of support and will remain dear friends. I am also grateful for the friendship of John Oliver, Stuart Perry and John Woodall.

My four-year solo sojourn in Adelaide came at a great cost to my family. I will remain forever grateful for the sacrifices made by Marijcke and Pieter, Eric and Cath, Nicky and Frazer, Bill and Marcia, Kyla and Simon, Ward, and especially Amber, in allowing me to pursue my dream. My parents instilled in me the self-belief to embark on this work and equipped me with the drive to persevere in the face of difficulty – for this I am thankful. To my wife Amber, I owe the greatest debt of gratitude – her unconditional support and encouragement have been central to my successes. As a small gesture of my appreciation I dedicate this work to Amber.

ABBREVIATIONS

$\leq$	less than or equal to
$\geq$	more than or equal to
~	approximately
#	number
°C	degrees Celsius
µg	microgram (10^{-6} g)
µl	microlitre (10^{-6} l)
µM	micromolar (10^{-6} M)
µm	micrometer (10^{-6} m)
A	adenine
aa	amino acid
a/bFGF	acidic/basic fibroblast growth factor
Ang 1	angiopoietin 1
Ang 2	angiopoietin 2
AP-1/-2	activator protein-1/-2
ARBP	Acidic Ribosomal Phosphoprotein
ARNT	aryl hydrocarbon receptor nuclear translocator (HIF-1β)
ARVO	Association for Research in Vision and Ophthalmology
ATP	adenosine triphosphate
BM	Bruch's membrane
bp	base pairs
C	cytosine
cDNA	complementary DNA
cGMP	cyclic-guanosine monophosphate
cm	centimetre
COX 2	cyclooxygenase 2
CRYO-ROP	the Multicentre Trial of Cryotherapy for Retinopathy of Prematurity
Da	Dalton
DA	Dark Agouti rat strain
DAG	diacylglycerol

DAO2	Dark Agouti rats exposed to cyclic hyperoxia and relative hypoxia for the first two days of life – day two follows a 24 hour period of relative hypoxia
DAO3	Dark Agouti rats exposed to cyclic hyperoxia and relative hypoxia for the first three days of life – day three follows a 24 hour period of hyperoxia
DAO8	Dark Agouti rats exposed to cyclic hyperoxia and relative hypoxia for the first 8 days of life – day 8 follows a 24 hour period of relative hypoxia
DAO9	Dark Agouti rats exposed to cyclic hyperoxia and relative hypoxia for the first 9 days of life – day 9 follows a 24 hour period of hyperoxia
DAO14	Dark Agouti rats exposed to cyclic hyperoxia and relative hypoxia for the first 14 days of life
DAO18	Dark Agouti rats exposed to cyclic hyperoxia and relative hypoxia for the first 14 days of life, followed by four days of sustained relative hypoxia in room air
DARA14	Dark Agouti rats exposed to room air for the first 14 days of life
ddH_20	double distilled water
DEPC	diethylpyrocarbonate
DNA	deoxyribonucleic acid
dNTP	dinucleotide triphosphate
DTT	dithiothreitol
ECM	extracellular matrix
EDTA	ethylene-diamine-tetraacetic-acid
EGF	epidermal growth factor
ELM	external limiting membrane
eNOS	endothelial nitric oxide synthetase
EPO	erythropoietin
ETDRS	Early Treatment of Diabetic Retinopathy Study
EtOH	ethanol
ETROP	the Early Treatment for Retinopathy of Prematurity Randomized Trial
$F_{(x,y)}$	F statistic (degrees of freedom, error)
F344	Fischer 344 rat strain
F344O2	Fischer 344 rats exposed to cyclic hyperoxia and relative hypoxia for the first two days of life – day two follows a 24 hour period of relative hypoxia

F344O3	Fischer 344 rats exposed to cyclic hyperoxia and relative hypoxia for the first three days of life – day three follows a 24 hour period of hyperoxia
F344O8	Fischer 344 rats exposed to cyclic hyperoxia and relative hypoxia for the first 8 days of life – day 8 follows a 24 hour period of relative hypoxia
F344O9	Fischer 344 rats exposed to cyclic hyperoxia and relative hypoxia for the first 9 days of life – day 9 follows a 24 hour period of hyperoxia
F344O14	Fischer 344 rats exposed to cyclic hyperoxia and relative hypoxia for the first 14 days of life
F344O18	Fischer 344 rats exposed to cyclic hyperoxia and relative hypoxia for the first 14 days of life, followed by four days of sustained relative hypoxia in room air
F344RA14	Fischer 344 rats exposed to room air for the first 14 days of life
FAK	focal adhesion kinase
FasL	Fas-ligand (CD95L)
FGF	fibroblast growth factor
Fig	figure
flk-1	foetal-liver kinase-1 (VEGFR-2)
flt-1	fms-like tyrosine kinase-1 (VEGFR-1)
g	gram
g	gravity
G	guanine
#G	# gauge
GAPDH	glyceraldehyde 3-phosphate dehydrogenase
GCL	ganglion cell layer
GH	growth hormone
GOI	gene of interest
GS-IB4	*Griffonia simplicifolia* type I isolectin B4-Alexa 488™ conjugate
HPRT	hypoxanthine guanine phophoribosyl transferase
HIF-1/-2	hypoxia inducible factor-1/-2
hr	hour
HRE	hypoxia response element
HuR	Hu protein R

HW	Hooded Wistar rat strain
ICAM-1	intercellular adhesion molecule-1
Ig	immunoglobulin
IGF-1	insulin-like growth factor-1
IL	interleukin
ILM	inner limiting membrane
IM	intramuscular
INL	inner nuclear layer
IP	intraperitoneal
IPL	inner plexiform layer
iU	international units
Kb	kilobases
kDa	kilo Daltons (10^3 Da)
KDR	kinase domain receptor (VEGFR-2)
Kg	kilogram (10^3 gram)
l	litre
LEW	Lewis rat strain
M	molar
m	metre
MAPK	mitogen-activated protein kinase
mg	milligram (10^{-3} g)
MHC	major histocompatibility complex
min	minutes
MIP-2	macrophage inhibitory peptide-2 (IL-8)
ml	millilitre (10^{-3} l)
mm	millimetre(10^{-3} m)
mM	millimolar (10^{-3} M)
mmHg	millimetres mercury
MMP	matrix metalloproteinase
mRNA	messenger ribonucleic acid
MW	molecular weight
n	number/sample size

NaCl	sodium chloride
NADPH	nicotinamide-adenine dinucleotide phosphate
NFL	nerve fibre layer
ng	nanogram (10^{-9} g)
NH&MRC	National Health and Medical Research Council of Australia
No.	number
NRP-1	neuropilin-1
NSW	New South Wales
NTC	no template control
OIR	oxygen-induced retinopathy
ONL	outer nuclear layer
OPL	outer plexiform layer
ORP150	oxygen-regulated protein-150
P#	postnatal day #
PAF	platelet activating factor
PBS	Dulbecco's A physiologic balanced salt solution
PCO_2	partial pressure of carbon dioxide
PCR	polymerase chain reaction
PDGF	platelet derived growth factor
PECAM-1	platelet-endothelial cell adhesion molecule-1
PEDF	pigment epithelium derived factor
pg	picogram (10^{-12} gram)
pI	isoelectric point
PI3-kinase	phosphatidylinositol 3-kinase
PlGF	placental growth factor
pmol	picomoles (10^{-12} moles)
PO_2	partial pressure of oxygen; oxygen tension
RNA	ribonucleic acid
RNAP2	RNA polymerase 2
ROP	retinopathy of prematurity
RPE	retinal pigment epithelium
rpm	revolutions per minute

rRNA	ribosomal RNA
RT	room temperature
RT1	rat MHC Class II
RT-	reverse transcriptase-free; negative control cDNA
RT-PCR	reverse transcription-polymerase chain reaction
sec	second
SA	South Australia
SD	standard deviation
sFlt	soluble fms-like tyrosine kinase
SNP	single nucleotide polymorphism
SPD	Sprague Dawley rat strain (conventionally abbreviated SD. SPD in this thesis to avoid confusion with the abbreviation for standard deviation)
SPDO14	Sprague Dawley rats exposed to cyclic hyperoxia and relative hypoxia for the first 14 days of life
SPDO18	Sprague Dawley rats exposed to cyclic hyperoxia and relative hypoxia for the first 14 days of followed by four days of sustained relative hypoxia in room air
SPDRA14	Sprague Dawley rats exposed to room air for the first 14 days of life
T	thymine
T_A	annealing temperature
TBE	tris borate EDTA
TGF α / β	transforming growth factor-α/-β
Tie2	tyrosine kinase with Ig and epidermal growth factor homology domain receptor 2: receptor for angiopoietin-1 & -2
T_m	melting temperature
TNF α	tumour necrosis factor-α
TUNEL	terminal deoxynucleotidyl transferase (TdT)-mediated deoxyuridine triphosphate (dUTP)-biotin nick end labelling
U	units
USA	United States of America
UV	ultraviolet light
V	volt
v	version; volume
v/v	unit volume per unit volume

VA	visual acuity
VCAM 1	vascular cell adhesion molecule 1
VEGF	vascular endothelial growth factor (VEGF A unless otherwise specified)
$VEGF_x$	VEGF, isoform$_x$ ($_x$ denotes number of amino acid residues)
VEGFR-1	vascular endothelial growth factor receptor-1
VEGFR-2	vascular endothelial growth factor receptor-2
VEGFR-3	vascular endothelial growth factor receptor-3
VHL	von Hippel-Lindau protein
VIC	Victoria
VPF	vascular permeability factor
V_T	tidal volume
w/v	unit weight per unit volume
WA	West Australia
WF	Wistar-Furth rat strain
WG	weeks of gestation
x	times / multiplication factor

CHAPTER 1

INTRODUCTION

1. CHAPTER 1: INTRODUCTION

1.1.　OVERVIEW

The work presented in this thesis relates to the identification of genetic determinants of susceptibility to neovascular retinopathy, principally retinopathy of prematurity (ROP). The introductory chapter will address several major themes related to retinal vascular development in health and disease, the features of ROP and the role of heredity in neovascular disorders. A majority of the literature cited in this chapter predates the commencement of my PhD candidature in February 2002. The chapter concludes with the central hypotheses and aims of this thesis.

1.2.　RETINAL ANATOMY

The following is a focussed overview of retinal anatomy with emphasis on the vascular system and cellular mediators of vascular development. It constitutes a distillation of material from primary sources and anatomy texts [1].

The retina lines the posterior two thirds of the globe, terminating anteriorly at the ora serrata, where its serrated processes attach to the pars plana of the ciliary body (Figure 1.1). The fovea, a shallow central retinal depression, unique to primates [2], serves the central visual field and visual acuity (Figure 1.2). The fovea lies within the macula (*area centralis*), a region bounded by the temporal retinal vascular arcades that has the shape of a horizontal ellipse, with an average maximal diameter of 5.5 mm. The optic nerve head (optic disc) lies approximately 4 mm medial and 0.8 mm superior to the fovea.

The retina is bounded at its inner and outer aspects by connective tissue membranes: at its inner aspect, the inner limiting membrane separates it from the vitreous; at its outer aspect Bruch's membrane separates it from the choriocapillaris (Figure 1.3). Within these confines the retina is comprised of an inner sensory layer, the sensory retina, and an outer pigmented layer, the retinal pigment epithelium (RPE). These layers are described below from outermost to innermost, reflecting the flow of visual information in the retina.
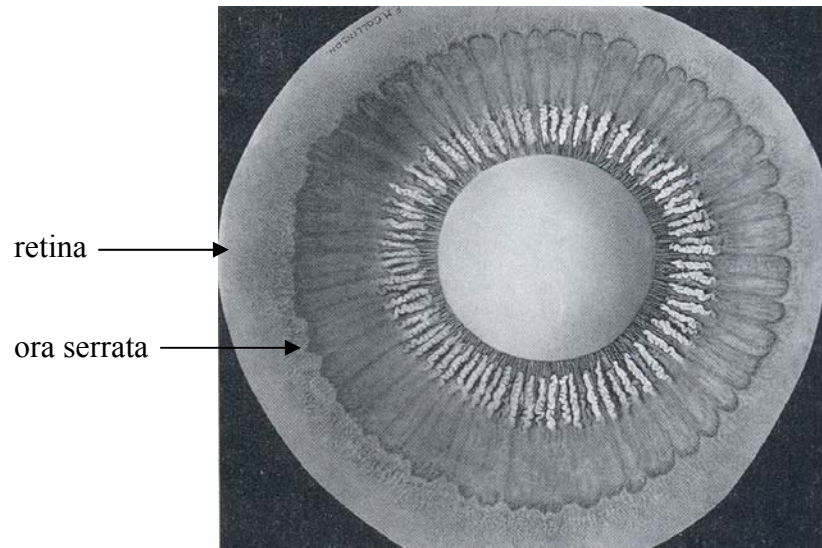
Figure 1.1 The retina and ora serrata. The retina lines the posterior two thirds of the globe, terminating anteriorly at the ora serrata where it attaches to the pars plana of the ciliary body. Figure from Bron *et al* [1].
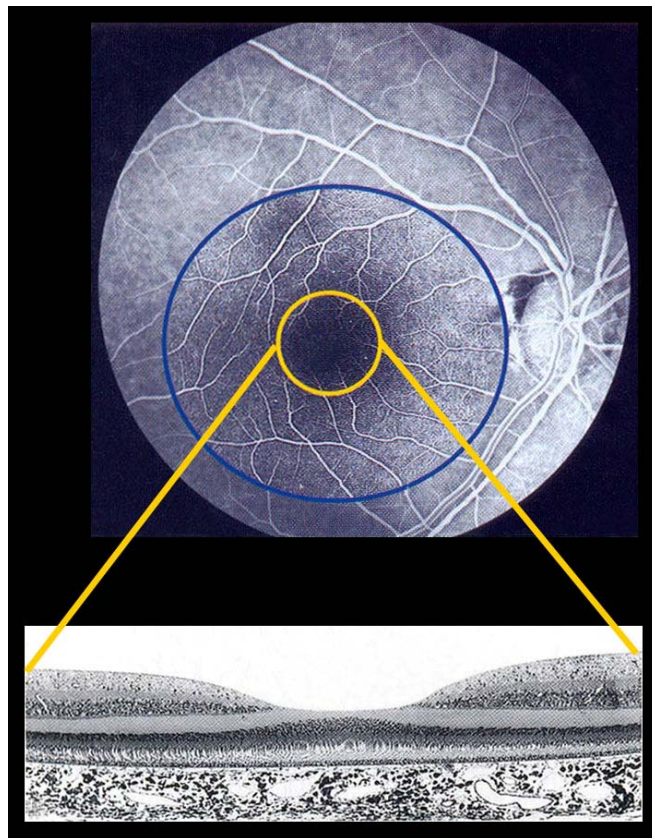
Figure 1.2 The macula and fovea. The macula is the region temporal to the optic disc bounded by the temporal vascular arcades (blue ellipse); the fovea is in the centre of the macula (bounded by the yellow circle) and is shown in histological cross section. Figures adapted from Kanski [3] and Bron *et al* [1].

Vitreous humour

Inner limiting membrane

Nerve fibre layer

Ganglion cell layer

Inner plexiform layer

Inner nuclear layer

Outer plexiform layer

Outer nuclear layer

External limiting membrane

Photoreceptor layer

Retinal pigment epithelium

Bruch's membrane

Choriocapillaris
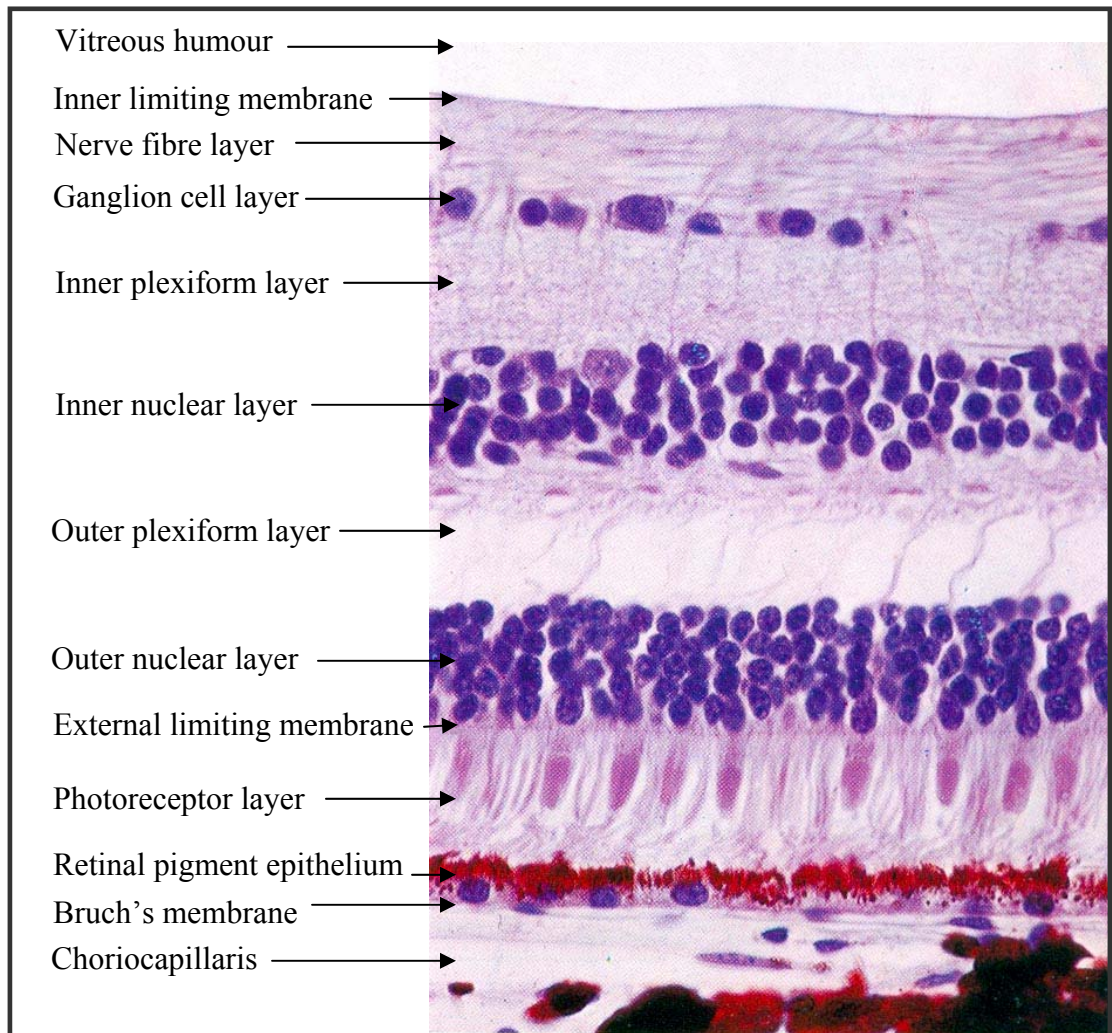
Figure 1.3 Histological cross-section of the retina. Figure adapted from Burkitt, Young and Heath [4].

1.2.a. The retinal pigment epithelium

The RPE is a monolayer of cuboidal cells that is continuous anteriorly with the pigmented layer of the ciliary epithelium. Basally, RPE cells are firmly adherent to Bruch's membrane, while apically their cytoplasm forms a series of brush-like microvillus projections that abut the outer segments of photoreceptors in the sensory retina (Figure 1.3). The phagocytic, nutritive and metabolic functions of RPE cells are central to photoreceptor function. The cells are melanin rich, aiding in the absorption of scattered light. Tight junctions between adjacent RPE cells contribute to the outer blood-retinal barrier.

1.2.b. The sensory retina

Nine layers of the sensory retina are typically described (Figure 1.3). Rod and cone photoreceptors, first order neurons vital for photo-reception and transduction, occupy the outermost layers: their inner and outer segments occupy the *photoreceptor layer*, while their somata and nuclei occupy the *outer nuclear layer*. The intervening *external limiting membrane*, comprised of the cytoplasmic extensions of Müller glial cells and associated connective tissue, provides structural support. Semantically the membrane delineates the junction between the 'inner' and 'outer' retina.

The *outer plexiform layer*, the site of communication between first and second order neurons, is comprised of the inner fibres of photoreceptors and dendrites of bipolar and horizontal cells. The somata of these neurons, as well as those of Müller cells, amacrine cells and inner plexiform cells, reside in the *inner nuclear layer*. Müller cells are the principal retinal glial cells and play important roles in the development of the retinal vasculature as well as the orientation and positioning of developing neurons. Müller cells have extensive cytoplasmic projections which span widely between the inner and external limiting membranes. In addition to providing structural support to neurons, the cells serve important metabolic functions including energy supply, waste removal and the maintenance of extracellular electrolyte homeostasis.

Accessory glial cells are distributed throughout the retina. Macroglia, the retinal astrocytes, are neural connective tissue cells that provide structural support, proliferating and hypertrophying in response to injury. Astrocytic foot processes attach to the exterior of retinal blood vessels, contributing to the inner blood retinal barrier. Microglia migrate throughout the retina serving phagocytic roles as tissue histiocytes.

Third order neurons reside in the *ganglion cell layer*. Synapses between second and third order neurons are made in the intervening *inner plexiform layer*. The axons of ganglion cells, which comprise the *nerve fibre layer*, converge at the optic nerve, transmitting information from the retina to the visual cortex for further processing.

The inner limiting membrane, the innermost retinal layer is a band of connective tissue that receives contributions from both the retina and vitreous (the hyaloid membrane). The membrane constitutes a structural barrier, ordinarily constraining blood vessels within the retina.

The typical adult human retina varies in thickness from 100 μm at the ora serrata, to 560 μm at the optic disc margin [1]. The fovea has an average thickness of 250 μm – it lacks inner nuclear and ganglion cell layers, as well as the inner plexiform and nerve fibre layers (Figures 1.2 and 1.3). The outer plexiform layer is replaced by *Henle's fibre layer*, comprised of the inner fibres of photoreceptors. The foveal photoreceptor layer is comprised exclusively of cones.

1.2.c. The retinal vasculature

The retina is supported by two anatomically and physiologically distinct vascular beds (Table 1.1): the choroidal and retinal circulations (Figure 1.4). Key anatomical and physiological features of these circulations will be reviewed in turn.

Table 1.1 Comparison of key features of the retinal and choroidal circulations

Retinal circulation	Choroidal circulation
Tight endothelial junctions [5]	No tight junctions
Non-fenestrated endothelial cells; few vesicles; little trans-cellular transport [5]	Fenestrated endothelial cells
Dense pericyte cover [1]	Sparse pericyte cover [1]
Low blood flow [6]	High blood flow [6]
High oxygen extraction [7]	Low oxygen extraction [7]
No autonomic innervation [8-10]	Sympathetic innervation [11]
Autoregulation* [6, 12, 13]	No autoregulation [6, 14]
Anastomotic [15]	Segmental supply [16]

* Autoregulation: the capacity of a vascular bed to modulate flow in response to altered perfusion pressure or metabolic demands of the supplied tissue [17].
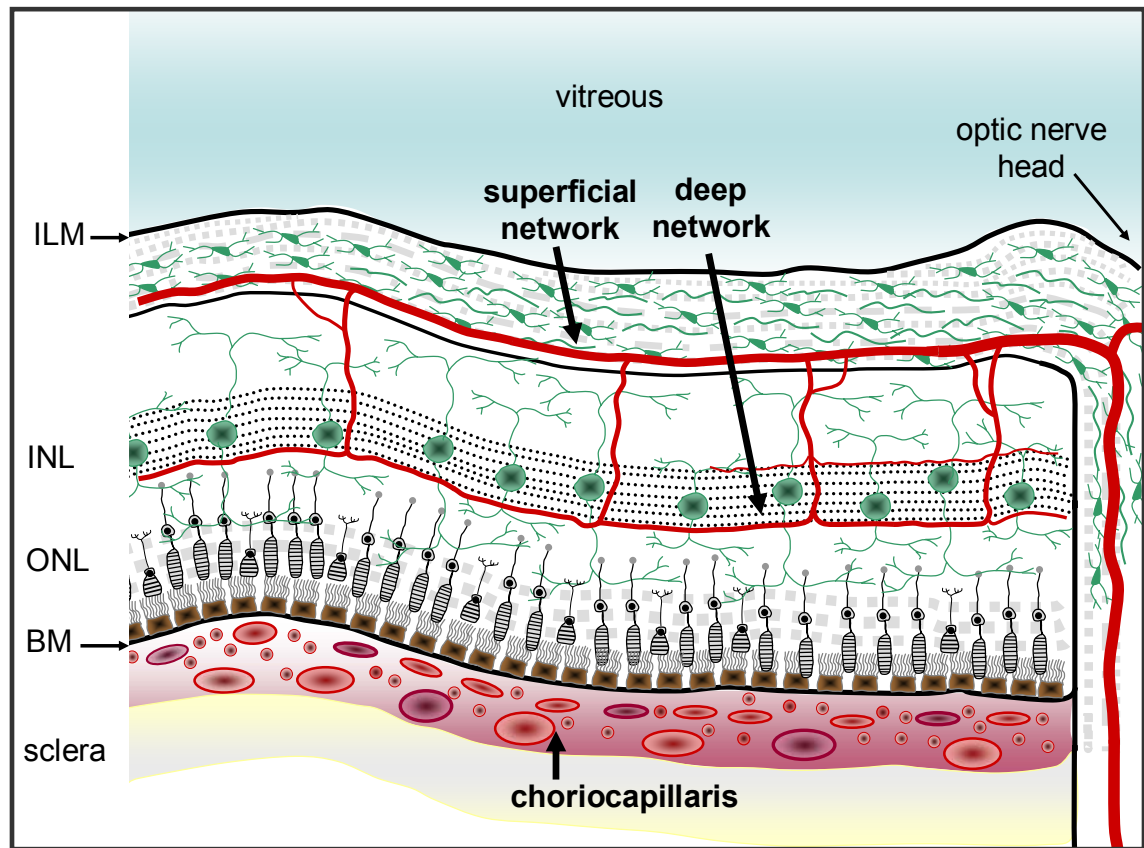
Figure 1.4 Schematic representation of a human retina in cross-section, demonstrating the dual retinal vascular supply. The retinal blood vessels radiate out from the optic nerve head and supply the inner retina via superficial and deep vascular networks. The metabolic demands of the outer retina are met by the choroidal circulation, a rich vascular network subjacent to Bruch's membrane (BM). Not to scale.

Key:

▢	vitreous	🔦	photoreceptor
▢	sclera	▨	pigmented epithelial cell
✬	astrocyte	◉	choroidal blood vessel
⚲	Müller cell	〜	retinal blood vessel

1.2.c.1   Retinal vascular anatomy

The retinal arteries, terminal branches of the central retinal artery, follow arcuate courses as they radiate out from the optic disc toward the retinal periphery. The arteries run superficially in the nerve fibre layer, where they give off numerous small arterioles, the *arteriae afferentes of His* [15]. The arterioles form planar anastomotic networks which give rise to capillary beds at two levels – the superficial capillary net, in the nerve fibre layer, and the deep capillary net, between the inner nuclear and outer plexiform layers.

The deep net is generally denser and more complex than the superficial net. The networks are largely planar in architecture, but communicate via numerous anastomotic capillaries. The superficial and deep networks – originally thought to be arterial and venous, respectively – have neither arterial nor venous predominance [15]. Venous capillaries unite to form venules, the *venae efferentes of His*, which in turn form anastomotic networks in the nerve fibre layer, in similar fashion to the arterioles. The venules converge on the retinal veins which course through the nerve fibre layer and unite as the central retinal vein at the optic disc. Retinal arteries and veins often run in close proximity and arteriovenous crossing is common. In distinction to the veins, retinal arteries are surrounded by capillary-free zones which average 50 μm in width, increasing towards the retinal periphery.

Several notable exceptions to this general architecture exist. In the central, thicker regions of the retina the deep network assumes a bilaminar arrangement, with a network of capillaries in the superficial part of the inner nuclear layer – referred to as the superficial inner nerve layer plexus [18]. In the fovea blood vessels are completely absent and the area, typically measuring 400-500 μm in diameter, is fittingly known as the foveal avascular zone [1]. Toward the retinal periphery both capillary nets become increasingly sparse, with the deep net disappearing entirely [15]. The peripheral margin of the retinal circulation is comprised of wide-calibre anastomotic arcades between terminations of the retinal arteries and veins. The circulation falls short of the extreme retinal periphery, leaving an avascular zone of approximately 1mm in width. The optic disc is a watershed between the retinal and optic nerve circulations. With the exception of the nerve fibre layer, which is supplied by the retinal vessels, the optic disc is supplied by the short posterior ciliary vessels.

The barrier properties of the retinal circulation are due, in large part, to the tight endothelial cell junctions and a lack of fenestrae [19, 20], coupled with dense abluminal coverage with pericytes and glial cellular-processes – the perivascular *glia limitans* [1, 21-23].

The choriocapillaris is a dense network of large-calibre capillaries which enmeshes the outer aspect of Bruch's membrane from the optic nerve head to the ora serrata [1]. The

choroidal circulation is largely segmental with multiple vascular lobules, each served by its own arteriole and venule. Beneath the macula, capillaries assume a dense honeycomb pattern and inter-arteriolar anastomoses, rare elsewhere in the choroid, are numerous. Choroidal capillaries are fenestrated and have sparse pericyte coverage, with average pericyte densities one third of their retinal counterparts [1]. Accordingly choroidal capillaries are highly permeable: more permeable to protein and glucose than the capillaries of skeletal muscle by factors of 10 and 80 respectively [24]. Oxygen and nutrients furnished by the choroidal circulation diffuse across Bruch's membrane to supply the outer retina, which lacks its own vasculature.

1.2.c.2   *Retinal vascular physiology – retinal oxygenation*

Retinal oxygen demands are enormous, well in excess of most other tissues on a unit mass basis, due to the high level of metabolic activity of the retina [25, 26]. *In vivo* microelectrode studies of the retinae of mammals with circulations similar to man, have provided important insights into retinal oxygenation (reviewed in [27-29]). These studies have demonstrated heterogeneity in oxygen consumption and supply at different retinal levels, such that the inner and outer retina differ markedly.

In the outer retina, oxygen tension (PO_2) in normoxia (21% O_2; $PO_2 \sim 150$ mmHg) decreases as a function of distance from the choriocapillaris [30], where typical PO_2 is in the order of 60 mmHg. The high choroidal PO_2 is achieved by its exceptionally high blood flow, which may be up to ten times higher per unit mass than that of grey matter of the brain [6, 31, 32]. Almost all oxygen consumption in the outer retina is accounted for by the photoreceptor inner segments, the mitochodria-rich powerhouses of the photoreceptors. Under conditions of illumination sufficient to saturate rod phototransductive responses ('light-adapted' – below normal room lighting) the oxygen demands of the inner segments are entirely met by the choroidal circulation [33]. With dark-adaptation, oxygen consumption in the outer retinae of rats, cats and monkeys increases dramatically, by between 32-64% [29], such that choroidal supply becomes insufficient [33]. Importantly, the choroidal circulation lacks substantive compensatory mechanisms to meet the oxygen demand as it is not subject to significant metabolic regulation (autoregulation) [6, 14]. As a result there is a reversal of the oxygen gradient at the junction of the inner and outer retina, and oxygen diffusing from the retinal

circulation supplies the inner segments. The choroidal circulation is thought to contribute approximately 50% of the total amount of oxygen consumed under dark-adaptation [34]. Much of the increase in oxygen consumption during dark-adaptation is thought to be related to the maintenance of intracellular ion gradients against the dark current – the intracellular flux of sodium ions across light-inactivated ion-channels in photoreceptors [29].

Oxygen homeostasis of the inner retina differs considerably from that of the outer retina. Average inner retinal PO_2 in normoxia is approximately 20 mmHg in the cat [29], however there is considerable heterogeneity in PO_2 at different levels of the inner retina [28]. The inner and outer plexiform layers are regions of significant oxygen consumption, purportedly due to the metabolic activity required to support synaptic transmission [28]. Studies in the rat demonstrate that inner retinal PO_2 is maximal in the nerve fibre and ganglion cell layers (~ 22 mmHg) and lowest in the deeper region of the inner plexiform layer (~ 5 mmHg), with a peak in PO_2 at the superficial outer plexiform layer, corresponding to the site of the deep retinal capillary network. The inner retinal PO_2 varies little with light- or dark-adaptation as there is no change in inner retinal oxygen consumption [29].

Changes in systemic oxygen tension have differing effects on inner and outer retinal PO_2. Studies in the cat and miniature pig demonstrate the tremendous capacity of the retinal circulation for autoregulation during hypoxia: inner retinal PO_2 remains relatively constant, provided that the systemic PO_2 level remains above 35 mmHg [29]. In the cat, retinal vasodilation has the capacity to more than treble blood flow [35]. At lower systemic oxygen levels these compensatory mechanisms are overwhelmed and retinal PO_2 falls more precipitously. The lack of choroidal autoregulation results in an almost linear reduction in outer retinal PO_2 with systemic PO_2. During systemic hyperoxia choroidal PO_2 increases dramatically – levels as high as 220 mmHg and 250 mmHg have been recorded in the miniature pig [36] and cat [37] ventilated with 100% oxygen – and outer retinal PO_2 increases proportionately. In contrast, inner retinal PO_2 is well regulated during hyperoxia. Retinal vascular autoregulation is central to this compensatory response, with marked vasoconstriction of retinal arteries. Increases in inner retinal oxygen consumption – possibly related to a switch from glycolytic to

aerobic metabolism – may also play a role in maintaining stable PO_2 [28]. Thus in hyperoxia, much of the inner retinal oxygen supply is met by the choroidal circulation. The vascular supply of the retina is anatomically and physiologically unique. Differences in oxygen delivery to the inner and outer retina are functional consequences of the dual circulation. These differences, coupled with regional variations in oxygen consumption, have important implications for our understanding of the drivers of retinal vascular development and the retinal response to changes in oxygen supply in disease.

1.3.　　VASCULAR DEVELOPMENT

An overview of general mechanisms of vascular development will precede a review of specific mechanisms of retinal vascular development.

1.3.a.　Blood vessel structure

Blood vessels are lamellated structures and three distinct cell layers, or tunics, are described (Figure 1.5). The *tunica intima* is comprised of a monolayer of endothelial cells, which lines the vessel lumen, surrounded by a basement membrane. Larger vessels also contain a layer of elastin-rich connective tissue. Endothelial cells in different vascular beds exhibit diverse functional specialisations due to differences in morphology, in the repertoire of cell surface molecules, in cell junctions and in barrier properties [38]. In addition to forming a vascular lining, endothelial cells have a range of paracrine signalling roles (reviewed in Cleaver and Melton [38]). The intima is surrounded by the *tunica media*, comprised of layers of smooth muscle cells and supporting connective tissue. The so called *mural cells* of the tunica media provide structural support to the intima and may have contractile functions and signalling roles. The *tunica adventitia* is composed of elastic and fibrous connective tissue. Small vessels lack this outer layer and have less substantial medial layers. Capillary endothelial cells are covered by scattered pericytes which vary significantly in density.
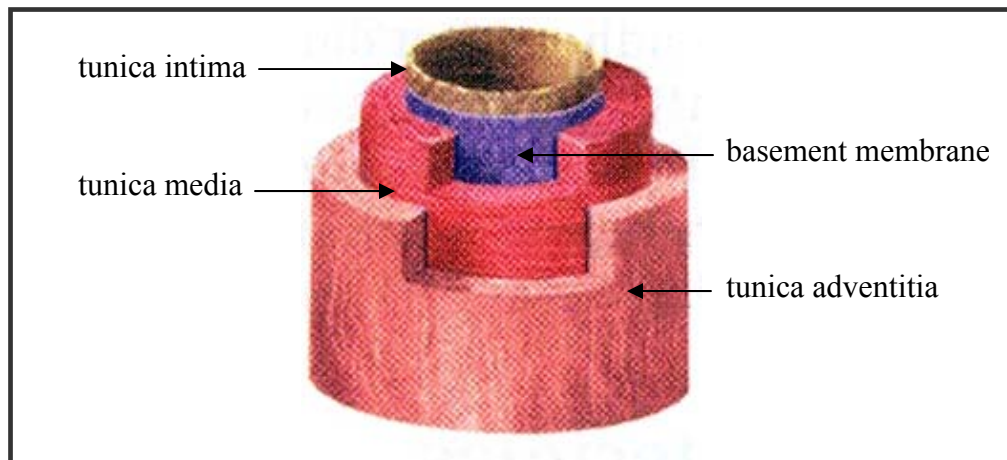
Figure 1.5 Blood vessel structure. A schematic representation of the three major cell layers, or tunics that comprise the wall of a typical arteriole. Figure adapted from Saladin [39].

1.3.b. Vasculogenesis and angiogenesis

Blood vessel formation involves complex synchrony between a large number of cellular and biochemical mediators. The development of blood vessels is an essential part of embryogenesis and in postnatal life it accompanies growth and sustains important physiological functions, such as ovulation and wound-healing. Furthermore, new vessel formation, termed *neovascularization*, is central to a host of disease processes including tumour growth, arthritis and psoriasis [40]. In the eye, aberrant blood vessel proliferation in association with premature birth, diabetes and macular degeneration is a major cause of vision loss. Two major processes of vascular development are described – vasculogenesis and angiogenesis.

Vasculogenesis is a process in which endothelial progenitor cells (*angioblasts*), typically of bone marrow origin, migrate into a tissue, proliferate and coalesce into cords, differentiating into endothelial cells which form vascular tubes [41]. These primitive vascular structures are subsequently remodelled and mural cells are recruited to produce mature vessels. In contrast, angiogenesis is a process in which new blood vessels are formed from pre-existing ones [42]. Endothelial cells are mobilised from existing vessels and proliferate to form nascent vessels which extend into the tissue, recruiting mural cells and assuming a mature phenotype. Historically vasculogenesis has been thought to account for most blood vessel development during embryogenesis, with the

exception of some tissues of ectodermal and mesodermal origin, such as the retina and kidney, which were thought to vascularize via angiogenesis [42, 43]. In the adult, new vessel formation was thought to be exclusively due to angiogenesis [44]. More recently these assumptions have been challenged by the finding that endothelial progenitor cells may contribute to many forms of vascular development [40, 45-47]. The extent of this contribution to human vascularization remains in question [48]. Nonetheless, angiogenesis remains central to retinal blood vessel formation in health and disease. Accordingly, an overview of the general mechanisms of angiogenesis will be followed by a specific review of mechanisms of retinal angiogenesis in development. The potential role of vasculogenesis in retinal vascularization will also be addressed.

1.3.c. Mechanisms of angiogenesis

Angiogenesis is a multi-step process involving a diverse range of biochemical factors. Numerous endogenous stimulators and inhibitors of the process – termed *pro-* and *anti-angiogenic factors*, respectively – have been characterised (Table 1.2). The large number and variety of factors implicated in angiogenesis attest to its complexity. It is the balance between these stimulatory and inhibitory influences that determines the angiogenic fate of a given tissue. In health the set-point of this balance may differ in different tissues: in the avascular cornea anti-angiogenic factors predominate; in the endometrium, during the proliferative phase, pro-angiogenic factor predominate. In disease, perturbation of this balance may lead to neovascularization – a concept aptly named the *angiogenic switch* [49, 50] (Figure 1.6).

The mechanisms of angiogenesis may conveniently be considered in five key stages: *initiation*, *migration*, *vasoproliferation, remodelling* and *stabilisation* (Figure 1.6). While such an approach fosters an understanding of new vessel formation, it represents a gross simplification of the process. It is important to appreciate that these events occur on a continuum and that present knowledge of the underlying mechanisms remains fragmentary.

Table 1.2 Some of the factors implicated in ocular neovascularization

Angiogenic	Anti-angiogenic
Vascular endothelial growth factor (VEGF) [51-53]	Endostatin [68]
	Angiostatin [69]
Fibroblast growth factor (FGF) [54]	Prolactin [70]
Placenta growth factor (PlGF) [55]	Matrix metalloproteinases (MMPs) [71]
Transforming growth factor-β (TGF-β) [56]	Tissue inhibitor of MMP (TIMPs) [72]
Integrins (αvβ3) [57]	Transforming growth factor-β (TGF-β) [73]
Insulin-like growth factor [58, 59]	Thrombospondin [74]
Platelet derived growth factors (PDGF) [60]	Pigment epithelium derived factor (PEDF) [75]
Matrix metalloproteinases (MMPs) [61]	Plasminogen kringle 5 [76]
Angiogenin [62]	
Hepatocyte growth factor (HGF) [63]	
Tumour necrosis factor-α (TNF-α) [64]	
Connective tissue growth factor (CTGF) [65]	
Interleukin-8 (IL-8) [66]	
Monocyte chemoattractant protein-1 (MCP-1)[67]	
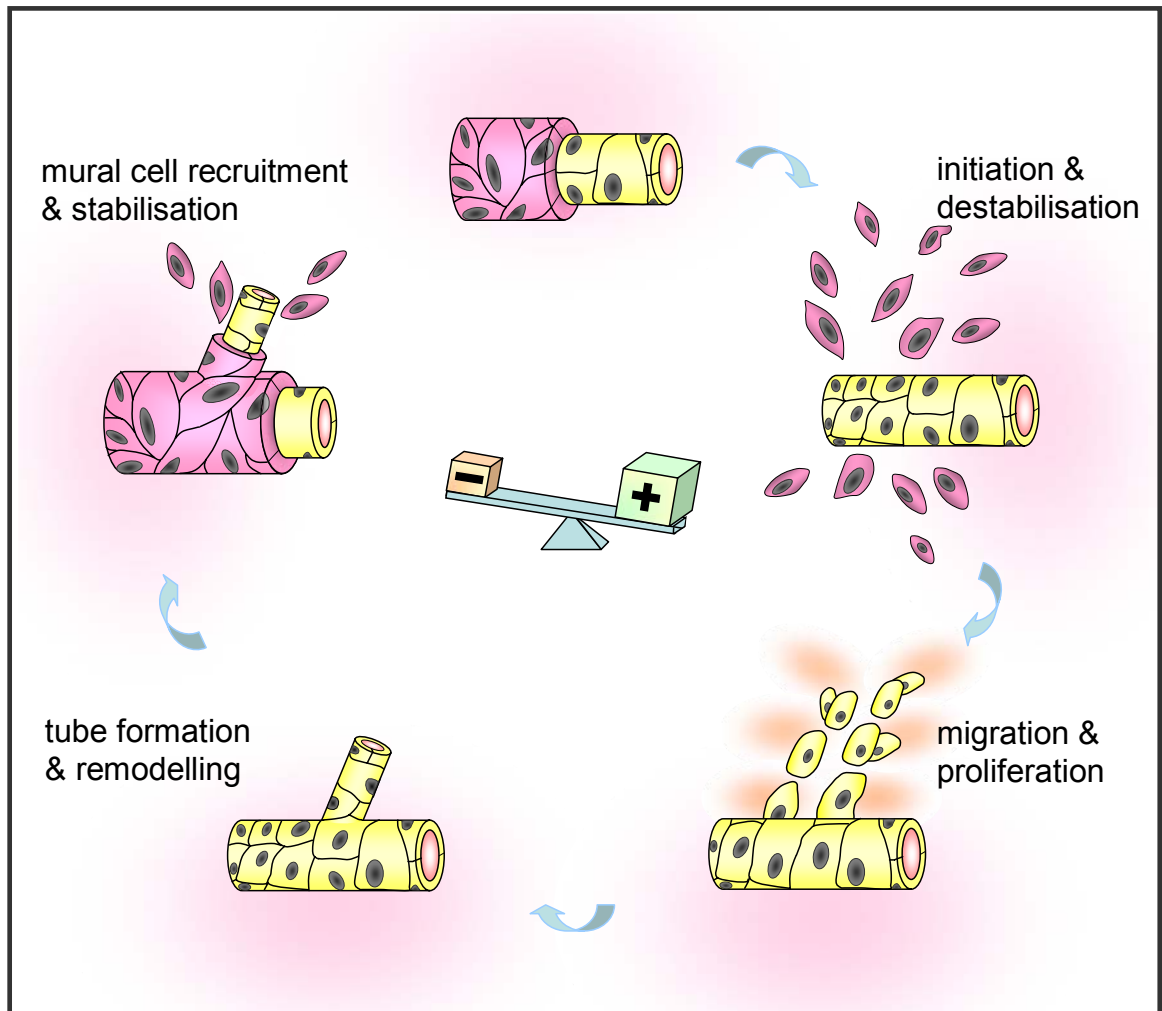
Figure 1.6 The angiogenic switch. The angiogenic activity of a given tissue rests on a balance between pro- and anti-angiogenic factors. A range of physiological and pathological stimuli can tilt the balance in favour of pro-angiogenic factors, triggering a switch to angiogenesis with the activation of a diverse range of molecular and cellular events that ultimately lead to new vessel formation. Key steps in the process are initiation and vascular destabilisation, endothelial cell migration and proliferation, vascular tube formation and remodelling, and finally mural cell recruitment and vascular stabilisation.

Neovascularization commences with an *initiation phase*, in which an inciting stimulus results in the activation of resident cellular mediators of angiogenesis. Common triggers include metabolic stressors, such as hypoxia or acidosis encountered in tissue ischaemia; mutation of genes that regulate angiogenic factors, as is seen in tumorigenesis; as well as inflammation and tissue injury [77]. The release of pro-angiogenic factors from cells initiates the switch to an angiogenic phenotype. Often considered the archetypal pro-angiogenic factor, vascular endothelial growth factor (VEGF) is of central importance in many cases of angiogenesis (Table 1.3) with biological activity at numerous levels of the angiogenic process (Table 1.4).

Amongst the soup of induced factors are many that recruit leucocytes and that up-regulate cellular adhesion molecules, such as vascular cell adhesion molecule-1 (VCAM-1), intercellular adhesion molecule-1 (ICAM-1) and E-selectin [78]. The complement of factors released may vary with the initiating stimulus [79]. Other factors induced during the initiation phase such as angiopoietin-2 (Ang 2), a ligand of the endothelial cell receptor Tie2, are responsible for the destabilisation of nearby vessels [80, 81]. Destabilisation of the association between endothelial and mural cells facilitates the subsequent migration and proliferation of endothelial cells that are essential for angiogenesis.

The release of a host of chemokines and angiogenic factors during the initiation phase stimulates the influx of leucocytes and vascular endothelial cells that denotes the commencement of the *migratory phase*. The release of proteases, such as the matrix metalloproteinases (MMPs), from the initiating cells, invading leucocytes and endothelial cells, causes breakdown of the extracellular matrix [82, 83]. Matrix degradation facilitates the ingrowth of vascular endothelial cells and liberates a range of proteases and angiogenic factors formerly sequestered in the matrix [82, 84-86]. These factors then feed into the ensuing biochemical cascade. The migration of endothelial cells from adjacent vessels is also facilitated by protease degradation of vascular basement membranes [82]. The initial ingrowth of vascular endothelial cells precedes cellular proliferation and involves the recruitment and migration of cells from established vessels [87, 88].

The beginning of the *vasoproliferative phase* is marked by the proliferation of vascular endothelial cells under the stimulatory influence of pro-angiogenic factors. The endothelial cells of nascent vessels contribute to the angiogenic stimulus by releasing factors with pro-angiogenic activity, such as VEGF [89]. The formation of tubular vascular structures from new endothelial cells and their subsequent differentiation and hierarchical organisation is also under biochemical control, with VEGF, the Ephrins, angiopoietin-1 (Ang-1) and Tie2 playing key roles [81, 90]. During this phase vessels are hyperpermeable. The associated extravasation of plasma proteins provides a structural supporting gel or scaffolding on which new vessels develop [85]. Vasoproliferation can be detected within hours of an inciting stimulus [91], and is at its peak within days [92].

The *remodelling phase* involves the selective pruning of nascent vessels, the development of vascular networks, lumen formation, as well as arterial and venous fate determination. While many elements of these processes remain to be delineated, several factors are known to play key roles. The family of membrane tethered Ephrin ligands, interacting with Eph tyrosine kinase receptors is critical for the assumption of arterial and venous identity [93]. The angiopoietin-Tie2 signalling axis plays a role in determining vascular density and lumen calibre [94-96]. The expression pattern of different VEGF isoforms has also been demonstrated to influence vessel lumen diameter and vascular patterning [97, 98]. These and other factors act in concert to orchestrate orderly vascular architecture.

In the *stabilisation phase*, endothelial cells, previously dependent on angiogenic growth factors for survival, recruit pericytes and smooth muscle cells. Factors such as platelet-derived growth factor-B (PDGF-B) expressed by endothelial cells are central to mural cell recruitment and proliferation [99, 100]. A population of bone marrow mural cell progenitors expressing PDGF-β, the receptor for PDGF-B, migrate to the site of angiogenesis, proliferate and mature on endothelial contact [101]. Association with these mural cells and with matrix macromolecules is proposed to confer upon endothelial cells an escape from a reliance on growth factors for survival and the assumption of a quiescent state [81, 102]. The association of mural cell derived angiopoietin-1 (Ang-1) with its cognate receptor, Tie2, on endothelial cells is important for vascular

stabilisation. Similarly, the interaction of the cell adhesion molecules integrin$\alpha_4\beta_1$ and VCAM-1, expressed by proliferating endothelial cells and mural cells respectively, is integral to vessel stabilisation [103]. In animal models, this phenomenon occurs within 7 to 14 days of the initiating stimulus [104]. In clinical terms, this is of significance as it imposes a narrow window, the so-called *plasticity window* [99], in which therapies directed against growth factors may exert anti-angiogenic effects. During the stabilisation phase, the vascular basement membrane is formed and endothelial cell junctions are established [82]. The expression of other factors, such as TGF-β, by mural cells may facilitate vascular stabilisation by inhibiting further matrix degradation and promoting endothelial cell differentiation [105]. Other anti-angiogenic factors, many of which are cleavage fragments of collagen (restin, endostatin, tumastatin) [106] and plasminogen (angiostatin) [107], serve to keep angiogenesis in check and are variously regulated by matrix metalloproteinases [82].

The activities of many of the key angiogenic factors are interrelated, such that a given factor may be either pro-angiogenic or anti-angiogenic in different contexts. Angiopoietin-2 provides a case in point [108, 109]. In the presence of VEGF – a potent endothelial cell survival signal – Ang-2 plays a permissive role in angiogenesis, destabilising established vessels and allowing endothelial cell mobilisation to the site of angiogenesis. In the absence of VEGF, Ang-2 mediated vascular destabilisation deprives endothelial cells of life-sustaining mural cell contact, leading to endothelial apoptosis [108]. The interrelationships between angiogenic factors extend further: some factors regulate the expression of others. VEGF is known to modulate the expression of many factors including Tie2 [110] and the anti-angiogenic factors pigment epithelium-derived factor (PEDF) [111, 112] and thrombospondin [74].

Thus it is clear that angiogenesis is a complex and highly orchestrated process. Disruption of the spatial, temporal or quantitative expression of any one of a large number of these factors can inexorably alter the process, arresting angiogenesis or causing the formation of dysfunctional vessels.

Table 1.3 VEGF in angiogenesis: VEGF plays a central role in angiogenesis in numerous contexts.

Physiological angiogenesis	Pathological angiogenesis
Endochondral bone formation [113]	Ocular neovascularization: corneal, iris, retinal and choroidal [119]
Cyclic endometrial [114] and corpus luteal development [115]	Tumour neovascularization [120]
Placentation and embryonal vascular development [116]	Arthritis [121]
Haematopoiesis [117]	Psoriasis [122]
Wound healing [118]	Atherosclerotic plaque formation [123]
Collateral vessel formation: brain and muscle (skeletal and cardiac) ischaemia [113]	von Hippel Lindau Syndrome [124]

Table 1.4 Some key biological activities of VEGF

Activity	Reference
Developmental vasculogenesis & angiogenesis	[51, 125-128]

Mitogen: vascular endothelial cells
      lymphocytes
      retinal pigment epithelial cells
      retinal photoreceptors
      Schwann cells
      neuroectodermal progenitor cells
	[129-133]
	[134]
	[135]
	[136]
	[137]
	[138]

Vascular endothelial cell hypertrophy	[139]
Spatial organisation of endothelial cells & lumen formation	[88, 97]

Survival signalling
      endothelial cells
      tumour cells (numerous)
      neuroectodermal progenitor cells
	
	[52, 140, 141]
	[142, 143]
	[137, 138]

Regulation of cellular adhesion molecules	[144, 145]
Modulation of protease activity	[82, 146, 147]
Vasopermeability	[85, 148, 149]

Chemotaxis
      vascular endothelial cells
      angioblasts
      pericytes & smooth muscle cells
      monocytes
      neural cells
	
	[127, 150, 151]
	[152]
	[127]
	[153]
	[137, 138]

Vasodilatation	[154]
Modulation of host antigen-presenting cell maturation	[155]
Regulation of retinal endothelial glucose transport	[156, 157]

1.4.   OCULAR VASCULARIZATION IN DEVELOPMENT

Development of the choroidal circulation and the hyaloid vessels occurs early in embryogenesis. These vascular networks play important roles in sustaining the developing retina prior to the formation of the retinal circulation. The development of the choroidal and hyaloid circulations will therefore be addressed briefly before retinal vascularization is discussed in detail.

1.4.a.   Development of the choroidal and hyaloid circulations

The choroid begins as a condensation of neural crest cells around the developing retina (optic cup) at approximately 28 days post conception [1]. In humans, primitive vessels are found in the developing choroid early on. Between four and five weeks of gestation (WG) the endothelial cells lining these vessels begin to proliferate and differentiate to form the primitive choriocapillaris. Association with the developing RPE is integral to this process [158]. By the beginning of the sixth WG the vascular network completely surrounds the developing retina. One week later endothelial cells begin to adopt the characteristic fenestrated phenotype. Endothelial cell differentiation proceeds during the ensuing weeks and mural cell recruitment, first identified at 6 WG, continues. The choroidal circulation expands and increases in density with eye growth, and vascular remodelling continues until the final mature vascular pattern is assumed by 8 months of gestation [1].

The hyaloid circulation develops in concert with the choroidal system. During the fourth WG, mesenchymal cells invade the developing retina via the centre of the nascent optic nerve (the optic stalk), giving rise to endothelial cells which aggregate to form the hyaloid artery [1]. The hyaloid artery gives off numerous branches which traverse the primary vitreous. Capillary networks form on the posterior aspect of the developing lens and by the ninth WG numerous anastomoses are made with anterior branches of the choroidal circulation, forming a transient vascular network, the *tunica vasculosa lentis*, which supplies the developing lens. Oxygen and nutrients furnished by the hyaloid system are also thought to sustain the inner portion of the developing retina [158]. As the retinal circulation begins to develop, the hyaloid vasculature regresses to disappear entirely by the ninth month of gestation [159].

1.4.b. Overview of retinal vascular development

Human retinal vascular development begins between 12 and 14 WG as spindle-shaped cells enter the developing retina at the optic disc from the hyaloid artery [128, 160-163]. These cells fan out in centrifugal fashion giving rise to primitive vessels [160]. The area occupied by vessels is butterfly-shaped, with lobules advancing superiorly and inferiorly into the nasal and temporal retina. Vascular development is more advanced temporally and superiorly than nasally and inferiorly [160]. During the initial phases of vascularization, vessels advance in planar fashion deep in the nerve fibre layer, forming the primitive superficial retinal circulation (Figure 1.7). Strikingly, vascularization is closely associated temporally and spatially with astrocytic development. As in the cat [164] and rat [165], astrocytes enter the retina via the optic nerve and radiate out toward the retinal periphery [162]. Two astrocyte layers are identifiable in the developing human retina: one in the superficial nerve fibre layer; the other near the junction of the nerve fibre and ganglion cell layers, in close association with the developing vasculature [162]. Astrocytes in the deeper layer move in advance of the vascularizing front, typically by distances of up to 150 μm [162]. By 21 WG dense branching vascular networks cover much of the retina and by 25WG vessels have almost reached the retinal periphery in some areas [128]. Between 25 and 26 WG new vessels sprout down from the superficial network to form the deep network, at the interface between the inner nuclear and outer plexiform layers [128] (Figure 1.7). By 32 weeks the superficial network has reached its peripheral limits [128, 160]. Remodelling of the circulation continues and the mature vascular pattern is finally assumed by the third month of postnatal life [1].
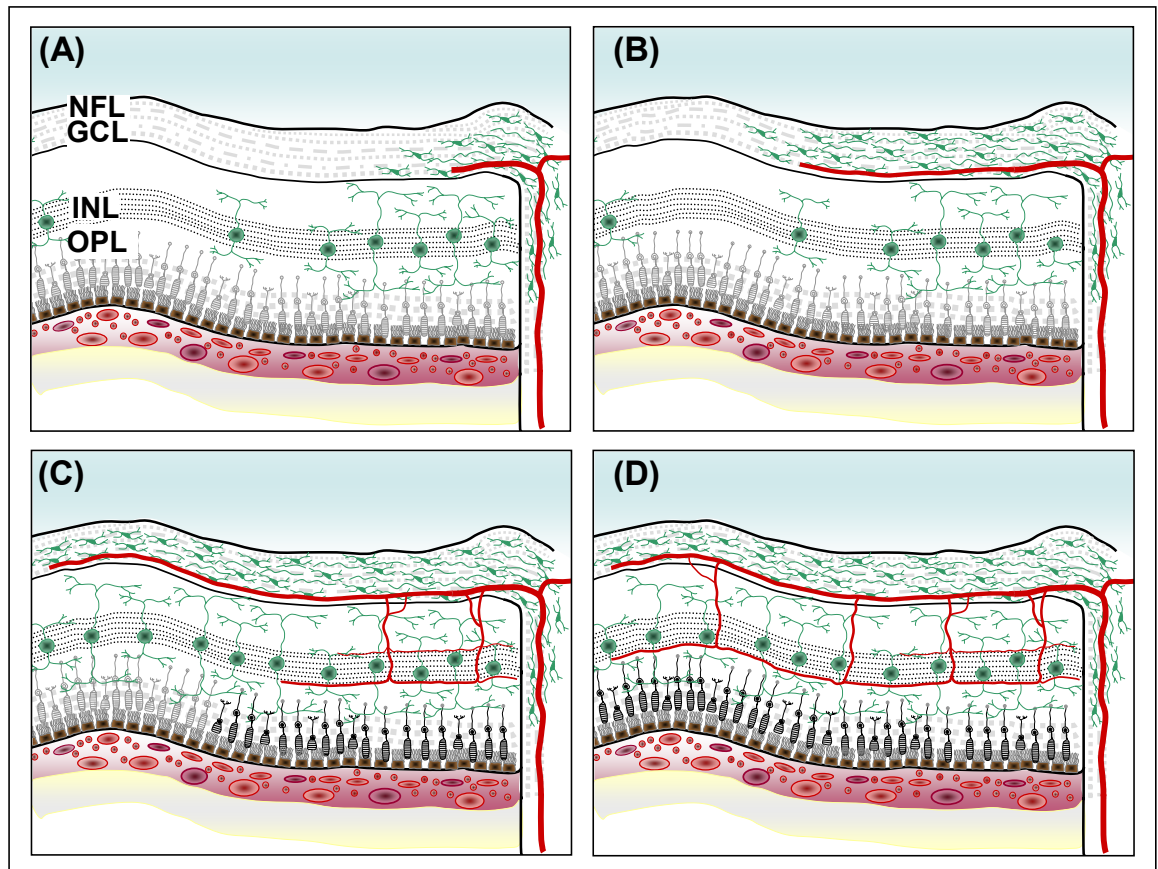
Figure 1.7 Schematic representation of human retinal vascular development (cross-sectional images). Retinal vessels emerge from the optic nerve and ramify at the interface of the nerve fibre (NFL) and ganglion cell layers to form the superficial vascular network. Vasoproliferation and astrocyte migration are closely related. Vascular sprouts from the superficial network descend to the junction of the inner nuclear (INL) and outer plexiform layers (OPL) before radiating toward the retinal periphery to constitute the deep circulation. Formation of the deep network is temporally and spatially associated with Müller cell migration and with photoreceptor maturation. (A) 15 weeks; (B) 20 weeks; (C) 26 weeks; (D) 36 weeks. Figure concept from Provis, J. M. (2001) [2]. Not to scale.

Key:
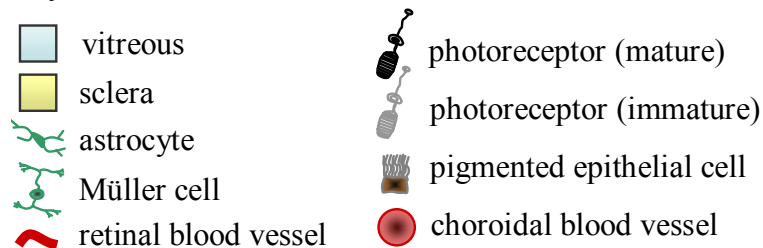
1.4.c.   Mechanisms of retinal vascular development

1.4.c.1   Historical insights

In his studies of retinal vascularization, Michaelson contributed a number of significant insights into the process, postulating the existence of a "vasoformative factor" and alluding to its association with "gradients of oxidative metabolism" [160]. He noted that capillaries bud predominately from the venous circulation and that their growth is preferentially away from arterioles. Where capillaries are associated with arterioles, their proximity is limited, such that a definite periarterial capillary-free zone is maintained. Michaelson concluded that vascular development is orchestrated by an extravascular biochemical factor and that concentration gradients of the factor determine the extent of vessel growth.   This hypothesis was explored by Campbell, who proposed that the capillary-free zones are due to the local inhibition of vessel growth, secondary to high periarterial oxygen tension [166]. Oxygen had long been associated with vascular development [167], but Michaelson was the first to propose a biochemical mechanism.

Michaelson's hypothesis was developed further by Ashton, Ward and Serpell [168]. Following a series of experiments, in which they studied the effect of hyperoxia on retinal vascularization in the kitten, the investigators proposed a mechanism for retinal vascularization. They postulated that ordinarily, in early retinal development, diffusion from the choroidal circulation is sufficient to maintain retinal oxygenation. With retinal maturation, the choroidal circulation becomes increasingly incapable of meeting retinal metabolic demands. They hypothesised that a "vasoformative stimulus…, closely related to want of oxygen" is central to subsequent retinal vascularization and that oxygen, furnished by newly developed retinal vessels, ameliorates the stimulus. The foresight of these investigators was confirmed some thirty years later when the "vasoformative factor" was identified as VEGF (initially named *vascular permeability factor*) [148]. Several years later it was confirmed that hypoxia-induced expression of VEGF is a central mediator of retinal vascular development [51-53].

1.4.c.2 Current concepts of retinal vascular development: vasculogenesis

In many of the earliest studies of retinal vascularization it was noted that spindle-shaped cells of indeterminate identity entered the retina from the hyaloid vessels [160, 169, 170]. These cells were noted to fan out in the deep nerve fibre layer forming solid cords which subsequently developed lumens, giving rise to the butterfly-shaped primitive superficial circulation. Similar observations were made in the rat [44], cat [171] dog [172] and monkey [18]. Michaelson suggested that these cellular aggregates constituted vascular buds from the hyaloid system and concluded that the retinal circulation in man does not develop from the local differentiation of mesenchymal progenitor cells [160]. Cogan arrived at a similar conclusion from his studies of digest preparations of foetal retina [169]. Ashton thought otherwise – he suggested that the invading cellular cords were not endothelial cells, but "mesenchymal precursor cells" [170]. The evidence for this latter hypothesis has continued to mount since [18, 44, 128, 171, 172], however the identity of these invading cells has remained the subject of contention [158].

Fruttiger has recently demonstrated that the spindle-shaped cells in advance of the developing vasculature in the murine retina express PDGFα, a marker for retinal astrocytes, but not VEGF receptor-2 (VEGFR-2), an endothelial lineage marker [173]. Thus in the mouse, at least, it appears that retinal vascular development occurs via angiogenesis alone [163, 173]. Recently and in contrast, Chan-Ling and colleagues have demonstrated that the spindle-cells in the developing human retina express the endothelial lineage markers VEGFR-2 and CD39, an ecto-ADPase [163]. This cell population was distinct from a second population, with immunohistochemical features of astrocytic precursor cells (expressing the transcription factor Pax-2, but not glial fibrillary acidic protein). Endothelial progenitor cells and astrocyte precursors were found ahead of the vascularizing front by approximately 1 mm and 0.1 mm, respectively. The investigators concluded that almost two thirds of the human primitive superficial retinal vascular network develops via vasculogenesis. The superficial network is thought to increase in density and in peripheral extent through angiogenesis, while the deep network is entirely the product of angiogenesis [128, 162, 163]. Thus on balance, vasculogenesis appears to be important for the initial phase of human retinal vascularization.

ADPase-expressing spindle cells are also found in the retinae of rats, cats, dogs and primates, supporting the notion that in these animals the retinal circulation develops in similar fashion to that of humans [163]. In the dog, Müller cells are thought to facilitate vasculogenesis by liberating an extracellular matrix that is conducive to angioblast migration [174]. Moreover, adenosine produced by the activity of a Müller cell ecto-enzyme may stimulate angioblast migration [175]. While the drivers of vasculogenesis are yet to be completely elucidated, evidence substantiating the importance of the process for retinal vascularization continues to accumulate.

1.4.c.3   *Current concepts of retinal vascular development: angiogenesis*

While some question the role of vasculogenesis in retinal vascularization [158], there is widespread consensus that the deep vascular network and much of the definitive superficial network are the products of angiogenesis. The accepted model of retinal angiogenesis, formulated by Stone *et al*. [51], resonates with the hypotheses of earlier investigators [160, 168]. In their studies of rat and feline retinal vascularization, Stone and colleagues noted – as had others before them – that vascular development occurs synchronously and proximately with astrocytic development: together, networks of nascent vessels and astrocytes radiate out from the optic nerve [51]. They identified VEGF as an important paracrine mediator of retinal vascular development and described a biphasic process [51, 52]. During the first wave of vascularization, astrocytes in the nerve fibre layer express VEGF immediately ahead of the vascularizing front. VEGF-expressing cells move progressively toward the retinal periphery and vessel development is followed by down-regulation of the factor. During the second wave of angiogenesis, VEGF expression by Müller cells in the inner nuclear layer precedes the proliferation of vessels in the deep vascular plexus [51, 53]. Vessels in the deep network arise as sprouts from the superficial vessels. The pattern of VEGF expression in the inner nuclear layer is similar to that of the nerve fibre layer, gradually moving out toward the retinal periphery, ahead of the spreading vasculature. Vessels in both networks are known to express VEGF receptors (flk-1, otherwise known as VEGFR-2) [51].

The investigators hypothesised that hypoxia, induced by maturation of the sensory retina and the associated rise in metabolic activity, triggers VEGF expression in astrocytes and

Müller cells. VEGF subsequently induces vascular proliferation, which in turn ameliorates the hypoxic drive for further VEGF expression. In this manner vascular supply is closely matched to the metabolic demands of neurons in the developing retina. This developmental hypoxic drive was named *physiological hypoxia* [176]. Stone and colleagues substantiated their hypothesis by demonstrating that hypoxia induces glial cell expression of VEGF *in vitro*. Additionally, exposure of newborn rats and kittens to hyperoxia impedes normal postnatal retinal vascularization as well as retinal VEGF expression [51], causing apoptosis of nascent endothelial cells [52]. The apoptosis of developing endothelial cells could be overcome by the intraocular administration of exogenous VEGF prior to the onset of hyperoxia [52]. Subsequent studies of human retinal vascularization have supported this model [162, 177].

The notion that VEGF expression is related to physiological hypoxia associated with neuronal differentiation is plausible on several grounds. Firstly, VEGF is known to be expressed in response to hypoxia [178, 179], under the control of a transcription factor up-regulated in hypoxia − hypoxia-inducible transcription factor-1 (HIF-1) [180, 181]. Secondly, vascularization is closely related to neuronal differentiation, both temporally and spatially. Neuronal differentiation commences centrally, in the fovea, and progresses peripherally with development [182-184]. The progression of neuronal maturation correlates closely with VEGF expression and vascular development [162]: spread of the superficial network in the human beyond 21 WG matches the gradient of retinal ganglion cell maturation [184]; while development of the deep circulation commences in concert with the onset of photoreceptor function [185]. The importance of precise temporal and spatial orchestration of VEGF expression in the formation of normal retinal vascular architecture is borne out by the disorganised vasculature of transgenic mice with photoreceptors that over-express VEGF [186, 187]. Additionally, it has been demonstrated that the directed movement of cytoplasmic extensions (*filopodia*) of retinal endothelial cells toward astrocytes at the vascularizing front is mediated by VEGF acting through VEGFR-2 [188]. Thirdly, neuronal differentiation is known to be associated with an increase in metabolic activity [189]. Together these lines of evidence provide robust evidence for the model.

To summarise then, retinal vascularization begins relatively late in gestation with formation of a primitive superficial vascular network deep in the nerve fibre layer, in a process of vasculogenesis. Hypoxia, accompanying the onset of ganglion cell maturation, is detected by developing astrocytes in the nerve fibre layer, which express VEGF in response. VEGF stimulates angiogenesis, with the sprouting of new vessels from the primitive superficial network. Vessels develop along a concentration gradient of VEGF that advances toward the retinal periphery with ganglion cell maturation. Oxygen furnished by newly developed vessels ameliorates physiological hypoxia in the ganglion cell and nerve fibre layers, with a resultant reduction in VEGF expression. The onset of photoreceptor function is associated with physiological hypoxia which is detected by Müller cells of the inner nuclear layer. The expression of VEGF by Müller cells leads to a second wave of angiogenesis, with the sprouting of new vessels from the superficial network down a VEGF concentration gradient. As photoreceptor maturation progresses in centrifugal fashion, so too does the deep vascular network, advancing along a VEGF concentration gradient deep in the inner nuclear layer.

While the model provides a cogent basis for development of the retinal circulation, it is important to note that VEGF does not act in isolation. A host of other angiogenic factors are also known to have important functions in retinal vascularization. Ang-2 expression is increased during normal development of the retinal vasculature in mice [190] and mice deficient in the factor have limited superficial retinal vascularization, with complete absence of the deep network [191]. *In vitro*, the expression of Ang-2 by endothelial cells is increased by hypoxia and by VEGF [192], as is retinal pericyte expression of Ang-1 and Tie2 [193]. Expression of the Ephrin ligands and their cognate receptors is also integral to normal retinal vascularization in the mouse [194]. In the dog, expression of adenosine has been associated with normal retinal vasculogenesis and angiogenesis and the factor has been shown to accumulate in hypoxia [175]. Other studies have demonstrated the importance of insulin-like growth factor-1 (IGF-1) in retinal vascularization in mice and in humans [59, 195]. Astrocytic expression of R-cadherin, a cell adhesion molecule and neuronal guidance cue, has also been shown to be important in directing retinal vascularization in mice – administration of an inhibitory antibody during vascular development resulted in paucity of branching of the superficial network and disordered architecture of the deep network [196]. Norrin, an activator of

the Wnt-β catenin signalling pathway, has recently been demonstrated to be essential for angiogenesis, as transgenic mice deficient in the factor have limited superficial retinal vascularization and absence of the deep circulation [197]. The pro-angiogenic factor, neuropeptide Y, has also been implicated in murine retinal vascular development [198], as have matrix metalloproteinases-2 and -9, which are up-regulated in response to hypoxia [199]. Regulation of anti-angiogenic factor expression during retinal angiogenesis is also important. Mice lacking the anti-angiogenic factor endostatin, a cleavage product of collagen XVIII, have excessive and aberrant retinal vascularization associated with astrocytic overgrowth [68]. In mice, expression of the anti-angiogenic factor PEDF by ganglion cells coincides with the cessation of retinal vascularization, pointing to an inhibitory role for this factor [200]. Thus many pro- and anti-angiogenic factors have been implicated in normal retinal vascular development.

It is likely that the factors regulating vascularization in the vicinity of the fovea differ from those directing retinal vascularization elsewhere (reviewed by Provis [2]). Owing to a high level of metabolic activity, the fovea would be expected to exert a substantial hypoxic drive for VEGF expression and therefore vascular development. However the fovea remains avascular. The mechanisms responsible for maintaining the foveal avascular zone remain to be determined [162].

Another point of interest is the apparent reciprocity in the relationship between developing astrocytes and endothelial cells [201]. It appears that an association with endothelial cells is important in stimulating astrocyte proliferation and differentiation. While the molecular basis of this association remains to be elucidated, leukemia inhibitory factor has been implicated [202]. Drawing on the observation that oxygen may trigger astrocyte maturation *in vitro*, others suggest that oxygen delivered by newly formed vessels may directly stimulate astrocyte differentiation [201]. Furthermore, the production of PDGF-A, the ligand for PDGF-α, by neurons of the developing sensory retina mediates astrocyte proliferation and differentiation [60, 201]. Thus the development and maturation of the sensory retina, astrocyte network and vasculature are intimately interrelated.

In summary, developmental retinal vascularization is a complex and highly orchestrated process involving numerous angiogenic factors and a host of cellular interactions amongst the developing sensory retina, endothelial cells, astrocytes and their precursors. Measured expression of these angiogenic factors – in quantitative, temporal and spatial terms – appears essential for normal vascularization.

1.5.   RETINOPATHY OF PREMATURITY

Retinopathy of prematurity, a disease characterised by aberrant retinal vascular development in premature neonates, is a leading cause of blindness and visual impairment in childhood. While numerous factors are implicated in the pathogenesis of ROP, altered retinal oxygen homeostasis is known to play a central role. Key clinical features of the disease will be discussed, as will current approaches to treatment. Several landmark clinical trials will be reviewed, with emphasis on the insights that they provide into the identification of risk factors for progression to advanced disease. The central clinical challenge of ROP – distinguishing the subgroup of infants at high risk of severe disease from the majority of infants in whom the disease will regress spontaneously – will be addressed. Genetic risk factors for neovascularization in general, and ROP in particular, will be discussed and the utility of a genetic screening test for ROP will be broached.

1.5.a.   Clinical features and the classification of retinopathy of prematurity

Retinopathy of prematurity (ROP) is a disorder of retinal vascular proliferation that affects neonates born prematurely. The condition – initially named *retrolental fibroplasia* after the end-stage sequelae of the disease – was first described as a distinct entity in 1942 by Terry [203], however case descriptions appeared in the medical literature as early as the beginning of the 19th century (reviewed by Ryan [204]). The disease is unique to premature neonates, who are born prior to completion of the normal process of intra-uterine retinal vascularization. The condition follows a biphasic course, with initial attenuation of developmental retinal vascularization, leading to hypoxia and the liberation of angiogenic growth factors which trigger the proliferation of retinal vessels into the vitreous (*neovascularization*). Retinal neovascularization may lead to haemorrhage and to the proliferation of fibrous tissue resulting in vitreoretinal traction

and ultimately in retinal detachment – the most advanced of the *involutional sequelae* of the disease [205]. An international classification system for key clinical features of the disease, the International Classification of Retinopathy of Prematurity (ICROP), was devised in 1984 [206], expanded in 1987 [205] and further refined in 2005 [207]. ICROP classifies the disease according to its location relative to the optic nerve (*zone*), its *stage* (increasing in severity from 1-5) and its extent (clock hours, or 30° sectors of disease) (Figures 1.8 & 1.9; Table 1.5). Additional reference is made to the presence or absence of plus disease, the dilatation of veins and increased tortuosity of arterioles in the posterior retina (Figure 1.9). Plus disease is thought to reflect extensive arteriovenous shunting and is often associated with progressive disease [208]. Other less common features of plus disease are vitreous haze, engorgement of iris vessels and impaired pupillary dilatation (rigid pupil) [207]. Together the zone, stage, extent and presence or absence of plus disease, allow for stratification of risk of progression to end-stage disease. Generally, the more posterior the disease, and the larger the area of involved retina, the greater the risk of progression [206, 208, 209]. Recent additions to the classification system include *pre-plus disease*, vascular tortuosity and dilatation insufficient to meet the criteria for plus disease; and aggressive posterior ROP, rapidly progressive, ill-defined retinopathy that does not follow typical step-wise progression through the stages [207].
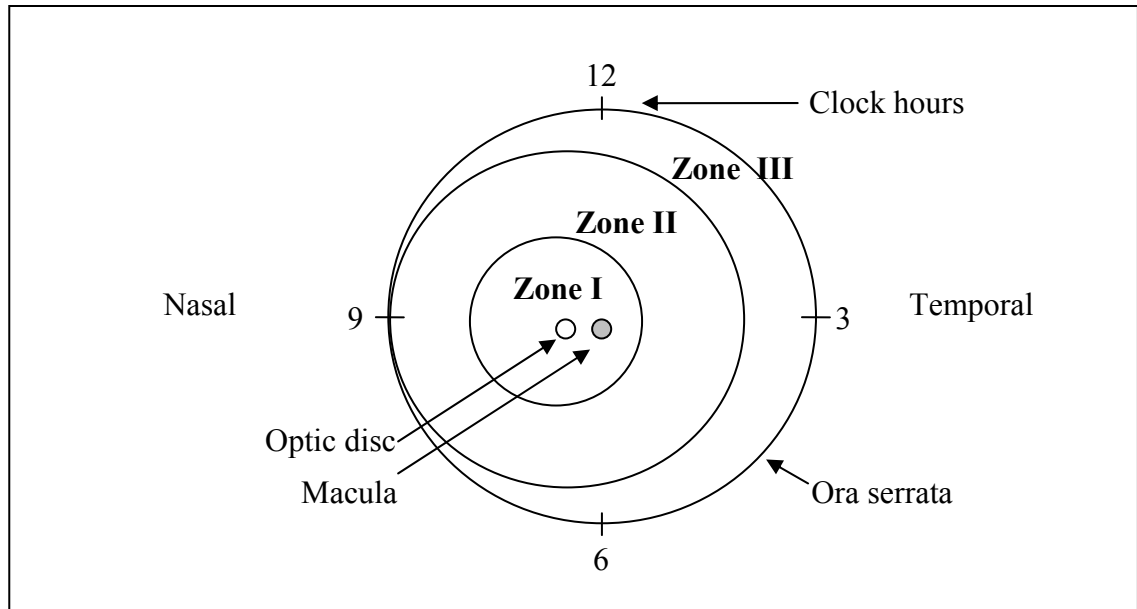
Figure 1.8 Zones of ROP (left eye): Zones are circular and centred on the optic disc. Zone 1: a circle with its radius twice the distance from the centre of the optic disc to the macula. Zone 2: a circle with its radius extending from the centre of the optic disc to the nasal ora serrata (excluding the area occupied by zone 1). Zone 3: the residual crescent of retina peripheral to zone 2. (Adapted from [207]).

Table 1.5 The ICROP stages of human ROP [207]**:** a scale of increasing disease severity, from 1-5.

Stage	Features
1	**Demarcation line**: flat, pale line delineating the interface between the avascular periphery and the vascularized posterior retina.
2	**Ridge**: tissue elevation above the plane of the retina in the region of the demarcation line; usually vascularized.
3	**Extra-retinal fibrovascular proliferation**: neovascularization and fibrous tissue extending from the ridge into the vitreous; mild, moderate or severe in extent.
4	**Partial retinal detachment**: external to, or involving the fovea (4A or 4B respectively).
5	**Total retinal detachment**: typically tractional; rarely exudative.
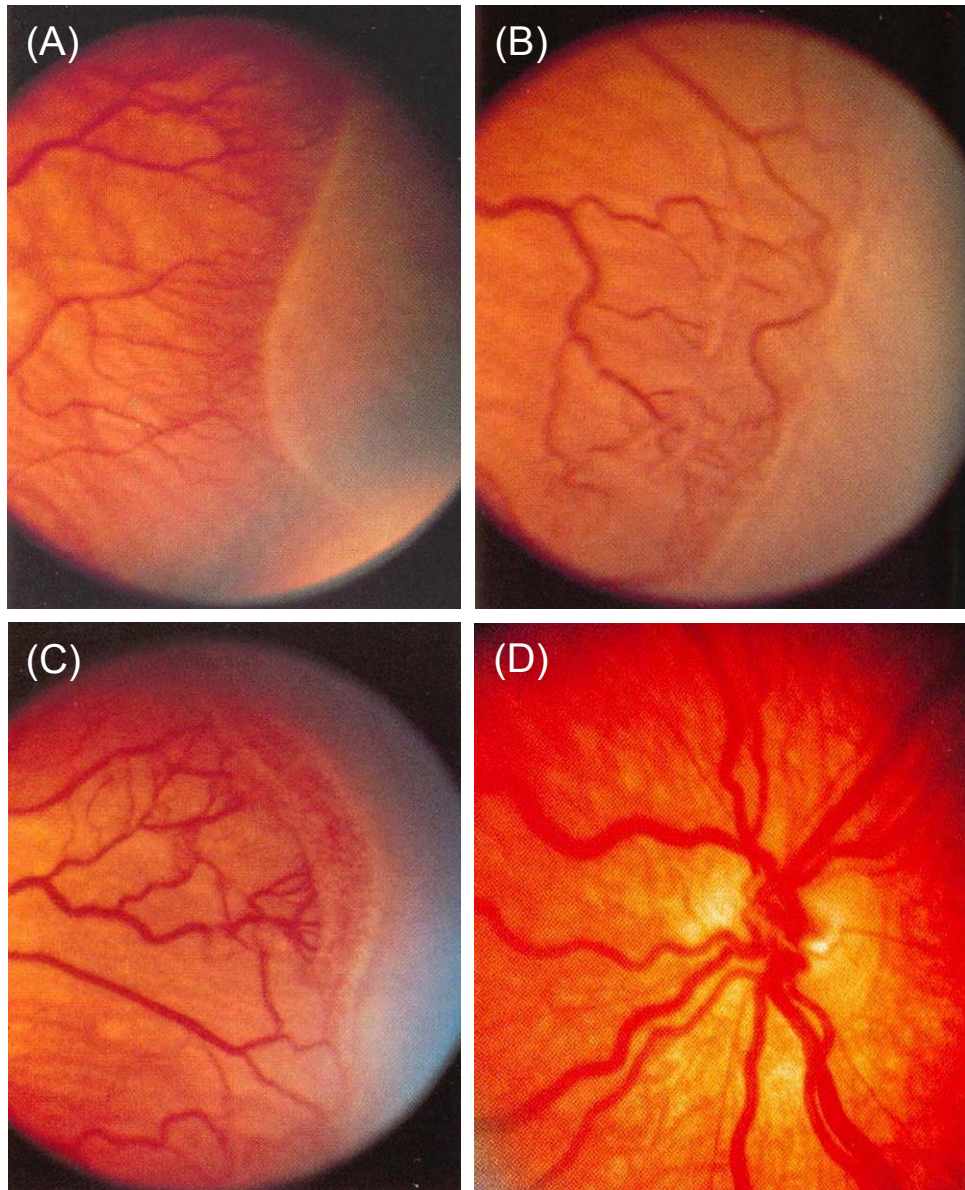
Figure 1.9 Retinopathy of prematurity: human fundus photographs. Stage 1 disease (A) is characterised by the presence of an abrupt transition between vascularized and avascular retina, known as a demarcation line. Stage 2 disease (B) is defined by the presence of an elevated ridge of tissue in the region of the demarcation line, while in stage 3 disease (C) blood vessels and fibrous tissue extend from the ridge into the vitreous. Photograph (D) depicts dilatation and tortuosity of the posterior vessels that is characteristic of plus disease. Sources: (A), (B) & (C) Hertle, R.W. *et al*. [210], (D) Kanski, J.J. [3].

1.5.b. ROP epidemiology and prognostic factors

In spite of advances in the clinical management of ROP, the disease remains a major cause of childhood blindness, second only to cortical visual impairment in the United States [211]. The prevalence of ROP is low in many developing countries; however reductions in infant mortality associated with industrialisation have been accompanied by increasing incidence of the disease [212]. A recent prospective study of infants admitted to tertiary care neonatal units in Australia and New Zealand provides insight into the local incidence of the disease [213]. Clinically severe ROP (defined as stage 3 or greater) developed in 203 of 2105 infants (9.6%) born before 29 WG and surviving to 36 weeks' postmenstrual age. Degree of prematurity was the single most important predictor of disease, with odds of severe ROP 20-fold higher for infants born before 25 WG, than for those born at 28 WG (p<0.01). For a given gestational age, birth weight was inversely related to the risk of severe disease and male gender was also identified as a significant risk factor (p<0.01) [213].

Perhaps the most informative data pertaining to risk factors for ROP and its natural history are those from the Multicentre Trial of Cryotherapy for Retinopathy (CRYO-ROP) [208]— a population-based, prospective study of infants enrolled at 23 study hospitals across the United States. The natural history cohort was comprised of 4099 infants weighing less than 1251 g at birth, born between January 1, 1986 and November 30, 1987. Some degree of ROP developed in 2699 (65.8%) infants (Figure 1.10). Infants weighing less than 1000 g at birth were at greater risk of retinopathy, with an overall incidence of 81.6%. A total of 245 (6%) infants met the severity criteria for entry into the randomised trial of cryotherapy ablation of the peripheral retina – so called *threshold disease*. Threshold disease was defined as 5 contiguous or 8 cumulative clock hours of stage 3 ROP, with plus disease [214]. *Prethreshold* disease – defined as any zone I ROP; any stage 2 ROP with plus disease; or any stage 3 ROP less than threshold severity –

developed in 17.8% of the cohort [214] (Figure 1.10). The median postconceptual[1] age at the onset of prethreshold disease was 36.1 weeks (5th percentile, 32.4 weeks; 95th percentile, 41.5 weeks), corresponding to a median chronological age of 9.6 weeks (5th percentile, 6.2 weeks; 95th percentile, 14.8 weeks). Thus prethreshold ROP manifests relatively late in the postnatal period. Of infants in the study with prethreshold disease, 33.5% progressed to threshold ROP [208, 214]. Eyes with threshold disease that went untreated had unfavourable structural outcomes – defined as posterior retinal detachment; posterior retinal fold involving the macula; or retrolental tissue precluding fundus examination – predictive of long term severe visual impairment, in 51.4% of cases at three months [216].

The findings of the recent multicentre Early Treatment for Retinopathy of Prematurity Randomized Trial (ETROP) [209] demonstrate that there has been little change in the overall incidence of ROP, its time of onset, or its rate of progression since the time of the CRYO-ROP study [217]. Zone I ROP occurred more often in the ETROP study (9.1% versus 2%). The lower gestational ages of infants in the ETROP study may account for this observation – in younger infants retinal vascularization is less advanced at the time of birth and the arrest of vascularization in zone I is therefore more likely [217]. Prethreshold disease was also more common in the ETROP study, with the latter developing in 36.9 % of infants with ROP, compared with 27.1 % in the CRO-ROP trial [217].

Multiple logistic regression analysis of data from the natural history cohort of the CRYO-ROP study has identified the contribution made by individual prognostic factors to the risk of progression to threshold disease [208]. Numerous demographic and ocular risk factors were identified to be of prognostic value. Birth weight was important, with a 27% reduction in the odds of progression for each additional 100 g of weight.

---

[1] Post-menstrual age – gestational age (the time elapsed between the first day of the last normal menstrual period and the day of delivery) plus chronological age – is currently preferred to describe the age of a preterm infant [215]. Conventionally, post-conceptual age is equivalent to post-menstrual age less two weeks. However the CRYO-ROP and ETROP studies defined post-conceptual age as "gestational age at birth plus chronological age" (i.e. post-menstrual age) [214, 216].

Gestational age was also important, with every extra week of age associated with a 19% lowering in the odds of reaching threshold. Furthermore, race was highly prognostic – in the entire cohort, black infants had 65% lower odds of developing threshold ROP than infants of other races. Black infants were also found to be at lesser risk of prethreshold disease than white infants in the ETROP study [217]. While the protective effects of additional birth weight and gestational age on progression to threshold disease diminished significantly once an infant reached prethreshold ROP, the risk reduction remained substantial for black infants in the CRYO-ROP trial. The rate of disease progression was also found to be predictive of the risk of threshold ROP – each additional week from the onset of ROP to the development of prethreshold disease was associated with a 23% odds reduction. Once threshold disease was reached, demographic factors were not prognostic of the risk of an unfavourable structural outcome, with the notable exception of birth weight. Ocular factors were however of predictive value. The location of disease was most predictive – the odds ratio (OR) of an unfavourable outcome for zone I ROP, as opposed to zone II ROP, was 8.24. Higher disease stage was associated with greater risk of an unfavourable outcome, especially in the presence of plus disease. Extent was also important, with a 26% odds increase for each additional clock hour beyond five clock hours. The rate of disease progression was significant, with a 35% lowering in odds for each additional week from onset to the development of threshold ROP [208]. ROP is often associated with other illnesses; however the contribution of these comorbidities to the overall risk of severe ROP cannot be ascertained from the CRYO-ROP study, as the relevant data were not collected.

Natural history cohort
4099 infants; birth weight
<1251 g

No ROP
1400 infants
* 34.2 % of cohort

Any ROP
2699 infants
* 65.8 % of cohort

Prethreshold ROP
731 infants
* 17.8 % of cohort
* 27.1 % of infants with ROP

Threshold ROP
245 infants
* 6 % of cohort
* 9.1 % of infants with ROP
* 33.5 % of infants with
  prethreshold ROP

**Untreated threshold ROP:
unfavourable outcomes at
15 yrs**
* Structural: 51.9 %
* Functional: 64.3 %

Figure 1.10 The natural history cohort of the CRYO-ROP: a simplification of the clinical course of infants enrolled in the study [214, 218].

1.5.c. Treatment of ROP

In the majority of cases ROP regresses spontaneously without significant visual loss [214]. Unfortunately, this is not the case for severe disease. The CRYO-ROP study has demonstrated a clear benefit of peripheral retinal ablation for eyes with threshold ROP – treatment was associated with a reduction in poor structural outcomes at three months from 51.4% to 31.1% (p<0.00001) [216]. At 15 year follow up of children with

threshold disease, 51.9% of control eyes and 30% of treated eyes had unfavourable structural outcomes (p<0.001) [218]. Unfavourable visual acuity outcomes (visual acuity [VA] of <20/200 by the Early Treatment of Diabetic Retinopathy Study charts [ETDRS]) were found in 64.3% and 44.7% of control and treated eyes, respectively (p<0.001) [218]. The study also provided evidence to support close clinical surveillance of infants with pre-threshold ROP until such time as their disease regresses, or progresses to threshold and treatment is initiated [214]. Additional evidence was provided to substantiate early intervention in the case of neonates with rapidly progressive prethreshold disease, in whom the prognosis of delayed treatment was generally poor [208].

While the CRYO-ROP study has provided a sound evidence-base to inform management decisions, many clinicians have advocated earlier treatment, suggesting that a subset of infants with prethreshold ROP at high risk of progression to threshold disease may benefit from early intervention [219]. This question was explored in the multicentre ETROP study [209]. Infants with birth weights of less than 1251 g and prethreshold ROP were stratified into *high-* and *low-risk* groups using a risk-factor analysis program based on the findings of the natural history data of the CRYO-ROP study. Those with high-risk prethreshold disease, estimated to have a greater than 15% risk of progression to an unfavourable outcome, were randomised to receive either conventional management, or early peripheral retinal ablation (generally laser photocoagulation). Early treatment of high-risk prethreshold ROP was associated with an overall reduction in unfavourable visual acuity outcomes (blind; light perception only; pattern vision only; or visual acuity <1.85 cycles per degree) from 19.5% to 14.5% (p=0.01). The incidence of unfavourable structural outcomes (identical to those of the CRYO-ROP study) reduced from 15.6% for eyes managed conventionally, to 9.1% for eyes treated early (p<0.001) [209].

For infants with high-risk prethreshold disease randomised to conventional therapy, the rate of progression to threshold was 66.4%, compared with 15.5% for those with low-risk prethreshold disease [209]. This finding is consistent with the notion that the two groups have different risks of severe disease. A corollary of this is that 33.6% of the infants randomised to conventional therapy never went on to develop threshold disease,

despite meeting the criteria for early peripheral retinal ablation. The implications of this finding are considerable – more than one third of those in the early treatment group would not have required treatment under the conventional management protocol. Aside from the ophthalmic morbidity attendant upon therapy, these infants were exposed to systemic adverse events associated with treatment. Importantly, adverse events – including apnoea, bradycardia and reintubation – occurred more than twice as often in the early treatment group than in the conventional management group (all adverse systemic events 23.6% versus 11.4%), presumably because treatment at a younger age is less well tolerated [209]. Analysis of the outcome data of infants with high-risk prethreshold ROP managed conventionally has identified subgroups at high and low risk of progression to threshold; so called *type 1* and *type 2* prethreshold ROP (Table 1.6). It is estimated that conventional management of infants with type 2 disease would reduce the number of unnecessary treatments by one third [209]. The study coordinators suggest that stratification on the basis of ICROP staging has the additional advantage of doing away with the need for complex risk factor analysis. They do however encourage consideration of individual demographic risk factors in the clinical decision-making process.

While the findings of the ETROP study have refined the guidelines for management of prethreshold ROP, difficulty remains in distinguishing those infants in whom disease will spontaneously regress from those who are likely to progress [220-222]. Insights into the molecular and genetic bases of disease susceptibility and severity may be of value in refining this stratification process.

Despite advances in treatment, ROP remains a major cause of disability associated with premature birth [223]. An assessment of health-related quality of life of 346 CRYO-ROP subjects at 10 year follow-up provides some insight into the long term morbidity of ROP [224]. Parental perceptions of poor health-related quality of life were associated with ROP severity and with the visual outcome following ROP. In fact, scores indicating a perceived health-status "worse than dead" were recorded for almost one third of those children who were blind or had low vision in the better eye (VA ≤20/200 by ETDRS), compared with less than 1.5% of those children with visual acuity greater than 20/200 (ETDRS) in the better eye. ROP is often associated with other major causes of perinatal

morbidity such as periventricular leukomalacia and intraventricular haemorrhage, necrotising enterocolitis and bronchopulmonary dysplasia [224]. Thus poor perceived quality of life may be related, in part, to comorbidities, of which ROP is a marker. Nonetheless, it is clear that ROP can have significant long term adverse effects.

Type 1	Zone I, any stage of ROP with plus disease
	Zone I, stage 3 ROP
	Zone II, stage 2 or 3 ROP with plus disease
Type 2	Zone I, stage 1 or 2 ROP without plus disease
	Zone II, stage 3 ROP without plus disease

Table 1.6 ETROP classification of prethreshold ROP [209]**:** early peripheral retinal ablation is recommended for type 1 disease.

1.5.d.   The role of oxygen in the pathogenesis of ROP

1.5.d.1   Oxygen – cause or cure?

The emergence of ROP in the 1940's and its inexorable rise in the ensuing decade triggered a multitude of studies aimed at identifying its cause. While many investigations focussed on environmental factors in neonatal nurseries, Dr Kate Campbell, an Australian paediatrician, was the first to present evidence implicating oxygen therapy as a major aetiological factor [225]. In her observational study of premature infants from three neonatal units with different protocols for oxygen therapy, Campbell noted that high-oxygen therapy was associated with an increased incidence of disease. On the basis of this observation, oxygen therapy was reduced and ROP incidence decreased accordingly [225]. Prophylactic oxygen therapy was routine practice in neonatal nurseries at the time, but its contribution to ROP remained a subject of contention for many years [226-228]. Some investigators identified hypoxia as a likely cause of ROP [229, 230], citing cases of the disease in cyanosed babies and in premature neonates not receiving oxygen therapy, as evidence [231]. This stance was further supported by the frequent onset of the proliferative phase of the disease on withdrawal of oxygen therapy and the regression of disease on oxygen re-exposure [230, 232]. Proponents of the counter-stance attributed increases in the incidence of ROP to

the introduction of routine high-oxygen therapy for premature infants [204, 225, 233]. Retinal vascularization ordinarily occurs during the third trimester in the 'hypoxic' intrauterine environment – foetal arterial oxygen tension is typically below 30 mmHg, less than one third that of a healthy neonate breathing room air [128, 204, 234]. It follows then that premature babies without significant pulmonary dysfunction are necessarily exposed to relative hyperoxia during the period of retinal vessel development. It was argued that the associated risk of ROP is further compounded by oxygen supplementation. However in her comprehensive review of the topic in 1952, Zaccharias concluded that "no strict correlation appears to exist between the use of oxygen and either the presence or absence of retrolental fibroplasia" [228].

1.5.d.2   *Oxygen induces retinopathy in animal models of ROP*

Investigators developed animal models of the disease, in an attempt to inform the debate [168, 235, 236]. The under-vascularized state of the premature human retina closely resembles that of various newborn animals, for which retinal vascularization ordinarily occurs *ex-utero*. Accordingly, Ashton, Ward and Serpell performed a series of experiments in which newborn kittens were exposed to high ambient oxygen tension, simulating the oxygen therapy of premature humans [168]. They described a biphasic process that bore close resemblance to the pathological features of ROP [237]. Retinal avascularity, following sustained hyperoxic exposure, was attributed to the obliteration of existing vessels and to the cessation of normal angiogenesis. Consequent room-air exposure was associated with strikingly abnormal retinal vascularization, with the proliferation of disorganised capillary networks. At the interface of vascular and avascular territories, new vessels ruptured through the inner limiting membrane, into the vitreous.

In further work on the *oxygen-induced retinopathy* (OIR) model it was found that retinal vasoobliteration is directly related to oxygen tension, as well as to the duration of oxygen exposure; and inversely to vascular maturity [226, 238]. With occasional exception [168, 236], vasoproliferation does not occur during continuous hyperoxia, only on subsequent exposure to normoxia or hypoxia [226]. Ashton, Ward and Serpell hypothesised that exposure of the developing circulation to hyperoxia would increase the

diffusion of oxygen from the choroidal circulation, attenuating the hypoxic drive for normal retinal vascularization [226]. Accordingly, retinal maturation could proceed in the absence of vascularization. Subsequent exposure of the mature, metabolically active, but avascular, neural retina to normoxia would result in retinal hypoxia, as the choroidal circulation would no longer meet retinal oxygen demands. Consequently an acute, profound accumulation of the "vasoformative factor" – now know to be VEGF – would induce retinal vasoproliferation. The choroidal circulation is much less prone to aberrant vascularization in the context of premature birth, owing to its development early in gestation. The investigators considered OIR as "a violent activation of the normal processes of retinal vascularization" [226] and postulated that the same factors were operational in ROP, as in OIR.

1.5.d.3   *Human clinical trials identify oxygen as a key risk factor for ROP*

A subsequent well-controlled multicentre clinical trial of "routine" high-oxygen therapy of premature babies versus "curtailed therapy" (fraction of inspired oxygen maintained below 40%), The Cooperative Study of Retrolental Fibroplasia, provided strong evidence of a causal association between early oxygen treatment and ROP [227]. The trial results were hailed as a major advance, and a dramatic decline in ROP accompanied the reduction in oxygen therapy [239]. In retrospect, the emergence of ROP had closely paralleled the introduction of routine oxygen therapy in the 1940's [239]. Fluctuations in blood oxygen saturation were associated with the risk of ROP and neonatologists have sought to titrate oxygen therapy to avoid large swings in oxygen saturation [240]. While ROP incidence declined with oxygen restriction, many investigators reported increases in mortality rates from lung disease and in the incidence of cerebral palsy [241-243]. A recent meta-analysis of five early trials of restricted versus liberal oxygen therapy found that oxygen restriction significantly reduced the incidence and severity of ROP without significantly increasing mortality [244]. Nonetheless, balancing the risks and benefits of oxygen therapy has become a key focus of neonatal intensive care. ROP remained uncommon until the late 1970's and early 1980's, when improvements in medical care led to the survival of younger, sicker infants who were at greater intrinsic risk of the disease [245, 246]. ROP remains a significant challenge for neonatologists and paediatric ophthalmologists alike. While oxygen does not account for all instances of

this multifactorial disease [247-249], it widely accepted as a key aetiological factor in ROP.

VEGF has provided a molecular explanation for the pathophysiology of OIR. It is a central mediator of angiogenesis in OIR in mice [53, 250], rats [51, 52, 251, 252], and cats [51, 253]. Hyperoxia-induced vasoobliteration is associated with profound down-regulation of VEGF messenger RNA (mRNA) and protein, as well as with apoptosis of immature vascular endothelial cells [52]. Intraocular administration of exogenous VEGF, prior to hyperoxic exposure, has a protective effect, minimising vasoobliteration [250] and endothelial cell apoptosis [52]. It is therefore thought that VEGF acts as a critical survival factor for the developing circulation [52, 250, 251]. In the OIR models, retinal hypoxia, consequent upon termination of sustained hyperoxic exposure, is associated with marked up-regulation of VEGF expression, leading to vasoproliferation. This vasoproliferation has been inhibited by the intraocular administration of a host of selective inhibitors of VEGF, substantiating VEGF as a key factor in OIR [254-260].

VEGF is thought to play a similar role in ROP. Increased expression of VEGF mRNA has been found in the avascular retina just anterior to the ridge in the eye of a premature neonate with stage 3 ROP [261]. Levels of the factor in the fellow eye, which had undergone laser peripheral retinal ablation, were reduced: ablation of the avascular, but metabolically active peripheral retina is thought to reduce the hypoxic stimulus for angiogenic factor expression [261-264]. Furthermore, VEGF was detected in 23 of 38 (65%) fibrovascular membranes removed from the eyes of infants with stage 5 ROP at vitrectomy [265]. The evidence linking VEGF to the obliterative and proliferative phases of OIR, coupled with the strength of the model in simulating human ROP, have led to broad acceptance of the importance of VEGF in the pathogenesis of ROP. However, as is the case for retinal vascularization in normal development, angiogenesis in the OIR model and in ROP is dependent on interactions between multiple angiogenic factors of which VEGF is just one – albeit of central importance. IGF-1 is one of the many factors presently implicated in ROP – low serum levels of the factor have been associated with risk of the disease [59]. Thus ROP is likely the consequence of disturbance in the precise temporal, spatial and quantitative expression of angiogenic factors required for normal retinal vascularization.

Given that retinal hypoxia is an important determinant of the proliferative phase of ROP, several investigators have experimented with supplemental oxygen therapy as a means of reducing neovascularization. Szewczyk [230, 232] and Bedrossain *et al.* [266] noted that rapid withdrawal of oxygen therapy often precipitated ROP, and that gradual oxygen-weaning was associated with a reduction in disease severity. These findings contrasted with those of animal experiments which demonstrated that oxygen weaning was associated with harm in the feline [267] and murine [268] OIR models. Furthermore, the Cooperative Study of Retrolental Fibroplasia identified an association between prolonged oxygen therapy and increased risk of ROP [227] and thus supplemental oxygen therapy was not accepted as routine practice. In subsequent experiments with the feline OIR model, Phelps and Rosenbaum demonstrated that following an initial hyperoxic exposure, kittens recovering in hypoxia develop more severe retinopathy than those exposed to normoxia [269]. Other investigations in the cat by Chan-Ling, Gock and Stone demonstrated significant reductions in the severity of retinopathy with carefully titrated supplemental oxygen therapy during the recovery phase of the model [270]. The investigators postulated that following a hyperoxic insult, the under-vascularized, but metabolically active retina, is rendered acutely hypoxic on exposure to room air. They suggested that mild hyperoxia during the recovery phase might recapitulate the more modest, *physiological* hypoxia that drives normal retinal vascularization.

The Supplemental Therapeutic Oxygen for Prethreshold ROP (STOP-ROP) study was undertaken to clarify the role of oxygen supplementation in ROP treatment [234]. Infants with prethreshold ROP and median blood oxygen saturation below 94% during a four hour period of pulse oximetry were randomised to receive either conventional oxygen therapy, or supplemental therapy. During conventional treatment, oxygen was titrated to maintain pulse oximetry readings between 89% and 94%; in the supplemental therapy group the target range was between 96% and 99%. Treatment was continued for at least two weeks and until one of the study endpoints was reached: either progression to threshold disease; or regression of retinopathy. The study had an asymmetric design: a higher standard for significance was applied to assessment of the treatment effect ($\alpha=0.025$), than to the analysis of adverse outcomes ($\alpha=0.01$).

When adjustments were made for baseline ROP severity, the trial demonstrated a trend toward a lower rate of progression to threshold disease in the supplemental oxygen group versus the conventional group (41% versus 48%) which failed to reach statistical significance (p=0.032, one-tailed test; α=0.025). Furthermore, there was no significant difference in the incidence of unfavourable structural outcomes at three months. Retrospective subgroup analysis suggested a benefit of oxygen supplementation for infants without plus disease – the risk of progression to threshold ROP was 32% versus 46% for the conventional treatment group (p=0.004) – however these *post hoc* findings must be interpreted with caution. Of note was the statistically significant increase in adverse systemic sequelae: infants in the supplementation group were more likely to suffer pneumonia and exacerbations of lung disease (13.2% versus 8.5%; p=0.066 [α=0.1]); and to require hospitalisation, oxygen therapy and diuretics at three months of corrected age (risk of any adverse event at three months: 56% versus 45%; p=0.04 [α=0.1]). Thus, while supplemental oxygen therapy does not appear to have a deleterious effect on established prethreshold ROP, it does not offer a statistically significant benefit and may increase the risk of systemic adverse effects.

It is important to recognise that the STOP-ROP trial was terminated prematurely due to slow recruitment. Consequently the sample size failed to reach the targets on which the significance criteria had been based. In their detailed statistical appraisal of the trial, Oden and Phelps take these considerations into account and conclude that the final treatment effect of oxygen supplementation on progression to threshold disease is small [234]. A similar conclusion was reached by the Cochrane Collaboration in their systematic review of supplemental oxygen therapy for prethreshold ROP [271]. Further trials are required to ascertain the role of supplemental oxygen therapy for infants with prethreshold ROP without plus disease. In addition, there is a pressing need for clinical trials examining the effect of restricted versus conventional oxygen therapy in the early postnatal period on ROP.

In a recent survey of oxygen therapy practices in neonatal intensive care facilities in the United States, considerable variation was found in pulse oximetry targets for premature infants treated with oxygen during the first two weeks of life [272]. Oxygen therapy guidelines for the early neonatal period are largely empirical due to a lack of clinical

trial evidence. In their review of the subject, Cole and colleagues lament that evidenced-based guidelines for safe oxygen therapy are lacking despite the fact that the association between oxygen and ROP was identified more than 50 years ago [273]. Silverman puts it more bluntly, "there has never been a shred of convincing evidence to guide limits for the rational use of supplemental oxygen in the care of extremely premature infants" [239]. Several recent observational studies suggest that oxygen restriction in the early postnatal period may reduce the incidence and severity of ROP, however definitive data are lacking [272, 274, 275].

An Australian multicentre double-masked randomised controlled trial – the Benefits of Oxygen Saturation Targeting (BOOST) trial – examined the effects of high (95-98%) versus standard (91-94%) pulse oximetry targets for extremely premature infants (gestational age <30 weeks) remaining on supplementary oxygen at 32 weeks of post-menstrual age [276]. No significant differences were found between the groups for the primary outcome measures of growth and major developmental abnormalities, including blindness (VA <6/60). With respect to the secondary outcome measures, significantly more infants in the high-saturation group had chronic lung disease and a longer mean duration of oxygen therapy. While the study lacked the statistical power to detect differences in secondary eye-related outcomes, there was a trend towards a reduction in the requirement for retinal ablation for the infants at highest risk of threshold ROP (gestational age <28 weeks) in the high-saturation group [276]. A second, larger trial – BOOST II – is currently underway. The trial will examine the effects of two different arterial oxygen saturation targets – 85-90% versus 91-95% – on oxygen-related health outcomes including ROP, bronchopulmonary dysplasia, neurological impairment and death, in infants born before 28 weeks gestation [277]. The trial will be performed in collaboration with another multicentre randomised controlled trial, the Pulse Oximetry Saturation Trial for Prevention of ROP (POST-ROP), with similar pulse oximetry targets [273]. These studies promise to clarify the role that early hyperoxic exposure has on the risk of ROP.

1.5.e.   Genetic risk factors for neovascularization and ROP

Several lines of evidence support a contribution of genetic factors to the occurrence of ROP and to its severity. Genetic factors may account for the significant effect of race on ROP, and for the heterogeneity in the risk of disease that remains once known demographic risk factors are taken into account. Moreover, the disease shares clinical features in common with several hereditary disorders of retinal vascularization, the causes of which may provide clues to the genetic basis of ROP. Numerous genetic polymorphisms of angiogenic factors have been identified, and it is possible that some of these genetic changes may contribute to the risk of disease. Given the complexity of the angiogenic process, abnormalities in the regulation of any one of a large number of factors could contribute to ROP risk.

Race was first identified as a significant factor in ROP in 1952, when Zacharias published her observation that of several cohorts of premature infants in the United States, black infants seemed less likely to develop retinopathy than white infants [228]. A more recent prospective study of ROP in the United Kingdom, confirmed the observation that black infants were at lower risk of ROP than white infants, despite lower mean gestational ages [278]. The CRYO-ROP study found the while the overall incidence of ROP was the same for all racial subgroups, black infants were at substantially lower risk of severe disease (refer to 1.5.b) [208]. In their review of the racial data of the natural history cohort of the CRYO-ROP study, Saunders *et al.* tested several hypotheses for the observed racial differences [279]. Of those infants in the study that never developed ROP, the rate of retinal vascularization was similar for all racial groups (p=0.19), excluding race-related differences in retinal vascular maturation as a cause of the observed effect. Furthermore, the effect of race was independent of gestational age and birth weight. The study survival data did not support the hypothesis of a selection bias in favour of healthier black infants, in whom severe retinopathy was less likely to develop. The investigators suggest that differences in ocular pigmentation may provide a plausible basis for a difference between the racial groups, but note that no assessment was made of the amount of ocular pigmentation of infants in the study [279]. One hypothesis, grounded in animal research [280], is that the more heavily pigmented eyes of black infants may be less susceptible to phototoxic injury than those of white

infants, and that this effect may account for the observed difference in ROP severity. However numerous animal experiments have failed to demonstrate an inhibitory effect of intense light exposure on retinal vascularization, even in the presence of hyperoxia [281, 282]. The recent multicentre randomised clinical trial, the Light Reduction in Retinopathy of Prematurity (LIGHT-ROP) study, found no significant difference in the incidence or severity of ROP in infants exposed to either reduced light or standard lighting [283]. Saunders *et al.* conclude that, "socioeconomic factors and other genetic differences beyond pigmentation could have an important effect in determining susceptibility to ROP" [279]. However socioeconomic factors might be expected to disadvantage, rather than benefit, black infants, and there is no compelling evidence of an effect of socioeconomic status within racial groups.

Other studies have identified an effect of race on retinopathy risk [284] [217]. A prospective study of all infants weighing less than 1500 g at birth, admitted to Alaskan neonatal intensive care units between 1989 and 2003, is of interest [285]. Threshold ROP was significantly (p<0.001) more common in Alaskan native (24.9%) and Asian Pacific (15.9%) races than white (6.3%) and black (4.6%) races. While the study was limited by small numbers in several racial groups, including the Asian Pacific group, the influence of race on the risk of severe disease was considerable. The authors state that the observed effect could not be attributed to dietary factors; however additional details are lacking [285]. The study does not support the hypothesis that ocular pigmentation has a protective effect on the risk of advanced ROP. A study of ROP in Australia and New Zealand found that infants born to Asian mothers were at increased risk of severe ROP (OR 1.83; 95% confidence interval [95% CI] 1.06-3.16), however the risk was not significant in multivariate analyses [213]. No significant differences in risk were found for infants of white, Indigenous Australian, Maori or Pacific Islander mothers. On balance, it seems likely that there is an effect of race on retinopathy risk, but it remains to be seen what, if any, genetic factors are responsible.

Several genetic disorders of the Wnt-β-catenin pathway – a signalling cascade thought to be important in angiogenesis [286]— have retinal phenotypes similar to the advanced stages of ROP [197]. Examples include Norrie disease and familial exudative vitreoretinopathy (FEVR). Norrie disease is a rare X-linked hereditary disorder, caused

by mutation of the Norrie disease pseudoglioma gene, that results in deficiency of functional Norrin protein, a ligand for the Wnt-receptor Frizzled-4 [286]. The disease is characterised by bilateral blinding retinopathy, deafness and mental retardation. In a knockout mouse model Norrin has been shown to be essential for endothelial sprouting in the process of retinal vascularization [197]. Deficiency of the protein causes retarded retinal vascularization, leading to retinal ischaemia and the accumulation of hypoxia-induced angiogenic factors. FEVR is a related disorder, characterised by deficient retinal vascularization often associated with exudation, retinal traction and ultimately, retinal detachment. Mutations of the Norrie disease gene are known to cause the X-linked form of FEVR, while other forms of the disease are associated with mutations of the genes for Frizzled-4 receptor and its coreceptor LRP5 [287, 288]. Thus FEVR and Norrie disease, disorders phenotypically similar to ROP, appear to be due to dysfunction of the same signalling axis [197].

Some investigators suggest that mutations of the Norrie disease gene may account for a proportion of advanced cases of ROP (reviewed in Wheatley *et al.* [212]) – Hiraoka *et al.* put the figure at 3% [289]. Evidence is emerging of significant genetic heterogeneity of FEVR and Norrie disease [290] and it is possible that mutations in these genes that would otherwise be phenotypically silent, become manifest under the circumstance of premature birth [291]. However a recent study has found no statistically significant increase in the prevalence of Norrie disease gene polymorphisms in infants with severe ROP (stage 3 or worse): sequence changes were identified in 6 of 54 (11%) affected individuals and in three of 89 unaffected individuals (3.4%) (p=0.063) [292]. The authors conclude that Norrie disease gene polymorphisms do not appear to play a major pathogenic role in severe ROP. A study of Kuwaiti premature infants identified a polymorphism in an untranslated region of the Norrie disease gene (C597A) that was associated with severe ROP [293]. The polymorphism was found in 20 of 24 (83.3%) infants with stage 4 or 5 ROP compared with none of 71 infants with regressing ROP, and 12 of 115 (10.4%) infants without ROP (p<0.0001). The functional significance of this polymorphism and its prevalence in other populations remains to be determined.

Polymorphisms of genes involved in retinal angiogenesis may be important in determining susceptibility to ROP. Several studies have identified polymorphisms in the VEGF gene that appear to segregate with the risk of progression to threshold disease. The VEGF gene is highly polymorphic, with more than 70 known polymorphic loci [294]. Of the known single nucleotide polymorphisms (SNPs), at least three have been associated with alterations in VEGF expression [294-297]. One of these polymorphisms, at position -634 (- 634 G→C, otherwise known as + 405 G→C [2]) in the 5'-untranslated region of VEGF gene, has been associated with the risk of progression to threshold ROP in two studies (Table 1.7). In their study of 91 infants with threshold ROP and 97 comparison infants without threshold disease, Cooke *et al.* demonstrated that carriage of the VEGF -634 G allele was an independent risk factor for threshold ROP (p=0.0008) [296]. Homozygotes for the G allele were twice as likely to progress to threshold ROP as other genotypes (OR 2.0, 95% CI 1.11-3.69). The opposite association was found by Vannay *et al.* [294]. The VEGF -634 C allele was significantly more common in the group of infants with threshold disease than in those without threshold ROP (p<0.05). The C allele was identified as an independent risk factor for severe disease, with doubling (OR 2.0; 95% CI 1.02-3.92) and greater than trebling (OR 3.37; 95% CI 1.17-9.65) of the risk for heterozygotes and homozygotes, respectively. These findings were consistent with those of Awata *et al.*, who identified an increased risk of retinopathy associated with the VEGF -634 CC genotype, in a cohort of Japanese patients with diabetes [297, 298]. Serum VEGF levels were higher in healthy individuals with the VEGF -634 CC genotype. Basal transcriptional activity of the VEGF -634 C allele was higher than the G allele in two different cell lines, as was translation of VEGF mRNA [297]. In contrast Watson *et al.* provided *in vitro* evidence for increased transcriptional activity of the -634 G allele in peripheral blood mononuclear cells [295].

It is likely that the effects of these polymorphisms on VEGF expression are highly context dependent. Investigators speculate that the VEGF -634 G→C polymorphism

---

[2] The +405 G→C nomenclature, used by *Vannay et al.* [294] describes the SNP position relative to the transcription start site, while the -634 G→C nomenclature, used by *Cooke et al.* describes the position of the same SNP relative to the first nucleotide of the start codon (ATG) – both terms describe the same SNP. For ease of understanding, the SNP position will be exclusively designated as -634 in this work.

may be differentially linked to other polymorphisms in the 5' flanking sequence and that the balance of polymorphisms may vary between ethnic groups and cell types [296, 297]. The work of Vannay *et al.* provides a case in point. The risk of threshold ROP for infants homozygous for the VEGF -634 C allele was increased dramatically in association with another polymorphism, VEGF -1498 T→C (otherwise known as -460 T→C: position relative to the transcription start site) – the odds ratio for infants with the VEGF -1498 TT/VEGF -634 CC haplotype was 16.2 (95% CI 1.96-134) [294]. At present our understanding of the contributions made by polymorphisms in the VEGF gene to the risk of ROP is incomplete. It is possible that the combined effects of these polymorphisms may differ in different racial groups, accounting for some of the observed differences in susceptibility. The situation may well be more complex – polymorphisms in a host of other angiogenic genes may also contribute to the overall risk of disease.

Table 1.7 Polymorphisms in the VEGF gene at position -634 may be of pathogenic significance for ROP.

VEGF SNP	Associations	Study
-634 G	Risk factor for threshold ROP: odds ratio=2.0 (-634GG).	[296]
	Increased transcriptional activity *in vitro* (mononuclear cells).	[295]
-634 C	Risk factor for severe ROP: -634 CG, odds ratio=2.0; -634 CC, odds ratio=3.4.	[294]
	Risk factor for diabetic retinopathy (-634 CC)	[298]
	Increased serum VEGF (-634 CC)	[298]
	Increased *in vitro* transcriptional activity compared with G allele (human glioma cells; lymphoblastic T-lymphocytes)	[297]

In summary, there is substantial evidence that genetic factors play a role in the pathogenesis of ROP. The identification of key genetic risk factors may inform clinical stratification of retinopathy risk, as well as the design of targeted therapeutic interventions.

1.5.f.   ROP: lessons learnt and scope for progress

The past five decades have taught us a tremendous amount about ROP. While oxygen is central to the pathogenesis of the disease, it does not appear to be a "sufficient, single cause" [273]. Demographic factors such as gestational age and birth weight contribute to the likelihood of progression to severe disease, and an effect of race on ROP severity points to the importance of genetic risk factors. Genetic factors are also likely to account for much of the heterogeneity in risk that remains once demographic factors have been taken into account. While several land-mark clinical trials have improved the management of ROP, progress is much needed on two fronts. Evidence-based guidelines for optimal oxygen therapy have been long awaited and are likely to revolutionise the delivery of neonatal intensive care. Similarly, improvements in the ability to identify the subset of infants at risk of progressive disease will facilitate timely intervention and the institution of prophylactic therapies. This development will reduce the need for intensive ophthalmic surveillance, as well as the morbidity associated with unnecessary peripheral retinal ablation. Ultimately, an understanding of the molecular basis of ROP may prove invaluable for risk stratification and for the design of rational therapeutics, further reducing the need for surgical intervention and improving ophthalmic outcomes.

1.6.   HYPOTHESIS AND AIMS

The hypothesis of this work is that heritable factors make important contributions to the risk of retinopathy in premature human infants. Rat oxygen-induced retinopathy (OIR), a surrogate model of human ROP, will be used to test this hypothesis. The overarching aims of this work are to identify genetic risk factors for OIR in the rat and to determine their effects on the retinal phenotype. Specifically, the susceptibilities of different inbred rat strains to OIR will be compared and the heritability of the identified susceptibility traits will be examined in cross-breeding experiments. Furthermore, the retinal expression of several candidate angiogenic factor genes, known to be important in retinal vascularization, will be compared amongst rat strains and correlated with differences in the susceptibility to OIR.

CHAPTER 2
MATERIALS & METHODS

2. CHAPTER 2: MATERIALS & METHODS

2.1.   MATERIALS

2.1.a.   Water

Double glass-distilled water (ddH$_2$O) was used for the preparation of buffers and solutions unless otherwise stated. Diethylpyrocarbonate (DEPC)-treated water was used for RNA extraction and cDNA synthesis (section 2.2.c). RNase-free water (autoclaved Milli-Q® water, Millipore, Billerica, MA) was used for RNA electrophoresis, while water free of nucleic acids and nucleases (Ultra Pure water, Fisher Biotech, West Perth, WA, Australia) was used for reverse transcription-polymerase chain reaction (RT-PCR).

2.1.b.   General chemicals

General chemicals were obtained from Sigma Chemical Company (St Louis, MO, USA), AJAX chemicals (Auburn, NSW, Australia) or BDH Chemicals (Kilsyth, VIC, Australia) and were of analytical reagent grade unless otherwise specified. Recipes for buffers and solutions are detailed in section 2.2.

2.1.c.   Enzymes

DNase treatment of RNA extracts was performed prior to cDNA synthesis using recombinant DNaseI (DNA-free®, Ambion, Austin, TX, USA). RNA reverse transcription was performed using Superscript III® Reverse Transcriptase (SuperScript III® First-Strand Synthesis System, Invitrogen, Carlsbad, CA, USA). Endpoint reverse transcription-polymerase chain reaction (RT-PCR) was performed using Platinum® Taq DNA polymerase (Invitrogen, Carlsbad, CA, USA). QuantiTect™ SYBR® Green PCR Master Mix was used for quantitative real-time reverse transcription-PCR (real-time RT-PCR) (Qiagen, Valencia, CA, USA). All enzymes were stored at -20°C.

2.1.d.   PCR primers

Primers used in real-time and endpoint RT-PCR experiments were synthesised by GeneWorks Pty Ltd (Thebarton, SA, Australia) at sequencing-grade purity. Primer design is described in section 2.3.i; primer sequences are listed in Table 2.1.

Table 2.1 Quantitative real-time RT-PCR primer sequences. Primers were designed for compatibility with SYBR Green and TaqMan chemistries. Accordingly, the sequences of putative TaqMan probes are included for each primer pair. Nucleotide position refers to the region of the mRNA sequence flanked by the primers. Reference is also made to the exons to which the primers hybridise. With the exception of IGF-1 and cyclophilin A, all primers amplify a single transcript, the identity of which has been confirmed by the sequencing of PCR products.

Gene (Accession No.)	Primer/Probe	Sequence (5' → 3')	Nucleotide position	T_m (^{o}C)	Amplicon size (bp)
Acidic Ribosomal Phosphoprotein (NM_022402.1)	ARBP(for)	AAAGGGTCCTGGCTTTGTCT		60	
	ARBP(rev)	GCAAATGCAGATGGATCG	766-856	59	91
	ARBP(probe)	ACTGACTACACCTTCCCACTGGCTGAAAAG	exons 5/6	71	
Actin, gamma 2 (NM_012893.1)	ACTG2(for)	GGAGAAGATCTGGCACCACT		59	
	ACTG2(rev)	CCCTGTTGGCTTTAGGGTTT	264-369	60	104
	ACTG2(probe)	CTTCTACAACGAGCTGCGAGTAGCACCAG	exons 2/3	71	
Angiopoietin 2 (XM_344544.1)	ANG2(for)	CAGCTTGCTGACCATGATGT		60	
	ANG2(rev)	GCACAGTCTCTGAAGGTGGTT	2244-2330	59	87
	ANG2(probe)	ATCGCCCGACTATAAGAGCTCTGTTGCTGT	exons 4/5	72	
Cyclooxygenase 2 (AF_233596)	COX2(for)	TCCTCCTTGAACACGGACTT		60	
	COX2(rev)	CTGCTTGTACAGCGATTGGA	1320-1421	60	102
	COX2(probe)	GCTCACTTTGTTGAGTCATTCACCAGACAG	exons 8/9	70	
Cyclophilin A (NM_017101.1)	CYCA(for)	GTCTGCTTCGAGCTGTTTGC		61	80
	CYCA(rev)	AATCCTTTCTCCCCAGTGCT	100-179	60	
	CYCA(probe)	CCAAAGACAGCAGAAAACTTTCGTGCTCT	exons 1/2	70	
Erythropoietin (NM_017001)	EPO(for)	ACCAGAGAGTCTTCAGCTTCA		57	
	EPO(rev)	GAGGCGACATCAATTCCTTC	361-464	60	104
	EPO(probe)	ATAGACAAAGCCATCAGTGGGCTACGTAGC	exons 4/5	70	

Table 2.1 (continued) Quantitative real-time RT-PCR primer sequences

Gene (Accession No.)	Primer/Probe	Sequence (5' → 3')	Nucleotide position	T_m (°C)	Amplicon size (bp)
Hypoxanthine Guanine Phosphoribosyl-transferase (NM_012583.2)	HPRT(for)	TTGTTGGATATGCCCTTGACT		59	
	HPRT(rev)	CCGCTGTCTTTTAGGCTTTG	629-733	60	105
	HPRT(probe)	TTGAATCATGTTTGTGTCATCAGCGAAAGT	exons 9/10	70	
Insulin-like Growth Factor 1 (NM_178866.2)	IGF1(for)	CACACTGACATGCCCAAGA		59	
	IGF1(rev)	GGGAGGCTCCTCCTACATTC	1091-1189	60	IGF1$_A$: 99
	IGF1(probe)	CACAAGTAGAGGAAGTGCAGGAAACAAGAC	exons 4/6	70	IGF1$_B$:151
Pigment Epithelium-Derived Factor (NM_177927.2)	PEDF(for)	CAGCCAGAATGTCCCTGAC		59	
	PEDF(rev)	GTCATCCTCCTCCACTACGG	98-176	60	79
	PEDF(probe)	CTCTCAGGATTCCCCAGCCCCTGAC	exons 2/3	73	
RNA Polymerase 2 (XM_343922.2)	RNAP2(for)	GTCCAATGACATCGTGGAGA		59	
	RNAP2(for)	CCATCAAAGGAGATGACATGG	4011-4106	60	96
	RNAP2(probe)	CTTCACGGTACTGGGCATTGAGGCT	exons 24/25	70	
Tie2 (XM_342863.2)	TIE2(for)	TGGAGAAGGACATCCTGGAC		60	
	TIE2(rev)	GCTGTCTGGCTTTTGGGTAG	1680-1778	60	99
	TIE2(probe)	TGAGAAGATTCACAACAGCGTCTATCGGAC	exons 11/12	71	

Table 2.1 (continued) Quantitative real-time RT-PCR primer sequences

Gene (Accession No.)	Primer/Probe	Sequence (5' → 3')	Nucleotide position	T_m (°C)	Amplicon size (bp)
Vascular Endothelial Growth Factor (NM_031836.1)	VEGF(for)	AATGATGAAGCCCTGGAGTG		60	
	VEGF(rev)	TATGTGCTGGCTTTGGTGAG	259-348	60	90
	VEGF(probe)	AGAGCAACGTCACTATGCAGATCATGC	exons 2/3	69	
Vascular Endothelial Growth Factor Receptor 2 (NM_013062.1)	VEGFR2(for)	TCTCGTACGGACCGTTAAGC		60	
	VEGFR2(rev)	CTCATCCAAGGGCAGTTCAT	2588-2681	60	94
	VEGFR2 (probe)	AGACAGGCTACTTGTCCATTGTCATGGATC	exons 15/16	70	

Abbreviations: T_m= melting temperature; bp= base pairs; for= forward primer; rev= reverse primer.

2.1.e.   Experimental animals

2.1.e.1   Ethical considerations

The animal experiments described in this thesis were approved by the Animal Welfare Committee of Flinders University of South Australia. Experiments conformed to the standards set out in the ARVO Statement for the Use of Animals in Ophthalmic and Vision Research [299], as well as those stipulated by the Australian Code of Practice for the Care and Use of Animals for Scientific Purposes [300] .

2.1.e.2   Rats

Five inbred rat strains, each derived from more than 20 consecutive brother-sister matings, and one outbred strain were used (Table 2.2). Lineage records and bi-annual allozyme electrophoresis of 14 biomarkers confirmed genetic integrity of inbred strains: there was no evidence of genetic variability within strains, or of genetic contamination of any strain (Genetic Monitoring Service, Evolutionary Biology Unit, South Australian Museum). Four albino and two pigmented strains were selected to examine the effects of ocular pigmentation on oxygen-induced retinopathy. Pigmentation and eye colour are listed in Table 2.2. An account of the origins of these strains is provided in Appendix 1. Rats were allowed unlimited access to water and rat chow ("New Joint Stock" Ridley Agriproducts, Murray Bridge, SA, Australia) and were exposed to a 12 hour light-dark cycle. Room temperature was maintained at 24°C. Ambient humidity was maintained at between 40-55% for all experimental groups. Animals were killed with an inhaled overdose of halothane anaesthesia.

Table 2.2 Rat strain characteristics

Strain	Inbred	RT1 haplotype	Coat colour	Eye colour	Mean litter size*	Source
Fischer 344 (F344)	Yes	$RT1^{vl}$	Albino	Red	11	Flinders University, Adelaide, SA, Australia
Wistar-Furth (WF)	Yes	$RT1^{u}$	Albino	Red	6	Flinders University, Adelaide, SA, Australia
Lewis (LEW)	Yes	RT^{l}	Albino	Red	8	Animal Resources Centre, Perth, WA, Australia
Sprague Dawley (SPD)	Yes	Unknown[†]	Albino	Red	6	Flinders University, Adelaide, SA, Australia
Dark Agouti (DA)	Yes	$RT1^{avl}$	Pigmented (agouti)	Dark Brown	8	Institute of Medical and Veterinary Science, Adelaide, SA, Australia
Hooded Wistar (HW)	No	Unknown; several expected	Pigmented (black)	Dark Brown	8	Flinders University, Adelaide, SA, Australia

* Based on breeding records of the Animal Housing Facility of Flinders Medical Centre for the 12 months ending January 2005.
[†] Locally inbred colony, RT1 (rat MHC class I) haplotype not tested.

2.1.f. Miscellaneous materials

A list of the sources of miscellaneous materials is presented in Table 2.3.

Table 2.3 Miscellaneous materials

Item	Description	Source
Agarose	Analytical grade	Promega, WI, USA.
DNA ladder 20 bp	20 bp – 1 kb fragments in 20 bp increments	GeneWorks, Thebarton, SA, Australia. Product No. DMW-20
DNA ladder 100 bp	100 bp – 1.5 kb fragments	Promega, WI, USA.
DNA ladder 1 kb	500 bp – 12 kb fragments 100 ng/μL	Invitrogen, Melbourne, VIC, Australia. Product No. 15615-016
DNA ladder 2 log	100 bp- 10 kb fragments	New England Biolabs, Beverly, MA, USA.
Ethidium bromide	10 mg/ml	Sigma, St.Louis, MO, USA.
Heparin	porcine mucous heparin sodium 1000 IU/ml	David Bull Laboratories, Mulgrave, VIC, Australia.
Indian ink	high-grade black Indian ink	Windsor & Newton, U.K.
Isolectin GS-IB4	*Griffonia simplicifolia* type I isolectin B4-Alexa 488™ conjugate (excitation 495 nm; emission 519 nm)	Molecular Probes, Eugene, OR, USA. Product No. I21411
RNA extraction column	RNeasy® mini-kit	Qiagen, Valencia, CA, USA.
Sodium chloride for irrigation	0.9% w/v isotonic, non-pyrogenic, sterile	Baxter, Old Toongabbie, NSW, Australia.
Superscript III RT	engineered Moloney murine leukaemia virus reverse transcriptase	Invitrogen, Carlsbad, CA, USA.
SYBR Green Master Mix	QuantiTect™ SYBR Green® PCR Master Mix: HotStarTaq® DNA polymerase, SYBR Green I, dNTPs and PCR buffer (5mM MgCl$_2$, Tris-Cl, KCl, (NH$_4$)$_2$SO$_4$, pH 8.7).	Qiagen, Valencia, CA, USA.
Tissue homogeniser	Qiashredder® column	Qiagen, Valencia, CA, USA.

2.2.   BUFFERS AND SOLUTIONS

2.2.a. Buffered formalin

50 ml	formalin (40% w/v)
450 ml	ddH_2O
2 g	$NaH_2PO_4.H_2O$
3.25 g	Na_2HPO_4

2.2.b. Chrome alum-subbed microscope slides

Prepare 0.05% $Cr(SO_4)_2.12H_2O$ w/v in ddH_2O. Submerge glass microscope slides for 5 min. Air dry in slide racks. Wipe clean with cotton gauze prior to use.

2.2.c. DEPC-H_2O

1 ml	diethylpyrocarbonate (DEPC)
up to 1 l	ddH_2O

Leave solution at room temperature overnight. Autoclave to inactivate DEPC prior to use.

2.2.d. DEPC-NaCl

1 ml	DEPC
up to 1 l	0.9% NaCl

Leave solution at room temperature overnight. Autoclave to inactivate DEPC prior to use.

2.2.e. Electrophoresis gel DNA/RNA loading buffer

1 ml	glycerol
1 ml	DEPC-H_2O
3 mg	bromophenol blue
3 mg	xylene cyanol

Store at 4°C. Mix 1 μl of loading buffer with 5 μl of DNA or RNA and load into agarose gel.

2.2.f. Eosin

Stock:	1 g	eosin Y
	20 ml	ddH_2O
	80 ml	95% ethanol

Add 25 ml eosin stock to 75 ml ethanol (80%). Add 0.5 ml glacial acetic acid immediately prior to use.

2.2.g. Ethidium bromide agarose plates

1 g	agarose
100 ml	ddH_2O

Combine and melt in a microwave oven. Add 5 μl ethidium bromide (10 mg/ml) and swirl to mix. Pour into Petri dishes, allow to set. Store at 4°C. Air-dry plate prior to

spotting with DNA.

2.2.h. Haematoxylin solution

1.25 g	haematoxylin powder
75 ml	glycerol
0.25 g	sodium iodate
12.5 g	aluminium potassium sulphate (alum)
0.5 ml	glacial acetic acid
2-4 ml	absolute ethanol
175 ml	ddH_2O

Stir alum in 100 ml water over gently heat until it forms a paste. Add remaining H_2O. Dissolve in ethanol. Cool and add haematoxylin powder. In fume hood, add sodium iodate, acid and glycerol. Store at RT for at least 24 h. Filter through Whatman No.1 paper (Whatman, Maldstone, UK) prior to use.

2.2.i. Ink perfusate

10% v/v black Indian ink (Windsor & Newton, U.K.) in ddH2O, filtered through Whatman No.1 paper (Whatman, Maldstone, UK) and warmed to $37^{o}C$.

2.2.j. PBS (10X)

28.55 g	$Na_2HPO_4.2H_2O$
(or 22.85 g	Na_2HPO_4)
6.25 g	$NaH_2PO_4.2H_2O$
70 g	NaCl
up to 1 l	ddH_2O or water for irrigation

Adjust pH to 7.3 and autoclave.

2.2.k. Sodium hydroxide stock 10 M

4 g	NaOH pellets
up to 10 ml	ddH_2O

Add pellets slowly to water in fume hood (reaction is exothermic). Dilute stock in ddH_2O to achieve desired molarity.

2.2.l. TBE buffer (10x)

108 g	Tris base
55 g	Boric acid
40 ml	0.5 M EDTA pH 8

Dissolve in 1 l ddH_2O and autoclave. Dilute with ddH_2O prior to use. RNase-free water is used in place of ddH_2O for RNA electrophoresis.

2.3.   MOLECULAR TECHNIQUES

2.3.a.   DNA quantification

The concentration of DNA in purified PCR products was estimated by spotting 1 µl of serial dilutions (neat, 1:2, 1:4) of each product onto ethidium bromide agarose plates (section 2.2.g). 1 µl of each of a series of herring sperm DNA standards of known concentration (5-200 ng/ml; Sigma, St. Louis, MO, USA) were spotted alongside. The fluorescence intensities of samples and standards were compared under UV light transillumination to estimate DNA concentration.

2.3.b.   Agarose gel electrophoresis

PCR products were analysed on ethidium bromide-stained 1-2.5% agarose gels. Gels were prepared by adding 0.8-2 g of agarose (Promega, WI, USA) to 80 ml of 0.5X TBE buffer (section 2.2.l) and heating in a microwave oven until completely dissolved. Ethidium bromide (5 µl, 10 mg/ml) was added and the solution was swirled to mix, before being poured into a gel tray with a well comb *in situ*. The gel was allowed to set prior to removal of the comb. The gel was transferred to an electrophoresis tank containing 0.5X TBE. Unless otherwise stated, 5 µl of PCR product mixed with 1 µl of loading dye (6X Loading Dye, Promega, WI, USA) was added to each well. One or more of the following molecular weight markers was used for product size estimation: 20 bp DNA ladder (GeneWorks, Thebarton, SA, Australia); 100 bp DNA ladder (Promega, WI, USA); 2 log DNA ladder (New England Biolabs, Beverly, MA, USA). Nucleic acid fragments were visualised under UV light following electrophoresis at 110 V for approximately 1 hr.

2.3.c.   RNA extraction

Rat eyes were enucleated immediately post-mortem into chilled (4°C) DEPC-NaCl (section 2.2.d) and retinae were removed with instruments washed in DEPC-NaCl, according to the method described in section 2.4.c.3. Retinae were transferred to freezing vials (1.8 ml; Nunc, Roskilde, Denmark) and immediately snap frozen in liquid nitrogen and stored at −80°C until processing. Gloves were worn at all times and tissue

handling was kept at a minimum to minimise RNA degradation.

Total RNA was isolated from each retina using an RNeasy mini-kit (Qiagen, Valencia, CA, USA) in accordance with the manufacturer's protocol. RNase-free reagents, tubes and pipette tips were used at all times. Briefly, 600 μl of lysis buffer (Buffer RLT) containing 1% v/v 2-mercaptoethanol (Sigma, St. Louis, MO, USA) was added to each retina immediately following removal from storage at -80°C. Retinal tissue was disrupted with vigorous pipetting. Tubes were kept on ice. The lysate was pipetted directly onto a Qiashredder (Qiagen, Valencia, CA, USA) spin column contained within a 2ml collection tube and centrifuged for 2 min at 10,000 g. The supernatant was transferred into a clean tube and centrifuged for 3 min at 10,000 g. One volume of 70% ethanol was added to the cleared lysate in a clean tube and mixed by pipetting. The sample was added in 700 μl increments to an RNeasy mini-column placed in a 2 ml collection tube and centrifuged for 15 sec at 8000 g. The flow-through was discarded and 700 μl of wash buffer (Buffer RW1) was added to the column prior to centrifugation for 15 sec at 8000 g. The column was transferred to a clean 2 ml collection tube and 500 μl of reconstituted Buffer RPE was added, prior to centrifugation for 15 sec at 8000 g. The flow-through was discarded and a further 500 μl of Buffer RPE was added before centrifugation at 10,000 g for 2 min. The column was centrifuged for 1 min at 10,000 g in a clean tube. The column was transferred to a clean collection tube and 30 μl of RNase-free water was added. Two min were allowed for resolution of column-bound RNA prior to elution by centrifugation at 8000 g for 1 min. Eluted RNA was kept on ice.

2.3.d.   DNAseI treatment of RNA extracts

Contaminating genomic DNA was removed using DNaseI (DNA-free, Ambion, Austin, TX, USA). 2.5 μl of DNaseI buffer and 1 μl of recombinant DNaseI were added to 25 μl RNA in a 0.5 ml tube and incubated at 37°C for 20 min. 2.5 μl of DNaseI inactivation slurry was added and mixed by vortexing. Mixing was repeated during a 2 min incubation at ambient temperature prior to centrifugation at 10,000 g for 1.5 min. The RNA-containing supernatant was transferred to a clean tube and stored on ice.

2.3.e. RNA quantification and qualitative assessment

Agarose gel electrophoresis was used to identify residual DNA contamination and to assess RNA quality. An electrophoresis tank, gel tray and comb were washed with detergent and rinsed in deionised water to minimise DNA contamination. A 1% agarose gel was prepared using TBE (1X) containing RNase-free water in a clean, autoclaved bottle, following the method described (section 2.3.b). 1 µl of RNA was mixed with 3 µl of RNase-free loading dye (section 2.2.e) and loaded into the gel. RNase-free 1 kb DNA ladder (Invitrogen, Melbourne, VIC, Australia) was also loaded to facilitate nucleic acid size discrimination. Examination of the nucleic acid bands visible under UV transillumination was used to provide an indication of sample quality. Samples free of visible DNA contamination, with a ratio of 28S:18S rRNA approximating 2:1 were deemed suitable for further use. Samples were quantified using spectrophotometry (BioPhotometer, Eppendorf, Hamburg, Germany). 48 µl of RNase-free water was added to a disposable spectrophotometry cuvette (Eppendorf, Hamburg, Germany) and a blank reading was taken. 2 µl of RNA was added and carefully mixed prior to quantification. RNA yields typically ranged from 4-16 µg per retina (mean 7.8 µg). The absorbance ratio at 260:280 nm was used as an additional guide to RNA purity – samples with a ratio of ≥ 1.9 were deemed satisfactory.

2.3.f. cDNA synthesis

RNA extraction and cDNA synthesis were performed on the same day, to avoid RNA degradation with freezing and thawing. cDNA was synthesised using a commercial kit (SuperScript III First-Strand Synthesis System, Invitrogen, Carlsbad, CA, USA) in accordance with the manufacturer's instructions. Briefly, 1 µg of RNA was added to 1 µl of random hexamers (50 ng/µl) and 1 µl of dNTP mix (10 mM). The volume was made up to 10 µl with DEPC-H_2O. The reaction components were mixed and collected by centrifugation and incubated at 65°C for 5 min prior to cooling on ice for 2 min. Ten µl of cDNA synthesis mix was added (2 µl of 10X RT buffer, 4 µl of 25 mM $MgCl_2$, 2 µl of 0.1 M dithiothreitol [DTT], 1 µl of RNaseOUT and 1 µl of SuperScript III reverse transcriptase) followed by vortex mixing and gentle centrifugation. A 10 min incubation at 25°C was followed by 50 min at 50°C. Incubation for 5 min at 85°C was used to

terminate the reaction. Contents of the tube were collected by centrifugation and 1µl of RNase H was added prior to a final 20 min incubation at 37°C. A reverse transcriptase-free (RT-) control sample was synthesised in parallel with each cDNA sample, with the substitution of DEPC-H$_2$O for reverse transcriptase. 1/20 v/v dilutions of each sample were prepared with Ultra Pure water (Fisher Biotech, West Perth, WA, Australia) and stored at 4°C. Residual neat cDNA was frozen at -20°C.

2.3.g. Preparation of the standard cDNA sample

Retinal RNA from rats of three strains – F344, SPD and DA – was pooled and used for the synthesis of a bulk standard cDNA sample. Aliquots of the standard sample were included in each PCR run and were used for the relative quantification of gene expression – the expression of a gene in a sample of interest was compared with the expression of the same gene in the standard sample. Furthermore, serial dilutions of the standard cDNA were used to generate standard curves for each primer pair. The standard pool was comprised of cDNA derived from oxygen-exposed rats, as well as room air control rats, from a range of developmental stages (Table 2.4). The RNA extracted from each retina was assessed by electrophoresis and spectrophotometry and all satisfactory samples were pooled and mixed. Pooled RNA was reverse transcribed as described in section 2.3.f. The products of 10 cDNA syntheses were combined to generate the standard sample. Two reverse transcriptase-free reactions were prepared as negative control samples (RT-).

Strain	Exposure	Number
F344	5 days of room air	1
SPD	10 days of room air	1
SPD	14 days of room air	1
SPD	14 days of cyclic hyperoxia and relative hypoxia	1
DA	14 days of cyclic hyperoxia and relative hypoxia	1
DA	14 days of cyclic hyperoxia and relative hypoxia, followed by four days of relative hypoxia	1
SPD	14 days of cyclic hyperoxia and relative hypoxia, followed by four days of relative hypoxia	1

Table 2.4 Rat retinae used in the pooled cDNA standard sample. The RNA extracted from both retinae of each of these rats was pooled and reverse transcribed to yield the pooled cDNA standard sample. The exposure period commenced during the first day of postnatal life.

2.3.h.   Preparation of test cDNA samples

Test cDNA samples used in real-time RT-PCR reactions were comprised of the cDNA products of pooled RNA samples. Each RNA pool was made up of equal quantities of RNA from the left retina of three rats, from at least two different litters, that had been exposed to identical experimental conditions (see Figure 2.1). Pooled RNA samples were vortex mixed, and 1 μg was reverse transcribed as described in section 2.3.f. The cDNA products of the pooled RNA samples were deemed *pooled cDNA samples* for convenience. A reverse transcriptase-free reaction was prepared in parallel with each test cDNA sample – the resultant product (RT-) was used as a negative control for real-time RT-PCR.
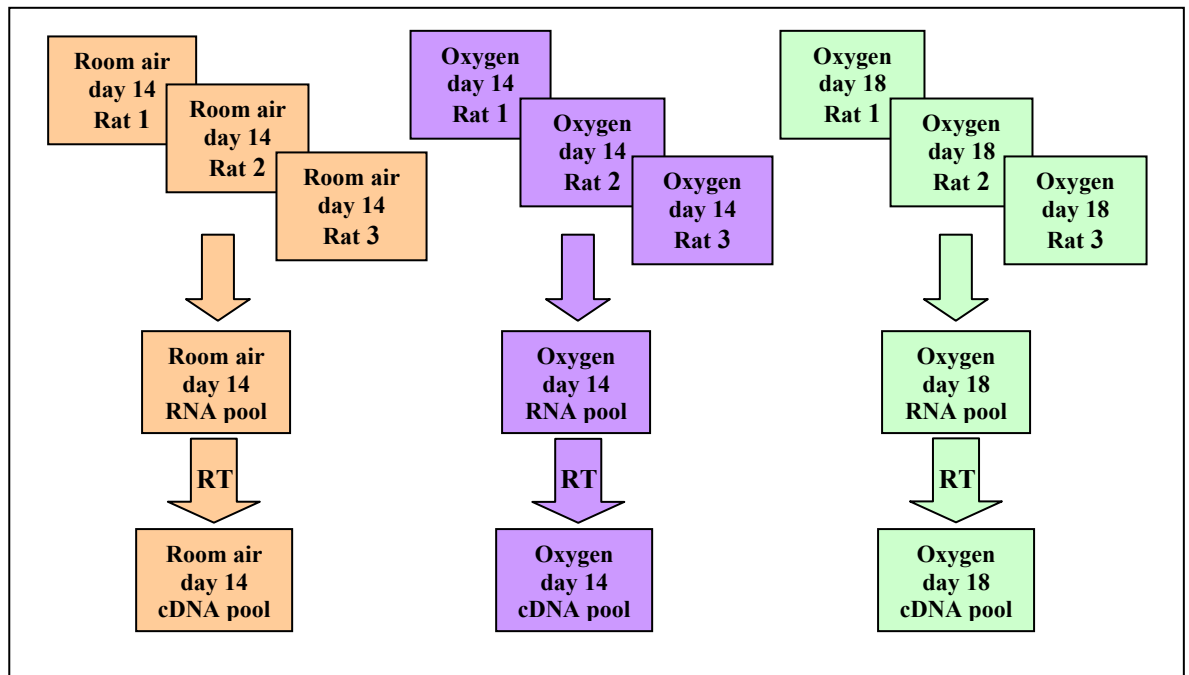
Figure 2.1 Preparation of pooled cDNA samples for a single rat strain. Equal quantities of retinal RNA from three rats were combined to make an RNA pool for each experimental group: room air day 14 (orange); oxygen day 14 (purple); oxygen day 18 (green). RNA pools were reverse transcribed (RT) to generate cDNA pools. cDNA pools were prepared for each of the three strains in this manner, giving a total of 9 different cDNA pools. Samples from each cDNA pool were then assayed in triplicate in each real-time RT-PCR reaction (see Figure 2.2).

2.3.i.   Polymerase chain reaction primer design

Primers and probes were designed using Primer3 software (http://frodo.wi.mit.edu/cgi-bin/primer3/primer3_www.cgi), in accordance with stringent parameters for optimal design [301] (Table 2.5). Primers were selected for compatibility with SYBR Green I [302] and TaqMan (Perkin-Elmer-Applied Biosystems) chemistries [301]. NCBI BLAST software (www.ncbi.nih.gov/BLAST/) was used to align the mRNA sequence of the gene of interest with the rat genome to identify putative intron-exon boundaries. Primers were designed to flank an intron, such that the products of genomic DNA amplification could be readily distinguished from the products of cDNA amplification on the basis of size. Probes were designed to span an intron-exon boundary – one half of a probe hybridised with the 3'-end of one exon, while the other half hybridised with the 5'-end of the adjacent exon. In the case of differentially spliced transcripts, those exons present in all of the major biologically-active isoforms were targeted for primer binding.

The mRNA sequence was copied to the Primer3 design application, the target region for probe hybridisation was specified, and primer and probe sequences were selected according to the conditions specified in Table 2.5 using a rodent mis-hybridisation library. Candidate primer pairs and probes were checked for compliance with the design parameters and were tested for specificity *in silico* using the nucleotide BLAST function of the NCBI BLAST software, against sequences for *Rattus norvegicus*. Primer pairs were then aligned with the rat genome (NCBI BLAST software) to identify the potential for genomic DNA amplification. In cases of predicted genomic DNA amplification, primers were considered acceptable if the genomic amplicon was more than twice the length of the target cDNA amplicon. Primers were tested in endpoint PCR, prior to testing in real-time PCR with SYBR Green chemistry. Real-time RT-PCR products of all genes of interest were purified, sequenced and compared with the predicted amplicon sequence to confirm their identity. The melting curve of each real-time PCR product was compared with that of the corresponding sequenced product to confirm its identity [303]. Primer sequences are listed in Table 2.1.

Table 2.5 Parameters for optimal primer and probe design [301]

Amplicon	length: 65-100 bases
Primers	length: 15-20 bases
	sequence: G/C content: 20-70%
	$\leq$2 G/C in terminal 5 bases of 3' end
	forward and reverse primers bind to separate exons
	(intron-spanning)
	T_m: minimum 58°C
	maximum 60°C
	$\leq$ 2°C difference between members of a primer pair
Probe	Length: ~ 30 bases
	sequence: G/C content: ~ 50%
	no overlap with primer-binding sites
	no complementarity with primers
	no terminal G at 5' end (reporter quenching)*
	ideally probe should span exon-exon boundary
	T_m: ~ 10°C > primers

T_m: melting temperature.

* Probe sequence for COX2 has a 5' G (Table 2.1). Omission of this residue will not adversely affect probe specificity, but may lower T_m by 1-2 ^{o}C.

2.3.j.   General precautions for polymerase chain reaction

Polymerase chain reactions were prepared in a dedicated area, free of PCR-product contamination. Gloves and a clean gown were worn at all times and plugged pipette tips, free of nucleic acids and nucleases (Edwards Instrument Company, Sydney, NSW, Australia), were used.

2.3.k.   Endpoint reverse transcription-polymerase chain reaction

Unless otherwise specified, endpoint PCR reactions contained 2 μl of cDNA template (appropriately diluted in DEPC-H$_2$O), 2.5 μl of PCR buffer (10X PCR buffer, Invitrogen, VIC, Australia), 100 μM dNTPs, 1.5 mM MgCl$_2$, 0.5 U Taq DNA polymerase (Platinum$^®$ Taq DNA polymerase, Invitrogen, VIC, Australia) and 10 pmol of each primer (forward and reverse) in a total reaction volume of 25 μl. The reaction mix was overlaid with light mineral oil (Sigma, St. Louis, MO, USA). Thermal cycling was performed in an OmniGene$^©$ Thermal Cycler (Hybaid Ltd, Middlesex, UK). An

initial denaturation at 94°C for 5 min was followed by cycles of denaturation (94°C for 30 sec), annealing (30 sec) and extension (72°C for 1 min). The reaction was completed with a final extension step at 72°C for 15 min. The number of amplification cycles and annealing temperature were modified for each primer pair. Agarose gel electrophoresis was used to analyse products.

2.3.l.   Quantitative real-time reverse transcription-polymerase chain reaction

Real-time RT-PCR was performed with a RotorGene 2000 Thermal Cycler (Corbett Research, Mortlake, NSW, Australia) in accordance with the manufacturer's instructions. A commercially prepared SYBR Green master-mix (QuantiTect SYBR Green PCR Master Mix), containing a hot-start Taq DNA polymerase, SYBR Green I, dNTPs and PCR buffer (5mM $MgCl_2$, Tris-Cl, KCl, $(NH_4)_2SO_4$, pH 8.7), was used. A bulk mixture comprised of the master-mix (10 µl/reaction), and primers (2 µl/reaction of each of the forward and reverse primers [20 µM]) was prepared, vortex mixed and collected by centrifugation. Fourteen µl of the bulk mixture was added to each tube (0.1 ml strip tubes, Corbett Research, Mortlake, NSW, Australia). cDNA samples were diluted 1/100 v/v with Ultra Pure water (Fisher Biotech, West Perth, WA, Australia), vortex mixed and collected by centrifugation. Six µl of the appropriate cDNA sample was added to each tube, giving a final reaction volume of 20 µl. Sealed tubes were placed in the thermal cycler and cycling was commenced. An initial denaturation (95 °C for 15 min) was followed by 50 cycles of denaturation (94°C for 20 sec), annealing (50°C for 20 sec) and extension (72°C for 30 sec). The reaction was completed with an extension step at 72°C for 4 min, followed by 25°C for 5 min. An annealing temperature 5-8°C below the T_m of primers was recommended by the master-mix instruction manual (QuantiTect SYBR Green PCR Handbook 08/2003), however a temperature of 50°C (7-10°C below estimated T_m of primers [Table 2.1]) was found to be optimal for the genes of interest. Melting of PCR products was performed with 0.5°C steps at 5 sec intervals from 60-99°C.

Each real-time RT-PCR run was used to quantify the expression of a single gene in each pooled cDNA test sample. Thus each PCR run contained 9 pooled test samples – one for each of the three test strains (F344, SPD and DA), for each of the three experimental

exposures (room air day14, oxygen day 14 and oxygen day 18) (see Figure 2.2). Every sample was tested in triplicate in each PCR run, and every gene of interest was tested in duplicate runs, giving a total of 6 replicates for each sample pool, per gene. Furthermore, a standard cDNA sample (section 2.3.g) was included in triplicate in each PCR run. The gene expression of each test sample was determined relative to the standard sample from the same run – giving a gene expression value for each test sample relative to the expression of the same gene in the standard sample. Expression values for duplicate runs were collated for statistical analysis.

A single RT- control (negative control) (section 2.3.h) for each sample was included in each PCR run, as were 2 tubes containing Ultra Pure water in place of cDNA (no-template control [NTC]). A negative control sample was considered to be negative if the threshold cycle (Ct) for amplification was more than five cycles greater than the than that of the corresponding test sample. In all cases in which the Ct value of a negative control sample was within 5 cycles of the test sample, melt-curve analysis confirmed the amplification of a non-specific product in the negative control sample.

Melt curve analysis was used to confirm product specificity, in accordance with the manufacturer's instructions (Corbett Research, Mortlake, NSW, Australia). In brief, the melt curves of specific products were expected to occupy a narrow temperature range and to have a single well-defined peak. In addition, the melt-curves of products from different samples, amplified with the same primer pair, were expected to be closely aligned. PCR products were randomly selected from each real-time RT-PCR run for agarose gel electrophoresis, to further confirm product identity. In addition, the PCR products of all primer pairs were purified and subjected to sequence analysis at least once. The gel electrophoresis photographs and melt-curves of these sequenced samples were used as references for comparison with each of the test samples.

F344 RA14	F344 O14	F344 O18	SPD RA14	SPD O14	SPD O18
F344 RA14	F344 O14	F344 O18	SPD RA14	SPD O14	SPD O18
F344 RA14	F344 O14	F344 O18	SPD RA14	SPD O14	SPD O18
DA RA14	DA O14	DA O18	STD	F344 RA14 RT-	SPD RA14 RT-
DA RA14	DA O14	DA O18	STD	F344 O14 RT-	SPD O14 RT-
DA RA14	DAO14	DA O18	STD	F344 O18 RT-	SPD O18 RT-
DARA14 RT-	STD –RT				
DAO14 RT-	NTC				
DAO18 RT-	NTC				

Figure 2.2 Schematic representation of the samples included in a single real-time RT-PCR run. A single gene was assayed in each run. Samples for the three representative strains were included in each run: F344 (yellow), SPD (blue), DA (pink). Each pooled sample (RA14; O14; O18) was assayed in triplicate. "RT-" samples (green) had not undergone reverse transcription and served as negative controls: an RT- sample was included for each group of pooled samples. No-template controls (NTC) contained water in place of cDNA. Each gene was assayed in duplicate PCR runs – setup of the duplicate plate was identical to the schema outlined above.

Abbreviations:
F344: Fischer 344; **SPD**: Sprague Dawley; **DA**: Dark Agouti; **RA14**: exposed to room air for 14 days; **O14**: exposed to cyclic hyperoxia for 14 days; **O18**: exposed to cyclic hyperoxia for 14 days followed by 4 days in room air; **STD**: standard cDNA sample.

2.3.m. Agarose gel PCR-product purification

Agarose gels were visualised under low intensity UV light, and gel slices containing desired DNA bands were removed with clean scalpel blades. DNA was extracted using the Qiaquick column purification system (Qiagen, Hilden, Germany) in accordance with the manufacturer's instructions and eluted in 10mM TrisCl (pH 8.5) for quantification and sequencing.

2.3.n. PCR product sequencing

Purified PCR products were sequenced by Mr Oliver van Wageningen (DNA sequencing facility, Flinders University, SA, Australia). Products were labelled using the BigDye® Terminator v3.1 Cycle Sequencing Kit and resolved using the ABI 3100 Genetic Analyser (Applied Biosystems, Foster City, CA, USA).

2.4.   ANIMAL AND TISSUE TECHNIQUES

2.4.a. Conventional histology

Enucleated eyes were pierced with a 21G needle and fixed in buffered formalin for at least 24 hr. Eyes were then dehydrated in 70% ethanol for one hr, 80% ethanol for one hr, 90% ethanol for one hr, before three 30 min washes with 100% ethanol. Eyes were placed in chloroform for 18 hr and then transferred into molten wax (Paraplast tissue embedding medium, Tyco Healthcare Group, Mansfield, MA, USA) for 45 min at 37°C. Eyes were transferred to fresh melted wax under vacuum at 37°C for a further 45 min and this was repeated again before tissues were embedded in wax blocks. Sections (5 μm) were cut at a microtome (Leica RM2/35; Leica Microsystems, Gladesville, NSW, Australia), mounted onto chrom alum-subbed microscope slides, and allowed to dry (section 2.2.b). Slides were cleared in xylene (2 x 4 min) and hydrated in 100% ethanol (2 x 2 min), 90% ethanol (2 min) and 70% ethanol (2 min) before being rinsed in ddH$_2$O. Slides were stained in haematoxylin (section 2.2.h) for 10 min and rinsed in tap water for 1 min. Samples were briefly dipped in acid alcohol and washed in tap water for 1 min. Sections were dipped in lithium carbonate solution and rinsed in deionised water before being stained with eosin (section 2.2.f) for 2 min and washed in tap water for 1 min. Sections were dehydrated in 100% ethanol (three brief washes), cleared in xylene (2 x 2 min) and mounted in DePex mounting medium (BDH Laboratory Supplies, Poole, UK) for examination at the light microscope.

2.4.b. Ink perfusion of rats

2.4.b.1   *Perfusion device*

A perfusion device, based on previously described designs [304-307], was constructed to deliver perfusate at a controlled pressure (Figure 2.3). The barrel of a 60 ml Luer-lock plastic syringe (Terumo, NSW, Australia) constituted the injection chamber. The chamber was secured in a vertical position 10 cm above the base of a 50 cm retort stand, with an adjustable clamp. A 20 cm length of polyethylene tubing (Minimum Volume Extension Set, Tuta Healthcare, Lane Cove, NSW, Australia) was attached to the distal end of the barrel. An injection cannula was attached to the free end of the tubing, via a three-way stopcock. The cannula was made by breaking a 21G needle 7mm from the

hub and sheathing the stump with a 10 mm length of polyethylene tubing (PE10 tubing, 0.28 mm internal diameter, Protech International, TX, USA).

The injection chamber was sealed with a rubber stopper (maximum diameter 29 mm, Selby Biolabs, Clayton, VIC, Australia). An 18G needle was pushed through the base of the stopper to communicate with the injection chamber and a 15 cm length of silicon tubing (3mm internal diameter) was attached to the needle hub via a three-way stopcock. The distal end of the tubing was attached to a sphygmomanometer dial and cuff, via a y-piece connector. The cuff was housed in a thick-walled glass jar. By pumping the inflation bulb of the sphygmomanometer cuff, pressure was transduced to the injection chamber and manometer dial simultaneously, allowing perfusion pressure to be precisely regulated. The stopper was secured in position with two 18G needles inserted 2 cm into the stopper, 2 mm below its base, in a plane parallel to the base of the retort stand. The hubs of these needles were secured to the flanges of the syringe with firmly-sprung metal document clips.

2.4.b.2   *Preparing rats for perfusion*

Adult rats were heparinised 30 min prior to perfusion (porcine heparin sodium, David Bull Laboratories, Mulgrave, VIC, Australia) with a dose of 5 iU/ml of plasma volume, estimated as 5.5% of body weight. Rats were lightly anaesthetised with inhalational halothane (Fluothane, Zeneca, Macclesfield, U.K.) and an intraperitoneal injection of heparin was delivered with a tuberculin syringe.

2.4.b.3   *Priming the perfusion device*

Immediately prior to perfusion, the apparatus was primed with 40 ml of warmed (37°C) 0.9% NaCl containing 100 μM papaverine hydrochloride (David Bull Laboratories, Mulgrave, VIC, Australia). The injection chamber and infusion tubing were submerged in warm water (37°C) contained in a beaker (1l) and a shallow kidney-dish, respectively. The volume of perfusate was kept below the tip of the needle penetrating the stopper, to prevent the introduction of bubbles into the perfusate. The injection chamber was sealed and the three-way stopcock, proximal to the cannula, was closed. The inflation bulb was pumped to generate a perfusion pressure of between 100-110 mmHg, approximating the systolic blood pressure of the normal adult rat [308, 309].
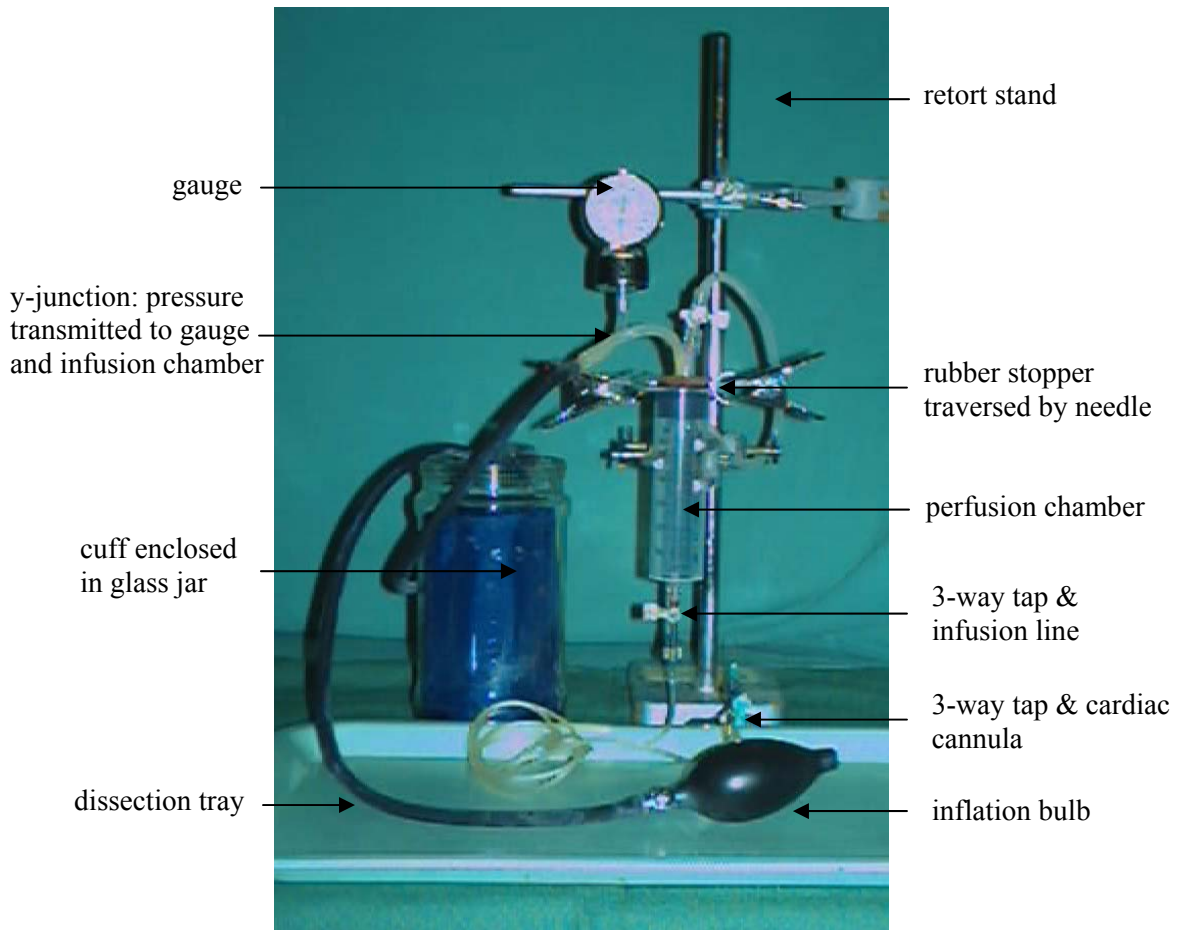
Figure 2.3 Pneumatic perfusion pump. A cardiac cannula is connected via narrow-bore infusion tubing to a 60 ml plastic syringe barrel containing the perfusate. Regulated perfusion pressure is provided by a pump made by modification of a standard sphygmomanometer. The cuff is contained in a glass jar such that compression of the inflation bulb transmits pressure directly to the gauge. A y-junction in the tubing transmits pressure equally to the gauge and to the perfusion-chamber. Continuity between the sphygmomanometer tubing and the chamber is achieved by a needle that pierces the rubber stopper lodged in the proximal end of the chamber.

2.4.b.4 Perfusion technique

The rat was killed with an overdose of inhaled halothane anaesthesia and placed in a supine position on a shallow plastic dissection tray. Its limbs were secured to the tray with masking tape. A midline thoraco-abdominal incision was made; skin and subcutaneous tissues were retracted and a transverse abdominal wall incision was made (Figure 2.4). Care was taken to avoid viscera. Bilateral cuts were made through the thoracic cage; the diaphragmatic attachments were freed and the thoracic cage was reflected superiorly and cross-clamped with artery forceps. The pericardium was dissected away. The left lung was retracted medially and the exposed descending aorta was clamped with fine artery forceps. The apex of the left ventricle was grasped with toothed forceps. Fine dissecting scissors were used to make an opening in the left ventricle 2 mm superior to the apex – entry into the chamber was confirmed by an efflux of blood. The injection cannula was carefully inserted deep into the cavity of the left ventricle. It was secured in position with a pair of curved artery forceps firmly applied around the ventricle, immediately superior to the insertion site (Figure 2.4). The tip of the right auricle was cut away to provide a portal of venous egress.

The three-way stopcock proximal to the cannula was opened and perfusion commenced. Perfusion pressure was maintained with intermittent compressions of the inflation bulb. The entire volume of saline/papaverine perfusate was used. The adequacy of the perfusion was demonstrated by clearing of the venous effluent and by pallor of the nose and upper limbs. Care was taken to avoid the entrainment of air into the perfusion tubing by closing the stopcock immediately before the chamber was emptied.

Pressure in the perfusion device was vented by releasing the sphygmomanometer valve. The stopper was removed and 20 ml of warm (37°C) ink perfusate (section 2.2.i) was poured into the injection chamber. The injection chamber was sealed and perfusion was continued at a pressure of 100-110 mmHg. Following perfusion bilateral enucleation and retinal flat-mounting was performed, as described (section 2.4.c.3).
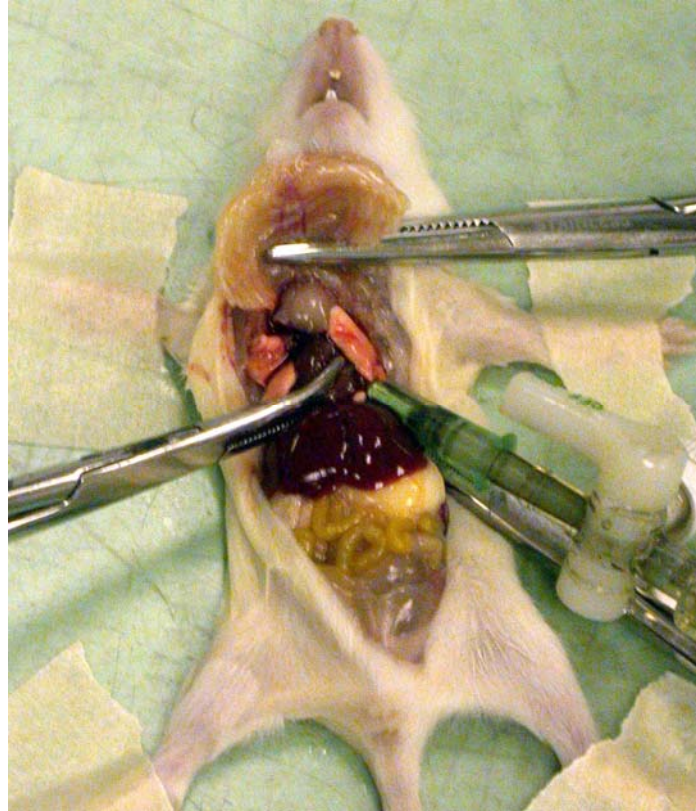
Figure 2.4 Ink perfusion of a neonatal rat. A 14 day old SPD rat was heparinised and killed with an inhaled overdose of halothane. A thoracotomy was performed and a cardiac catheter, fashioned from blunt-ended 21G needle sheathed with polyethylene tubing, was inserted into the left ventricle and secured with artery forceps. The right auricle was removed and perfusate was delivered into the left ventricle via the pneumatic perfusion pump.

2.4.c.   Oxygen-induced retinopathy

2.4.c.1   Oxygen chamber

A custom-made chamber designed to deliver oxygen to rat litters under precisely controlled conditions was constructed by Ms Anne-Louise Smith (Biomedical Engineering Department, Flinders Medical Centre, SA, Australia) (Figure 2.5). The chamber was comprised of a wooden box mounted with Perspex doors. Rubber door seals and plastic electrical tape were used to make the chamber air-tight. An anaesthetic blender (Bennett AO-1, CIG Medishield-Ramsay, Melbourne, VIC, Australia) and high-flow oxygen regulator (Anaequip, Adelaide, SA, Australia) were used to deliver blended oxygen and air to the chamber. Gas was vented via an exhaust pipe positioned in the roof of the chamber. Oxygen levels were continuously monitored with a fuel-cell oxygen monitor (Hudson Oxygen Monitor, model 5550, Temecula, CA, USA) and were recorded with a data logger (Tinytalk II, Gemini Dataloggers Ltd, Chichester, West Sussex, UK) for subsequent analysis (Gemini Logger Manager, v2.6, Gemini Dataloggers Ltd, Chichester, West Sussex, UK). The oxygen monitor was regularly calibrated with room air and 100% oxygen prior to experiments, to ensure the accuracy of monitoring. A gas flow rate of 25 l/min was found to maintain stable oxygen levels when the chamber was loaded to capacity with four rat litters. Gas flow within the chamber was enhanced by large vents in the shelf dividing the upper and lower halves of the chamber. Even gas flow was confirmed by observations of smoke circulation within the chamber (Air Current Tubes, Dräger, Lübeck, Germany). Movement of the fuel-cell probe to various positions in the chamber during a period of 80% oxygen gas flow yielded uniform results, confirming the homogeneity of oxygen levels within the chamber. Humidification was achieved by placing a water reservoir below the gas inflow pipe. During several 24 hr periods of monitoring with a hygrometer, chamber humidity ranged between 40-55%. Temperature within the chamber was constant at 24°C and a 12 hr light-dark cycle was adhered to.
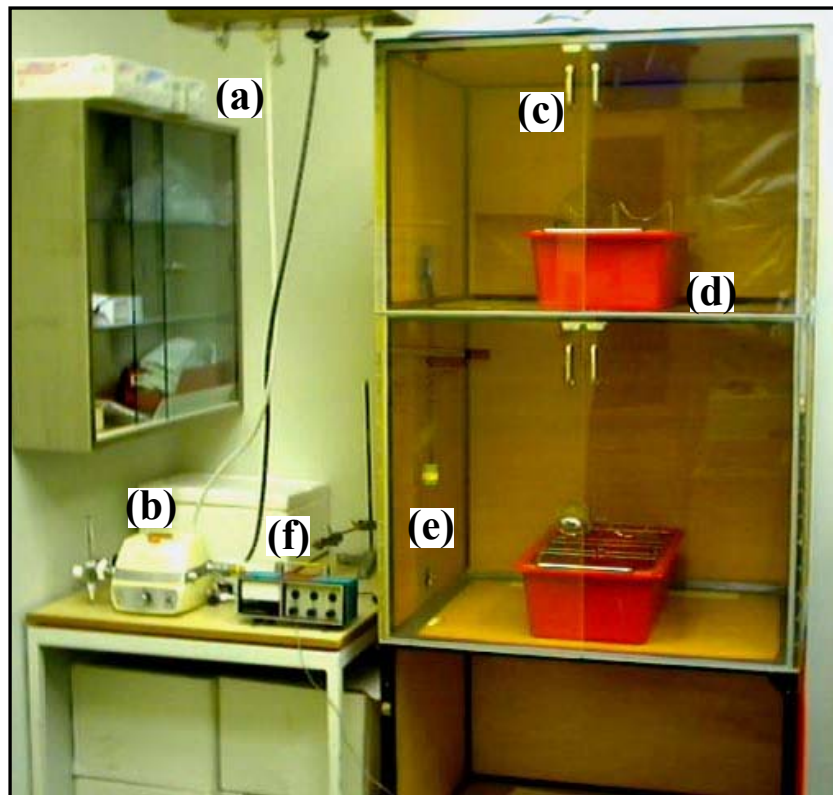
Figure 2.5 Oxygen chamber. Air and oxygen (a) were mixed with an anaesthetic blender (b) and delivered to the chamber (c) with a high-flow regulator. The chamber was constructed from a wooden cabinet, which was mounted with Perspex doors and made airtight. Four rat cages (d) could be housed simultaneously. Oxygen levels in the chamber were continuously monitored with a fuel cell oxygen sensor (e) and an oxygen monitor (f) attached to a data recorder.

2.4.c.2   *Oxygen exposure protocol*

The cyclic oxygen exposure protocol used in these experiments was a modification of those described in other studies of rat oxygen-induced retinopathy (OIR) [310-314]. Unless otherwise stated, female rats and their newborn litters were placed in the oxygen chamber within 12 hr of birth and exposed to alternating 24 hr cycles of hyperoxia (80% O_2) and normoxia (21% O_2) for the first 14 days of life (cyclic hyperoxia) (Figure 2.6). An oxygen concentration of $80 \pm 1\%$ was maintained for the duration of hyperoxic cycles. At the day 14 time-point, rats were either killed for retinal dissection, or exposed to room air for a sustained period of 4 days prior to analysis (day 18). Day 14 of cyclic hyperoxia was deemed the *vascular attenuation time-point*, whilst day 18 was named the *vascular proliferation time-point*.

Cage positions within the chamber were randomly allocated and often changed during the 14 day exposure period. Survival rates were in excess of 95% for hyperoxia exposed neonatal rats and there was no obvious maternal oxygen toxicity. Rats reared in room air were used as controls. Pups from at least 2 different litters of each of the six rat strains studied, were analysed at each exposure endpoint to distinguish inter-strain from intra-strain variation. In those instances in which an entire litter was not used for analysis, pups were selected at random. Mean litter sizes of each strain are provided in Table 2.2.
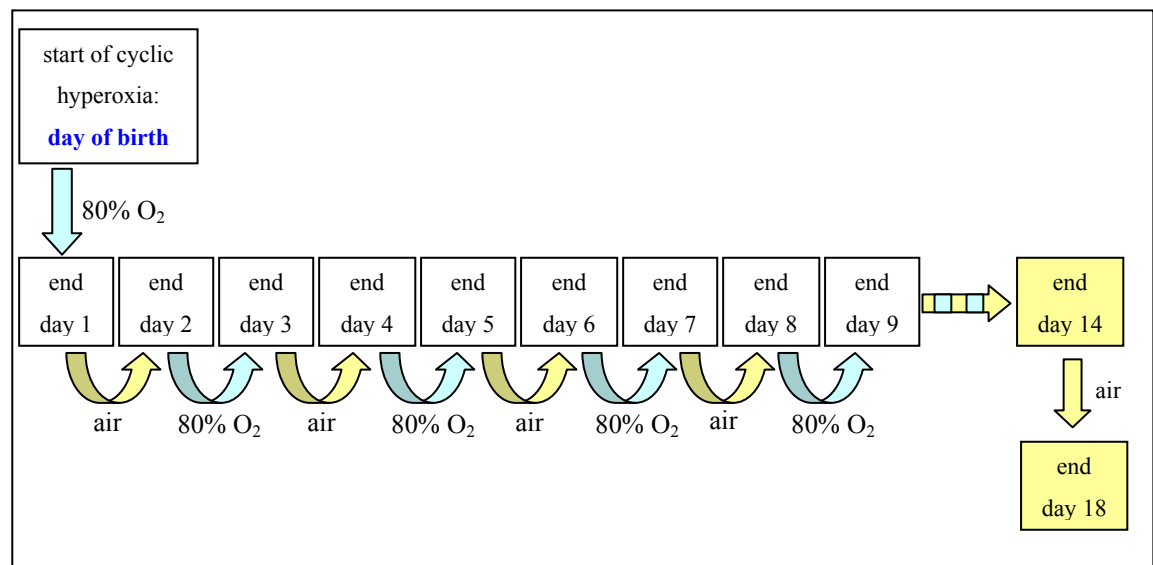
Figure 2.6 Cyclic hyperoxia protocol. Newborn rats were exposed to 24 hours of 80% oxygen (blue arrow) on the first day of postnatal life. The end of this initial cycle of hyperoxia marked the end of exposure day 1. During the subsequent 24 hour period, rats were exposed to room air (yellow arrow). Room air constituted relative hypoxia for the avascular retinae. The alternating exposure to hyperoxia and room air continued for 14 days at which point rats were either killed for retinal dissection, or exposed to room air for a sustained period of 4 days prior to processing. The day 14 and day 18 time-points were the *vascular attenuation* and *vascular proliferation* time-points, respectively.

2.4.c.3   *Retinal dissection and flat-mounting*

Rats were killed with an overdose of inhalational halothane anaesthesia and weighed. Enucleation was performed using fine curved forceps and curved-tip scissors. Care was taken to avoid excessive pressure on the globe. Eyes were fixed in 2% w/v paraformaldehyde in PBS (pH 7.4) at 4ºC for 90 min. Retinal flat-mounts were prepared with a modification of the methods of Stone [315] and Chan-Ling [316] (Figures 2.7, 2.8 and 2.9).

Dissection was performed in a petri-dish lid in 1-2 ml of chilled PBS (4°C) under an operating microscope (Wild Heerbrugg M690, Heerbrugg, Switzerland). Peribulbar fat and connective tissue were dissected away to expose the sclera. A short stump of optic nerve was left protruding from the globe. The eye was cradled between the tips of a pair of curved forceps. An incision was made immediately anterior to the corneoscleral limbus with a scalpel (No.11 blade). Fine-toothed forceps were used to grasp the cornea. The incision was continued circumferentially with curved-tip microdissection scissors. The cornea, iris and crystalline lens were discarded. Forceps were used to avulse the hyaloid vessels and vitreous gel from their retinal attachments: particular attention was paid to the regions posterior to the ora serrata and around the optic nerve head, where the attachments were most marked [316]. Care was taken to remain above the retinal surface.

Four equally-spaced radial relaxing incisions, extending 2/3 of the way from the retinal periphery to the optic nerve head, were made with a scalpel to flatten the eyecup. Incisions were placed so as to avoid major vessels. The flattened eyecup was turned face-down, the optic nerve stump was grasped with forceps and the tissue was carefully transferred, face-down, to a chrom-alum subbed microscope slide (section 2.2.b). The remainder of the dissection was performed on the microscope slide. A drop of chilled PBS was added to the tissue and a bubble of air was injected beneath the retina with an angled 26G anterior chamber injection cannula (Accutome, PA, USA) attached to a 1 ml syringe, lifting it from the slide and aiding in manipulation of the tissue. The cannula was used as a blunt probe and inserted into the sub-retinal space via the cut edges of the eyecup. The choroid and sclera were carefully separated from each quadrant of the retina and removed with microdissection scissors. The optic nerve stump and the surrounding rim of choroid and sclera were cut away and the retina was carefully turned, inner aspect up, with two blunt probes. The ora serrata was cut away from the retinal periphery. Two pairs of fine forceps were used simultaneously to tease away residual vitreous and hyaloid vessels. A drop of chilled PBS was added to prevent dehydration of the retina. The microscope slide was transferred to a humid box for isolectin histochemistry.

2.4.c.4 Isolectin histochemistry

Retinal flat-mounts were stained with a fluorophore-conjugated isolectin with specificity for alpha-galactosylated glycoprotein residues on vascular endothelial cells and macrophages (*Griffonia simplicifolia* type I isolectin IB4 [317], Alexa Fluor 488 conjugate, Molecular Probes, OR, USA) according to a modification of the method of Cunningham [252]. Retinae were permeabilized with pre-chilled 70% v/v ethanol for 30 min at 4ºC, followed by PBS-1% v/v Triton X-100 (Ajax Chemicals, Sydney, NSW, Australia) for 20 min. Each retina was washed twice with PBS and incubated with 50 μL of 4 μg/ml isolectin in PBS overnight, in the dark at 4ºC. Retinae were washed in PBS seven times, covered with PBS:glycerol (2:1 v/v, pH 7.4) and coverslipped. In all cases, histochemistry was commenced within 6 hours of enucleation.
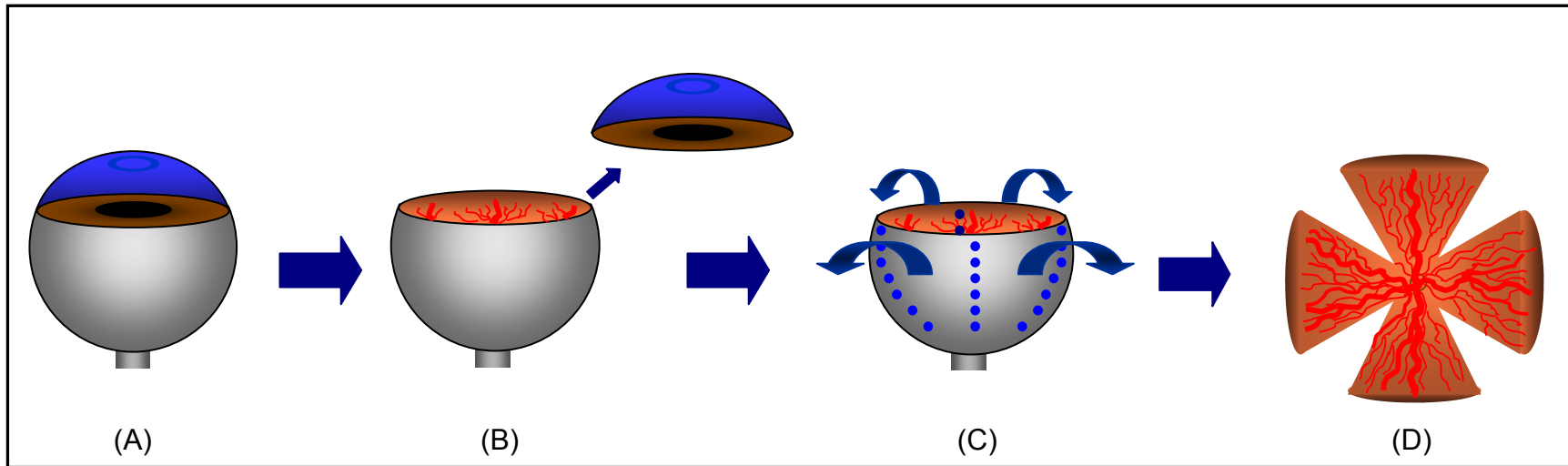
Figure 2.7 Retinal flat-mounting: The eye is enucleated (A) and the anterior segment is removed (B). Four radial relaxing incisions (C) are used to flatten the eyecup (D). The eyecup is transferred to a microscope slide; vitreous and hyaloid vessels are removed, as are the choroid and sclera.
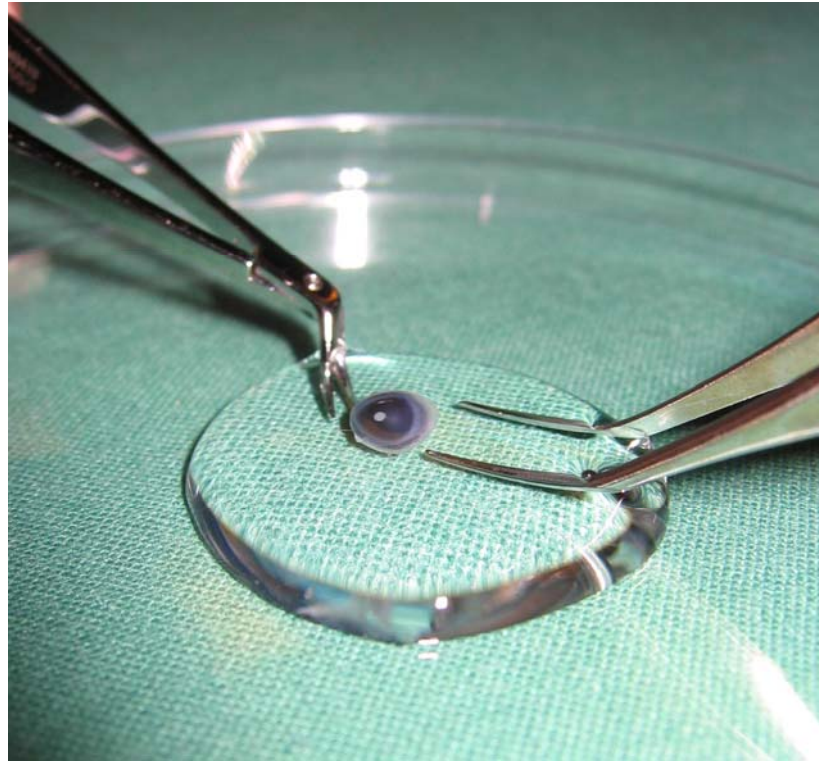
Figure 2.8 Retinal dissection. Dissection of a pigmented neonatal rat eye. The pupil is visible centrally.
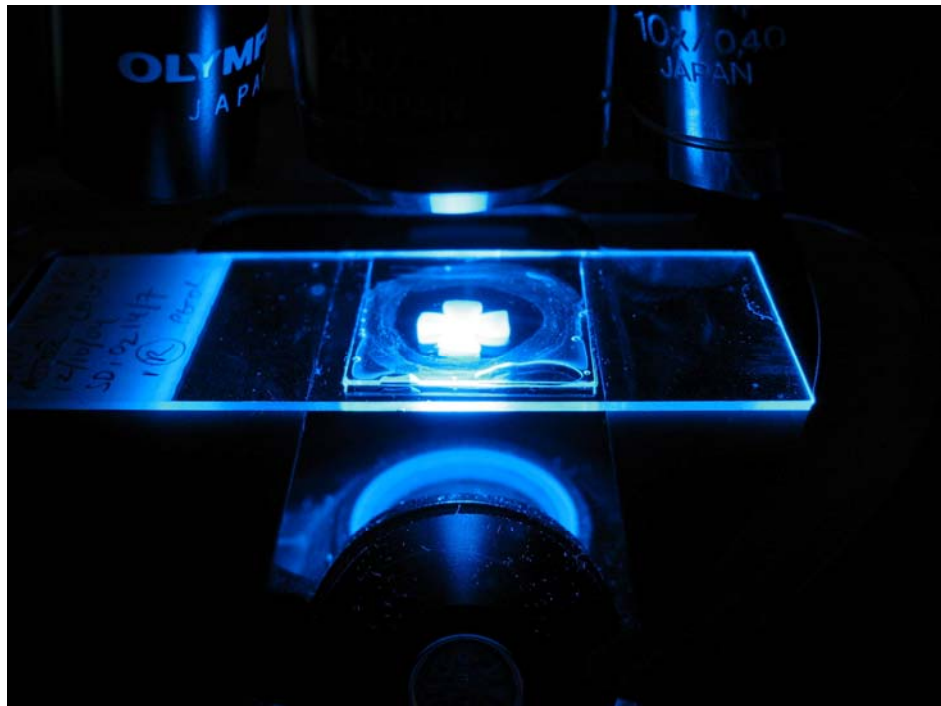
Figure 2.9 Flat-mounted retina. The retina has been dissected, mounted flat on a glass slide and stained with a fluorophore conjugated endothelial cell stain (isolectin GS-IB4). A coverslip has been applied and the retina is being examined at a fluorescence microscope.

2.4.c.5   *Image analysis of labelled retinae*

The right retina of each animal was used for image analysis. Imaging was performed within 12 hr of isolectin labelling using a fluorescence microscope (BX50F, Olympus Optical Co. L.T.D., Japan) coupled with a CCD-digital camera (Photometrics Coolsnap *fx*, Roper Scientific, Trenton, NJ, USA) and image acquisition software (RS Image, v1.01, Roper Scientific, Trenton, NJ, USA). Sequential, overlapping high-resolution images of the entire retina were captured using a 4X objective. Images were manually arranged, merged to construct a montage image of the retina (Figure 2.10) (Adobe Photoshop v7.0, Adobe Systems Inc, San Jose, CA, USA) and analysed using image analysis software (ImageJ v1.30, National Institutes of Health, Bethesda, MD, USA). Each montage was analysed in a window measuring 20 x 20 centimetres on a high definition LCD computer monitor (17 inch Apple Studio Display, Apple, CA, USA). Avascular areas were manually outlined and measured as a percentage of the total retinal area by a masked observer. Repeat analyses by the same observer were highly concordant (mean difference $2.1 \pm 1.9\%$). The central avascular zone was defined as the capillary-free region surrounding the optic nerve head. Peripheral avascular zones were capillary-free regions not in continuity with the optic nerve head.

A semi-quantitative system was used to grade vascular morphology. The retinal montages of postnatal day 18 (P18) cyclic oxygen-exposed rats were compared with reference images of room air-exposed controls. Montages were scored for vascular morphological abnormalities and tortuosity. Morphological abnormalities were defined as features not seen in the course of normal retinal vascularization, including regions of exceptionally dense vascular budding, vascular ridges, marked vascular dilatation and neovascular tufts [318]. Neovascular tufts were defined as vascular projections anterior to the superficial vascular plexus. Each retinal quadrant was divided into thirds to give a total of 12 clock hours of retina, and each clock hour was scored for the presence (1) or absence (0) of any of these morphological abnormalities [313, 314, 319] (Figure 2.11). The tortuosity of retinal vessels was assessed by eye in masked fashion, using reference images for comparison (Figure 2.12). First-order vessels were considered along their entire length and an overall grading was determined for each retina as normal (1); minimally increased (2); moderately increased (3); or markedly increased (4).
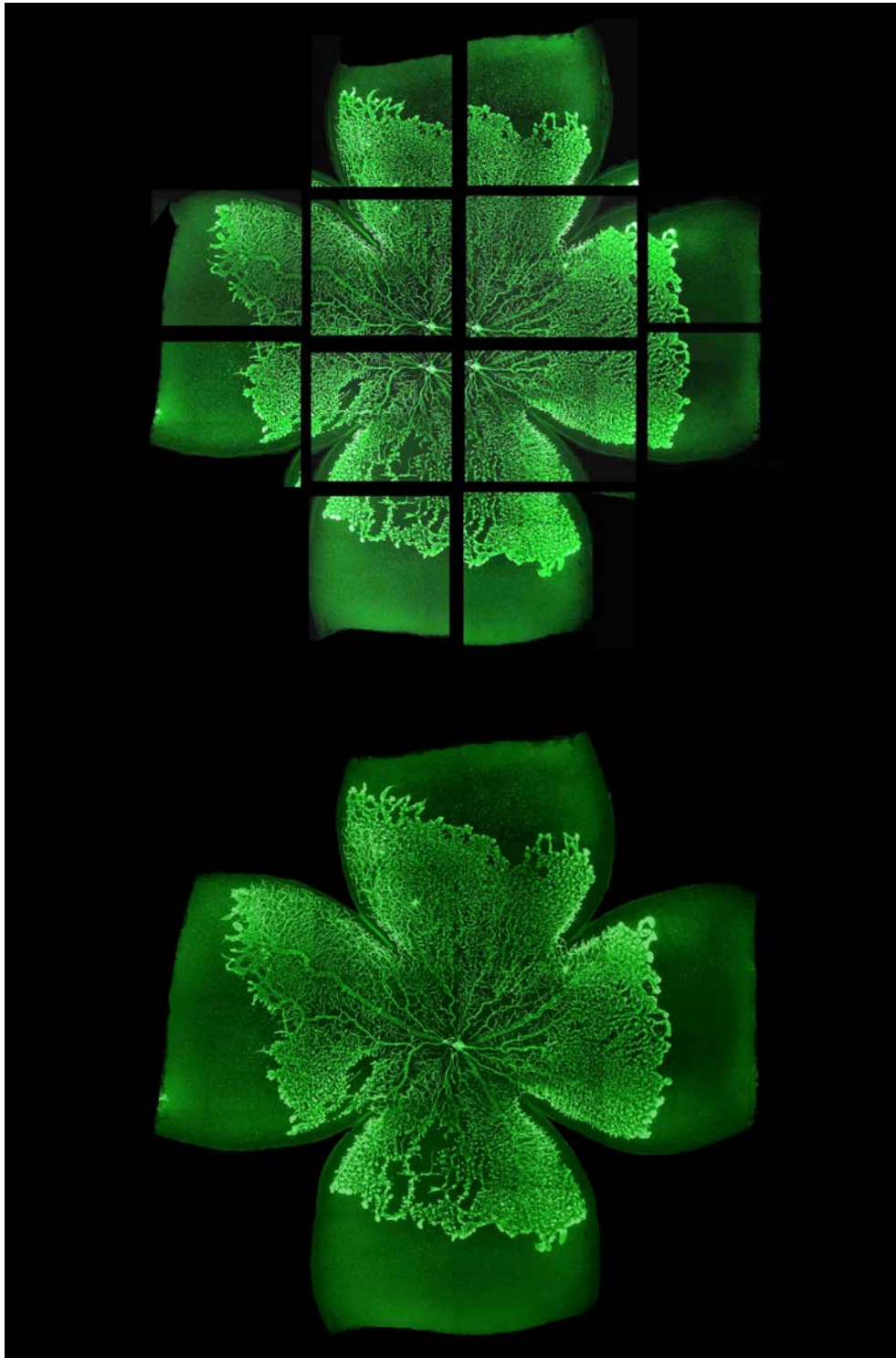
Figure 2.10 Schematic representation of the process of compiling montage retinal images. Sequential, overlapping fluorescence microscopy images were manually arranged and merged to form a composite image. This is a representation only – in reality, montages were compiled from between 30 and 40 sequential images**.**
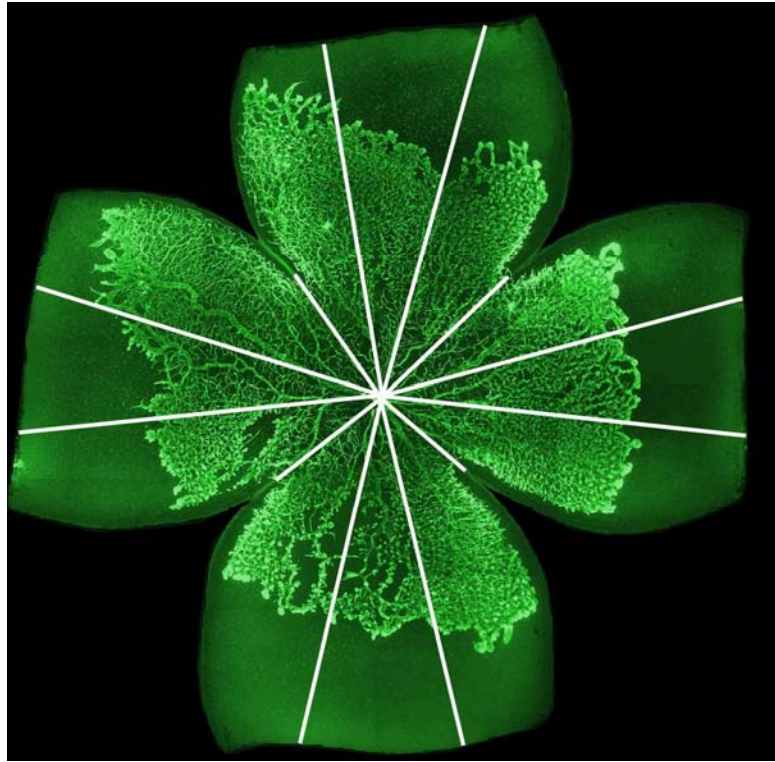
Figure 2.11 Clock hour method for scoring vascular morphological abnormalities. Each retinal quadrant was divided into three approximately equal segments, giving a total of 12 segments or clock hours per retina. A score of 1 was given to each clock hour containing vascular morphological abnormalities. The scores were summed to give an abnormal morphology score, ranging from 0 to 12, for the entire retina.
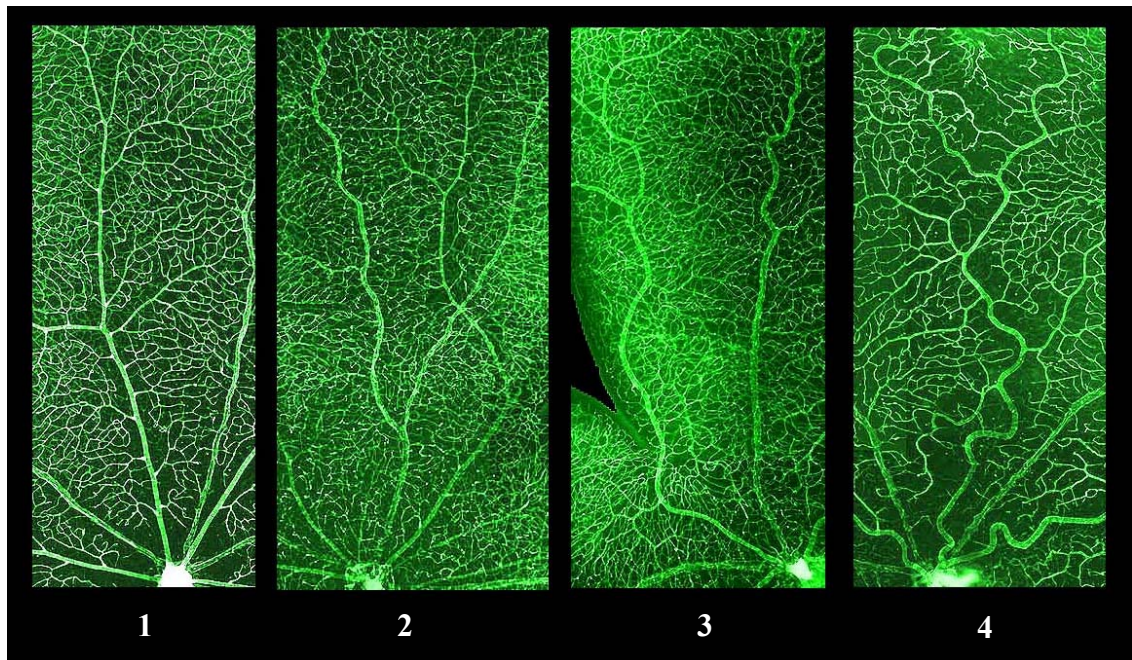
Figure 2.12 Grades of retinal vascular tortuosity. First order vessels were scored for vascular tortuosity. The median tortuosity score was used as the overall score for a given retina. Key:1= normal; 2= mild tortuosity; 3= moderate tortuosity; 4= marked tortuosity.

2.4.d.   Mechanical ventilation of neonatal rats

Following an extended period of 18 days of cyclic hyperoxia neonatal rats were anaesthetised and mechanically ventilated to assess the extent of lung-injury induced by hyperoxia. Modification was made to the method described by Martinez *et al* [320]. Each rat was weighed and anaesthetised with an intraperitoneal injection (100 mg/kg) of thiopentone (25 mg/ml in 0.9% NaCl) administered with a 27G tuberculin syringe. Deep anaesthesia was confirmed by loss of the pedal reflex. Bilateral thigh intramuscular injections (total dose 100 µg/kg) of pancuronium bromide (20 µg/ml in 0.9% NaCl) were administered and a small midline neck incision was made to expose the trachea. A length of 3.0 silk suture was passed around the trachea and a small tracheostomy was made proximal to the suture with fine dissecting scissors. A tracheal cannula, made from a broken 18G needle cuffed at its distal end with a 5 mm length of 18G silicon tubing, was inserted and the encircling suture was pulled tight and tied to prevent air leak (Figure 2.13). The needle hub was immediately attached to a computer-controlled small animal ventilator (Flexivent, module 2, SCIREQ Scientific Respiratory Equipment, Montreal, Canada) and ventilation with 100% oxygen was commenced. Dead-space in the ventilation tubing had been reduced to a minimum. A tidal volume (V_T) of 10 ml/kg was delivered at a rate of 150 breaths per min, with an inspiratory/expiratory ratio of 1:2. A positive end expiratory pressure equivalent to 2 cm H_2O was used to avoid lung atelectasis. These ventilatory parameters yielded optimal blood gas values in healthy aged-matched control rats in pilot experiments. Lung mechanics were recorded 2 minutes after sigh breaths (2.5 x V_T) at 2, 10 and 20 min.

After 20 minutes of ventilation, a midline laparotomy was performed and 100 µl of blood was drawn from the aorta using a 25G needle attached to a 1ml syringe pre-coated with heparin (porcine heparin sodium, David Bull Laboratories, Mulgrave, VIC, Australia). Air was expelled and blood gas analysis was performed immediately (ABL-5 Blood Gas Analyser, Radiometer, Copenhagen, Denmark). The rat was exsanguinated, ventilation was ceased and the lungs and mediastinum were removed *en bloc*, with the tracheal cannula *in situ* (Figure 2.14). The right upper lobe of the lung was tied off with 3.0 silk suture, excised and transferred to a pre-weighed 1.5ml tube. The excised lung tissue was weighed (wet weight) and set aside for overnight freeze-drying (Dynavac Freeze Drier, Adelab Scientific, Adelaide, SA, Australia) and subsequent determination

of the wet:dry weight ratio. The lungs and heart were suspended in a 50 ml beaker of chilled (4°C) 0.9% NaCl, with the proximal end of the trachea above the fluid level. The lung was degassed in a water vacuum-chamber for 1 min prior to bronchoalveolar lavage. Two ml of chilled 0.9% NaCl was injected into the lungs via the tracheal cannula. The saline was aspirated and reinjected a total of three times, the aspirate was transferred to a 50 ml centrifuge tube (Beckton Dickinson, NJ, USA) and the volume was recorded. The process was repeated twice for a total injected volume of 6 ml 0.9% NaCl. Following centrifugation (150 g for 10 minutes) the supernatant was collected and frozen (-20°C) for later total protein quantification.

Figure 2.13 Mechanical ventilation of an 18 day old F344 rat. Rats were anaesthetised and paralysed prior to the insertion of an endotracheal cannula and the commencement of mechanical ventilation with 100% oxygen.

Figure 2.14 Bronchoalveolar lavage of neonatal rat lungs. Following 20 minutes of mechanical ventilation, arterial blood was collected for gas analysis, the rat was exsanguinated and the heart and lungs were removed *en bloc*. The right upper pulmonary lobe was ligated and excised, the lungs were degassed and bronchoalveolar lavage was performed by instilling chilled saline into the lungs via the endotracheal cannula.

2.5.   STATISTICAL ANALYSIS

The statistics program SPSS v11.0.2 (SPSS Inc, Chicago, IL) was used for all statistical analyses.

2.5.a.   Retinal avascular area and vascular morphology

Prior to statistical analysis, percentages were transformed with the angular (arcsin) transformation in order to normalise the variances of the data [321]. The transformed data were analysed using analysis of variance, including repeated measures designs where appropriate. Comparisons between subsets of data were made with pre-planned single degree of freedom contrasts, Ryan-Einot-Gabriel-Welsch F tests (REGWF tests) or Bonferroni tests, with significance levels (alpha) set at 0.05 in each case. Summary data were expressed as means with 95% confidence intervals (95% CI). Chi-Square and Kruskall Wallis tests were used for the analysis of vascular morphology data.

2.5.b.   Real-time PCR data

The gene expression data were transformed ($\log_{10}$) and subjected to tests of homogeneity of variance: Levene's test of equality of error variance ($p>0.05$) and quantile plots (Q-Q plots) of residual values were used. In all cases transformed expression data were normally distributed and thus two-way analysis of variance was used to compare gene expression amongst different experimental groups. Bonferroni adjustment was made for multiple comparisons, with significance levels (alpha) set at 0.05. Detailed accounts of the methodologies used in the normalisation of gene expression data and in relative quantification are provided in Chapter 4 (sections 4.2.b and 4.2.c).

CHAPTER 3

RESULTS

STRAIN-DEPENDENT DIFFERENCES IN RAT

OXYGEN-INDUCED RETINOPATHY

3. CHAPTER 3: RESULTS – strain comparison of oxygen-induced retinopathy

3.1.   INTRODUCTION

3.1.a.   Overview

Animal models of oxygen-induced retinopathy (OIR) have provided many valuable insights into the pathogenesis of human retinopathy of prematurity (ROP). This chapter describes the identification and characterisation of strain-dependent differences in the susceptibility of inbred rats to OIR. The effect of strain on susceptibility to OIR is shown to be independent of other putative risk factors including birth weight, litter size and respiratory dysfunction. The chapter also details cross-breeding experiments between relatively resistant and susceptible rat strains, which provide evidence for the heritability of susceptibility to OIR. Collectively, these experiments provide strong evidence for the importance of genetic factors in the risk of OIR. The potential significance of these risk factors for human ROP is discussed.

3.1.b.   Risk factors for OIR

The need for more precise retinopathy risk stratification in premature human infants is clear and pressing. Owing to obvious ethical considerations, studies involving human infants are limited in scope. Animal models of OIR are therefore indispensable for the study of human ROP. All OIR models share two key features in common – an initial hyperoxic exposure, causing attenuation of the normal process of postnatal vascular development; and a subsequent hypoxic period, inducing retinal vascular proliferation (section 1.5.d.2). In most instances, the second phase involves the exposure of animals to room air – an exposure that constitutes relative hypoxia for the poorly vascularised, but metabolically active retinae – rather than to ambient hypoxia. The two stages of OIR recapitulate the biphasic nature of human ROP.

Animals differ in their susceptibility to OIR, and also in the extent to which the retinopathy resembles human ROP (reviewed by Madan *et al.* [322]). In comparison with mice, cats and dogs, rats are relatively resistant to OIR [323-327]. Accordingly, retinopathy is more consistently induced in rats by alternating cycles of hyperoxia and hypoxia during the first phase of the model, than by hyperoxia alone [311, 313] [312]. Cycles of hyperoxia and hypoxia are thought to approximate the fluctuations in arterial oxygen tension that are experienced by premature human infants at risk of ROP [252,

314]. The OIR model used in this work had, as its initial exposure phase, 14 alternating 24-hour cycles of hyperoxia (80% oxygen in air) and relative hypoxia (21% oxygen in air) – referred to as *cyclic hyperoxia* (section 2.4.c.2). A subsequent four day period in the relative hypoxia of room air constituted the second phase of the model. The pattern of retinopathy induced by cyclic hyperoxia in the rat is similar to that seen in premature human infants – neovascularization typically occurs just posterior to the vascularizing front, and adjacent neovascular tufts occasionally unite to form a pre-retinal ridge [322]. However, the model also differs from human ROP in several respects. The concomitant proliferation of connective tissue with neovascularization is limited, such that the formation of a true fibrovascular ridge – a pathognomonic feature of human ROP – is rare, as is retinal detachment [311, 313, 322]. OIR in rodents regresses spontaneously in almost all cases and neovascularization persists for a relatively short period of time [312, 328]. Furthermore, rats and other animals used in models of ROP are not premature and therefore lack many of the comorbidities of premature infants, such as problems resulting from pulmonary and gastrointestinal immaturity. Many of these comorbid ailments have the potential to modulate the risk ROP and its rate of progression. Despite these shortcomings, animal OIR models are still of value in the study of human ROP [311, 326].

Human ROP and animal models of OIR share several risk factors for disease severity. In rats, the extent of the avascular area in the peripheral retina has been correlated with both the risk of neovascularization and its severity – the larger the avascular area following the initial hyperoxic phase of the model, the greater the subsequent risk of hypoxia-induced proliferative disease [251, 312, 313, 323]. A similar association applies in ROP – the more posterior the zone of vascular arrest, the higher the risk of severe disease [208]. In other studies of OIR, the severity of retinopathy has been associated with metabolic acidosis [329] and with increased inspired carbon dioxide levels [330-332]. Acidosis and hypercarbia are often associated with severe illness in premature infants and may contribute to the increased prevalence of the disease in the sickest infants. As is the case in ROP, OIR risk is correlated with growth retardation – the incidence and severity of retinopathy are greater in malnourished rat pups raised in large, expanded litters, than in well-nourished pups from small litters [318, 333]. Furthermore, early postnatal insulin-like growth factor-1 deficiency appears to be a risk

factor for retinopathy in mice and premature human infants alike [58, 59].

Evidence is mounting for an effect of genetic factors on the risk of neovascularization in mice and in rats. A recent study has identified differences in the susceptibility of two rat strains – the Brown Norway (BN) and the Sprague Dawley (SPD) – to OIR [334]. The BN strain was significantly more susceptible to OIR than was the SPD strain. It was concluded that differences in the ischaemic regulation of the pro-angiogenic factor VEGF, and the anti-angiogenic factor pigment epithelium-derived factor (PEDF), were responsible for the strain difference. It was also suggested that differences in ocular pigmentation may have contributed to the strain difference in susceptibility to neovascularization. This stance was supported by another study of ocular angiogenesis in the rat. In a model of VEGF-induced choroidal neovascularization, vascular proliferation was more advanced in two pigmented rat strains – BN and Long Evans – than in two albino strains – Lewis and Wistar-Kyoto [335]. However the association between ocular pigmentation and retinopathy is far from straight-forward – other work has demonstrated greater susceptibility of albino rats, than pigmented rats, to ischaemic retinal injury [336] and to retinal gliosis following trauma and inflammation [337]. Furthermore, epidemiological studies of human ROP confirm that the association between ocular pigmentation and retinopathy risk is not simple – African American infants appear to be at lower risk of severe disease than Caucasian infants [208]; however Alaskan native infants are at higher risk [285] (section 1.5.e). It is likely that genetic factors, other than those regulating ocular pigmentation, may contribute to the risk of OIR. In support of this hypothesis, the risk of OIR has been shown to vary considerably between different two different populations of the same inbred rat strain raised under similar environmental conditions [338].

Strain-related heterogeneity of ocular angiogenesis in rodents is not limited to the retina. Rohan *et al.* have identified murine strain-dependent variation in the corneal response to angiogenic factors [339] – corneal stromal implantation of basic fibroblast growth factor (bFGF)-impregnated micropellets was associated with angiogenesis that differed by up to 10-fold amongst strains. Similar heterogeneity was seen in the response to VEGF. Chan *et al.* have demonstrated that the extent of the resting limbal vasculature differs considerably amongst mouse strains and is predictive of the response to bFGF in the

corneal neovascularization model [340]. Together, these studies suggest that genetic factors play important roles in regulating angiogenesis.

Of the various animal and human studies implicating genetic factors in the risk of ROP, none have provided direct evidence of a heritable susceptibility trait. Accordingly, the overarching aims of these experiments were to identify whether inbred rat strains differed in their susceptibility to OIR and, if so, to determine the heritability of the susceptibility trait. In addition, these experiments sought to clarify the role played by ocular pigmentation in the risk of OIR.

Thus the specific aims of this work were to:

- systematically compare the susceptibilities of 6 different rat strains to OIR.
- examine the heritability of the identified susceptibility trait in the offspring of matings between OIR-susceptible and OIR-resistant rat strains.
- test the association between ocular pigmentation and susceptibility to OIR.

The rats selected for study included five inbred strains – Fischer 344 (F344), Lewis (LEW), Wistar Furth (WF), Sprague Dawley (SPD) and Dark Agouti (DA) – and a single outbred strain – Hooded Wistar (Figure 3.1). Each of the inbred strains constituted a genetically homogeneous population (section 2.1.e.2). Two of the 6 strains – the DA and HW – have ocular pigmentation, while the remainder are albino. A brief account of the genealogy of these rat strains is provided in Appendix 1.
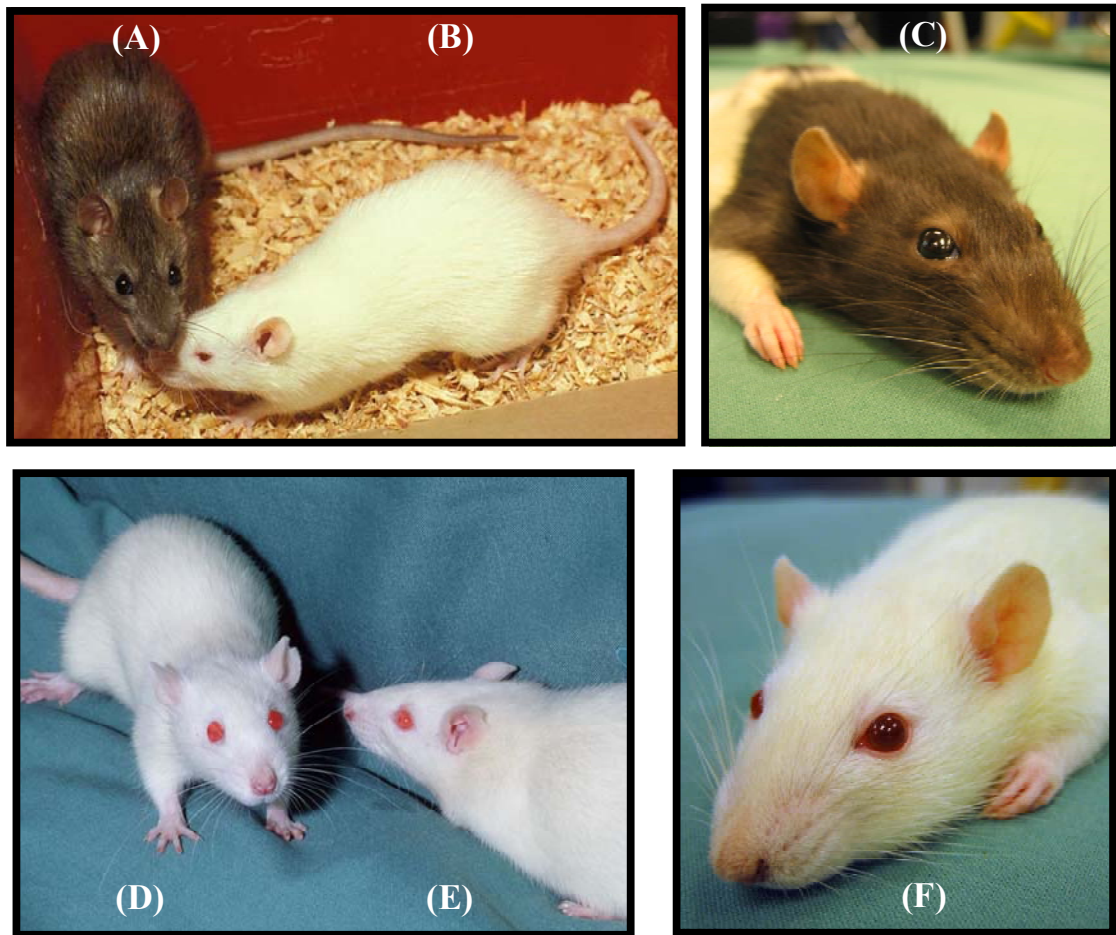
Figure 3.1 Rat strains examined in this thesis. Five inbred strains and a single outbred strain were used in studies of OIR. (A) Dark Agouti & (B) Fischer 344; (C) Hooded Wistar (outbred); (D) Wistar Furth & (E) Sprague Dawley; (F) Lewis. Note the dark brown eye colour of the DA and HW strains and the red eye colour of the albino strains.

3.2.   RESULTS

3.2.a.   Strain comparisons of retinal vascularization in normoxia

Control rats of each strain were raised in room air from the time of birth. The extent of retinal vascularization in control rats was assessed after either one day, or 14 days of room air exposure. Fluorescence microscopy and video image analysis were used to measure the extent of vascularization in whole, flat-mounted retinae, stained with the endothelial cell marker isolectin GS-IB4 (section 2.4.c). Preliminary experiments had demonstrated that labelling of the retinal vasculature was more complete with isolectin GS-IB4 than with ink perfusion (section 2.4.b) – perfusion was often incomplete and nascent vessels lacking lumens were not labelled (Figure 3.2). Accordingly, isolectin-labelling was used in preference to ink perfusion.
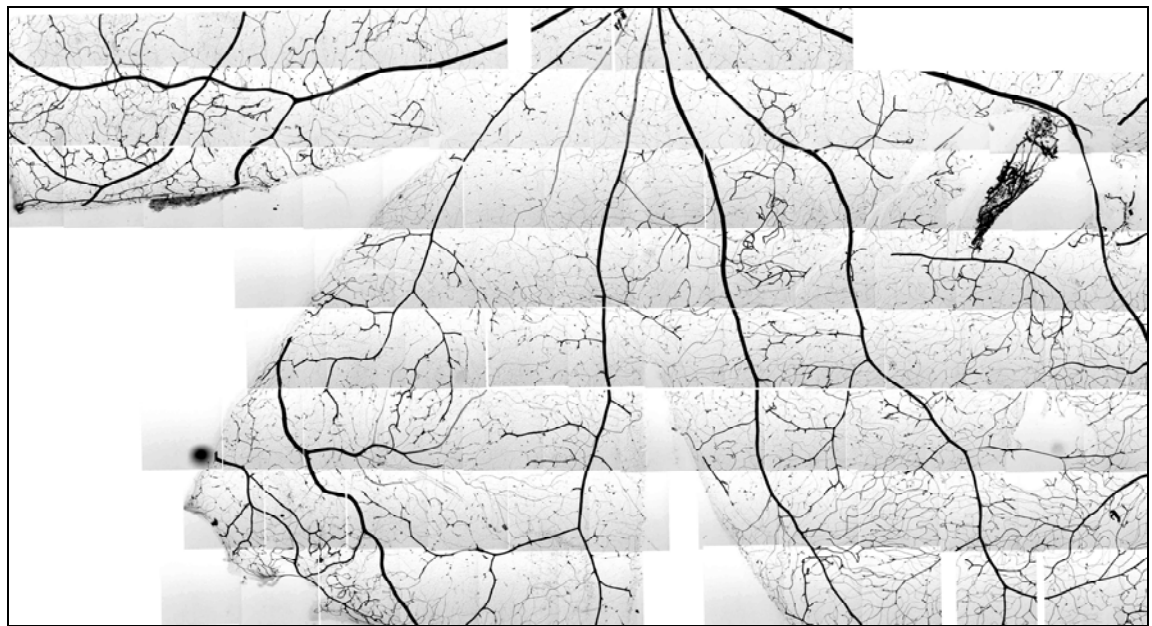
Figure 3.2 Partial montage image of an ink-perfused adult rat retina. Pilot experiments were performed to test the adequacy of ink-perfusion for the quantification of retinal vascular extent. As is illustrated, vascular perfusion was often incomplete, precluding accurate vascular area quantification. Accordingly, vascular imaging was performed using fluorophore-conjugated isolectin GS-IB4.

As was expected, retinal vascularization was limited in one day-old rats, and nearly complete in 14 day-old rats (Figures 3.3, 3.4 & 3.5). Small but statistically significant differences in the extent of retinal vascularization were identified amongst control rats of different strains at the day one and day 14 time-points. Control rats raised in room air for one day segregated into two groups with respect to retinal avascular area: mean avascular areas were slightly but significantly larger for the F344, WF and DA strains (mean 86.5%; 95% CI 85.6-87.4%), than for the SPD, LEW and HW strains (mean 81.2%; 95% CI 80.2-82.3%) (p<0.001) (Figure 3.3; Table 3.1). Representative retinal montage images for each strain are provided in Figure 3.4.

Significant differences were also found in the size of the mean avascular retinal area amongst control rats of different strains following 14 days in room air (p<0.001) (Figures 3.3 & 3.5; Table 3.1). The central retina was fully vascularized in all strains by day 14 – differences were due entirely to variation in the extent of peripheral retinal vascularization. The peripheral avascular areas of the two pigmented strains, the HW and DA, were larger than those of other strains (p<0.05). Although the avascular area of HW rats was more than twice that of F344 rats, it was still less than 10% of the total retinal area.
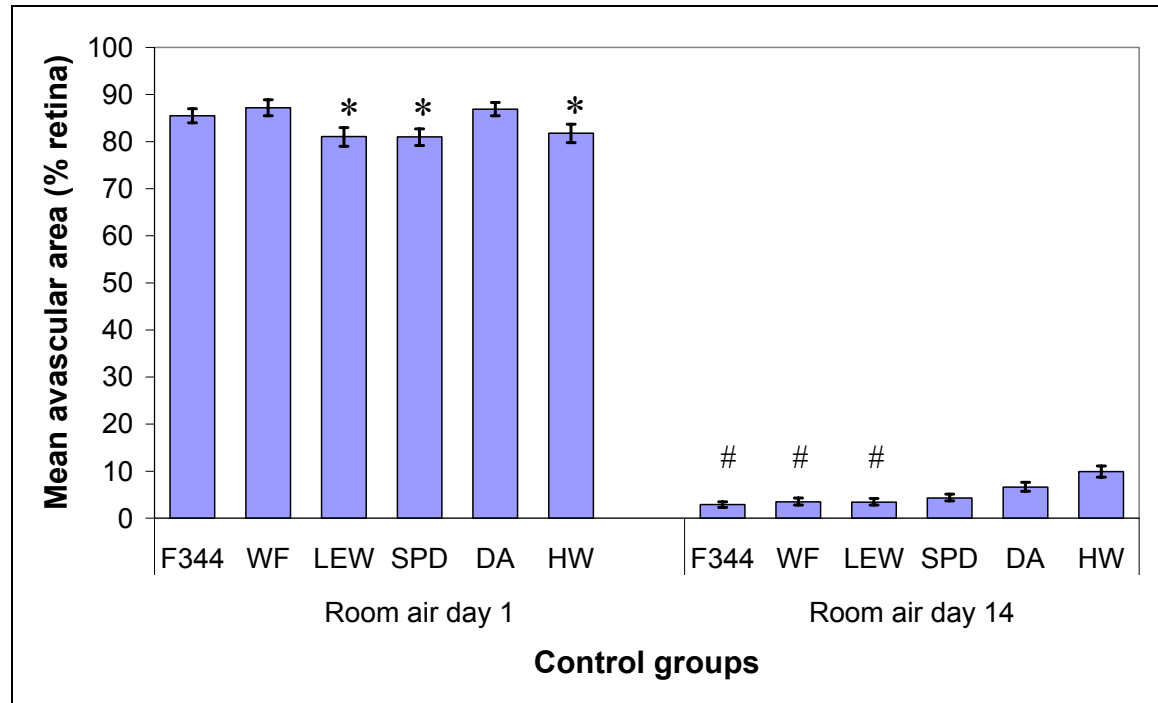
Figure 3.3 Retinal avascular area by strain for control rats exposed to room air for one day or 14 days. Newborn rat pups were exposed to room air for one day, or 14 days, prior to measurement of the extent of the avascular retinal area. Mean avascular area is presented as a percentage of the total retinal area. At day one, avascular areas were large in all strains. The area of avascular retina was slightly, but significantly smaller in rats of the LEW, SPD and HW strains than in rats of the other strains (* p<0.001). At 14 days all retinae were almost completely vascularized. The extent of the avascular area was marginally, but significantly smaller in F344, WF and LEW rats than in rats of the other strains (# p<0.001). Error bars: ± 95% CI. Room air day 1: *n*= 3-4 rats per strain. Room air day 14: *n*= 9-14 rats per strain.

Abbreviations:
F344: Fischer 344 rat strain
WF: Wistar Furth rat strain
LEW: Lewis rat strain

SPD: Sprague Dawley rat strain
DA: Dark Agouti rat strain
HW: Hooded Wistar rat strain (*outbred*)
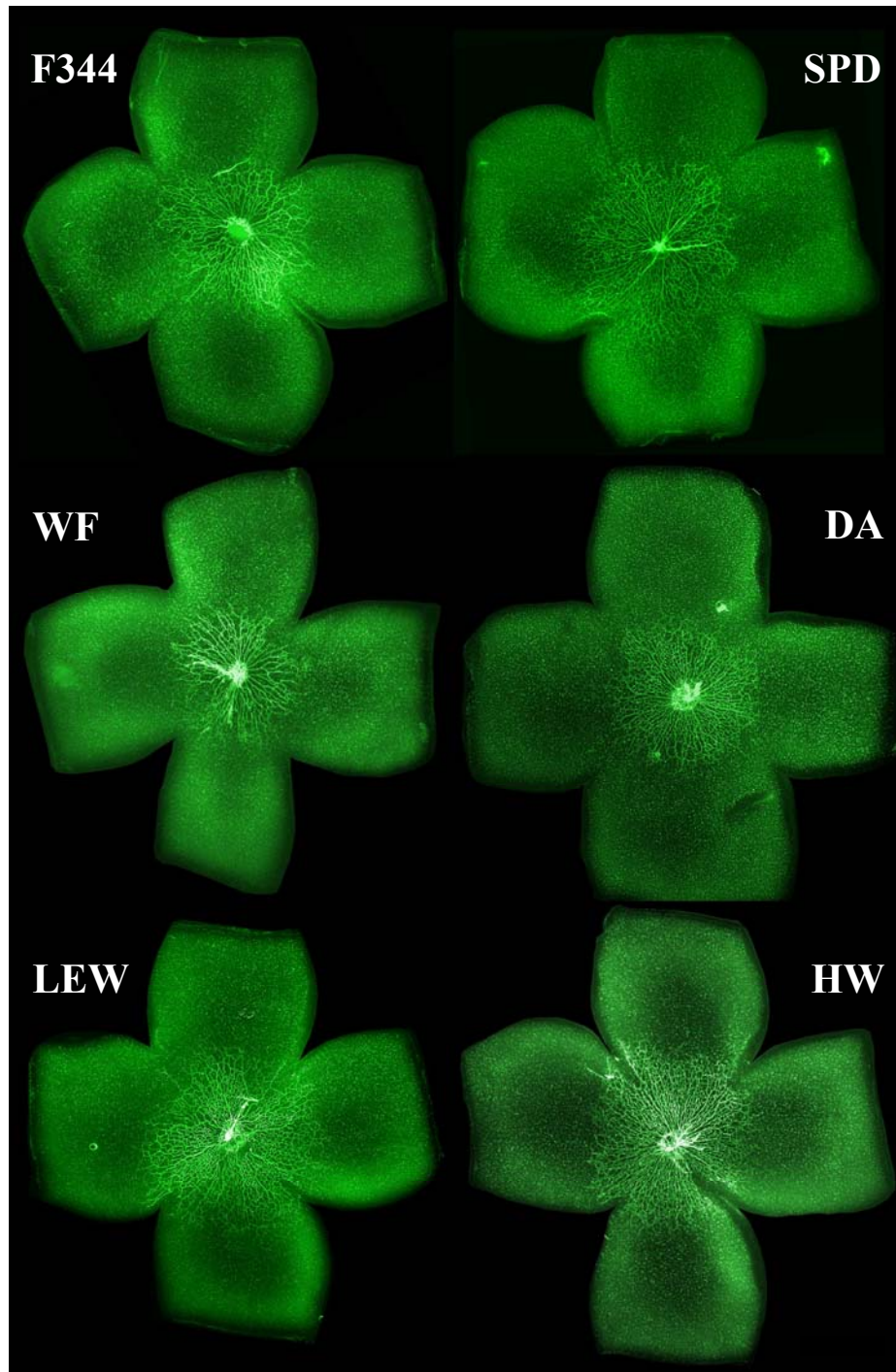
Figure 3.4 Representative images of the retinae of one day-old room air exposed control rats. Retinae were flat-mounted and stained with an endothelial cell label – fluorophore conjugated isolectin GS-IB4. Images were captured with a CCD-camera attached to a fluorescence microscope, and merged to form a single montage image for vascular analysis. Retinal vascularization was limited to a small central zone at this early stage in development. **F344**: Fischer 344; **SPD**: Sprague Dawley; **WF**: Wistar Furth; **DA**: Dark Agouti; **LEW**: Lewis; **HW**: Hooded Wistar.
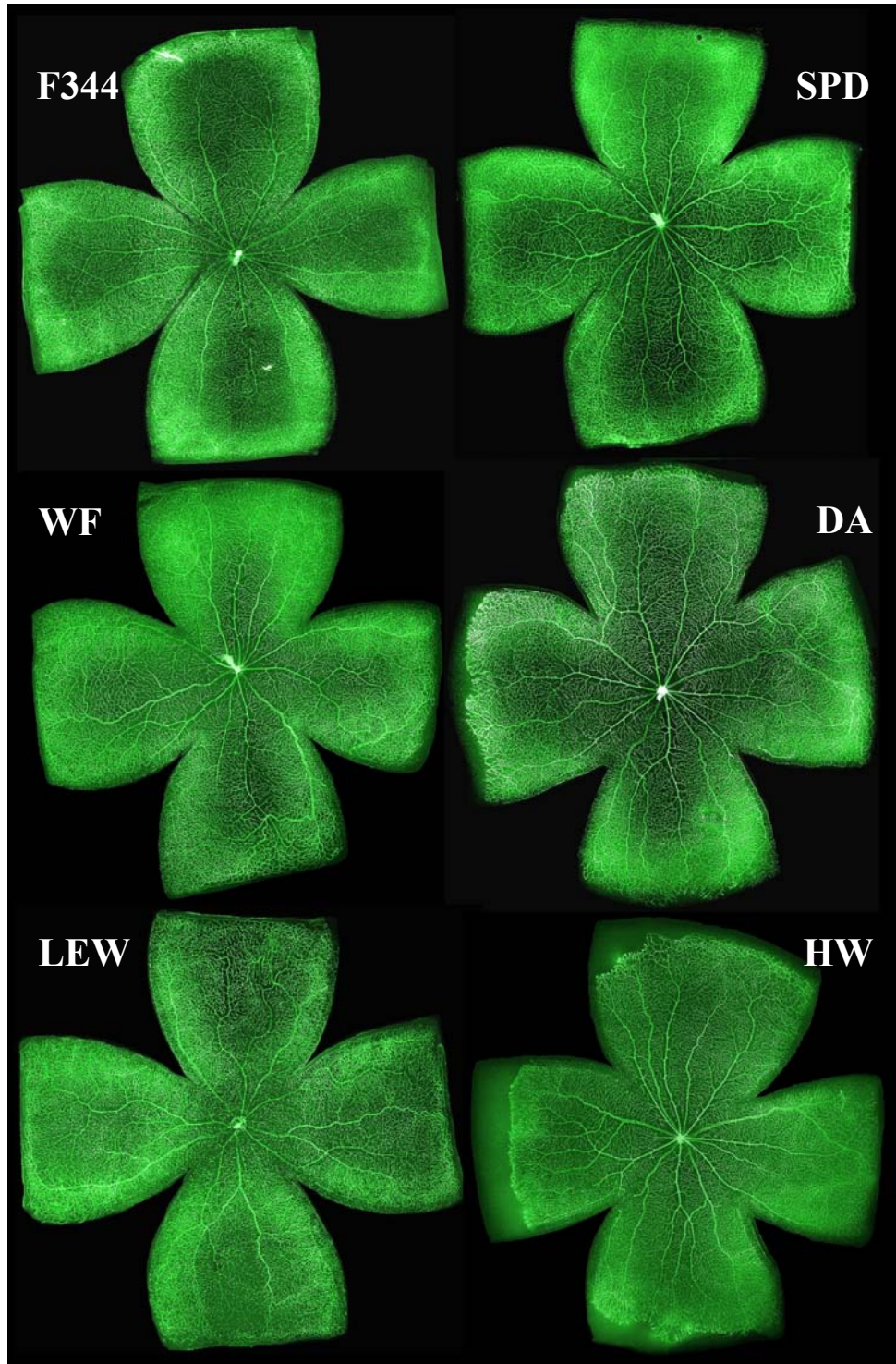
Figure 3.5 Representative images of the retinae of 14 day-old room air exposed control rats. Vascularization was almost complete in all strains by 14 days – small avascular zones remained in the extreme retinal periphery. **F344**: Fischer 344; **SPD**: Sprague Dawley; **WF**: Wistar Furth; **DA**: Dark Agouti; **LEW**: Lewis; **HW**: Hooded Wistar.

3.2.b. Strain comparisons of retinal vascularization following exposure to cyclic hyperoxia

3.2.b.1 Avascular retinal area

Rats exposed to cyclic oxygen for 14 days had significantly larger areas of avascular retina than rats exposed to room air for the same period (p<0.001) (Table 3.1; Figures 3.6 & 3.7). However the effect of oxygen exposure on total retinal avascular area differed amongst strains (p<0.001). Avascular areas were smallest for the F344, WF and LEW strains, larger for the SPD strain and largest for the DA and HW strains (p<0.05 per comparison).

At day 14, rats of all strains exposed to cyclic hyperoxia exhibited avascular areas in the central retina that were not seen in rats exposed to room air (Figures 3.6 & 3.7). The extent of central avascular area differed amongst strains (p<0.001): those of the F344, WF and LEW were smaller than those of other strains (p<0.05) (Table 3.1).

Rats exposed to cyclic hyperoxia had larger avascular areas in the peripheral retina at day 14 than did those exposed to room air (p<0.001). The size of peripheral avascular areas also differed amongst strains (p<0.001). Peripheral avascular areas of DA and HW rats were more than double those of F344, WF and LEW rats (p<0.05). The peripheral avascular area of SPD rats was less than those of DA and HW rats but greater than those of other strains (p<0.05 per comparison).

Mean litter sizes for oxygen exposed rats ranged from 6 to 10 for all strains and no association was found between litter size and retinal avascular area at day 14 (linear regression, r= 0.17, p= 0.13).

At day 18 (14 days of cyclic oxygen, followed by 4 days in room air) rats had total retinal avascular areas that were intermediate in size between those of the control groups and the oxygen exposed groups at day 14 (p<0.05 per comparison) (Figures 3.6 & 3.7; Table 3.1). Comparison between oxygen exposed rats at the day 14 and day 18 time-points yielded two key findings: (1) for all strains central retinal vascularization was

nearly complete by day 18; and (2) F344, WF and LEW rats had smaller peripheral avascular areas at day 18 than at day 14 ($p<0.05$ per comparison). In contrast, there were no significant changes in peripheral avascular area for SPD, DA and HW rats between these two time-points ($p>0.05$).
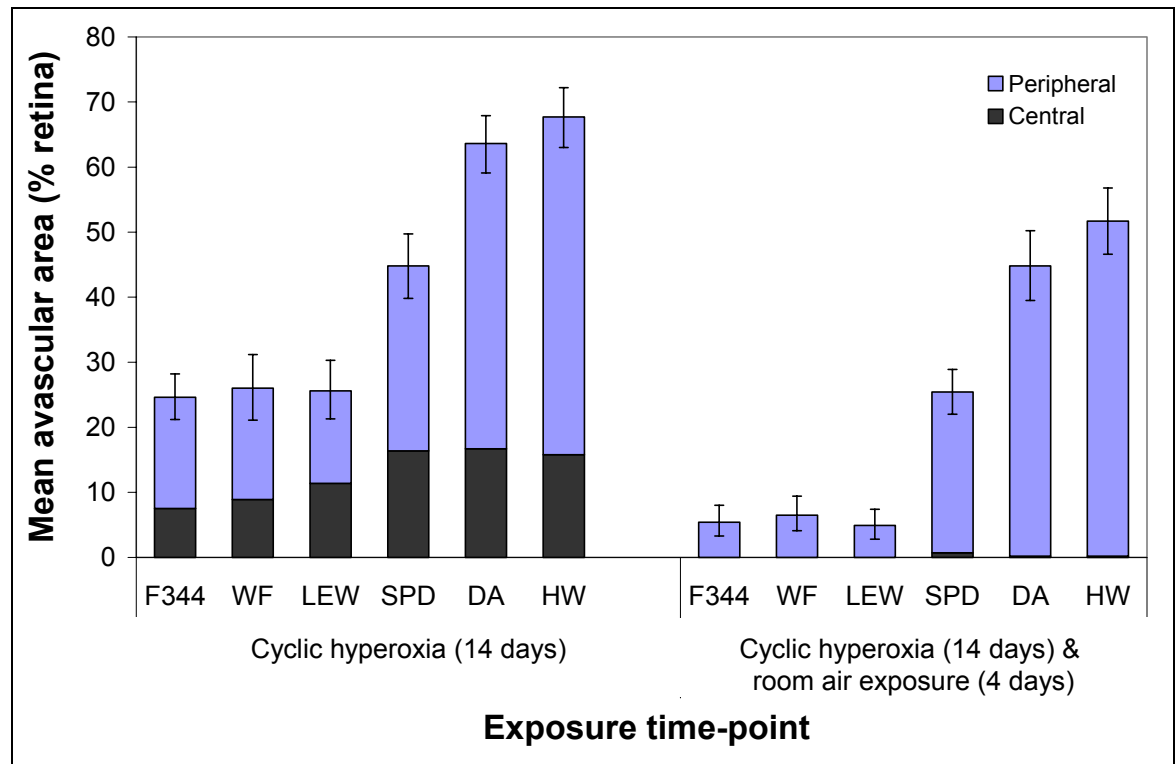
Figure 3.6 Retinal avascular area by strain for rats exposed to cyclic hyperoxia. Newborn rats of 6 strains were exposed to cyclic hyperoxia for 14 days. Retinal vascular analysis was performed at day 14 or following a further four days in room air (day 18). Mean central avascular area (peripapillary capillary-free zone) and peripheral avascular area (peripheral capillary-free zone, not in continuity with the optic nerve head) are presented as a percentage of the total retinal area. Error bars: ± 95% CI; *n*= 9-18 rats per group.
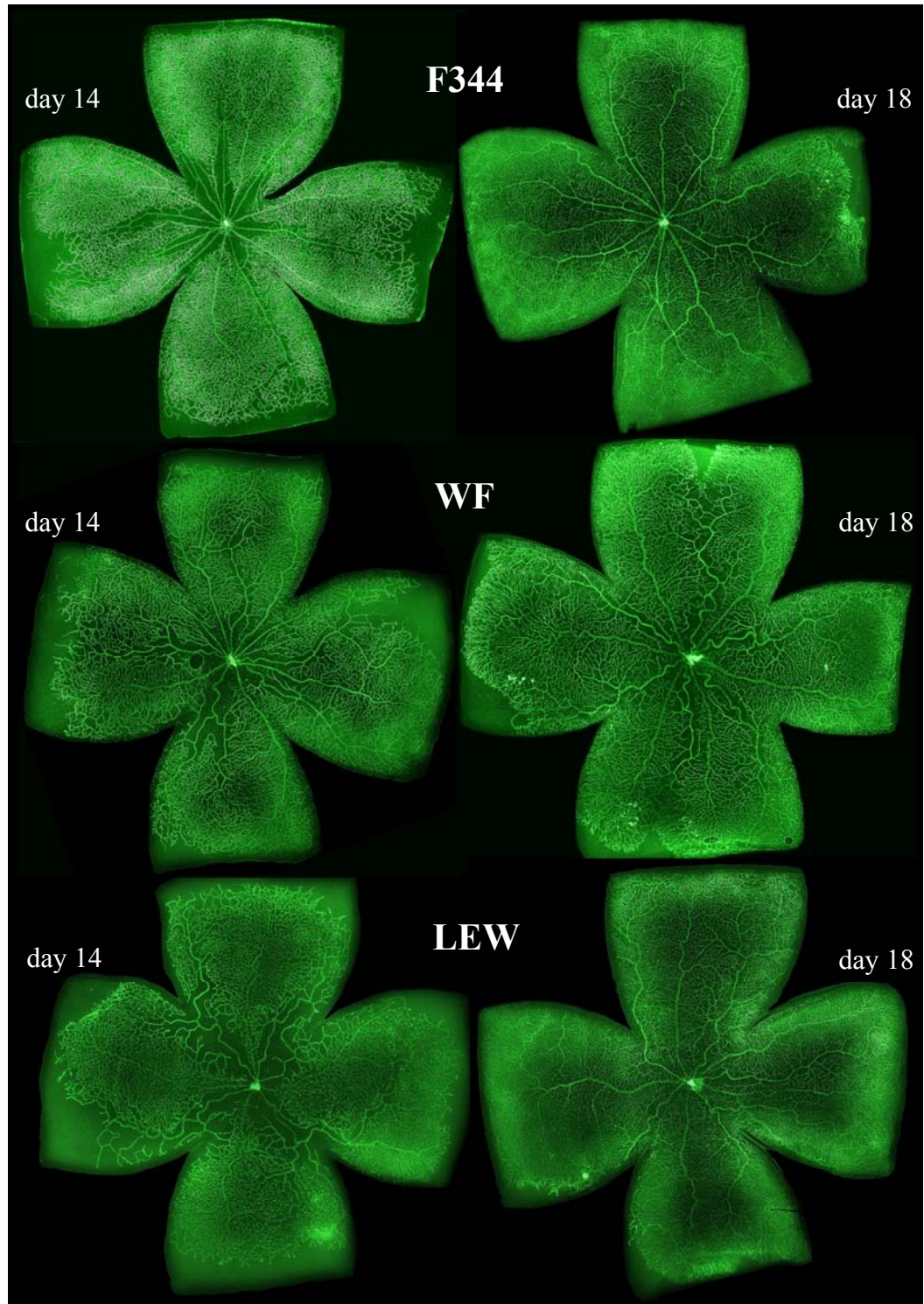
Figure 3.7 (A) Comparison of retinal vascular extent and morphology by strain, for rats exposed to cyclic hyperoxia at the day 14 and day 18 time points. Representative digital montage images of isolectin GS-IB4 labelled retinae. The Fischer 344 (**F344**), Wistar Furth (**WF**) and Lewis (**LEW**) strains were relatively resistant to cyclic hyperoxia – retinal avascular areas at day 14 were small and vascularization was near complete following a further 4 days in room air (day 18).
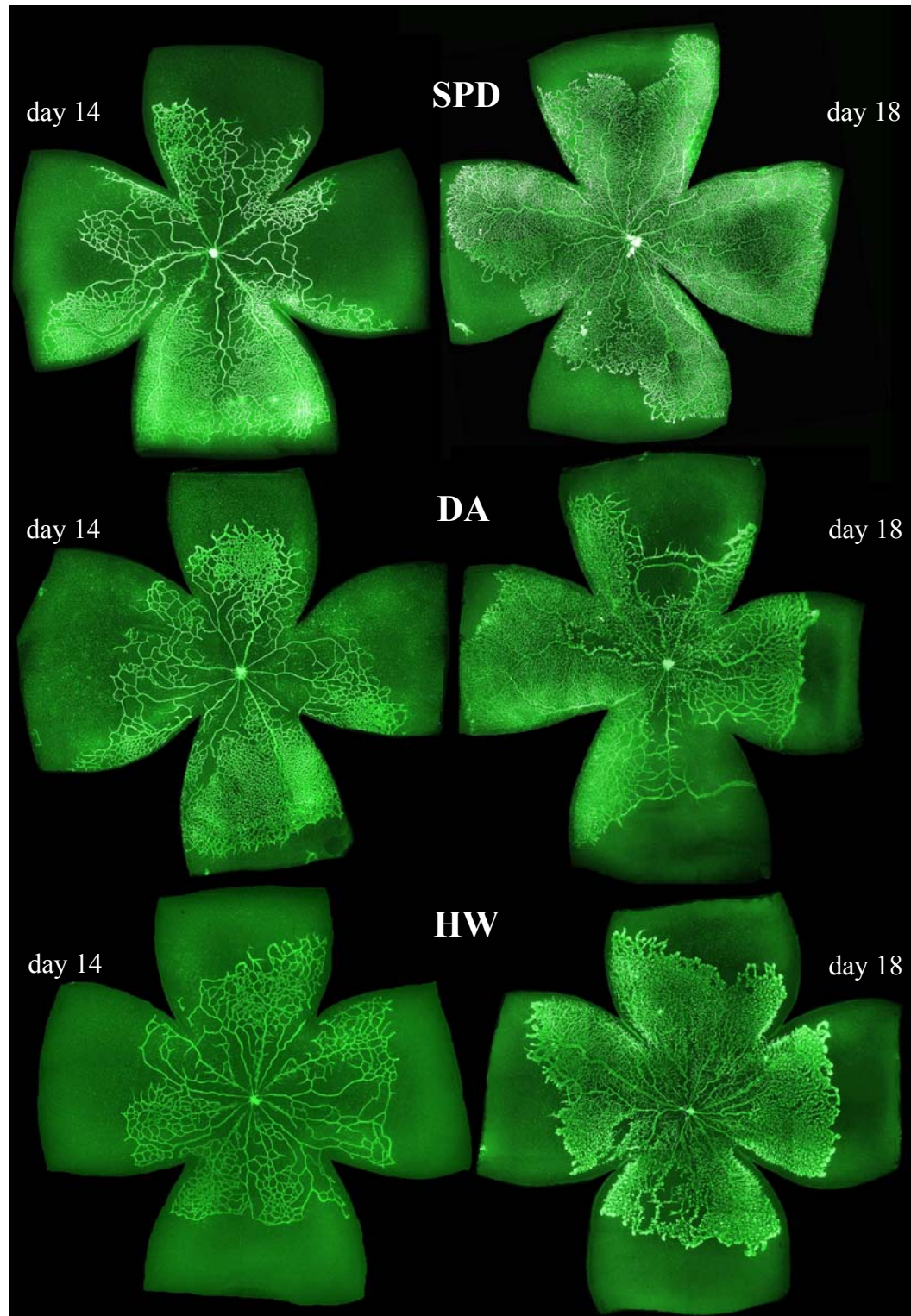
Figure 3.7 (B) Comparison of retinal vascular extent and morphology by strain, for rats exposed to cyclic hyperoxia at the day 14 and day 18 time points. Representative montage images are shown. The Sprague Dawley (**SPD**), Dark Agouti (**DA**) and Hooded Wistar (**HW**) strains were relatively susceptible to the attenuating effects of cyclic hyperoxia on retinal vascularization – avascular areas at day 14 were large. Dense central retinal vascularization occurred during a subsequent four day period in room air (day 18), without significant peripheral vascularization. Vascular morphology was abnormal.

Table 3.1 Retinal avascular areas of rats by strain following room air exposure or cyclic hyperoxia.

Strain	Day 1 (control)		Day 14 (control)		Day 14 (oxygen)		Day 18 (oxygen & room air)[*]	
	n[†]	% avascular[‡]	n	% avascular	n	% avascular	n	% avascular
F344	4	**85.5** (84.0-87.0)	12	**2.9** (2.3-3.5)	18	**24.6** (21.2-28.2)	11	**5.4** (3.3-8.0)
WF	3	**87.2** (85.5-88.9)	9	**3.5** (2.8-4.3)	9	**26.0** (21.1-31.2)	10	**6.5** (4.1-9.4)
LEW	3	**81.1** (79.0-83.0)	10	**3.4** (2.8-4.2)	11	**25.6** (21.3-30.3)	10	**4.9** (2.8-7.4)
SPD	4	**81.0** (79.2-82.7)	14	**4.3** (3.7-5.1)	12	**44.8** (39.8-49.7)	18	**25.4** (22.0-28.9)
DA	4	**86.9** (85.5-88.3)	11	**6.6** (5.7-7.6)	14	**63.6** (59.1-67.9)	10	**44.8** (39.5-50.2)
HW	3	**81.8** (79.8-83.7)	10	**9.9** (8.7-11.1)	12	**67.7** (63.0-72.2)	11	**51.7** (46.6-56.8)
TOTAL	21	**84.1** (83.3-84.7)	66	**4.8** (4.5-5.2)	76	**41.6** (39.6-43.6)	70	**20.7** (18.4-21.6)

[*] Exposed to cyclic hyperoxia for 14 days followed by 4 days of sustained room air exposure
[†] n = number of animals
[‡] Mean avascular area as a percentage of total retinal area (95% CI)

3.2.b.2 Vascular morphology

Retinal vascular morphology was assessed in flat-mounted retinae at the day 18 time-point. As pre-retinal neovascular tufts were relatively infrequent, the enumeration of preretinal endothelial cells in transverse retinal sections was not practicable. Instead, a semi-quantitative system was used to score vascular morphological abnormalities (section 2.4.c.5). Morphological abnormalities were defined as features not seen in the course of normal retinal vascularization, including regions of exceptionally dense vascular budding, vascular ridges, marked vascular dilatation and neovascular tufts. Vascular morphology data are summarised in Table 3.2; Figures 3.7 and 3.8 provide representative images. There were significant differences in clock hours of vascular morphological abnormality amongst strains ($\chi^2_{(60)} = 142.7$, p<0.001). The F344, WF and LEW strains had fewer clock hours of abnormality than the SPD strain which, in turn, had fewer than the DA and HW strains. Tortuosity of the major retinal vessels was minimally increased for F344, DA and HW rats, moderately increased for WF rats and markedly increased for LEW and SPD rats, relative to room air controls (Table 3.2; Figure 2.12). Photographs of representative histological sections demonstrating pre-retinal neovascular tufts are provided in Figure 3.9.

Table 3.2 Abnormal retinal vascular morphology and vascular tortuosity of cyclic oxygen exposed rats analysed by strain at day 18.

Strain	n^{*}	Abnormal morphology,[†] median (range)	Vascular tortuosity,[‡] median (range)
F344	11	2 (2,4)	2 (1,2)
WF	10	3 (0,7)	3 (2,4)
LEW	10	3 (0,5)	4 (3,4)
SPD	18	7 (2, 9)	4 (3,4)
DA	10	11 (8,12)	2 (2,3)
HW	11	12 (9,12)	2 (2,3)

[*] n = number of rats.
[†] Clock hours (0-12) of retina with morphological abnormality, including dense vascular budding, vascular ridges, vascular dilatation and neovascular tufts.
[‡] Vascular tortuosity (1-4) from normal (1), to markedly increased (4).
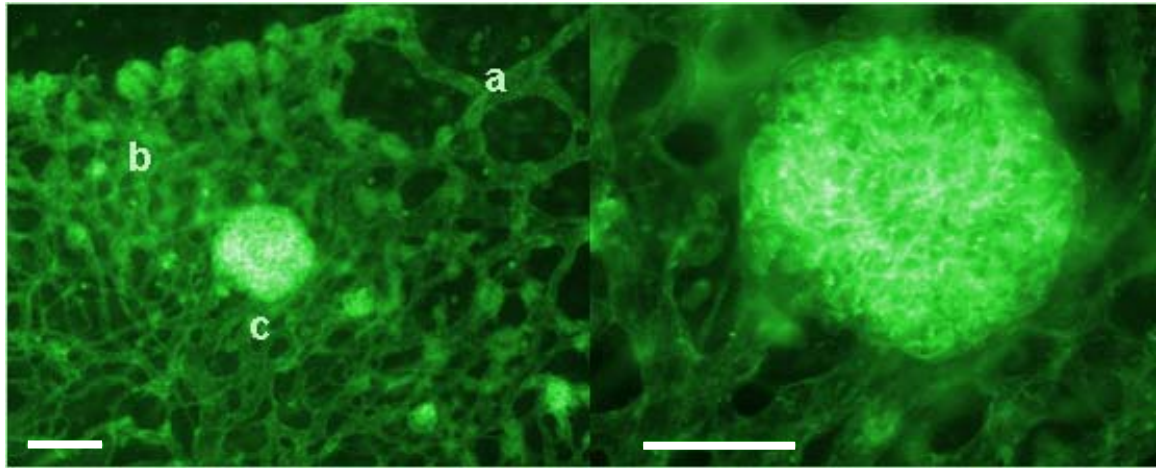
Figure 3.8 Retinal vascular morphological abnormalities. A representative image of vascular morphological abnormalities seen in the retina of an 18-day-old SPD rat exposed to cyclic hyperoxia for the first 14 days of life. Dilated vessels (a) and dense capillary networks (b) are apparent. A large glomerular neovascular tuft (c) is seen projecting anterior to the underlying retina. This is shown at higher magnification in the right-hand panel (scale bar = 100 μm).
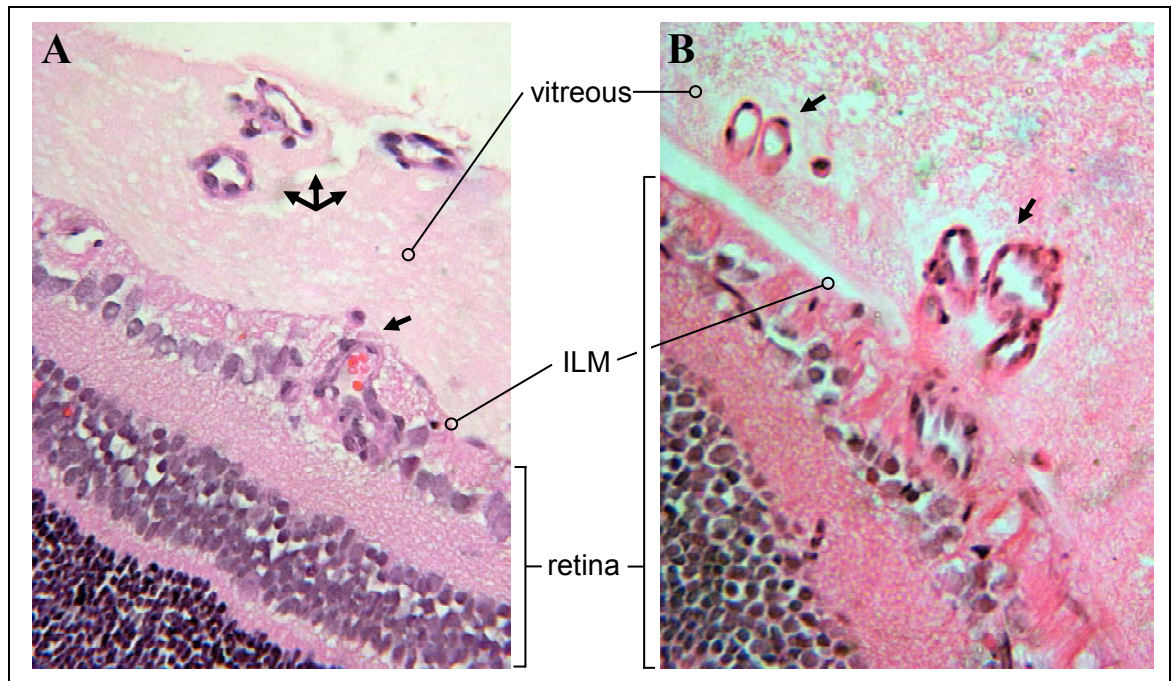
Figure 3.9 Retinal neovascularization. Representative histological sections of pre-retinal neovascular tufts in two 18-day-old Dark Agouti rats (A and B) following exposure to the oxygen-induced retinopathy model. Retinal vessels breach the inner limiting membrane (ILM) and proliferate in the vitreous humour (black arrows). Original magnification 200x prior to resizing.

3.2.c. Body mass

There were significant strain differences in body mass amongst control rats raised in room air for 14 days (p<0.001) (Table 3.3). SPD rats were significantly heavier than HW rats, which in turn were heavier than rats of other strains (p<0.05 per comparison). Across all strains oxygen exposure had a small, but statistically significant inhibitory effect on mass (mean difference 1.67g; 95% CI 0.36-2.98g, p= 0.013). However, when mass was used as a covariate, there was no change in the strength of association between strain and retinal avascular area – only 10% of the strain difference in avascular area could be attributed to differences in mass ($r^2 = 0.10$).

Table 3.3 Relationship between rat body mass and exposure to room air or cyclic oxygen.

Strain	Day 14 (control)		Day 14 (oxygen)		Day 18 (oxygen & room air recovery)	
	n^*	Body mass, g mean (95% CI)	n	Body mass, g mean (95% CI)	n	Body mass, g mean (95% CI)
F344	12	**24.4** (22.1-26.6)	18	**21.2** (19.4-23.0)	11	**26.7** (24.4-29.0)
WF	9	**26.3** (23.8-28.9)	9	**25.3** (22.8-27.9)	10	**28.8** (26.3-31.2)
LEW	10	**27.1** (24.7-29.5)	11	**26.9** (24.6-29.2)	10	**36.7** (34.3-39.1)
SPD	14	**37.5** (35.5-39.6)	12	**36.6** (34.4-38.8)	18	**45.9** (44.1-47.8)
DA	11	**24.0** (21.7-26.3)	14	**22.5** (20.5-24.6)	10	**31.9** (29.5-34.3)
HW	10	**33.2** (30.7-35.6)	12	**29.9** (27.7-32.1)	11	**41.2** (38.8-43.5)

* n = number of animals.

3.2.d. Respiratory function

Sustained exposure to hyperoxia is known to induce lung injury in rats [341, 342]. Strain differences in the susceptibility to hyperoxic lung injury may lead to differences in retinal oxygen delivery and in the severity of OIR. Oxygen-exposed rats of two strains, the relatively OIR-resistant F344 and the relatively OIR-susceptible DA, were selected for a comparative study of susceptibility to hyperoxia-induced lung injury. Anaesthetised rats were mechanically ventilated with 100% oxygen for 20 minutes prior to arterial blood gas analysis, bronchoalveolar lavage and assessment of wet and dry

lung weights (section 2.4.d). The technical challenges of ventilating such small animals necessitated the use of 18 day-old rats. Accordingly, for these experiments alone, rats were exposed cyclic hyperoxia for 18 days, as opposed to the conventional 14 days. It was thought that prolonged exposure to cyclic hyperoxia might exacerbate, rather than diminish hyperoxia-induced lung injury, making it more readily detectable. Despite this prolonged exposure, no statistically significant differences were found in arterial blood gas parameters between rats of the F344 and DA strains immediately after the period of ventilation ($p > 0.05$) (Figure 3.10). In addition, there were no significant strain differences in the protein concentration of bronchoalveolar lavage fluid (Figure 3.11). Lung wet-to-dry weights were marginally, but significantly lower for F344 rats than for DA rats ($p = 0.008$; two-tailed Mann-Whitney U-test) (Figure 3.12). Ventilator-derived measurements of lung mechanics were uninterpretable, owing to the small size of the 18 day-old rats. Thus, the different retinal responses of F344 and DA rats to cyclic hyperoxia could not be attributed to underlying differences in lung function.
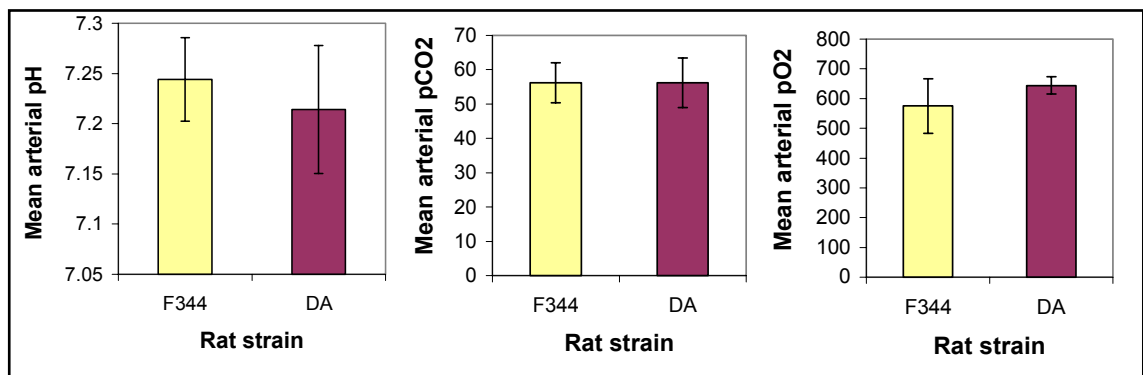
Figure 3.10 Arterial blood gas comparisons between cyclic hyperoxia exposed F344 and DA rats following 20 minutes of mechanical ventilation with 100% oxygen. Newborn rats were exposed to cyclic hyperoxia for 18 days. Rats were anaesthetised and mechanically ventilated with 100% oxygen prior to blood gas analysis. Error bars: $\pm$ standard deviation (SD); *n* = 5 rats per strain. Abbreviations: F344: Fischer 344 rat strain; DA: Dark Agouti rat strain; pCO_2: partial pressure of carbon dioxide (mmHg); pO_2: partial pressure of oxygen (mmHg).
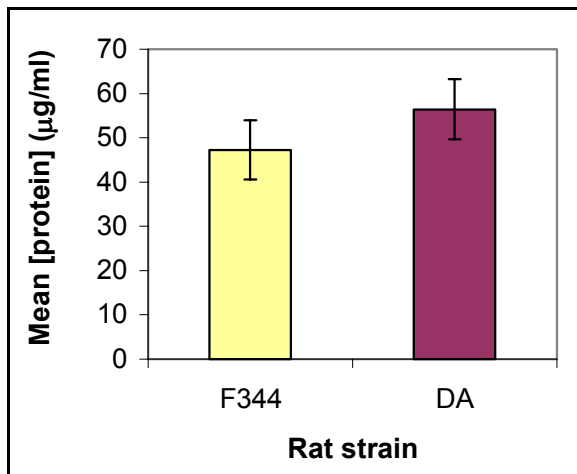
Figure 3.11 Strain comparison of bronchoalveolar lavage fluid protein concentrations. Newborn rats of the Fischer 344 (F344) and Dark Agouti (DA) strains were exposed to cyclic hyperoxia for 18 days. Rats were anaesthetised and mechanically ventilated with 100% oxygen prior to bronchoalveolar lavage with chilled isotonic saline. Samples were centrifuged and the protein concentrations were estimated using the Bradford method. Error bars: $\pm$ SD. n(F344) = 4; n(DA) = 5.
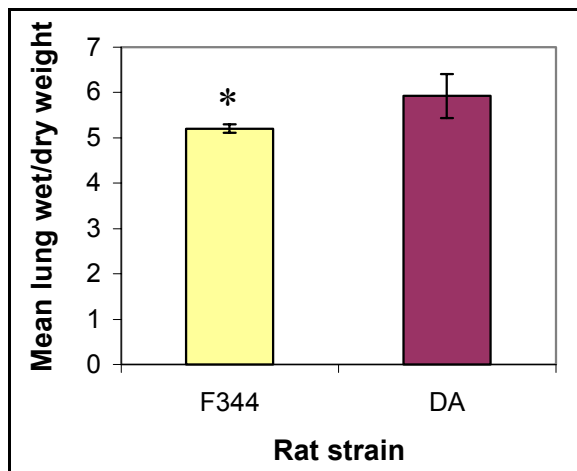
Figure 3.12 Lung wet-to-dry weight ratios. Newborn rats were exposed to cyclic hyperoxia for 18 days prior to mechanical ventilation with 100% oxygen for 20 minutes. Following ventilation, each rat was killed and the right upper pulmonary lobe was ligated and excised. The wet mass of the excised tissue was recorded. The tissue was freeze-dried overnight and reweighed. The ratio of wet mass to dry mass was determined. Error bars: $\pm$ SD. n = 5 rats per strain. * p =0.008.

3.2.e. A hereditary basis for susceptibility to OIR: cross-breeding studies

The heritability of strain differences in susceptibility to OIR was examined in a series of cross-breeding experiments. The F344 and DA rat strains were selected as representative of relatively OIR-resistant, and OIR-susceptible strains, respectively. Each genetic cross was performed twice, and different gender pairings were used in each cross. All of the offspring of each cross were exposed to cyclic hyperoxia for the first 14 days of life, prior to retinal vascular area measurement (section 2.4.c).

3.2.e.1   The susceptibility of the offspring of F344 x DA crosses to OIR

All of the offspring of the two F344 x DA inter-crosses, deemed the F_1 generation, had ocular and coat pigmentation that was similar to that of the DA strain – eye colour was dark brown; coat colour was agouti, with white patches on the abdomen and paws (Figure 3.13). The mean retinal avascular area of F_1 rats exposed to cyclic hyperoxia for 14 days was 72.8% (95% CI: 68.6-76.9%) of the total retinal area (Figure 3.14). All oxygen exposed F_1 pups had large avascular regions in the central and peripheral retina (Figure 3.15). The extent of the retinal avascular area of F_1 rats was slightly larger than that of oxygen exposed pups of the DA parental strain at the same time-point (mean difference 1.1%; 95% CI: 0.02-3.8%; p= 0.02) and substantially larger than that of the F344 parental strain (mean difference 23.6%; 95% CI 16.7-31.3%; p<0.001) (Figures 3.14 & 3.15).

Figure 3.13 14 day-old F1 rat pups. The offspring of crosses between DA and F344 rats, the F1 generation, resembled the DA parental strain, having similar coat and eye colour.
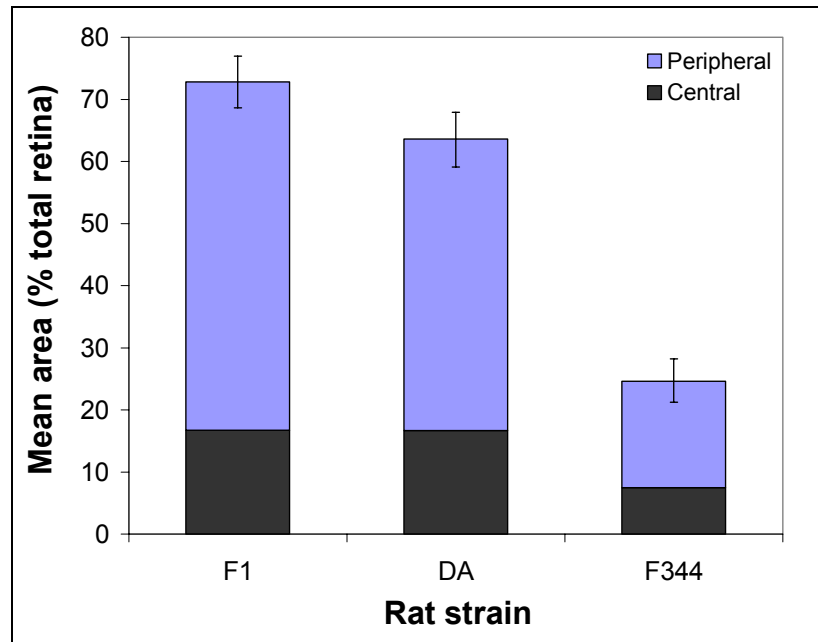
Figure 3.14 Retinal avascular area for rats exposed to cyclic hyperoxia for 14 days. Newborn pups of the DA and F344 rat strains, as well as F_1 pups – the offspring of crosses between DA and F344 rats – were exposed to cyclic hyperoxia for 14 days. The mean central avascular area and peripheral avascular area for each group are presented as percentages of the total retinal area. Error bars: $\pm$ 95% CI; $n(F_1)$ =16; n(DA) =14; n(F344) =18.
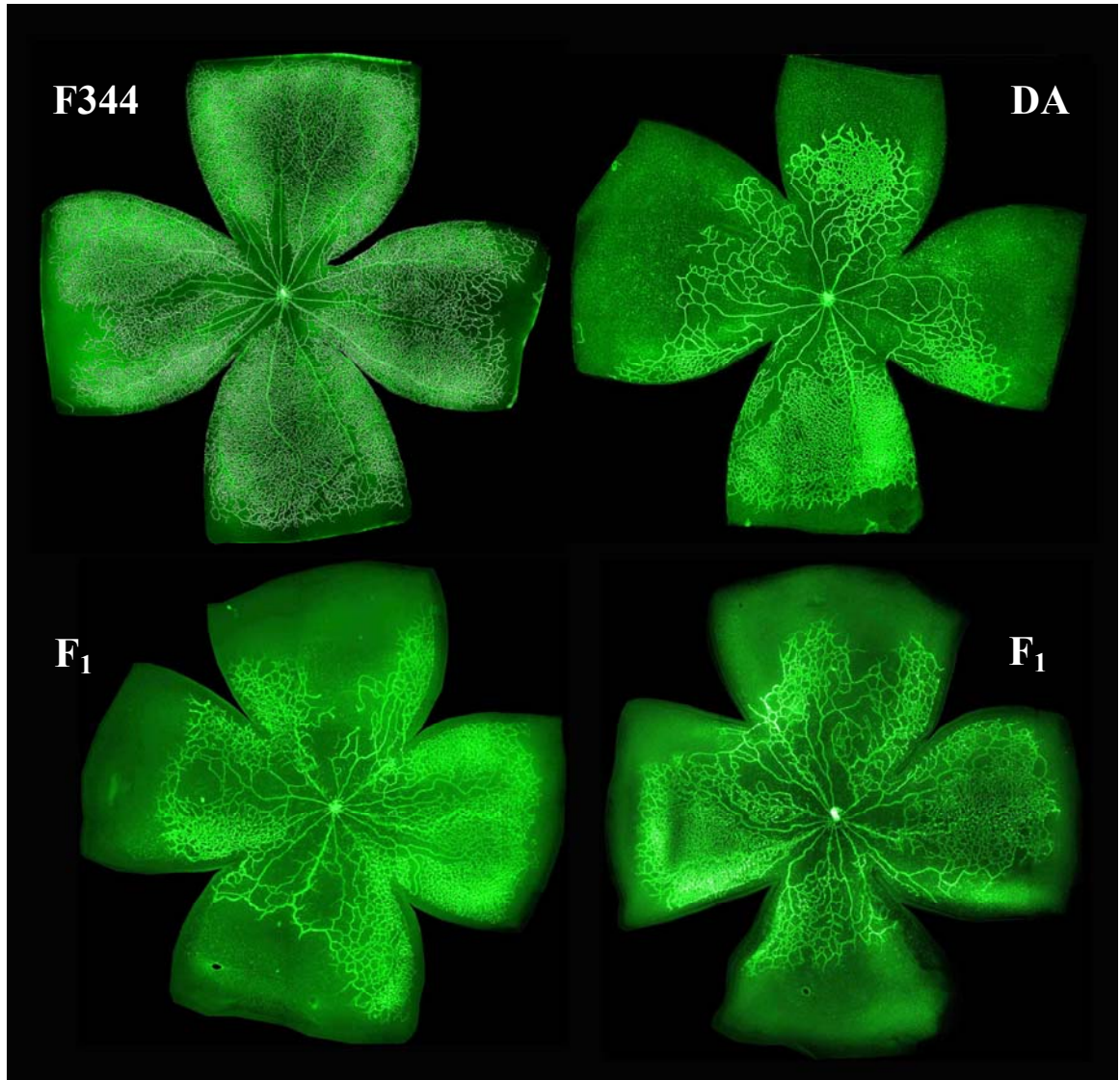
Figure 3.15 Comparison of retinal vascularization in rats exposed to cyclic hyperoxia for 14 days. Newborn Fischer 344 (**F344**), Dark Agouti (**DA**) and F_1 generation rats (**F_1**) – the offspring of crosses between F344 and DA rats – were exposed to cyclic hyperoxia for 14 days prior to the measurement of retinal vascular extent. The avascular retinal areas of the F_1 rats were similar in size to those of the DA strain and significantly larger than those of the F344 strain. Representative montage images are shown.

3.2.e.2   *The susceptibility of the back-cross offspring to OIR*

Adult rats of the F_1 generation were mated with F344 and DA rats to yield back-cross offspring. A total of four back-crosses were performed to accommodate each gender pairing (Figure 3.16). The offspring of the DA back-crosses (DA x F_1) were indistinguishable from F_1 pups: all had dark brown ocular pigmentation and agouti coat colour (Figures 3.13 & 3.16). In contrast, the offspring of the F344 back-crosses (F344 x F_1) exhibited a wide range of coat colours (Figures 3.16 & 3.17). Albino rats had red eyes, while all rats with coloured coats had dark brown ocular pigmentation. All newborn offspring of each back-cross were exposed to cyclic hyperoxia for 14 days and the extent of the retinal avascular area was measured.

The offspring of the DA back-crosses were universally susceptible to the attenuating affects of oxygen on retinal vascularization, with a mean avascular area of 76.3% (95% CI: 72.9-79.8%) of the total retinal area. Greater variation was found in the extent of retinal vascularization in the offspring of the F344 back-crosses (mean avascular area 47.3%; 95% CI: 37.5-57.0%) (Figure 3.16). A strong association was identified between ocular pigmentation and retinal vascularization – highly significant differences were found in the extent of retinal avascular area between albino and pigmented offspring of the F344 back-crosses ($z = 4.14$; $p<0.001$, two-tailed Mann-Whitney U-test). Accordingly, when the pigmented offspring of the F344 back-crosses were considered together, the mean retinal avascular area was 71.3% (95% CI: 64.5-78.0%), compared with 27.0% (22.9-31.1%) for albino offspring of the same crosses. The pigmented rats of each of the four back-crosses had large areas of avascular retina that were slightly larger than those of the DA strain (mean difference 1.6%; 95% CI: 0.1-4.9%; $p=0.003$) and substantially larger than those of the F344 strain (mean difference 25.6%; 95% CI: 18.1-33.7%; $p<0.001$). In contrast, the albino back-cross progeny had avascular areas that were similar in size to those of the F344 strain ($p=1.0$ for difference).
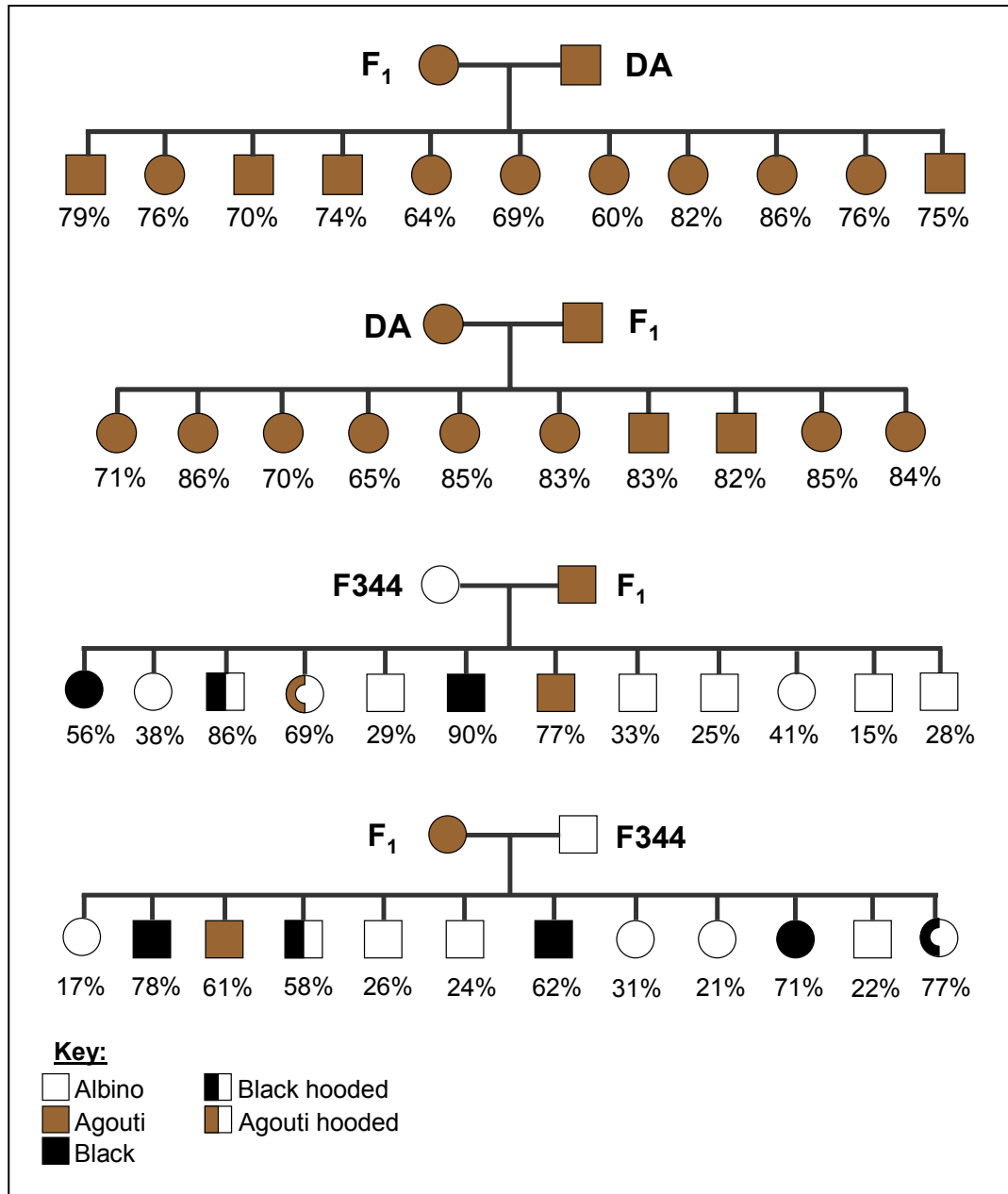
Figure 3.16 Back-cross offspring: coat colours and retinal avascular areas. Newborn back-cross offspring were exposed to cyclic hyperoxia for 14 days prior to measurement of the avascular retinal area. Values for avascular area are expressed as a percentage of the total retinal area. Coat colours are provided. Albino rats lacked ocular pigmentation (red eyes), while all those rats with pigmented coats had dark brown eye colour.

Figure 3.17 Back-cross pups and an F_1 dam. The offspring of a cross between a female F_1 rat and a male F344 rat had a wide range of coat colours including white (albino); agouti; black; and hooded (either black or agouti). Albino rats had red eyes; all rats with coat pigmentation had dark brown eye colour.

3.3. DISCUSSION

This study has identified marked and consistent variation in the response of different inbred rat strains to cyclic hyperoxia in a model of oxygen-induced retinopathy. Significant inhibition of retinal vascularization occurred in newborn rats of all strains following exposure to 14 days of cyclic hyperoxia. However the extent of this inhibition differed significantly amongst strains and was associated with ocular pigmentation, but not with body mass, litter size, or with significant differences in pulmonary function. Those rats that were exposed to the relative hypoxia of room air for four days following 14 days of cyclic oxygen, underwent complete central retinal vascularization. Peripheral vascularization was, however, incomplete and differed significantly in extent amongst strains, as did vascular morphological abnormalities. Rats that were resistant to the attenuating effects of cyclic hyperoxia on retinal vascularization exhibited fewer vascular morphological abnormalities following the period of relative hypoxia. In addition, cross-breeding experiments between relatively susceptible and relatively resistant rat strains provided strong evidence for the importance of hereditary factors for

the risk of OIR.

Two distinct patterns of retinal vascularization were observed amongst rats exposed to cyclic hyperoxia. Those strains that were relatively resistant to cyclic hyperoxia, the F344, WF and LEW, had comparatively small avascular territories in the peripheral retina at day 14. During the four day post-exposure period, these strains underwent complete central vascularization, with near complete vascularization of the retinal periphery. Vascular architecture was relatively normal and few morphological abnormalities were identified. In contrast, those strains that were more susceptible to cyclic hyperoxia, the SPD, DA and HW, had large peripheral avascular territories at day 14. During the period of relative hypoxia there was dense and disordered vasoproliferation both centrally and in those peripheral regions that were already vascularized at day 14. The retinal vascular morphology in these strains (SPD, HW and DA) was highly abnormal with dense tufts of endothelial cells, distended central vessels and grossly dilated vascular buds at the avascular periphery.

In studies of the effects of different hyperoxic exposures on retinal vascularization in the SPD rat, a strong association has previously been identified between the extent of retinal avascular area at the cessation of hyperoxia and the development of neovascularization on subsequent room air exposure [251, 312, 313]. The present study confirms these findings and demonstrates that rat strains differ significantly in their susceptibility to hyperoxic retinal vascular attenuation and to subsequent vascular abnormalities. Interestingly, vascular tortuosity, a marker of disease severity in human ROP ("plus" disease) bore no obvious relationship to either the degree of retinal vascularization or to other morphological abnormalities [206].

In contrast to the F344, WF and LEW strains, no significant vascularization of the avascular retinal periphery was observed during the period of relative hypoxia (day 14 to day 18) for those strains most susceptible to hyperoxic vascular attenuation (SPD, DA and HW). The basis for this delay in peripheral vascularization remains in question. It may be that the large avascular territories seen in the retinae of these strains are subjected to a more profound hypoxic insult on room air exposure than the smaller avascular regions of the more vascularized strains. The delay in vascularization may

therefore relate to transient ischaemic compromise of glial cells that ordinarily play critical roles in vascular patterning of the retina, or to disruption of other mediators of vascular development such as extracellular matrix proteases and cellular adhesion molecules [51, 196, 253, 343].

In all strains, central retinal vascularization occurred at a more rapid rate than peripheral vascularization during the period of relative hypoxia. The central retina was vascularized in all strains at birth and exposure to hyperoxia was associated with vasoconstriction of the central vessels [168, 312]. Revascularization of the central retina is likely to have been facilitated by surviving endothelial cells and residual extracellular matrix may have aided the ingrowth of nascent vessels. Furthermore angioblasts, important in developmental retinal vascularization, would be expected to have more ready access to the central retina than to more peripheral regions [45, 46].

A small but significant strain difference was found in the extent of retinal vascularization amongst control rats exposed to room air for 14 days. Control rats of those strains relatively resistant to cyclic hyperoxia, the F344, WF and LEW, had smaller avascular areas than those of strains susceptible to hyperoxia, the HW and DA. While a marginally slower rate of retinal vascularization in room air conditions may predispose to increased susceptibility to hyperoxia, it is unlikely to constitute the sole basis for the observed differences in susceptibility. Other strain-dependent genetic factors are likely to be involved. Differences in the regulatory effects of oxygen tension on retinal angiogenesis, such as the ubiquitination and degradation of the constitutively expressed α subunit of HIF-1, or in glial cell sensitivity to hyperoxia, may be responsible [344].

It was considered possible that the observed strain differences in retinal vascularization following cyclic hyperoxia might have been due to differences in retinal oxygenation, rather than to intrinsic differences in the regulation of vascularization. As measures were taken to ensure identical environmental conditions for all oxygen exposed rats (section 2.4.c.2), the only potential sources of variation in retinal oxygen delivery amongst strains were differences in respiratory function. Hyperoxia is known to induce lung-

injury in rats, and recent studies have identified strain-related differences in the susceptibility to this effect [341, 342, 345, 346]. Interestingly, F344 rats were found to be at greater risk of oxygen-induced lung injury than rats of other strains, including SD [341, 342]. Although there was no overt evidence of respiratory distress in oxygen exposed rats of any strain, a strain comparison of respiratory function was undertaken.

The relatively OIR-resistant F344 strain, and the relatively OIR-susceptible DA rat strain were selected for respiratory function testing. There were no significant differences in systemic oxygenation between F344 and DA rats following 18 days of cyclic hyperoxia. Similarly, there were no significant differences in bronchoalveolar lavage fluid protein concentration. While a statistically significant difference was found in lung wet-to-dry weight ratios (a measure of pulmonary oedema), the magnitude of this difference was small. Were strain differences in the susceptibility to lung injury to account for the observed differences in retinal vascularization, it might be expected that the F344 strain would be more susceptible to lung injury than the DA strain – systemic oxygen tensions would be lower in the more severely lung-injured strain and therefore retinal hyperoxic vasoattenuation would be less marked. It follows then that the lung wet-to-dry weight ratio would be higher for the F344 strain, than the DA strain. This was not the case – the lung wet-to-dry weight ratio was marginally higher in the DA strain, than in the F344 strain. Taken together, these results suggest that the observed strain differences in OIR were not due to differences in retinal oxygenation. Rather, the findings support the hypothesis that differences in OIR susceptibility were a consequence of strain differences in the regulatory effects of oxygen on retinal angiogenesis.

Similarly, the observed strain differences in retinal vascularization could not be attributed to differences in litter size, or in mass. The importance of body mass in the risk of retinopathy is significant. In human infants birth weight has been identified as an independent predictor of the risk of progression to threshold ROP, as well as the risk of an unfavourable structural outcome once threshold disease is manifest [208]. Furthermore, postnatal growth restriction has been associated with an increase in the risk of retinopathy [347]. Holmes and colleagues have identified a strong association between growth restriction and the risk of retinopathy in the rat model of OIR – the

severity of retinopathy was significantly increased in rats reared in expanded litters and there was an inverse correlation between weight gain and retinopathy risk [318, 348]. While birth weight was not measured in the present study, the strain differences in body mass and in weight gain relative to control rats, following 14 days of cyclic hyperoxia, could not account for the observed strain differences in retinal vascularization.

The cross-breeding experiments undertaken in this work substantiate the importance of heritable genetic factors in determining the susceptibility of rats to OIR. As is illustrated in Figure 3.18, the segregation of the susceptibility trait can be modelled using an autosomal dominant pattern of inheritance. If susceptibility to vascular attenuation is defined as a retinal avascular area in excess of 50 percent of the total retinal area following 14 days of cyclic hyperoxia, and the susceptibility allele is assumed to be dominant, then all of the offspring of crosses between F344 and DA rats would be susceptible, as would all of the progeny of the back-crosses between DA and F_1 rats (DA x F_1). Furthermore, the ratio of susceptible to resistant offspring of backcrosses between F344 and F_1 rats (F344 x F_1) would be expected to approximate 1:1. The findings of the cross-breeding experiments closely matched these predictions (Figures 3.14 & 3.16). This modelling was based on several assumptions: the continuous variable, avascular retinal area was assigned a categorical value; and the value for categorisation – avascular area of greater than, or less than 50 percent of the total retinal area – was arbitrarily selected. While these assumptions are simplistic, the observed segregation of susceptibility to OIR does appear to follow an autosomal dominant pattern. However, the extent of variation in avascular retinal areas of back-cross rats argues against a monogenic mode of inheritance (Figure 3.16). Studies of a larger pedigree are required to clarify the mode of inheritance of the susceptibility to OIR. Nonetheless, the results of these experiments demonstrate that hereditary factors are central to the risk of OIR in the rat.
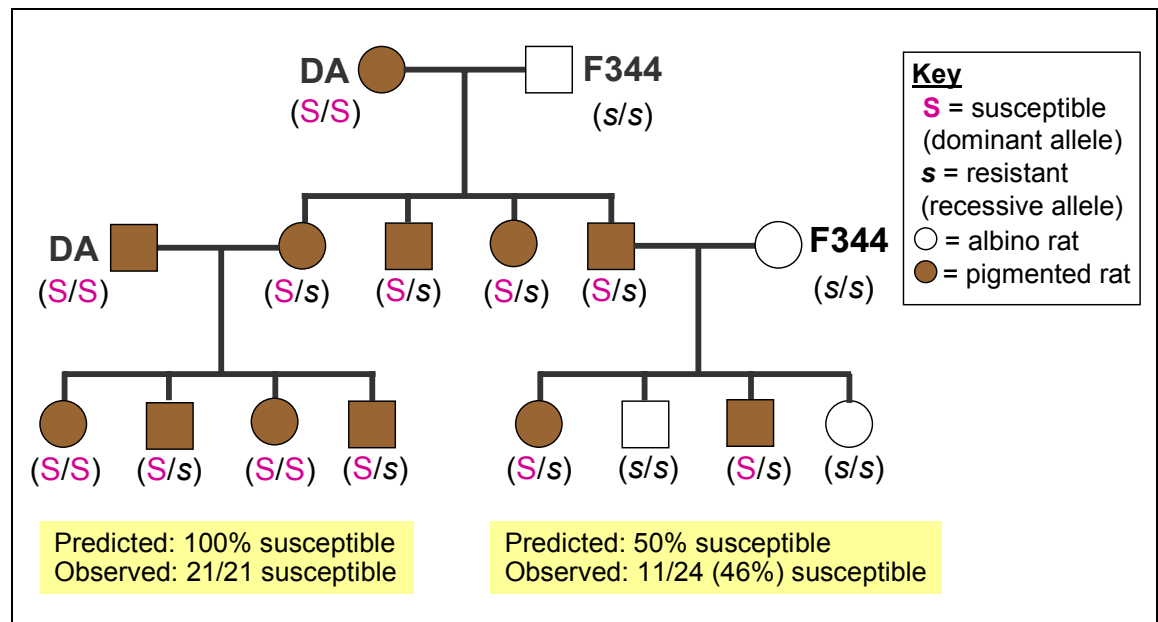
Figure 3.18 Genetic modelling of the susceptibility to OIR. If it is assumed that the susceptibility to retinopathy is a monogenic trait, and if an avascular area of greater than 50% of the total retinal area after 14 days of cyclic hyperoxia is adopted as the definition of susceptibility to OIR, then the inheritance of the susceptibility trait can be predicted as shown. All of the progeny of the DA x F344 cross (F_1 generation) would carry the dominant susceptibility allele and would therefore be expected to exhibit susceptibility to OIR. Likewise, all of the offspring of the DA back-cross (DA x F_1) would carry at least a single susceptibility allele and therefore express the susceptible phenotype. In contrast, approximately 50% of the offspring of the F344 back-cross (F344 x F_1) would carry the susceptibility allele, while the remaining 50% would not. Accordingly 50% of the offspring of this back-cross would be expected to exhibit the susceptible phenotype, and 50% would be expected to be relatively resistant to OIR (avascular area <50%). The predicted pattern of inheritance closely matches the findings observed for the cross-bred offspring (Figure 3.16). The inheritance of susceptibility to OIR also closely matches the inheritance of ocular pigmentation (all pigmented rats have dark brown eye colour; all albino rats have red eye colour).

Ocular pigmentation appears to be strongly associated with susceptibility to oxygen-induced retinal vascular attenuation in rats. The pigmented DA and HW rat strains had significantly larger avascular retinal areas than all of the albino strains. Moreover, all of the offspring of the F_1 generation (DA x F344), as well as the progeny of the DA back-cross (DA x F_1) had dark brown eye colour and large avascular retinal areas that were similar in extent to those of the DA strain and substantially larger than those of the F344 strain. The pigmented offspring of the F344 back-cross (F344 x F_1) also had large retinal avascular areas, while the albino pups had significantly smaller avascular areas that were similar to those of the F344 strain. These results provide compelling evidence of a link

between ocular pigmentation and susceptibility to OIR in the rat.

The association between ocular pigmentation and susceptibility may be causal or coincident – the lack of ocular pigment may directly confer resistance to OIR; alternatively a genetic determinant of susceptibility to oxygen-induced vascular attenuation may be linked with the gene locus for ocular pigmentation. Albinism is caused by mutations in the genes involved in melanin production and accumulation [349]. The gene encoding tyrosinase, an enzyme in the melanin biosynthetic pathway, is often mutated in albinos. In fact, albinism in the Wistar rat was recently attributed to a missense mutation in the tyrosinase gene [350]. Dihydroxyphenylalanine (DOPA), a product of tyrosinase catalysis is known to play an important role in cell cycle regulation and a deficiency of the factor is thought to account for the increase in neuronal proliferation and disordered maturation found in albino retinae [351-353]. Further, a deficiency of DOPA has been associated with alteration of the balance between the neurotransmitters gama-aminobutyric acid (GABA) and glutamate [354]. This balance ordinarily plays an important role in neuronal direction selectivity and its perturbation may account for the misrouting of optic nerve fibres commonly found in albinos [354]. It is possible therefore that the biochemical ramifications of impaired melanin biosynthesis may confer resistance of albino strains to the attenuating effects of oxygen on retinal vascularization. Oxygen free radicals are generated in the process of melanin biosynthesis, and the accumulation of these toxic molecules is enhanced in hyperoxia [351]. *In vitro* experiments demonstrate that vascular endothelial cells are particularly sensitive to the DOPA-mediated oxidative damage [351, 352]. Thus it is possible that DOPA-mediated endothelial cell damage and death is responsible for the susceptibility of pigmented rats to hyperoxia-induced vascular attenuation. Furthermore, retinal pigment epithelial cells are known to play important regulatory roles in retinal angiogenesis, including the production of pigment epithelium-derived factor (PEDF), a potent inhibitor of angiogenesis [355]. It may be that the biochemical sequelae of aberrant melanin biosynthesis in albinos impede this regulatory role.

Support for this hypothesis comes from a study comparing the susceptibility of the pigmented BN and albino SPD rat strains to OIR [334]. The study found that retinal expression of PEDF protein was increased 3.8-fold over controls, for BN rats at the

conclusion of hyperoxic exposure [334]. No significant increase in PEDF levels was found for SPD rats at the same time-point. Oxygen excess has been associated with an increase in retinal PEDF expression *in vivo* and in RPE cell culture [75, 356]. It may be that pigmented eyes express PEDF to a greater extent under hyperoxia than do non-pigmented eyes. This would lead to an increase in PEDF-mediated inhibition of retinal angiogenesis during the hyperoxic exposure, rendering the retinae of pigmented eyes more ischaemic on room air exposure. It is possible that a difference in the expression of PEDF expression by retinal pigment epithelial cells may account for the difference in retinal vascularization in the eyes of pigmented and albino rats identified in the present study.

As has been discussed previously (section 1.5.e), the association between ocular pigmentation and the risk of ROP in humans is far from straightforward. While epidemiological studies have identified an effect of race on retinopathy risk, the evidence for a link with ocular pigmentation is conflicting – African American infants appear to be at lower risk of severe disease than Caucasians, while Alaskan natives are at significantly greater risk [279, 285]. Another study found no difference in the risk of retinopathy for infants of white, Indigenous Australian, Maori or Pacific Islander mothers [213]. Collectively these data suggest that hereditary factors other than those related to ocular pigmentation are of primary importance in the risk of retinopathy. The finding of a hierarchy of susceptibility amongst albino rat strains in the present work lends support to this notion.

Studies in the murine OIR model have identified a role for nitric oxide (NO) in hyperoxia-induce retinal vasoattenuation [357]. Transgenic mice deficient in endothelial nitric oxide synthase (eNOS), as well as mice treated with a nitric oxide synthase inhibitor, demonstrated substantially less hyperoxia-induced vasoobliteration than wild type mice. Following a period of relative hypoxia the NO-deficient mice developed less extensive neovascularization than wild type mice [357]. While the mechanism for NO-mediated retinal vascular attenuation remains to be established, it is possible that toxic NO-derived oxidants, such as peroxynitrite, may play a key role. It follows that the strain differences observed in the present study may relate to differences in eNOS activity or in differences in the expression of anti-oxidants such as glutathione.

Furthermore, NO is known to inhibit VEGF expression via an effect on the accessory transcription factor activator protein-1 (AP-1) [357]. Thus a deficiency of NO in the retinae of relatively resistant rat strains may result in higher levels of VEGF expression during hyperoxia, facilitating more complete vascularization. The extent to which differences in NO expression account for the strain differences identified in the present study remains to be established.

Strain-dependent differences in the susceptibility to hyperoxia may, in part, account for the abandonment of the rat model of OIR for more than 30 years. In the 1950's and early 1960's Ashton *et al.* were unable to demonstrate significant retinopathy in WF rat pups in studies of oxygen-induced retinopathy [324]. The present study identifies the WF strain as relatively resistant to hyperoxic exposure. It was not until the 1990's that the rat model became widely accepted as a valid model of proliferative retinopathy, due largely to the studies of Reynaud and Penn, who exposed the more susceptible SPD strain to cyclic hyperoxia [311-314]. It has been demonstrated more recently that neovascularization may be consistently induced in some rat strains, such as the BN, but not others, such as the SPD, by exposure to constant hyperoxia during the first phase of the model [358].

This study is the first to attribute rat strain differences in OIR to differences in the susceptibility to the inhibitory effects of cyclic hyperoxia on developmental retinal vascularization. While Gao and colleagues have previously identified a strain difference between BN and SPD rats in OIR, their conclusions differ from those of the present work in several respects [334]. In the study by Gao *et al.* rats were exposed to a period of sustained hyperoxia (vasoattenuation phase) prior to a period of relative hypoxia in room air (vasoproliferation phase). The chief finding of their study was that retinal vascular abnormalities were more marked in the BN strain during the vasoproliferation phase. This was associated with a higher ratio of expression of VEGF to the PEDF, in the BN compared with the SPD strain [334]. Accordingly, the BN strain was deemed to be more susceptible to retinal *hypoxia*. However, the investigators did not take account of differences in the relative susceptibilities of each strain to the hyperoxic exposure (vasoattenuation phase). While the results demonstrate that BN retinae were less well vascularized than those of SPD rats immediately after the hyperoxic exposure, the

significance of this observation was not appreciated. As SPD retinae were more completely vascularized at the end of the hyperoxic exposure than those of BN rats, it is probable that the stimulus for hypoxia-induced angiogenic factor expression during the period in room air was less in SPD rats than in BN rats. This would imply that the strain difference observed by Gao and colleagues was not the result of a difference in susceptibility to hypoxia, but rather a difference in the susceptibility to hyperoxia.

In conclusion, the experiments described in this chapter are the most comprehensive comparison of OIR in different inbred rat strains to date. These experiments have demonstrated a significant effect of rat strain on susceptibility to retinopathy and cross-breeding studies have confirmed the heritability of this susceptibility trait. At present the relevance of these observations to human ROP remain in question. Granted that genetic risk factors are important in human ROP, and given that opportunities for the examination of these risk factors is limited by ethical considerations, further study of the rat strain differences identified in this work is justified. Identification of the aetiology of the strain-related differences will enhance understanding of the rodent model of oxygen-induced retinopathy and further clarify the role of oxygen tension in the regulation of retinal angiogenesis. These findings may prove to be of relevance to human ROP, facilitating advances in the screening and treatment of at-risk neonates.

CHAPTER 4

<u>**RESULTS**</u>

**QUANTIFICATION OF RETINAL ANGIOGENIC FACTOR
GENE EXPRESSION IN RAT OXYGEN-INDUCED
RETINOPATHY**

4. CHAPTER 4: RESULTS – Retinal gene expression

4.1.   INTRODUCTION

Strain differences in the susceptibility of inbred rats to OIR and the apparent heritability of this trait, point to differences in angiogenic factor gene expression amongst strains. The characterisation of these genetic differences may provide insights into the regulation of rodent retinal angiogenesis and be of value in the understanding of human ROP. Quantitative real-time reverse transcription-polymerase chain reaction (real-time RT-PCR) is the most sensitive method for the quantification of gene expression [359]. The experiments described in this chapter sought to exploit real-time RT-PCR to compare the expression of angiogenic genes in the retinae of rats exposed to the hyperoxia-hypoxia model. Candidate genes considered for inclusion in the study were those that are known to be important in angiogenesis – specifically those implicated in retinal vascularization, and those that are regulated by oxygen. Ultimately eight genes were selected for inclusion in the study: vascular endothelial growth factor, vascular endothelial growth factor receptor-2, angiopoietin 2, Tie2, cyclooxygenase-2, erythropoietin, insulin-like growth factor-1 and pigment epithelium-derived growth factor. The characteristics of each of these factors and the roles that they are known to play in retinal angiogenesis will be addressed in turn.

4.1.a.   Vascular endothelial growth factor

VEGF is a peptide growth factor with at least five different isoforms in humans, ranging in size from 121 to 206 amino acid residues [360]. As has already been discussed (section 1.3.c), VEGF plays a central role in angiogenesis, with actions at numerous levels of the multi-step process (Table 1.4; Figure 4.1). The factor is important in many contexts of developmental and pathological angiogenesis (Table 1.3), and is a key mediator of OIR in the mouse [53, 250], the rat [51, 52, 251, 252], and the cat [51, 253] (section 1.5.d.2). VEGF expression is regulated by hypoxia-inducible transcription factors (HIFs) – it is induced by hypoxia, and suppressed by hyperoxia [178-181]. The inhibition of VEGF expression is central to hyperoxia-induced vasoattenuation in OIR, while hypoxic induction of the factor is essential for vascular proliferation. VEGF was therefore a necessary inclusion in the study of strain differences in rat OIR.

4.1.b. Vascular endothelial growth factor receptor-2

Vascular endothelial growth factor receptor-2 (VEGFR-2 [KDR; flk-1]), the principal receptor for VEGF-mediated angiogenic activity, is a tyrosine kinase receptor and member of the platelet-derived growth factor receptor subfamily. VEGF binding triggers receptor homodimerisation and transphosphorylation. Resultant activation of the receptor tyrosine kinase domain triggers a series of intracellular signalling cascades (Figure 4.1). VEGFR-2 expression is induced within hours of hypoxia and it has been demonstrated to play a central role in retinal vascularization in development and in OIR, making it a logical candidate for gene expression analysis in the present study [361-363].

Stone *et al*. demonstrated an increase in VEGFR-2 mRNA expression in the inner retina and in association with proliferating preretinal vessels in during the hypoxic phase of feline OIR [253]. Similarly, Suzuma *et al.* demonstrated increased retinal expression of VEGFR-2 protein and mRNA during the proliferative phase of murine OIR [364]. Expression of the receptor was localised to zones of active vascular proliferation, including neovascular tufts. VEGFR-2 protein expression was increased above control levels from days 8 to 22 in newborn dogs, following four days of constant hyperoxia [365]. Another study found increased levels of VEGFR-2 mRNA in rat retinae after five days of relative hypoxia that followed 11 days of cyclic hyperoxia [366]. In another rat OIR model, retinal VEGFR-2 protein levels were increased after two days of relative hypoxia, and even more after 6 days [367]. Werdich *et al.* compared VEGFR-2 protein levels in the retinae of rats exposed to room air with those of rats exposed to 14 days of alternating hyperoxia and hypoxia, using Western immunoblotting assays of whole retinal lysates [368]. At the end of this exposure VEGFR-2 levels were lower than control levels. Expression of the receptor increased progressively during the subsequent period of relative hypoxia, reaching control levels by day 20.
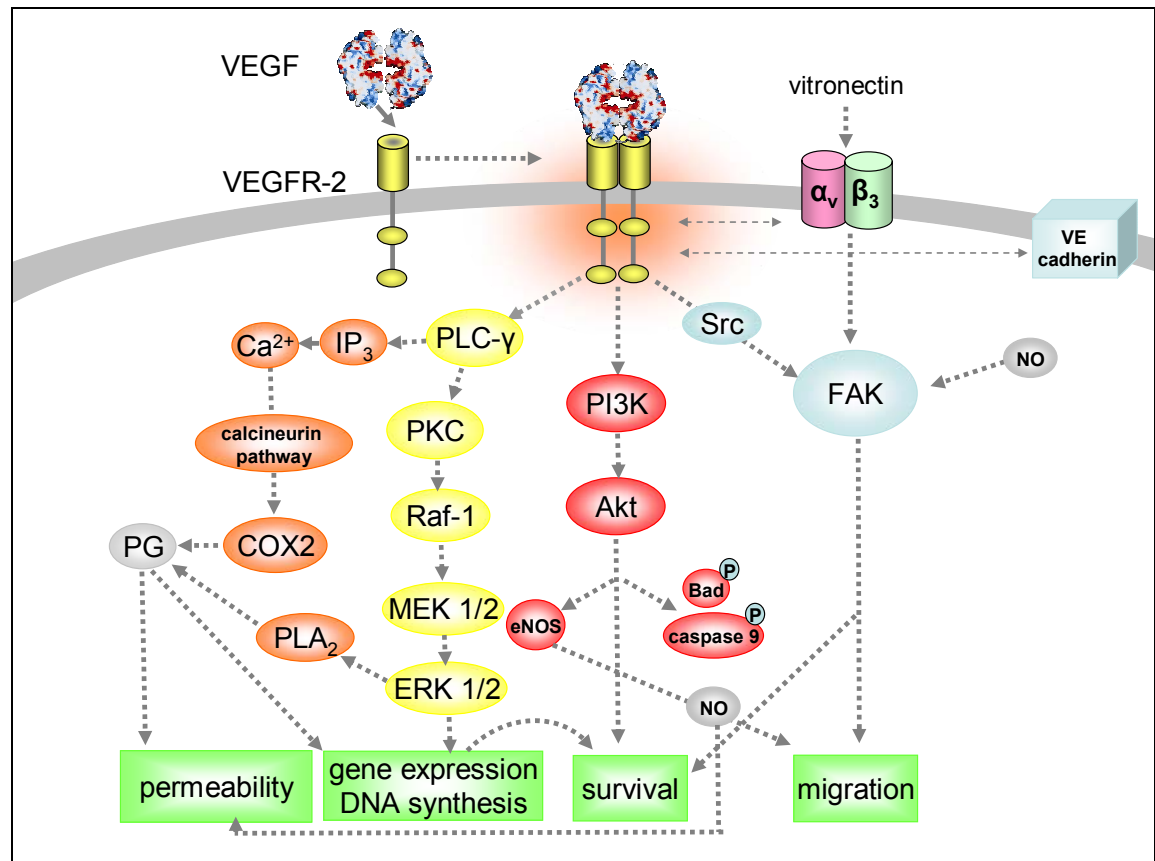
Figure 4.1 VEGF signalling pathways [369]**.** VEGF binds to VEGFR-2 on the endothelial cell surface, triggering receptor dimerisation, transphosphorylation, activation of the intracellular tyrosine kinase domain and a tyrosine kinase signalling cascade. Much of the endothelial survival signalling of VEGF is mediated via phosphatidylinositol-3 kinase (PI3K). PI3K activates anti-apoptotic kinase (Akt) which phosphorylates pro-apoptotic factors such as Bad and caspase 9. Akt also activates endothelial nitric oxide synthase (eNOS) – the resultant increase in nitric oxide (NO) is important in endothelial cell migration and permeability. Survival signalling and cell migration is also mediated via activation of Src tyrosine kinase and focal adhesion kinase (FAK). VEGF and integrin signalling axes converge at FAK. Direct interactions between VEGFR-2 and the integrins, and cell adhesion molecules may also be important in survival signalling. Activation of the phospholipase C-γ (PLC-γ) pathway is central to the mitogenic action of VEGF. Inositol-trisphosphate, a product of PLC-γ, activates the calcineurin pathway, inducing cyclooxygenase-2 (COX-2) expression. Prostanoids, such prostacyclin and prostaglandin-E$_2$, generated by COX-2 and phospholipase-A$_2$ (PLA$_2$) activity, regulate vascular permeability, stimulate angiogenesis and induce VEGF gene expression. (Adapted from Zachary [369]).

Key:

VEGF: vascular endothelial growth factor
VEGFR-2: vascular endothelial growth
              factor receptor-2
α$_v$β$_3$: integrin α$_v$β$_3$
PI3K: phosphatidylinositol-3 kinase
Akt: anti-apoptotic kinase
eNOS: endothelial nitric oxide synthase
NO: nitric oxide
Src: Src tyrosine kinase
FAK: focal adhesion kinase
PLC-γ: phospholipase C-γ
PKC: protein kinase C

Raf-1: Raf serine/threonine kinase-1
ERK1/2: extracellular-signal-regulated protein
             kinase 1 and 2
MEK1/2: mitogen-activated protein kinase/ERK
             kinase 1/2
IP$_3$: inositol trisphosphate
COX-2: cyclooxygenase-2
PLA$_2$: phospholipase A$_2$
PG: prostaglandins/prostanoids

4.1.c.   Angiopoietin 2 & Tie2

Angiopoietin 2 (Ang2) is an angiogenic factor that interacts with endothelial cell Tie2 (tyrosine kinase with immunoglobulin and epidermal growth factor homology domains) receptors. Ang2 is thought to function principally as an antagonist of Tie2, inhibiting angiopoietin 1 (Ang1) binding and Tie2 signalling [80], although on occasion Ang2 may act as an agonist of Tie2 [370]. Ang2 and Tie2 are expressed at sites of angiogenesis and vascular remodelling [80, 371]. Ang2 is selectively up-regulated in hypoxia and is instrumental in destabilising the association between mural cells and endothelial cells, permitting endothelial cell mobilisation for migration and proliferation [80]. The effect of Ang2 expression appears to be context dependent – in the presence of VEGF, Ang2 expression promotes angiogenesis; in the absence of VEGF, Ang2-mediated vascular destabilisation leads to endothelial cell apoptosis and vascular regression [80, 108].

Retinal Ang2 expression is temporally and spatially correlation with vessel formation during development – Ang2 mRNA is expressed by horizontal cells at the outer extremity of the inner nuclear layer during formation of the deep retinal circulation in the mouse, and to a lesser extent by neurones in the superficial retina [190, 191]. In Ang2-deficient mice retinal vascular development is impaired – the superficial network is sparse and the deep network is absent [96, 191]. Furthermore, Ang2 expression is known to correspond with vascular proliferation in OIR: mRNA expression in the inner retina increased within hours of hypoxia in murine OIR models, and peak expression was coincident with maximal neovascularization [190, 192]. Ang2 potentiates VEGF-induced NV [190]. Thus Ang2 was an attractive target for examination in the study of strain differences in retinal vascularization in rat OIR.

As Ang2 exerts its effects via interaction with Tie2, the expression of this receptor was also of interest in the study of strain differences in rat OIR. Tie2 is constitutively expressed by endothelial cells, and its expression is induced at sites of active angiogenesis [372]. Tie2 expression is induced in hypoxia by HIFs [373] – in a model of rat myocardial ischaemia, Tie2 protein expression was increased within hours [362]. Thus Tie2 was included in the study of gene expression in the rat retinopathy model.

4.1.d. Cyclooxygenase-2

The inducible prostaglandin synthase cyclooxygenase-2 (COX-2) is an important mediator of angiogenesis. COX-2 expression is up-regulated by nuclear factor-κB (NF-κB), a transcription factor induced in hypoxia, and to a lesser extent by VEGF, signalling through VEGFR-2 [369, 374] (Figure 4.1). The hypoxic induction of COX-2 has been demonstrated in murine and rat retina [375]; in rat lung [374]; in rabbit cornea [376]; in human vascular endothelium [377]; in tumour cells [378, 379]; in cultured neurones [380] and in primate retinal vascular endothelial cells [374]. COX-2 catalyses the production of prostaglandins from arachidonic acid and several of these products, including prostaglandin E_2 (PGE_2) and prostacyclin (PGI_2), are important in angiogenesis. PGE_2 stimulates VEGF expression, and thus constitutes a HIF-independent inducer of VEGF expression in hypoxia [374]. Moreover PGE_2 and PGI_2 are important in modulating vascular permeability and tone [369].

Hypoxia-induced expression of COX-2 is known to occur in human diabetic retinopathy and in rodent OIR [375, 381]. In the OIR model, expression of the enzyme has been localised to retinal astrocytes [381], with maximal expression during the period of relative hypoxia at sites of active vascular proliferation [375]. Selective inhibition of COX-2 has been shown to impede normal retinal vascular development in mice, as well as vascular proliferation in OIR in mice [375] and in rats [381].

4.1.e. Erythropoietin

Erythropoietin (EPO) is the archetypal hypoxia-induced protein − its transcription is regulated by HIF-1 and HIF-2 [382]. While EPO has long been regarded as a haemopoietic cytokine, recent studies have implicated the factor in angiogenesis and neuronal survival signalling [383, 384]. EPO was demonstrated to induce endothelial cell proliferation and migration in cultured endothelial cells, which were shown to express EPO receptors (EPO-R) [383, 385]. The addition of EPO to cultured human vascular endothelial cells triggered EPO-R phosphorylation, the activation of intracellular cell signalling cascades and the induction of a pro-angiogenic phenotype [384]. EPO stimulated angiogenesis *in vitro*, in cultured rat aortic explants [386], and *in vivo*, in the chick chorioallantoic membrane [384]. Furthermore EPO has recently been shown to play a role in murine OIR [387]. Mice deficient in hypoxia-inducible factor-2α

(HIF-2α), failed to undergo hypoxia-induced retinal neovascularization, in contrast to wild-type mice. EPO was the only one of a series of angiogenic factors to be differentially expressed between the two groups of oxygen exposed mice. The administration of exogenous EPO prior to the hyperoxia-hypoxia exposure largely restored the susceptibility of HIF-2α-deficient mice to the proliferative phase of OIR [387]. Furthermore EPO-R were expressed in the inner nuclear layer and the neovasculature of these retinae. Collectively, these data support a role for EPO in OIR.

4.1.f.   Insulin-like growth factor-1

Insulin-like growth factor-1 (IGF-1) has been implicated in developmental retinal angiogenesis and ROP [58, 59, 195]. IGF-1 stimulates the proliferation of retinal endothelial cells *in vitro* [388, 389] and, acting via IGF-1 receptors (IGF-1R), it augments VEGF-mediated activation of the ERK and Akt signalling pathways [58, 59] (Figure 4.1). Furthermore, IGF-1 has been shown to induce the accumulation and nuclear translocation of the alpha subunit of HIF-1 (HIF-1α), augmenting VEGF expression [390, 391]. This effect is enhanced by IGF-1-induced increases in the accessory transcription factors, activator protein-1 (AP-1) and NF-κB [391]. Accordingly, mice deficient in IGF-1, or IGF-1R, fail to develop neovascularization in the OIR model, as do mice treated with an IGF-1R antagonist, even when VEGF expression is high [58, 392, 393]. Thus IGF-1 appears to be important for realisation of the full angiogenic potential of VEGF [58]. Prospective studies of premature infants are consistent with this hypothesis – low serum IGF-1 was identified as a risk factor for ROP [59]. It is thought that a deficiency of IGF-1 in premature infants leads to impaired retinal vascularization, predisposing to retinal hypoxia and a marked increase in VEGF expression. Delayed production of IGF-1 in these infants has been demonstrated to correlate with the proliferative phase of ROP [59]. While retinal IGF-1 expression did not vary with oxygen exposure in a study of rat OIR [394], it is possible that strain differences in IGF-1 expression may contribute to the differential susceptibility to OIR observed in the present study. Although there is evidence that serum IGF-1 may be more predictive of retinopathy risk than retinal IGF-1 in diabetes, the examination of retinal IGF-1 production in OIR remains of interest [395].

4.1.g.   Pigment epithelium-derived factor

Pigment epithelium-derived factor (PEDF) is a secreted anti-angiogenic protein and neurotrophic factor that is widely expressed in the eye [75, 355]. The PEDF gene is a member of the serine protease inhibitor (serpin) gene family, although PEDF is not thought to function as a protease inhibitor [396, 397]. PEDF is the most potent of the known endogenous inhibitors of ocular angiogenesis [75, 398]. The factor inhibits endothelial cell migration in a dose-dependent fashion [75] and induces the expression of Fas ligand (FasL) by nascent endothelial cells, inducing their apoptosis via the Fas/FasL pathway [399]. Neural PEDF receptors have been identified, however little is known of endothelial cell receptors for the factor [400, 401]. PEDF is expressed by numerous ocular cell types including corneal, lens and ciliary epithelial cells as well as retinal ganglion cells, Müller cells and retinal pigment epithelial cells [402, 403]. PEDF protein has also been detected in the inner and outer plexiform layers of the rat retina [402]. PEDF inhibited neovascularization in a rat model of corneal wounding [75].

PEDF down-regulation has been associated with ischaemic proliferative retinopathy in diabetic humans and in animal models of choroidal neovascularization [402, 404-406]. In addition, sustained intraocular expression of PEDF by gene therapy inhibited neovascularization in murine OIR [406]. PEDF expression is regulated by oxygen: protein expression was inhibited by hypoxia in retinoblastoma cell culture, and increased following hyperoxia in the murine retina [75]. The regulatory effects of oxygen on PEDF expression are mediated, in part at a post-translational level [75, 407]. In a study of rat OIR, PEDF expression was positively correlated with oxygen tension at both the mRNA and protein levels – PEDF expression was increased in hyperoxia and reduced in hypoxia [356]. Changes in mRNA expression preceded changes in protein expression. Reciprocal regulation of PEDF and VEGF was mediated in part by a cleavage fragment of plasminogen, plasminogen kringle 5 [76]. In contrast, other research has demonstrated that VEGF, acting via VEGF receptor-1 (VEGFR-1) can induce the expression of PEDF mRNA and protein in cultured RPE cells [111]. Given the central role of PEDF as an inhibitor of retinal angiogenesis, it was included as one of the candidate genes in the study of strain differences in rat OIR.

Using real-time RT-PCR, the expression of each of these candidate genes was studied in the retinae of rats exposed to the cyclic hyperoxia and hypoxia model, detailed previously. The results of this analysis were interpreted in light of the observed differences in retinal vascularization. Significant differences in the expression of several angiogenic genes were identified and an integrated hypothesis was generated to account for the differences in retinal vascular extent amongst strains.

This chapter is divided into two sections: the design of and validation of the gene expression studies are described in section 1; the results are presented in section 2.

CHAPTER 4
SECTION 1

EXPERIMENTAL DESIGN &
METHODOLOGICAL VALIDATION

4.2.   Overview of the experimental design

cDNA samples, derived from pooled retinal RNA samples, were used to compare gene expression patterns amongst experimental groups. Three rat strains representing the spectrum of susceptibility to oxygen-induced retinopathy were selected for gene expression profiling. The DA strain was highly susceptible to OIR; the SPD strain was intermediate; and the F344 strain was relatively resistant. The retinal expression of 8 candidate angiogenic genes was examined in an attempt to identify a genetic basis for the differing susceptibilities to oxygen exposure. In some rats, retinal gene expression was assessed at the conclusion of the 14 day period of cyclic hyperoxia (O14); while in others, it was evaluated following an additional four days in room air (O18). The gene expression patterns of control rats, exposed to room air for 14 days (RA14), were compared with those of the oxygen-exposed rats to identify changes induced by the exposure. Comparisons were made between strains, for each reference time-point; as well as within strains, between time-points (Figure 2.2).

RNA pools were comprised of equal quantities of retinal RNA from three rats, drawn from at least two different litters that had been exposed to identical experimental conditions. Each RNA pool was reverse transcribed to yield a pooled cDNA sample. A standardised methodology was followed for all cDNA syntheses (section 2.3.f). Real-time reverse transcription-polymerase chain reaction (real-time RT-PCR) was then used to quantify gene expression in the cDNA pools. Real-time RT-PCR was performed using SYBR Green, a dye that is fluorescent only when bound to double-stranded DNA [302]. The accumulation of fluorescence with DNA amplification was used to quantify gene expression. The fluorescence emitted during the exponential phase of PCR amplification was a function of the initial quantity of the template cDNA. The amplification cycle at which the emitted fluorescence exceeded a threshold value corresponding with the beginning of the exponential phase of amplification – the threshold cycle (Ct) – was used to determine relative concentration of the template in the cDNA sample.

All real-time RT-PCR experiments were conducted in the same thermal cycler under identical cycling conditions (section 2.3.l). Unless otherwise specified, data are derived from duplicate PCR runs, with each sample assayed in triplicate and normalised to two

reference genes – hypoxanthine guanine phosphoribosyltransferase (HPRT) and acidic ribosomal phosphoprotein (ARBP). A single gene was amplified in each PCR run and all experimental samples, as well as a standard sample (section 2.3.g), were included in each run.

Control samples (RT- and NTC) were negative for all reactions (section 2.3.l). At the conclusion of each PCR run the products were subjected to melting-curve dissociation analysis. The change in fluorescence with time was monitored while the temperature was increased from $60^{o}C$-$99^{o}C$. The dissociation of double-stranded products at a critical temperature – the melting-temperature – was marked by a reduction in SYBR Green fluorescence. Analyses of these data were used to confirm the specificity of each primer pair (section 2.3.l). In addition the products of randomly selected samples from each PCR run were subjected to agarose gel electrophoresis (section 2.3.b). Product specificity was further confirmed by comparing the electrophoresis photographs and melting-curve analysis plots of test samples with those of a sequenced reference sample (sections 2.3.m & 2.3.n). For each sample, gene expression was quantified relative to the level of expression of the same gene in the pooled standard sample (section 2.3.g), using the delta Ct method with correction for amplification efficiency (sections 4.2.a.2 & 4.2.b). Variance of the transformed ($\log_{10}$) data was homogeneous for each experimental group as demonstrated by Levene's test of equality of error variance ($p > 0.05$) and by quantile plots (Q-Q plots) of residual values. Therefore two-way analysis of variance was used to compare mRNA expression amongst different experimental groups. Bonferroni adjustment was made for multiple comparisons.

4.2.a. Methodological validation

4.2.a.1   Confirmation of primer specificity

Primers were designed for each of the 8 genes of interest – VEGF, VEGFR-2, Ang2, Tie2, COX-2, EPO, IGF-1 and PEDF – in accordance with the method outlined in section 2.3.i (primer sequences: Table 2.1). Primer pairs were tested on a standard cDNA sample derived from RNA extracted from pooled rat retinae (section 2.3.g). Real-time RT-PCR was performed in accordance with the method outlined in section 2.3.l. A representative fluorescence amplification plot for each gene is presented below

(Figures 4.2(A), (C), (E), (G) and (I)). In all cases, aside from IGF-1, the melting-curve analysis was consistent with a single reaction product – indicated by a single, narrow peak in the first derivative plot for each primer set (Figures 4.2(B), (D), (F), (H) and (J)). The first derivative plot of the IGF-1 melting-curve had two distinct peaks, indicating the amplification of two products (Figure 4.2(J)).

These findings were confirmed by agarose gel electrophoresis – a single DNA band of the expected size was identified for each primer set, with the exception of IGF-1 (Figure 4.3). The agarose gel photograph demonstrates two DNA bands for IGF-1 – a major product of approximately 100 base pairs and a minor product of approximately 150 base pairs. All PCR products were purified and sequenced (sections 2.3.m & 2.3.n). Sequence analysis confirmed that the product amplified by each primer pair was identical to the predicted sequence, confirming primer specificity (Appendix 2). Of the two products amplified by the IGF-1 primers, the sequence of the smaller product matched that of the major splice variant of IGF-1 – IGF-1A. The larger product contained an additional 52 base pairs corresponding with the sequence encoded by exon five of IGF-1, an alternatively-spliced cassette exon (Appendix 2) [408-410]. Thus the specificity of each primer pair was confirmed.
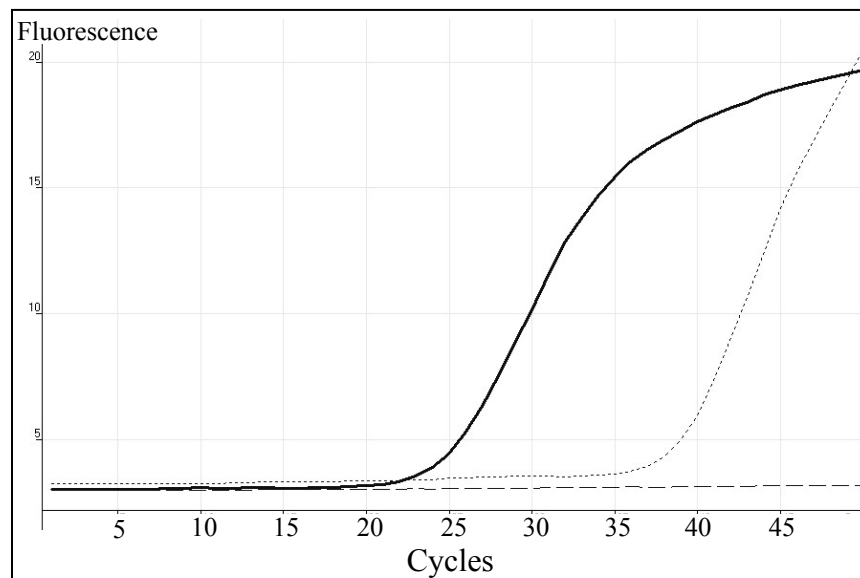
Figure 4.2(A) Real-time RT-PCR fluorescence amplification plots: VEGF primer pair. The amplification plots display the change in fluorescence of each sample with cycles of polymerase chain reaction: fluorescence of the DNA-binding dye, SYBR Green, increases in proportion with amplicon copy number. Quantification is based on the number of cycles required for the fluorescence signal to exceed a threshold value – the more abundant the target transcript in the cDNA sample, the earlier the fluorescence signal exceeds the threshold value. It is apparent that the product amplified in the standard cDNA sample (**solid line**) is more abundant than the product amplified in the negative control sample (RT-; **dotted line**). There was no amplification of the non-template control (water; **dashed line**).
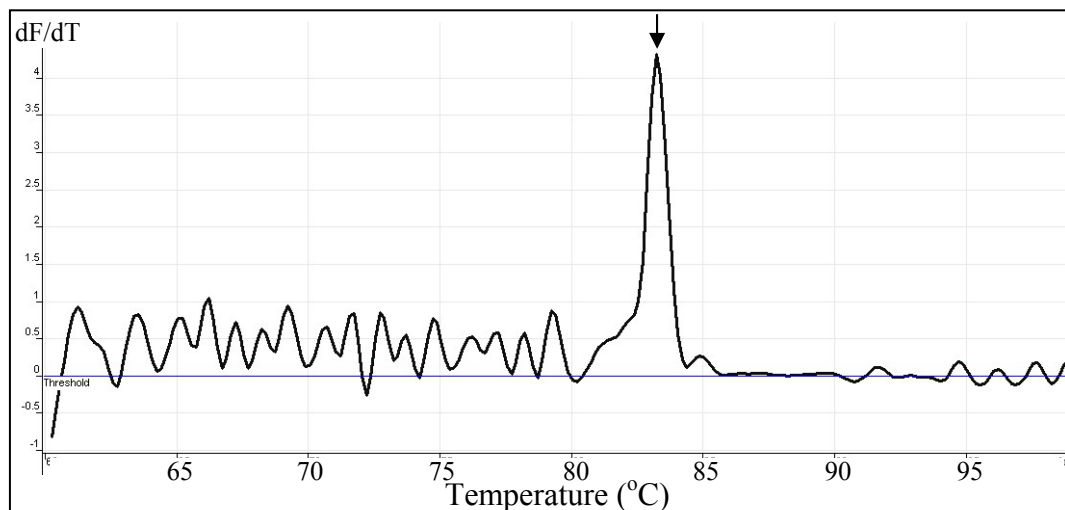
Figure 4.2(B) Melting-curve first derivative plot: VEGF primer pair. The products amplified by the VEGF primer pair were subjected to increasing temperatures. The dissociation of double-stranded amplicons at a critical temperature (melting temperature) was accompanied by a loss of SYBR Green fluorescence. The peak of the first derivative plot (dF/dT) (**arrow**) marked the point at which the change in fluorescence was maximal – this point corresponded with the melting temperature of the amplicon. In this case, the first derivative plot had a single, well-defined peak, suggestive of a single product.
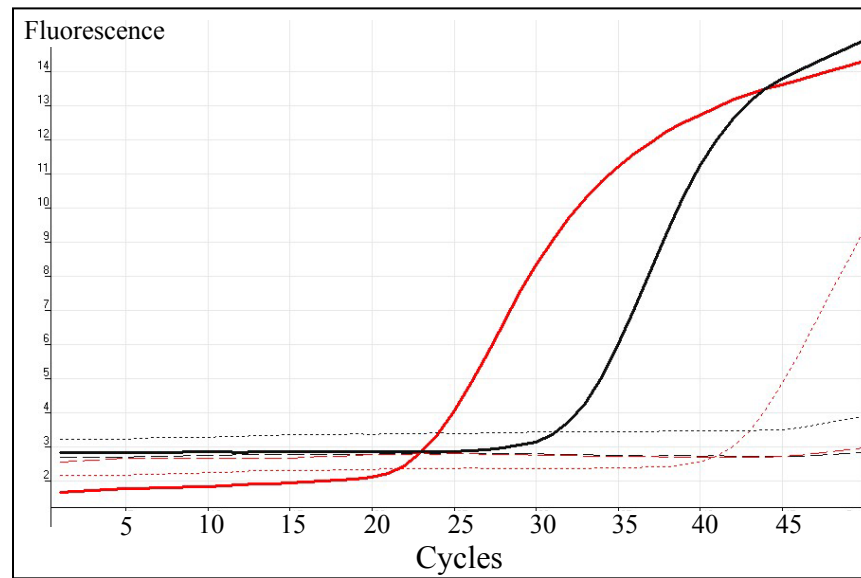
Figure 4.2(C) Real-time RT-PCR fluorescence amplification plots: VEGFR-2 and PEDF primer pairs. Key: VEGFR-2 (**solid red line**); PEDF (**solid black line**); VEGFR-2 negative control (RT-; **dotted red line**); PEDF negative control (RT-; **dotted black line**); VEGFR-2 non-template control (water; **dashed red line**); PEDF non-template control (water; **dashed black line**).
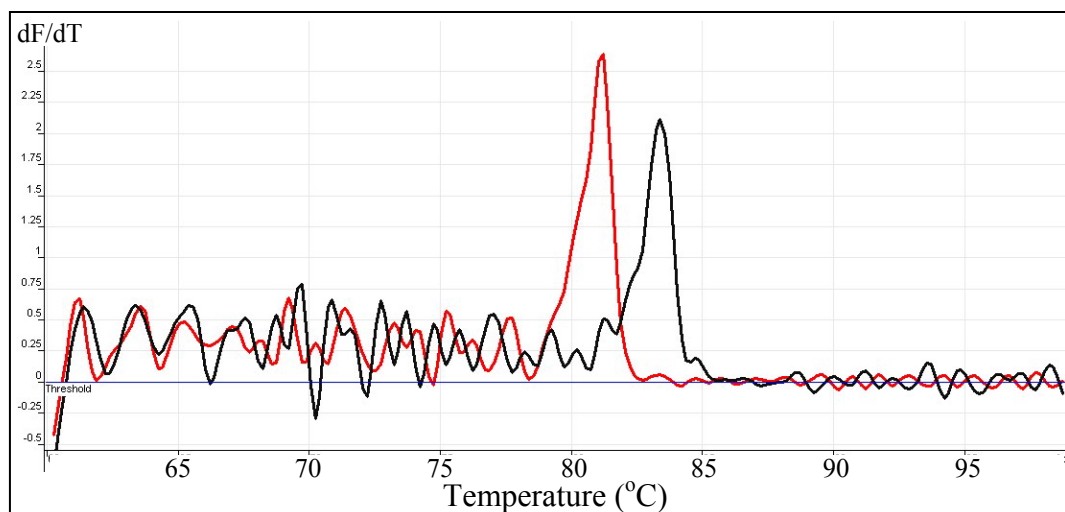
Figure 4.2(D) Melting-curve first derivative plots: VEGFR-2 and PEDF primer pairs. A single product is amplified by each primer pair. **Key:** VEGFR-2 (**red line**); PEDF (**black line**).
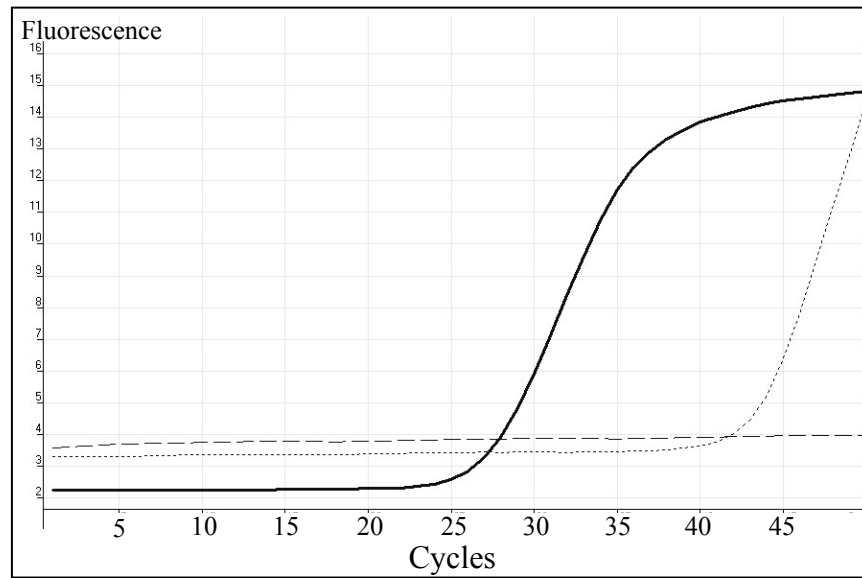
Figure 4.2(E) Real-time RT-PCR fluorescence amplification plots: Ang2 primer pair. Key: standard cDNA sample (**solid black line**); negative control sample (RT-; **dotted black line**); non-template control (water; **dashed black line**).
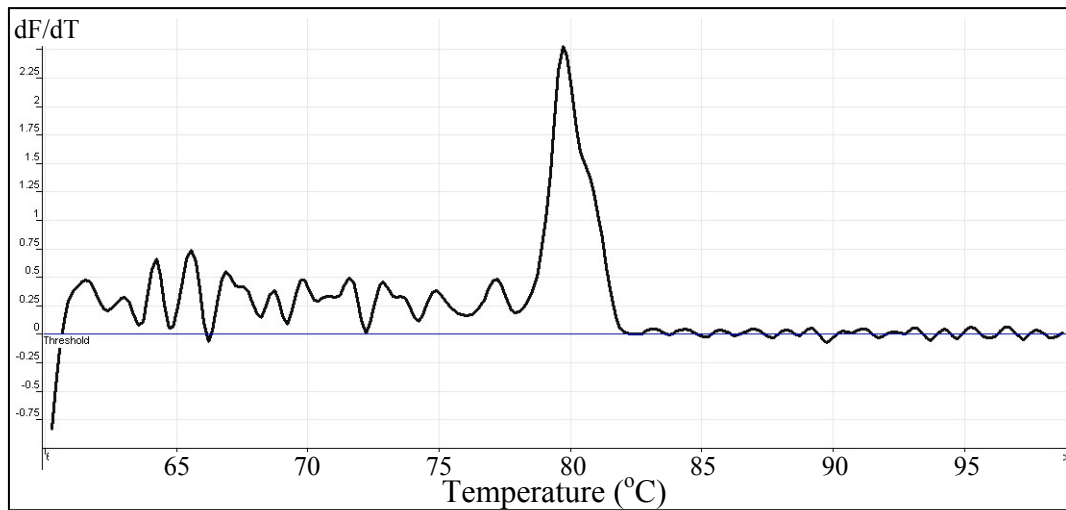
Figure 4.2(F) Melting-curve first derivative plot: Ang2 primer pair. A single product is amplified by this primer pair.
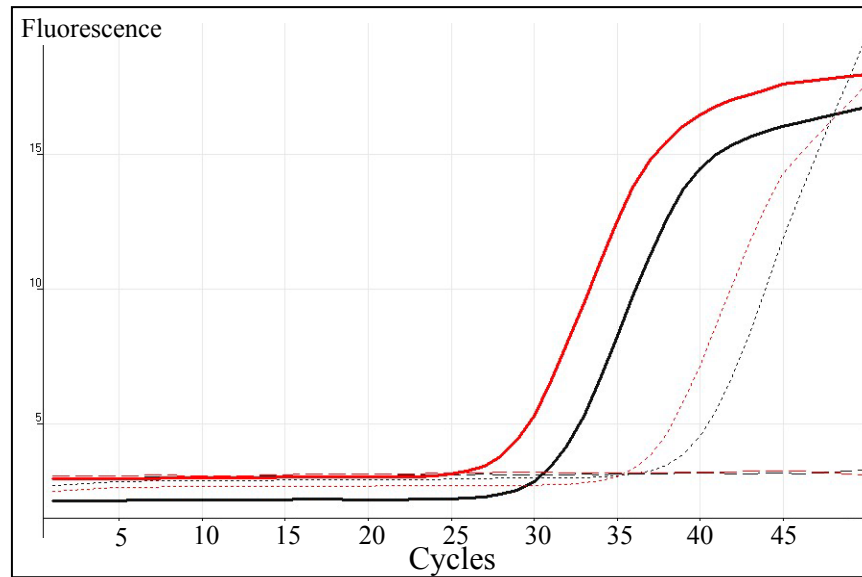
Figure 4.2(G) Real-time RT-PCR fluorescence amplification plots: Tie2 and EPO primer pairs. Key: Tie2 (**solid red line**); EPO (**solid black line**); Tie2 negative control (RT-**dotted red line**); EPO negative control (RT-; **dotted black line**); Tie2 non-template control (water; **dashed red line**); EPO non-template control (water; **dashed black line**).
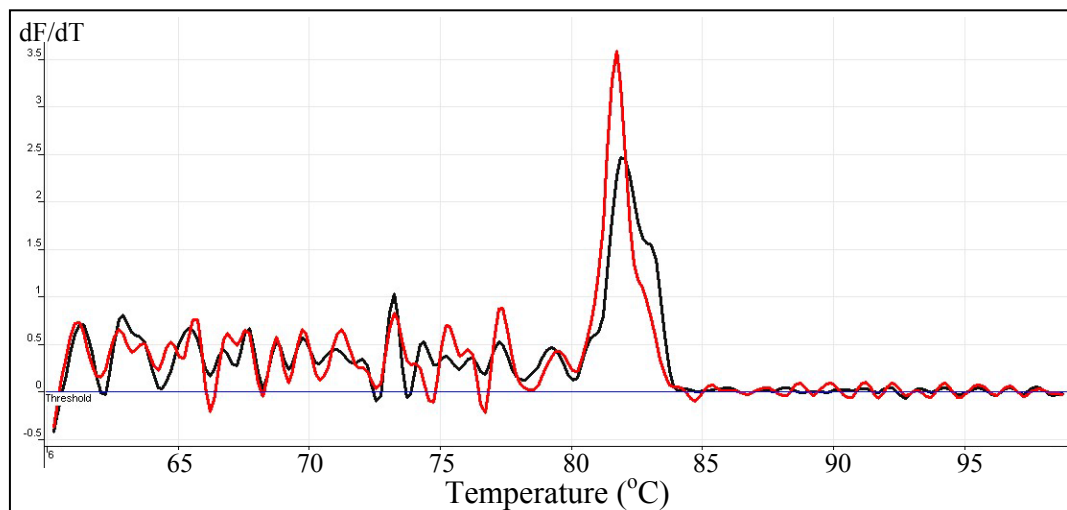
Figure 4.2(H) Melting-curve first derivative plots: Tie2 and EPO primer pairs. A single product is amplified by each primer pair. **Key:** Tie2 (**red line**); EPO (**black line**).
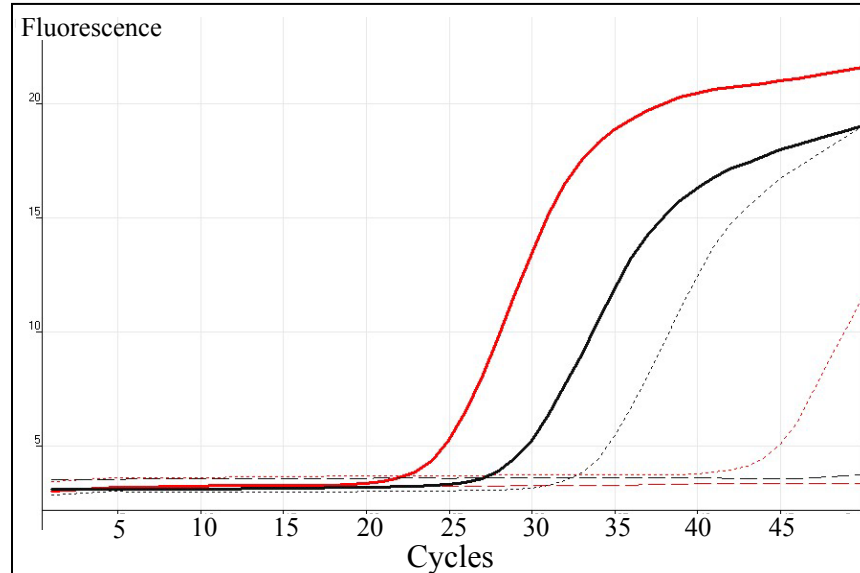
Figure 4.2(I) Real-time RT-PCR fluorescence amplification plots: IGF-1 and COX-2 primer pairs. IGF-1 (**solid red line**); COX-2 (**solid black line**); IGF-1 negative control (RT-; **dotted red line**); COX-2 negative control (RT-; **dotted black line**); IGF-1 non-template control (water; **dashed red line**); COX-2 non-template control (water; **dashed black line**).
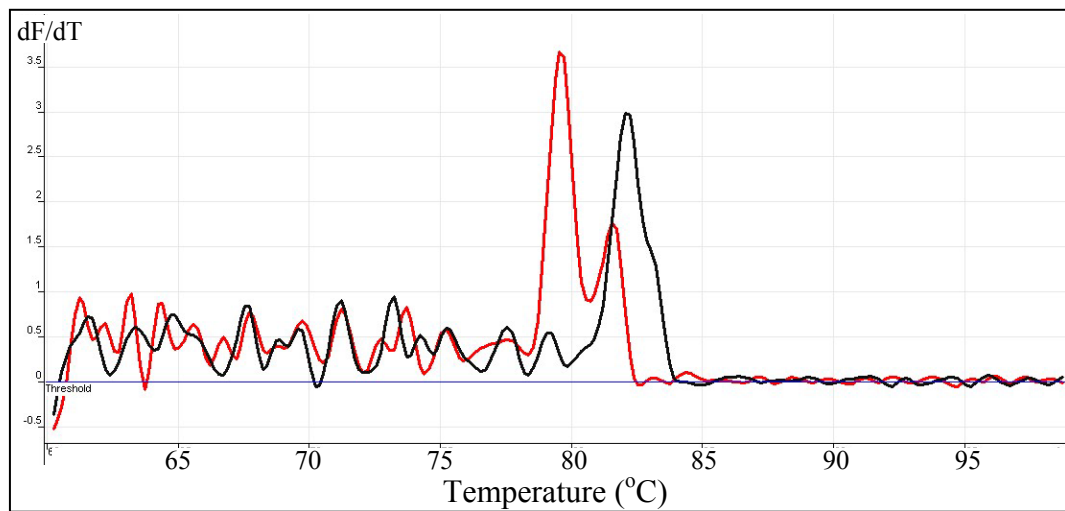
Figure 4.2(J) Melting-curve first derivative plot: IGF-1 and COX-2 primer pairs. A single product is amplified by the COX-2 primer pair (**black line**). The curve for IGF-1 has two distinct peaks, suggestive of two products (**red line**).

Lanes	primers	size (bp)
2/3	ARBP	91
4/5	HPRT	105
6/7	VEGF	90
8/9	PEDF	79
10/11	Ang2	87

DNA markers:
Lane 1: log 2 ladder

Lane 12: 20 bp ladder
(bright band: 200 bp)

Lanes	primers	size (bp)
2/3	VEGFR2	94
4/5	IGF-1	99
6/7	EPO	104
8/9	COX-2	102
10/11	Tie2	99

DNA markers:
Lane 1: log 2 ladder

Lane 12: 20 bp ladder
(bright band: 200 bp)
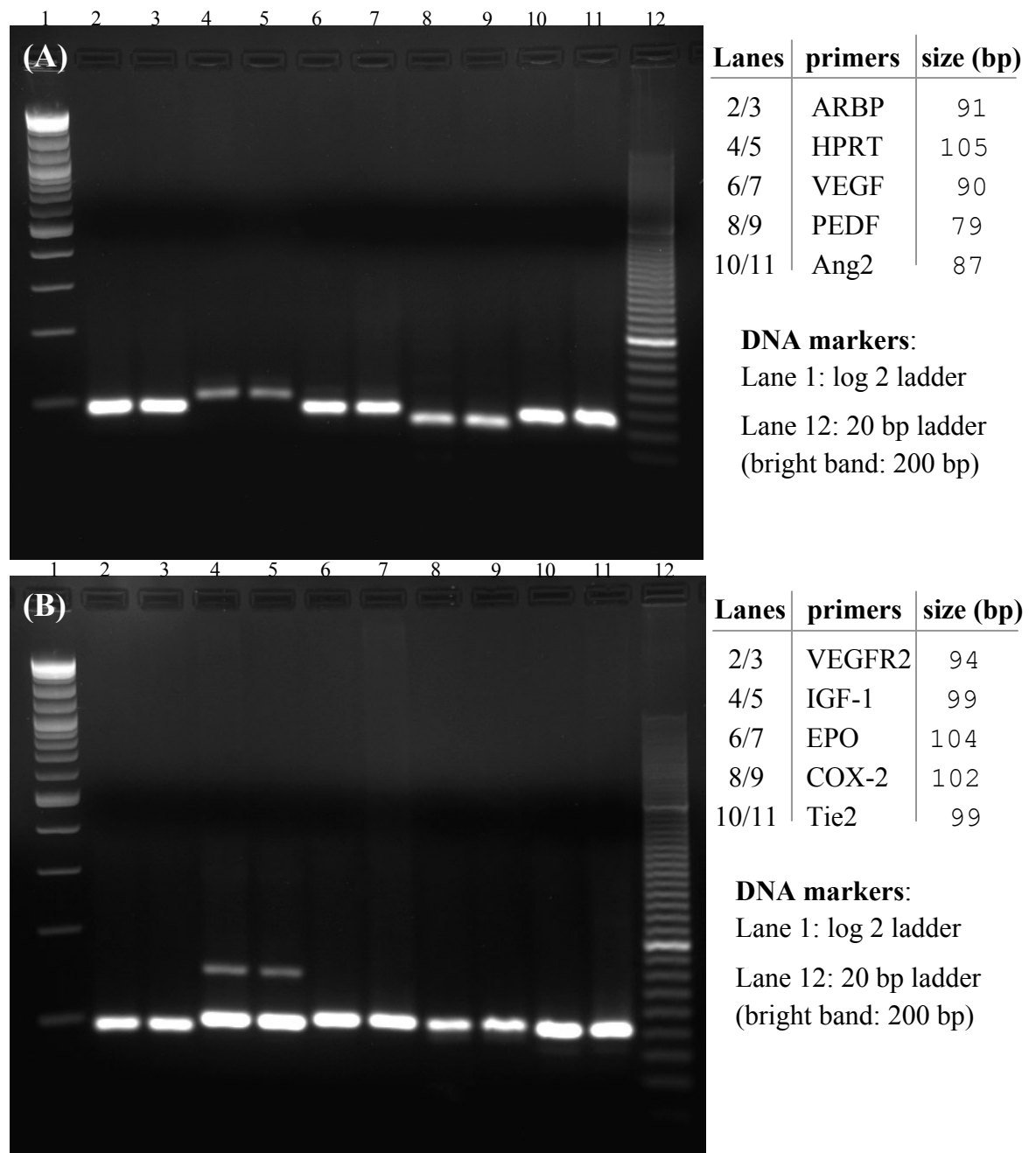
Figure 4.3 Reverse transcription-polymerase chain reaction products of candidate angiogenic factor gene primers (agarose gel electrophoresis photographs). A single PCR product is visible for each primer pair, with the exception of IGF-1 (photograph (B) lanes 4 and 5). In each case, the PCR product is of the predicted size (column 3 of table).

Abbreviations:

bp: base pairs
ARBP: acidic ribosomal phosphoprotein
HPRT: hypoxanthine guanine phosphoribosyl-
transferase
VEGF: vascular endothelial growth factor
PEDF: pigment epithelium-derived factor

Ang2: angiopioetin 2
VEGFR-2: vascular endothelial growth factor
receptor 2
IGF-1: insulin-like growth factor-1
EPO: erythropoietin
COX-2: cyclooxygenase-2

4.2.a.2 Determination of primer amplification efficiency

Sevenfold serial dilutions of the standard cDNA sample were prepared. Real-time RT-PCR was used to generate a standard curve for each set of primers. The PCR cycle number at which the fluorescence signal of a given sample exceeded a threshold value – threshold cycle (Ct) – was used to generate a standard curve. A threshold value was automatically determined for each sample using the Rotor-Gene analysis software (v.5.0). In brief, threshold was defined as a point on the second derivative curve for change in fluorescence with time (d2F/dt2), 80% below the peak of the curve – an approximation of the commencement of the phase exponential amplification. The mean Ct values of the triplicates of each cDNA dilution were plotted as a linear function against the logarithm ($\log_e$) of cDNA concentration (Appendix 3). The gradient of the standard curve regression line for each primer pair was used to calculate the PCR amplification efficiency (Equation 1).

Equation 1:

$$AE = [e^{(1/-g)}] - 1 \quad \text{(reference [411])}$$

where:
AE= amplification efficiency, the percentage change in fluorescence per cycle of PCR (100% efficiency corresponds with a doubling of fluorescence per cycle).
e= Euler's number (where the natural logarithm [$\log_e$] was used to transform cDNA concentration values)
g= gradient of the standard curve regression line

The derivation of this equation is provided in Appendix 3.

The amplification efficiencies of each primer pair and the *r*-squared value of the standard curve regression lines are provided in Table 4.1. Figure 4.4 displays the standard curve for the VEGF primer pair. Amplification efficiency values were used for the quantification of gene expression.
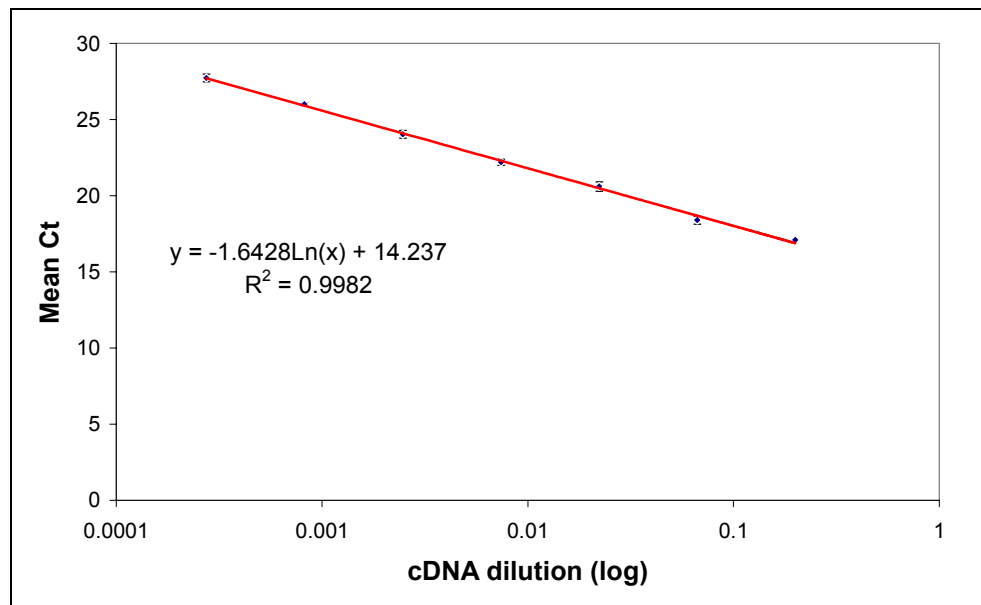
Figure 4.4 Standard curve for VEGF primer pair. A sevenfold serial dilution of the standard rat retinal cDNA sample in water was prepared. Each dilution was amplified in triplicate with the vascular endothelial growth factor (VEGF) primer pairs. The mean threshold cycle value (Ct) for each dilution was plotted against the natural logarithm of the fractional cDNA concentration, where 1= neat cDNA. The slope of the regression line fitted to these points (red line) was used to determine the amplification efficiency for the reaction. *n*= mean of three reactions per data point; error bars: ± SD.

Primer pair	Amplification efficiency (%)	R^2
VEGF	83.81	0.998
VEGFR-2	98.60	0.999
PEDF	104.72	0.998
Ang2	96.42	0.999
Tie2	96.47	0.999
EPO	92.17	0.999
IGF-1	91.46	0.998
COX-2	93.53	0.999

Table 4.1 Standard curve derived amplification efficiencies of candidate gene primers. Real-time RT-PCR was performed in triplicate on a dilution series of a standard cDNA sample. For each dilution the mean cycle (mean Ct) at which the emitted fluorescence exceeded the threshold value was plotted against the logarithm of the cDNA dilution. The regression line fitted to these points was used to determine amplification efficiency – the percentage change in fluorescence per PCR cycle. R^2 indicates the goodness of fit of the regression line. Note that the amplification efficiency for PEDF exceeded 100% — a practical impossibility. Calculated efficiencies in excess of 100% are not uncommon and reflect the fact that this method of efficiency determination provides an overestimate of true efficiency [359, 412].

4.2.a.3   Optimisation of experimental conditions

The real-time RT-PCR conditions selected for the initial experiments required little optimisation (section 2.3.l). The cycling parameters were selected in accordance with the instruction manual for the thermal cycler, with adjustment for the primer melting temperatures. Each primer was designed to have a melting temperature as close to $60^{o}C$ as possible, such that a single set of cycling parameters could be utilised for all primer pairs. The estimated primer melting temperatures ranged from $57\text{-}61^{o}C$ (Table 2.1). An annealing temperature $5\text{-}8°C$ below the melting temperature of each primer was recommended by the SYBR Green master-mix instruction manual (QuantiTect SYBR Green PCR Handbook 08/2003). Accordingly, efficient and specific amplification was achieved for all primer pairs with an annealing temperature of $50°C$. An increase of $5^{o}C$ in the annealing temperature had no appreciable effect on the specificity or sensitivity of the reaction (data not shown). The buffering conditions of the SYBR Green master-mix are known to facilitate specific primer annealing over a wide temperature range and a wide range of magnesium concentrations (QuantiTect SYBR Green PCR Handbook 08/2003). Accordingly, titration of $MgCl_2$ was not required.

A working dilution of cDNA of 1/100 was selected on the basis of the findings of the standard sample dilution series. In all cases, dilutions of the standard cDNA sample of 1/1215 remained on the linear portion of the standard curve. Accordingly, at a dilution of 1/100, gene expression in an experimental sample of more than 10-fold greater than, or 10-fold less than, that of the standard sample could be reliably detected.

4.2.b. Relative quantification of gene expression

Relative quantification of gene expression was performed using the delta Ct method [413], with adjustment for amplification efficiency and subsequent normalisation. The expression of each gene in each sample was determined relative to the geometric mean expression of the same gene in triplicates of the standard sample (section 2.3.g). Thus gene expression values were relative to the standard cDNA sample. The use of a standard sample precluded the need for calibration between duplicate PCR runs. The method was developed as a modification of the quantification algorithm described in the public   domain   software   application   GeNorm   [414]   (accessible   at:

http://medgen.ugent.be/~jvdesomp/genorm/).

The relative quantity (Q) of each gene, in each cDNA sample was calculated as a function of reaction efficiency raised to the power of the difference in threshold cycle between the sample of interest (Ct_A) and a standard sample (Ct_S) (Equation 2). Reaction efficiency – the fold change in fluorescence per cycle – was equal to the percentage change in fluorescence per cycle – the amplification efficiency (E) – plus one. The value for Ct_S was the geometric mean of the Ct for triplicates of a standard sample amplified by the same primer pair, in the same PCR, as the sample of interest.

Equation 2:

$$Q=(E+1)^{(Cts-CtA)}$$

The derivation of this equation is appended (delta Ct method; Appendix 3). Note that for each PCR run the value for Ct_S was the geometric mean of the Ct values of triplicates of the standard sample. The relative quantity value was calculated for each replicate for each primer pair, in each cDNA sample. The relative expression values were then normalised to the geometric mean of two reference genes assayed in parallel.

4.2.c. Normalisation of gene expression

4.2.c.1 Reference gene selection and validation

Reference genes were used for normalisation – a means of controlling for variation in cDNA loading between samples. Candidate reference genes were selected for appraisal on the basis of a literature review (Appendix 4). Reference genes that were stably expressed during retinal development and in hypoxia were considered for selection. Accordingly, acidic ribosomal phosphoprotein (ARBP), cyclophilin A (CYCA), hypoxanthine guanine phosphoribosyltransferase (HPRT), RNA polymerase 2 (RNAP2) and gamma actin (ACTG2) were chosen as potential reference genes. These genes play roles in a diverse range of cellular processes (Table 4.2).

Table 4.2 Candidate reference genes considered for inclusion in the study of rat strain differences in OIR.

Gene name	Accession number	Cellular function (OMIM*)
Actin, gamma 2 (ACTG2)	NM_012893.1	Structural/cytoskeletal protein (102545)
Acidic ribosomal phosphoprotein (ARBP; 36B4)	NM_022402	Ribosomal protein (180510)
Cyclophilin A [peptidylprolyl isomerase A] (CYCA)	NM_017101.1	Protein folding and intracellular transport (123840)
Hypoxanthine guanine phosphoribosyltransferase (HPRT)	NM_012583.1	Purine biosynthesis (308000)
RNA polymerase 2 (RNAP2)	XM_343922.1	mRNA transcription (180660)

* OMIM: Online Mendelian Inheritance in Man –

http://www.ncbi.nlm.nih.gov/entrez/query.fcgi?db=OMIM

Primers were designed for each of the candidate reference genes (Table 2.1), using the method described previously (section 2.3.i). Primer pairs were tested on a control sample of cDNA derived from the RNA extracted from a DA rat retina. cDNA was used at a dilution of 1/10 in water for the pilot experiment. Real-time RT-PCR was performed in accordance with the method outlined in section 2.3.l. The candidate reference genes were expressed to varying extents in the test cDNA sample, with CYCA being the most abundant, and ACTG2 the least abundant (Figure 4.5). When real-time RT-PCR was repeated at the working cDNA dilution of 1/100, as opposed to the 1/10 dilution used in the pilot experiment, the expression of ACTG2 was so low as to preclude its use as a reference gene.

In all cases, with the exception of CYCA, the melting-curve analysis was consistent with a single reaction product (Figure 4.6). The curve for CYCA was broad and had three distinct peaks, suggestive of three different products. To confirm these findings, the products of each primer pair were separated via agarose gel electrophoresis. All primers other than CYCA amplified a single product, and in each case the amplified product

matched the predicted size (Figure 4.7). In contrast, the CYCA primers amplified three distinct products, one of which corresponded in size with the target sequence. CYCA is known to have numerous processed pseudogenes and it is likely that the additional CYCA products are the result of pseudogene amplification [415, 416]. It has been found that CYCA pseudogene amplification may persist even when rigorous efforts are undertaken to minimise genomic DNA contamination [417]. CYCA was therefore abandoned as a candidate reference gene.

To further confirm primer specificity, the PCR products of the remaining three candidate reference genes were purified and subjected to sequence analysis (sections 2.3.m & 2.3.n). In each case, sequencing confirmed the amplification of a single product identical to the predicted sequence (Appendix 2). The primer pairs for ARBP, HPRT and RNAP2 were then used in real-time RT PCR experiments with pooled cDNA samples as described in section 2.3.l. Relative expression values of each reference gene were determined for each of the three cardinal rat strains (F344, SPD and DA) at each of the three experimental end-points – room air control at day 14; cyclic hyperoxia at day 14; cyclic hyperoxia for 14 days plus four days in room air (day 18). These values were used in the assessment of candidate reference gene expression stability, to guide the final selection of reference genes.
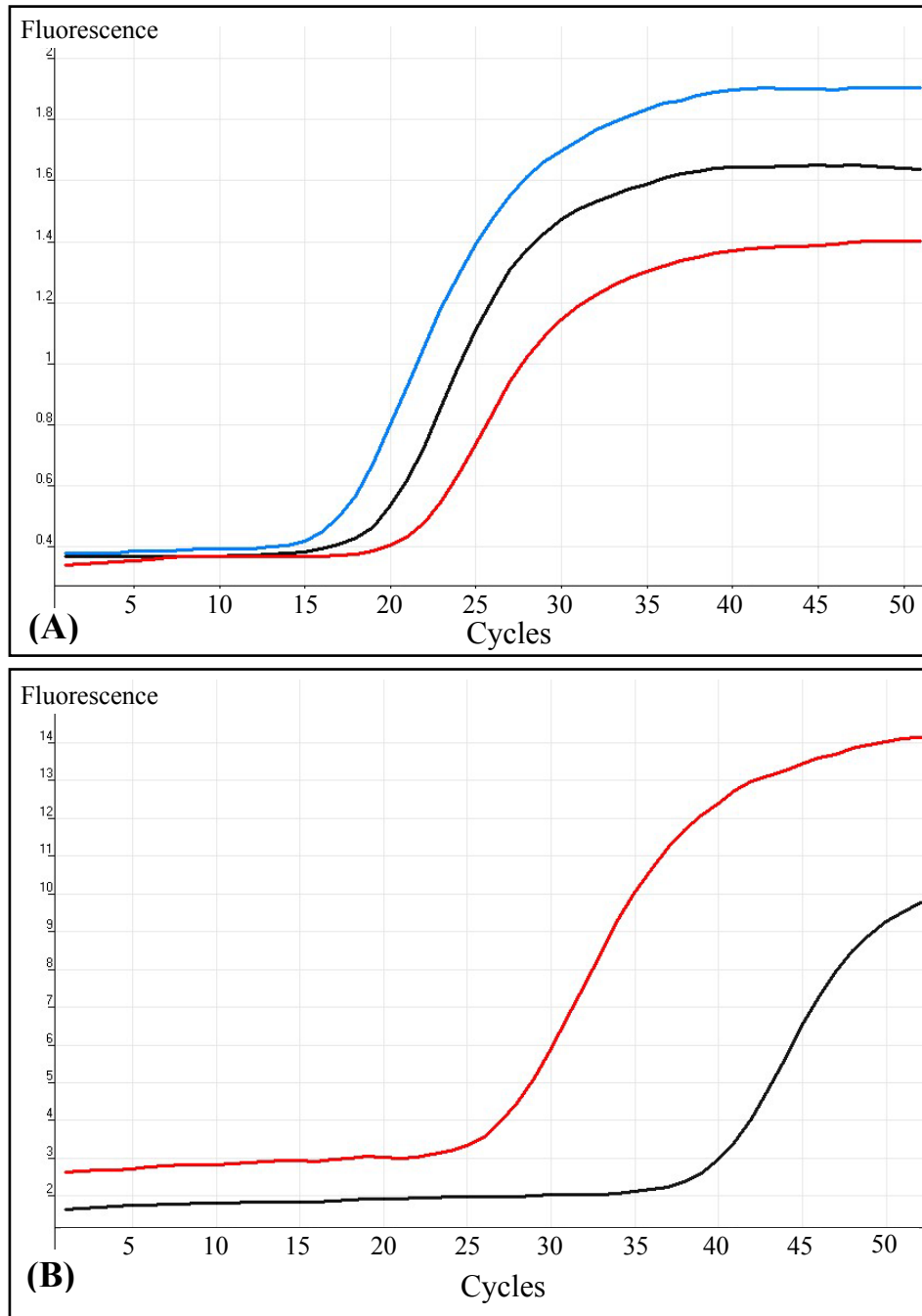
Figure 4.5 Real-time RT-PCR fluorescence amplification plots of candidate reference genes. Real-time RT-PCR was performed on a sample of rat retinal cDNA (1/10 dilution). Figure (A): Cyclophilin A (**blue**) is more abundant in the sample than RNA polymerase 2 (**black**) which, in turn, is more abundant than acidic ribosomal phosphoprotein (**red**). Figure (B): hypoxanthine guanine phosphoribosyl-transferase (**red**) is more abundant than gamma actin (**black**).
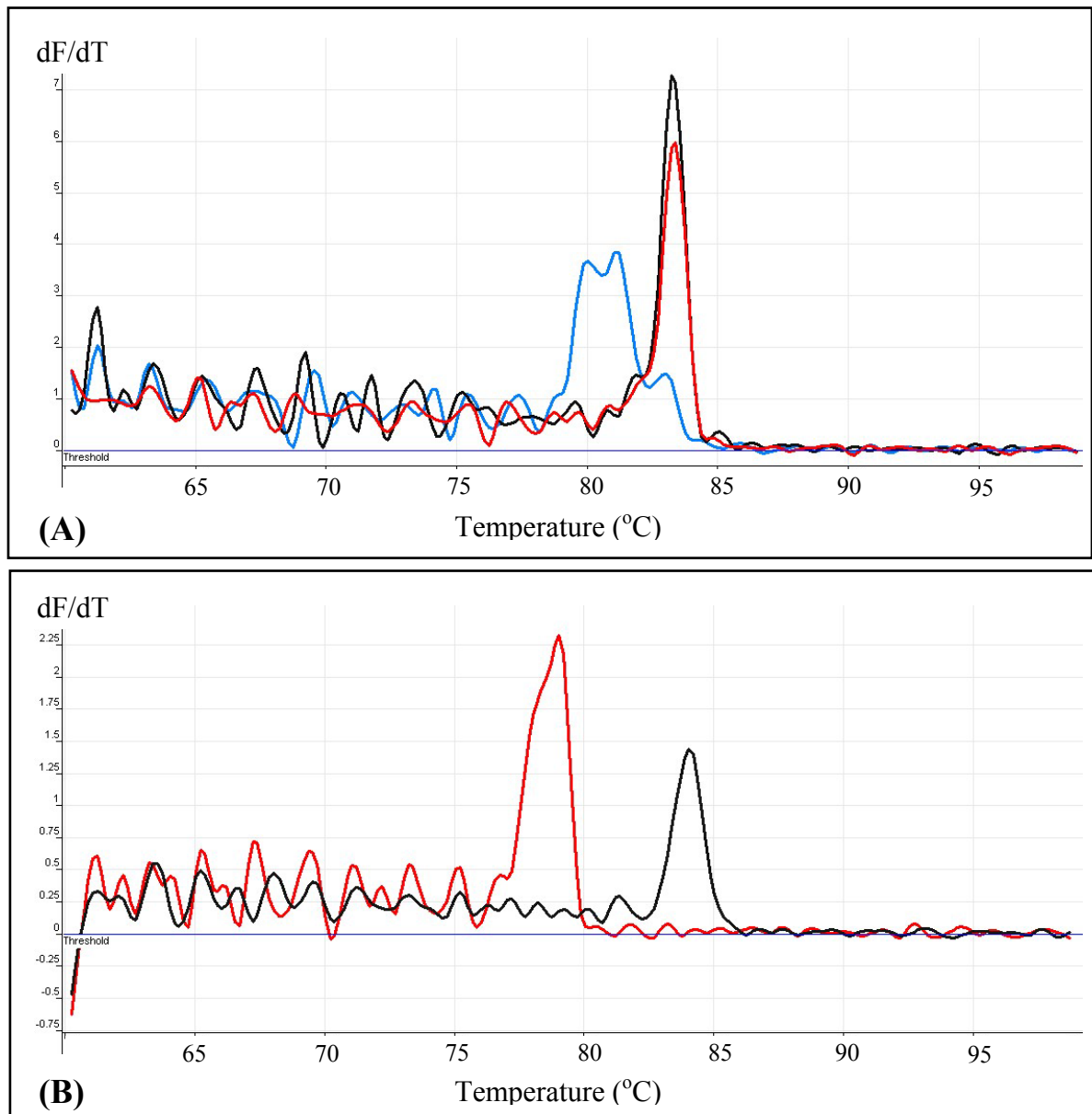
Figure 4.6 Melting-curve analysis of candidate reference genes. The products of each reference gene primer pair were subjected to increasing temperatures. With the exception of cyclophilin A (blue curve, figure (A)), the melting-curve of each primer pair has a single, well-defined peak, suggestive of a single product. The curve for cyclophilin A occupies a broad temperature range and has three distinct peaks, suggestive of three different products.

Key. Figure (A): **Blue curve**: cyclophilin A (CYCA); **Red curve**: RNA polymerase 2 (RNAP2); **Black curve**: Acidic ribosomal phosphoprotein (ARBP). **Figure (B)**: **Red curve**: hypoxanthine guanine phosphoribosyltransferase (HPRT); **Black curve**: actin, gamma 2 (ACTG2).
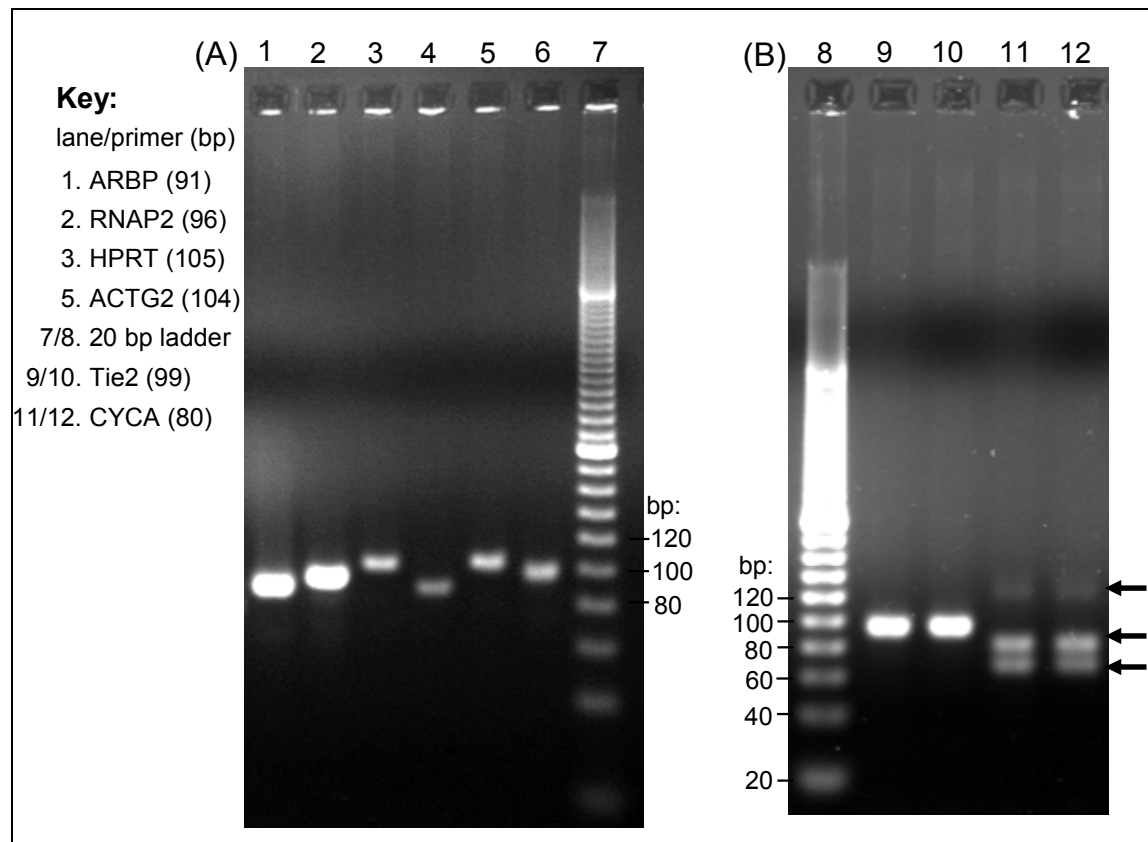
Figure 4.7 Reverse transcription-polymerase chain reaction products of candidate reference gene primers (agarose gel photographs). A single product of the expected size is amplified by all of the reference gene primer pairs tested in panel (A). In contrast, the primers for cyclophilin A amplify three separate products of approximately 70 bp, 80 bp and 120 bp (black arrows, lanes 11 and 12). The predominant product is of the expected size (80 bp), while the other two products are likely to be the result of pseudogene amplification.

Abbreviations:
ARBP: acidic ribosomal phosphoprotein
RNAP2: RNA polymerase 2
HPRT: hypoxanthine guanine phosphoribosyltransferase
ACTG2: actin, gamma 2
CYCA: cyclophilin A

4.2.c.1.1 Reference gene expression-stability

The expression data for each of the three candidate reference genes in each of the retinal cDNA pools was subjected to expression-stability analysis using the GeNorm software application (Appendix 4) [414]. RNAP2 was identified as the least stably expressed of the three genes. In accordance with this finding, a comparison of the relative expression of each of the reference genes in the 9 different cDNA pools demonstrated that the

expression of RNAP2 differed amongst samples to a greater extent than did either ARBP or HPRT (Figures 4.8 & 4.9). There was greater correlation for the expression ARBP and HPRT (r^2=0.80) than for the other gene pairs – ARBP and RNAP2 (r^2= 0.31) or HPRT and RNAP2 (r^2=0.25). The exclusion of RNAP2 from the GeNorm analysis significantly improved the average gene expression stability value. On this basis, the reference genes ARBP and HPRT were retained for normalisation.

Thus ARBP and HPRT were stably expressed in each of the pooled cDNA samples. Expression of these genes did not differ significantly between strains, nor did they vary with oxygen exposure or developmental stage. ARBP and HPRT were therefore validated as reference genes for this study.
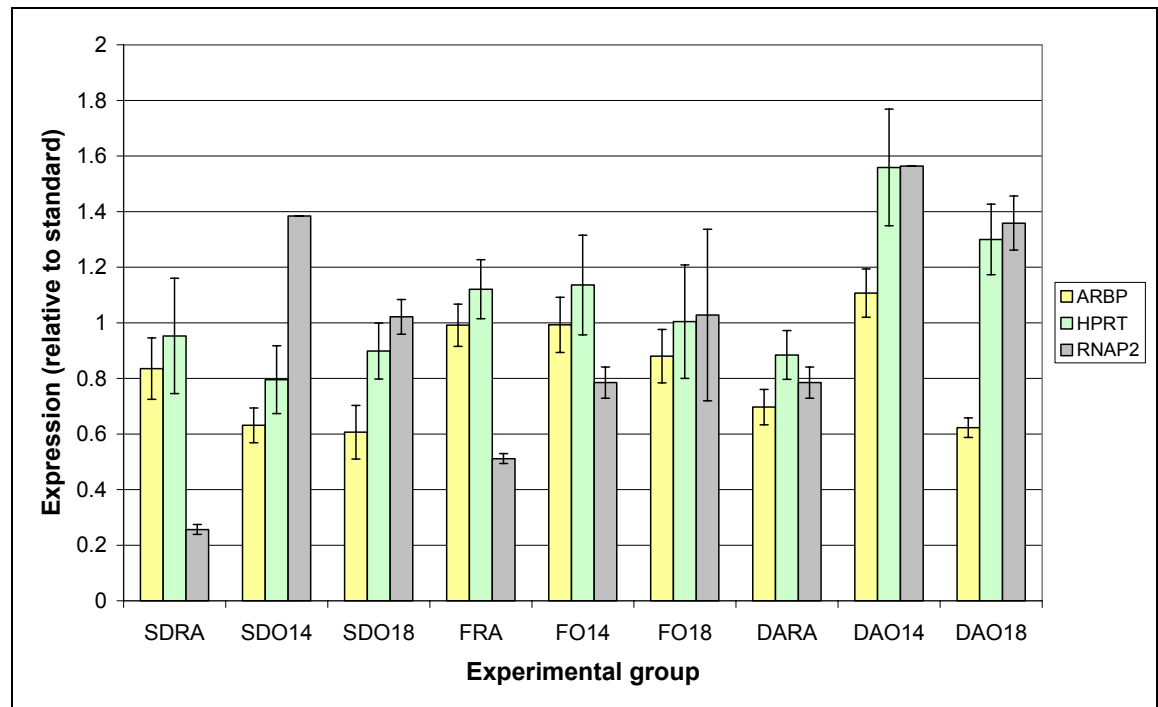
Figure 4.8 Candidate reference gene expression in rat retinal cDNA pools. The expression of each reference gene, in each sample, was determined relative to the expression of the same gene in a standard sample. The non-normalised, relative expression values were plotted. The average of the variation in relative expression between each pair of genes within each of the 9 cDNA samples was used as a guide to the stability of gene expression. The relative expression values for ARBP and HPRT were more closely correlated than were those for either gene with RNAP2. RNAP2 appeared to have the lowest expression stability. As the expression of ARBP and HPRT were closely matched within samples, differences in the average expression levels of these genes between different samples reflected differences in cDNA loading – this is the principle on which normalisation was based.

n=6 replicates per experimental group of three pooled rat retinae. Error bars: ± SD.

Key:
ARBP: Acidic ribosomal phosphoprotein
HPRT: hypoxanthine guanine phosphoribosyltransferase
RNAP2: RNA polymerase 2

F344RA14: Fischer 344 room air day 14 (control)
F344O14: Fischer 344 cyclic hyperoxia day 14
F344O18: Fischer 344 day 18 (cyclic hyperoxia 14 days + 4 days room air)
SPDRA14: Sprague Dawley room air day 14 (control)
SPDO14: Sprague Dawley cyclic hyperoxia day 14
SPDO18: Sprague Dawley day 18 (cyclic hyperoxia 14 days + 4 days room air)
DARA14: Dark Agouti room air day 14 (control)
DAO14: Dark Agouti cyclic hyperoxia day 14
DAO18: Dark Agouti day 18 (cyclic hyperoxia 14 days + 4 days room air)

Figure 4.9 (facing page) Normalised expression of reference genes in rat retinal cDNA pools. Gene expression in each pooled sample was normalised by dividing the raw expression value by the geometric mean of the expression levels of the two selected reference genes, ARBP and HPRT, in the same sample. There is little variation between groups for the normalised expression of ARBP (A) or HPRT (B). In contrast the expression of RNAP2 (C) varies considerably between groups: within each strain expression is higher in the oxygen exposed groups (O14 & O18), than in the room air group.

n=6 replicates per experimental group of three pooled rat retinae. Error bars: ± SD.

Key:
ARBP: Acidic ribosomal phosphoprotein
HPRT: hypoxanthine guanine phosphoribosyltransferase
RNAP2: RNA polymerase 2

F344RA14: Fischer 344 room air day 14 (control)
F344O14: Fischer 344 cyclic hyperoxia day 14
F344O18: Fischer 344 day 18 (cyclic hyperoxia 14 days + 4 days room air)
SPDRA14: Sprague Dawley room air day 14 (control)
SPDO14: Sprague Dawley cyclic hyperoxia day 14
SPDO18: Sprague Dawley day 18 (cyclic hyperoxia 14 days + 4 days room air)
DARA14: Dark Agouti room air day 14 (control)
DAO14: Dark Agouti cyclic hyperoxia day 14
DAO18: Dark Agouti day 18 (cyclic hyperoxia 14 days + 4 days room air)

(A) ARBP

(B) HPRT

(C) RNAP2

4.2.c.2 Normalised retinal gene expression

The relative expression value of each gene, in each sample replicate, calculated by the delta Ct method (Equation 2, 4.2.b), was normalised using the reference genes HPRT and ARBP. A normalisation factor for each sample replicate was calculated as the geometric mean of the relative expression values for HPRT and ARBP in the same sample, in accordance with the method outlined in the GeNorm software application. An example calculation outlining the steps involved in relative quantification and normalisation is provided in Figure 4.10. The mean expression value for each gene in each pooled cDNA sample was calculated as the mean of the normalised relative expression values for the six replicates of that sample.

4.2.d. Intra-run and inter-run variation

The standard deviation (SD) in Ct values of replicate amplifications were used to provide an overall estimate of the reproducibility of PCR reactions. All replicate amplifications included in the strain comparison of gene expression (n= 180 reactions in triplicate) were used for this estimate. Overall, the variation in SD of Cts of replicate amplifications within each PCR run ranged from 0 to 0.84 cycles, with an average of 0.182 cycles. This corresponded with an average intra-run coefficient of variation in Ct of 0.69% (range 0-2.67%), and in mean normalised gene expression of 10.9% (range 0-61%). Variation in the SD of Ct values of replicate runs – inter-run variation – was between 0.07 and 0.79 cycles, with a mean of 0.21 cycles. The overall inter-run coefficient of variation was 0.81% (range 0.30-3.11%) for Ct and 14.2% (range 3.7-46.6%) for mean normalised expression. These values compared favourably with those of other published studies [412, 418]. Thus the overall precision of PCR reactions was satisfactory.

Figure 4.10(A) Quantification algorithm

Sample A ← One of three replicates of the pooled cDNA sample for SPD room air control rats (SPDRA) in run 1 of 2 duplicate PCR runs for the gene of interest, VEGF

← Real time RT-PCR: VEGF primer pair; run includes triplicates of each pooled cDNA sample and a standard sample

Ct_A ← Amplification cycle at which emitted fluorescence exceeds threshold value

	VEGF		ARBP		HPRT	
	Run1	Run2	Run1	Run2	Run1	Run2
SPDRA	23.2	22.7	20.6	21	32.2	31.6
SPDRA	23	23	20.8	20.8	31.4	31.1
SPDRA	23.1	22.7	20.6	20.7	31.2	31.7
STD	22.2	22.3	20.6	20.6	31.6	31.6
STD	22.3	21.9	20.4	20.3	31.9	31.2
STD	22	22.1	20.6	20.3	31.6	30.4

Q= non-normalised VEGF expression in sample A relative to the expression of VEGF in the standard sample.
E= Amplification efficiency for VEGF; calculated from the gradient of the standard curve for VEGF.
Ct_S= geometric mean of the Ct values for each of the three replicates of the standard sample (STD) in this PCR run

$Q_A=(E+1)^{(Cts-CtA)}$ ←

	VEGF		ARBP		HPRT	
	Run1	Run2	Run1	Run2	Run1	Run2
SPDRA	0.532	0.693	0.957	0.672	0.801	0.787
SPDRA	0.601	0.577	0.838	0.767	1.143	0.984
SPDRA	0.566	0.693	0.957	0.819	1.249	0.753
STD	0.979	0.885	0.957	0.876	1.045	0.787
STD	0.922	1.129	1.092	1.068	0.915	0.941
STD	1.107	1.000	0.957	1.068	1.045	1.343

X_A= normalised VEGF expression in sample A relative to the expression of VEGF in the standard sample.
NF_{SPDRA}= normalisation factor for SPD room air samples: the geometric mean of the relative quantity values for ARBP and HPRT in SPDRA samples (6 replicates per reference gene)

$X_A = Q_A / NF_{SPDRA}$ ←

	VEGF		ARBP		HPRT	
	Run1	Run2	Run1	Run2	Run1	Run2
SPDRA	0.605	0.788	1.087	0.763	0.910	0.895
SPDRA	0.684	0.656	0.952	0.871	1.298	1.118
SPDRA	0.643	0.788	1.087	0.931	1.419	0.856
STD	0.980	0.885	0.957	0.876	1.406	0.788
STD	0.922	1.130	1.093	1.069	0.915	0.941
STD	1.107	1.000	0.957	1.069	1.046	1.343

Figure 4.10(B) Example calculation

Sample A

$Ct_A = 23.2$

$Ct_S = (22.2 \times 22.3 \times 22)^{1/3} = 22.1663$

$E = 83.81\% = 0.84$

$Q_A = (0.84+1)^{(22.1663 - 23.2)}$

Ct_A

$Q_A = 1.84^{-1.0337} = 0.532$

$NF_{SPDRA} = (\Pi \ ARBPQ_{SPDRA} x \ \Pi \ HPRTQ_{SPDRA})^{1/12}$

$\Pi \ ARBPQ_{SPDRA} = 0.957 \times 0.838 \times 0.957 \times 0.672 \times 0.767 \times 0.819$

$= 0.324$

$\Pi \ HPRTQ_{SPDRA} = 0.801 \times 1.143 \times 1.249 \times 0.787 \times 0.984 \times 0.753$

$= 0.667$

$Q_A = (E+1)^{(Cts-CtA)}$

$NF_{SPDRA} = (0.324 \times 0.667)^{1/12} = 0.880$

$X_A = Q_A / NF_{SPDRA}$

$X_A = Q_A / NF_{SPDRA}$

$X_A = 0.532 / 0.880 = 0.605$

$X_{SPDRA} = (0.605 + 0.684 + 0.643 + 0.788 + 0.656 + 0.788)/6$

$X_{SPDRA} = 0.694$

	VEGF		ARBP		HPRT	
	Run1	Run2	Run1	Run2	Run1	Run2
SPDRA	23.2	22.7	20.6	21	32.2	31.6
SPDRA	23	23	20.8	20.8	31.4	31.1
SPDRA	23.1	22.7	20.6	20.7	31.2	31.7
STD	22.2	22.3	20.6	20.6	31.6	31.6
STD	22.3	21.9	20.4	20.3	31.9	31.2
STD	22	22.1	20.6	20.3	31.6	30.4

	VEGF		ARBP		HPRT	
	Run1	Run2	Run1	Run2	Run1	Run2
SPDRA	0.532	0.693	0.957	0.672	0.801	0.787
SPDRA	0.601	0.577	0.838	0.767	1.143	0.984
SPDRA	0.566	0.693	0.957	0.819	1.249	0.753
STD	0.979	0.885	0.957	0.876	1.045	0.787
STD	0.922	1.129	1.092	1.068	0.915	0.941
STD	1.107	1.000	0.957	1.068	1.045	1.343

	VEGF		ARBP		HPRT	
	Run1	Run	Run1	Run2	Run1	Run2
SPDRA	0.605	0.788	1.087	0.763	0.910	0.895
SPDRA	0.684	0.656	0.952	0.871	1.298	1.118
SPDRA	0.643	0.788	1.087	0.931	1.419	0.856
STD	0.980	0.885	0.957	0.876	1.406	0.788
STD	0.922	1.130	1.093	1.069	0.915	0.941
STD	1.107	1.000	0.957	1.069	1.046	1.343

4.2.e. Experimental design and methodological validation: concluding remarks

The preliminary real-time RT-PCR experiments confirmed that the primer pairs for each of the eight angiogenic factor genes, and the two reference genes, amplified a specific product with satisfactory efficiency. Primer specificity was assured by melting curve analysis, coupled with agarose gel electrophoresis as well as product sequencing. Gene expression in each sample was determined relative to a standard sample, with adjustment for reaction efficiency. Raw gene expression values were normalised using two reference genes that were validated for the experimental conditions. Normalisation provided an important control for variation in cDNA quantity, ensuring the comparability of test samples. Each sample was tested in triplicate, in duplicate runs, with satisfactory precision. Together, these measures facilitated highly specific quantification of retinal gene expression using the SYBR-Green system, without the need for probe-based detection chemistry.

CHAPTER 4
SECTION 2

RESULTS

4.3.   INTER-ANIMAL VARIATION IN GENE EXPRESSION

As gene expression studies were to be conducted using cDNA samples derived from pooled retinal RNA samples, a pilot experiment was conducted to evaluate the extent of variation in retinal gene expression amongst individual rats within a given pool. As the selected rat strains were inbred, it was likely that inter-animal variation within one strain was representative of the variation within other strains. Accordingly, the expression of an arbitrarily selected gene – VEGF – in an arbitrarily selected strain – the SPD – was used for the pilot experiment. Each of the three SPD cDNA pools was examined: room air control rats at 14 days (SPDRA14); rats exposed to 14 days of cyclic hyperoxia (SPDO14); and rats exposed to cyclic hyperoxia for 14 days, followed by four days in room air (SPDO18). One microgram of retinal RNA from each rat of the three pools was reverse transcribed in parallel with 1 μg of the pooled samples. Quantitative real-time RT-PCR was used to compare relative retinal gene expression amongst individual rats within each pool to assess inter-animal variation in VEGF gene expression. The retinal expression levels of VEGF mRNA in the three experimental groups are shown in Figures 4.12-4.14. Values are relative to the expression of VEGF in the pooled standard sample. Data are derived from a single PCR run, with each sample assayed in triplicate and normalised to the two reference genes.

Figure 4.11 displays the expression data for rats following 14 days in room air. Overall, there was a statistically significant difference in VEGF expression between individual rats in this group ($F_{(2,6)}=42.352$; $p<0.001$). The retinal VEGF expression of rat 1 (SPDRA14.1) was 117% greater than that of rat 2 (SPDRA14.2) and 145% greater than that of rat 3 (SPDRA14.1). Figure 4.12 demonstrates a similar finding for rats exposed to cyclic hyperoxia for 14 days – there was a statistically significant difference between individual rats ($F_{(2,6)}=16.3$; $p=0.004$) for VEGF expression. The mean retinal VEGF expression of rat 3 (SPDO14.3) was 52% greater than that of rat 1 (SPDO14.1) and 30% higher than rat 2 (SPDO14.2). No significant difference was found for the expression of VEGF in the retinae of three rats at SPDO18 ($F_{(2,6)}=2.0$; $p=0.21$) (Figure 4.13). When the three exposure groups were compared, there was an overall effect of oxygen exposure on VEGF expression ($F_{(2,6)}=9.87$; $p=0.013$). Furthermore, when a two-way nested analysis of variance was performed, with rat identity allocated as a random factor,

there was still a statistically significant difference in VEGF expression between the three exposure groups (F(6,18)=28.59; p<0.001). Thus the overall effect of oxygen exposure on VEGF expression was greater than the effect of inter-animal variation within the treatment groups. Of the observed variance in VEGF expression within treatment groups 90.2% was attributable to inter-animal variation, while 9.8% was due to measurement error.

Real-time RT-PCR was used to determine the extent of VEGF expression of each of the three sample pools. These values (*pooled RNA*) were then compared with the overall mean expression level of the three corresponding individual samples, which together represent a surrogate of a pooled cDNA sample, or a virtual *cDNA pool* (Figure 4.14). The pooled RNA values were greater than those of the corresponding virtual cDNA pools. However, when the VEGF expression levels of the oxygen exposed groups were compared with the matched room air control group, the changes in gene expression induced by oxygen exposure were similar in magnitude for the two sets of pooled data (Table 4.3).

In summary, significant variation was identified in retinal VEGF mRNA expression amongst inbred rats of the same strain, in the same treatment group, with differences as great as 2.4-fold in magnitude. Nevertheless, when the inter-animal variation was taken into account, there was still an overall difference in gene expression between exposure groups. The comparison of pooled samples suggested that there was little difference between the pooling of samples before or after reverse transcription, as long as care was taken in the initial process of RNA quantification.
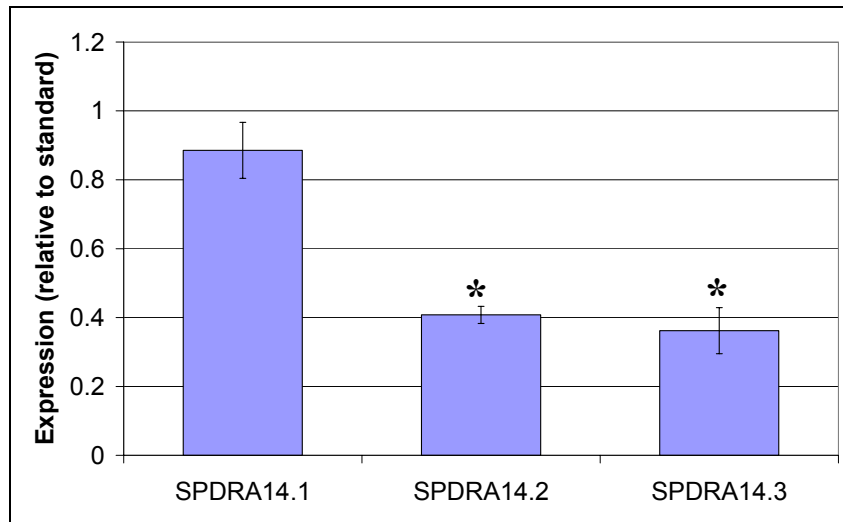
Figure 4.11 Variation in VEGF mRNA expression amongst SPD rats reared in room air for 14 days. VEGF expression was significantly greater for rat 1 (SPDRA14.1), than for rats 2 (SPDRA14.2) and 3 (SPDRA14.3). * p<0.001; error bars: ± SD.

Comparison	Mean difference	95% CI	Significance
SPDRA14.1>SPDRA14.2	117%	53-207%	p<0.001
SPDRA14.1>SPDRA14.3	145%	72-247%	p<0.001
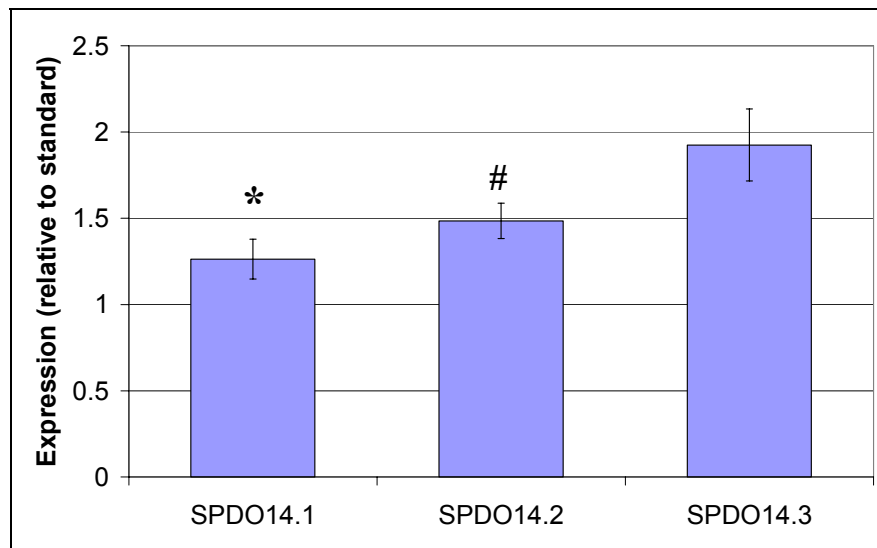
Figure 4.12 Variation in VEGF mRNA expression amongst oxygen exposed SPD rats at 14 days. VEGF expression was significantly higher for rat 3 (SPDO14.3) than for rats 1 (SPDO14.1) (* p=0.004) and 2 (SPDO14.2) (# p=0.04). Error bars: ± SD.

Comparison	Mean difference	95% CI	Significance
SPDO14.3>SPDO14.1	52%	20-95%	p=0.004
SPDO14.3>SPDO14.2	30%	2-66%	p=0.04
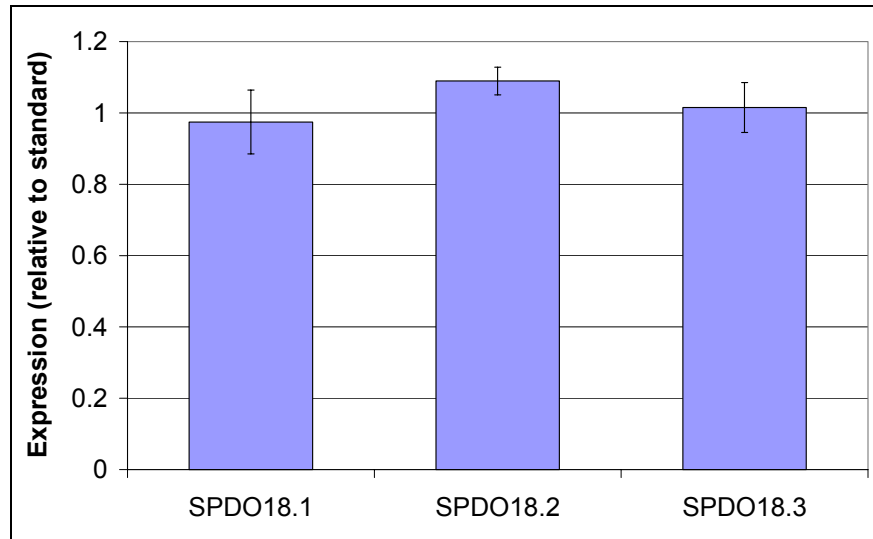
Figure 4.13 Variation in VEGF mRNA expression amongst oxygen exposed SPD rats at 18 days (14 days cyclic hyperoxia + 4 days room air). VEGF expression was similar for each of the 3 rats. Error bars: ± SD. **Key:** SPDO18.1= rat 1; SPDO18.2= rat 2; SPDO18.3= rat 3.
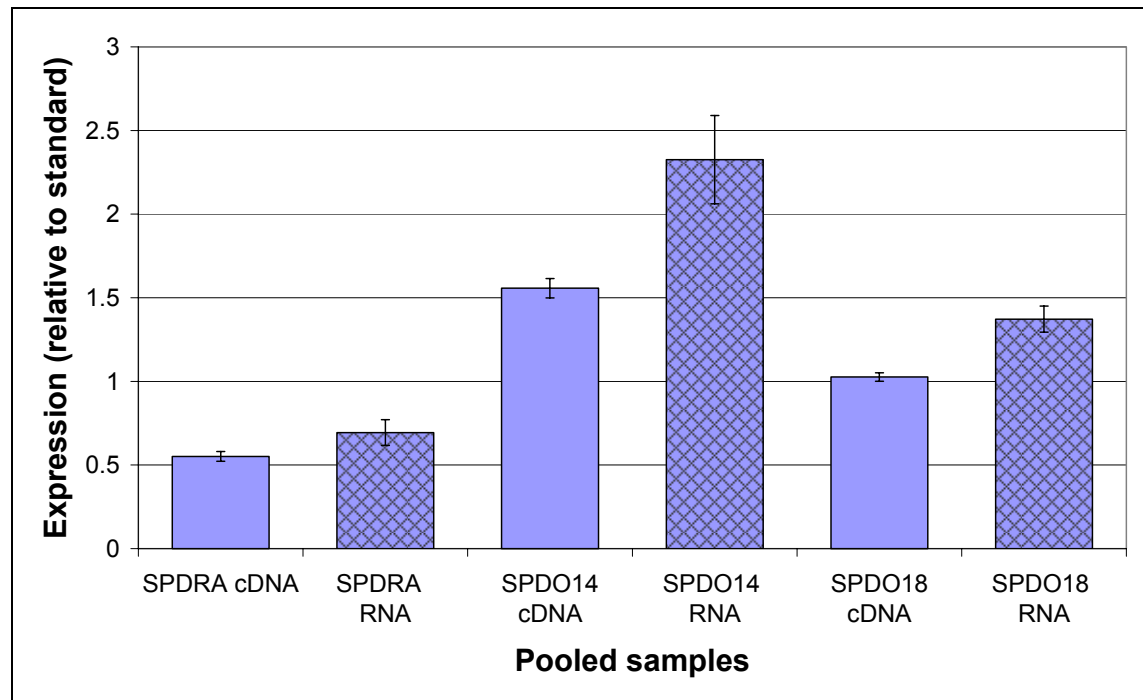
Figure 4.14 Comparison of VEGF mRNA expression levels in pooled samples. For each experimental group, the expression level of the RNA pool sample (made by combining equal amounts of retinal RNA from three rats and reverse transcribing the pooled sample –*hatched bars*) is plotted beside that of the *virtual* cDNA pool (the overall mean expression level of samples from the same three rats, reverse transcribed and assayed independently). Values for the RNA pool samples are greater than those of the virtual cDNA pools. Error bars: ± SD.

Key:
SPDRAcDNA = SPD day 14 room air cDNA pool
SPDRARNA = SPD day 14 room air RNA pool
SPDO14cDNA= SPD day 14 cyclic hyperoxia cDNA pool
SPDO14RNA = SPD day 14 cyclic hyperoxia RNA pool
SPDO18cDNA= SPD day 18 (14 days cyclic hyperoxia + 4 days room air) cDNA pool
SPDO18RNA = SPD day 18 (14 days cyclic hyperoxia + 4 days room air) RNA pool

Table 4.3 Changes in VEGF expression in pooled samples following oxygen exposure. Values for the oxygen exposed RNA pools and virtual cDNA pools are expressed relative to those of the matched room air exposed controls. The relative changes in gene expression are alike, irrespective of the pooling method.

Experimental group	RNA pool: % RA14 RNA pool (95% CI)	cDNA "pool": % RA14 cDNA pool (95% CI)	p value for difference between pools
SPDO14	282 (245-320%)	335 (286-398%)	0.062
SPDO18	186 (177-195%)	198 (169-232%)	0.12

4.4. STRAIN DIFFERENCES IN RETINAL GENE EXPRESSION FOLLOWING EXPOSURE TO CYCLIC HYPEROXIA AND RELATIVE HYPOXIA

Expression levels of the 8 candidate genes in each of the pooled samples from the three cardinal rat strains – F344, SPD and DA – were assessed using quantitative real-time RT-PCR in accordance with the method outlined previously. Expression data for each of the candidate genes, in turn, are presented below. A synthesis of the major changes in gene expression is presented in section 4.4.i and in figures 4.23 and 4.24.

4.4.a. The effect of cyclic hyperoxia and hypoxia on VEGF mRNA expression

VEGF expression data for the three rat strains are displayed in Figure 4.15. Overall, oxygen exposed rats exhibited higher retinal VEGF expression than control rats exposed to room air ($F_{(1,48)}$= 156.0; p<0.001). However the relative difference was substantially lower for the F344 strain (mean increase from FRA14: 50%; p<0.001) than for the SPD (mean increase from SPDRA14: 166%; p<0.001]) and DA (mean increase from DARA14: 154%; p<0.001) strains. Thus, an overall influence of strain on the effect of oxygen exposure on retinal VEGF expression was identified (strain-treatment interaction: $F_{(4,45)}$=40.6; p<0.001).

Two different patterns of VEGF expression were apparent. In the DA strain, VEGF mRNA levels were increased above room air control levels in rats exposed to 14 days of cyclic hyperoxia (mean increase=114%) and they continued to rise during the subsequent four days of relative hypoxia (mean increase from DARA14=195%). The other two strains exhibited a biphasic pattern of gene expression. VEGF mRNA levels were maximal at the end of the cyclic hyperoxia period (O14) for the F344 and SPD strains. By the end of the subsequent four day period of relative hypoxia, VEGF expression had fallen significantly in both strains (p<0.001 for the difference between O14 and O18), but remained above room air control levels. While strain differences in VEGF expression in the room air pools achieved statistical significance (F344RA14<SPDRA14, p=0.015; F344RA<DARA14, p<0.001), the magnitudes of these differences were small.

Figure 4.15 Retinal VEGF mRNA expression in three rat strains – the influence of cyclic hyperoxia and relative hypoxia. * p<0.001; *n*= 6 replicates per experimental group of three pooled rat retinae. Error bars: ± SD.

Key:

F344RA14: Fischer 344 room air day 14 (control)

F344O14: Fischer 344 cyclic hyperoxia day 14

F344O18: Fischer 344 day 18 (cyclic hyperoxia 14 days + 4 days room air)

SPDRA14: Sprague Dawley room air day 14 (control)

SPDO14: Sprague Dawley cyclic hyperoxia day 14

SPDO18: Sprague Dawley day 18 (cyclic hyperoxia 14 days + 4 days room air)

DARA14: Dark Agouti room air day 14 (control)

DAO14: Dark Agouti cyclic hyperoxia day 14

DAO18: Dark Agouti day 18 (cyclic hyperoxia 14 days + 4 days room air)

Comparison	Mean difference	95% C.I.	Significance
DAO14>DARA14	114%	83-151%	p<0.001
DAO18>DARA14	195%	152-246%	p<0.001
F344O14>F344RA14	77%	51-108%	p<0.001
F344O18> F344RA14	22%	4-43%	p=0.007
SPDO14>SPDRA14	235%	186-293%	p<0.001
SPDO18>SPDRA14	98%	69-132%	p<0.001

4.4.b.   The effect of cyclic hyperoxia and hypoxia on VEGFR-2 mRNA expression

The expression of retinal VEGFR-2 mRNA in the cardinal rat strains was examined (Figure 4.16). An overall effect of oxygen exposure on VEGFR-2 gene expression was identified ($F_{(2,45)}$=54.1, p<0.0001), and this effect differed amongst strains (strain-treatment interaction: $F_{(4,45)}$=40.2, p<0.0001). Two different patterns of gene expression were apparent. The levels of VEGFR-2 expressed in each of the two oxygen exposed pools of the F344 strain were slightly, but statistically significantly lower than that of room air control group of the same strain. In contrast, VEGFR-2 expression increased substantially in oxygen exposed SPD and DA rat strains at the 18 day time-point, with increases of 84% and 70% above control levels, respectively. Of the room air groups, the expression of VEGFR-2 mRNA was significantly higher in the SPD strain, than in the F344 and DA strains.

4.4.c.   The effect of cyclic hyperoxia and hypoxia on PEDF mRNA expression

Overall, oxygen exposure had a slight, but statistically significant effect on the expression of PEDF mRNA ($F_{(2,45)}$=6.59; p=0.003) (Figure 4.17). The effect of the exposure on gene expression differed amongst strains (strain-treatment interaction: $F_{(4,45)}$=3.49; p=0.015). In the F344 and SPD strains, PEDF mRNA levels were marginally increased in the O14 pools, and marginally reduced in the O18 pools, relative to room air control levels, however the differences were not statistically significant. The differences in PEDF expression between the O14 and O18 pools were statistically significant for both strains. Levels of PEDF mRNA in each of the three DA pools were alike. Room air control pools differed significantly amongst strains: PEDF was lower in the F344 strain, than in the SPD and DA strains.

Figure 4.16 Retinal VEGFR-2 mRNA expression in three rat strains – the influence of cyclic hyperoxia and relative hypoxia. * $p<0.001$; *n*= 6 replicates per experimental group of three pooled rat retinae. Error bars: ± SD.
Key:
F344RA14: Fischer 344 room air day 14 (control)
F344O14: Fischer 344 cyclic hyperoxia day 14
F344O18: Fischer 344 day 18 (cyclic hyperoxia 14 days + 4 days room air)
SPDRA14: Sprague Dawley room air day 14 (control)
SPDO14: Sprague Dawley cyclic hyperoxia day 14
SPDO18: Sprague Dawley day 18 (cyclic hyperoxia 14 days + 4 days room air)
DARA14: Dark Agouti room air day 14 (control)
DAO14: Dark Agouti cyclic hyperoxia day 14
DAO18: Dark Agouti day 18 (cyclic hyperoxia 14 days + 4 days room air)

Comparison	Mean difference	95% C.I.	Significance
F344O14<F344RA14	25%	14-36%	$p<0.001$
F344O18<F344RA14	25%	14-36%	$p<0.001$
SPDO18>SPDRA14	84%	60-113%	$p<0.001$
DAO18>DARA14	70%	47-97%	$p<0.001$
SPDRA14>F344RA14	43%	23-65%	$p<0.001$
SPDRA14>DARA14	37%	19-59%	$p<0.001$

Figure 4.17 Retinal PEDF mRNA expression in three rat strains – the influence of cyclic hyperoxia and relative hypoxia. * p=0.044; # p=0.007; *n*= 6 replicates per experimental group of three pooled rat retinae. Error bars: ± SD.
Key:
F344RA14: Fischer 344 room air day 14 (control)
F344O14: Fischer 344 cyclic hyperoxia day 14
F344O18: Fischer 344 day 18 (cyclic hyperoxia 14 days + 4 days room air)
SPDRA14: Sprague Dawley room air day 14 (control)
SPDO14: Sprague Dawley cyclic hyperoxia day 14
SPDO18: Sprague Dawley day 18 (cyclic hyperoxia 14 days + 4 days room air)
DARA14: Dark Agouti room air day 14 (control)
DAO14: Dark Agouti cyclic hyperoxia day 14
DAO18: Dark Agouti day 18 (cyclic hyperoxia 14 days + 4 days room air)

Comparison	Mean difference	95% C.I.	Significance
F344O14>F344O18	38%	1-90%	p=0.044
SPDO14>SPDO18	60%	16-121%	p=0.007
SPDRA14>F344RA14	88%	36-159%	p<0.001
DARA14>F344RA14	146%	78-238%	p<0.001

4.4.d. The effect of cyclic hyperoxia and hypoxia on Ang2 mRNA expression

The expression data for Ang2 are displayed in Figure 4.18. Oxygen exposure had a small, but significant effect on Ang2 mRNA expression overall ($F_{(2,45)}$=11.3; p<0.001). Modest increases in Ang2 gene expression above room air control levels were identified in oxygen exposed SPD and DA rats. In the F344 strain, a small reduction in Ang2 expression was observed following the period of relative hypoxia. Rat strains differed significantly in the expression of Ang2 in room air: mRNA levels were lower in the F344 than in the SPD and DA strains.

4.4.e. The effect of cyclic hyperoxia and hypoxia on Tie2 mRNA expression

Tie2 mRNA expression was modulated by oxygen exposure in the three rat strains studied ($F_{(2,45)}$=245.0; p<0.001) and the effect varied amongst strains (strain-treatment interaction $F_{(4,45)}$=30.8; p<0.001) (Figure 4.19). Cyclic hyperoxia was associated with a reduction in Tie2 mRNA expression in the F344 and DA strains. Following four days of relative hypoxia, Tie2 expression increased to room air control levels and beyond, in the DA and F344 strains respectively. There was no statistically significant difference in Tie2 expression between room air and O14 pools for the SPD strain. However, Tie2 expression was significantly increased above room air control levels at the O18 time-point in SPD rats. Tie2 expression differed significantly amongst the room air groups: levels were lower in the F344 strain than in the SPD and DA.
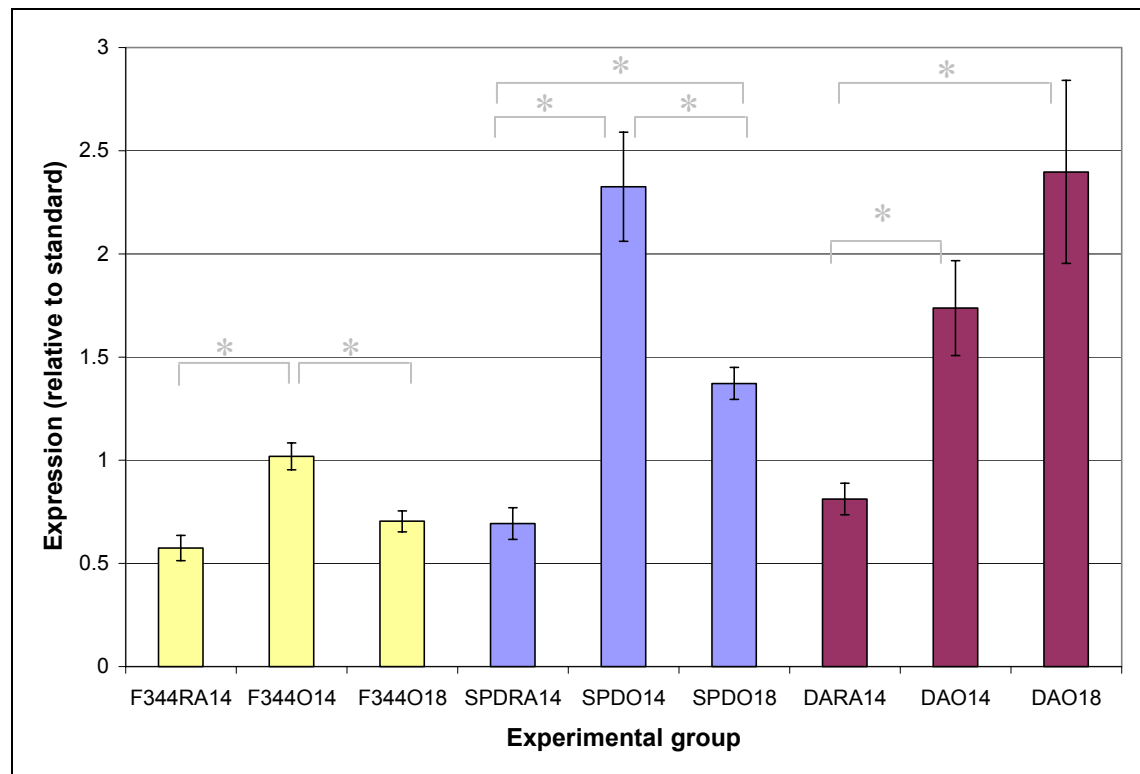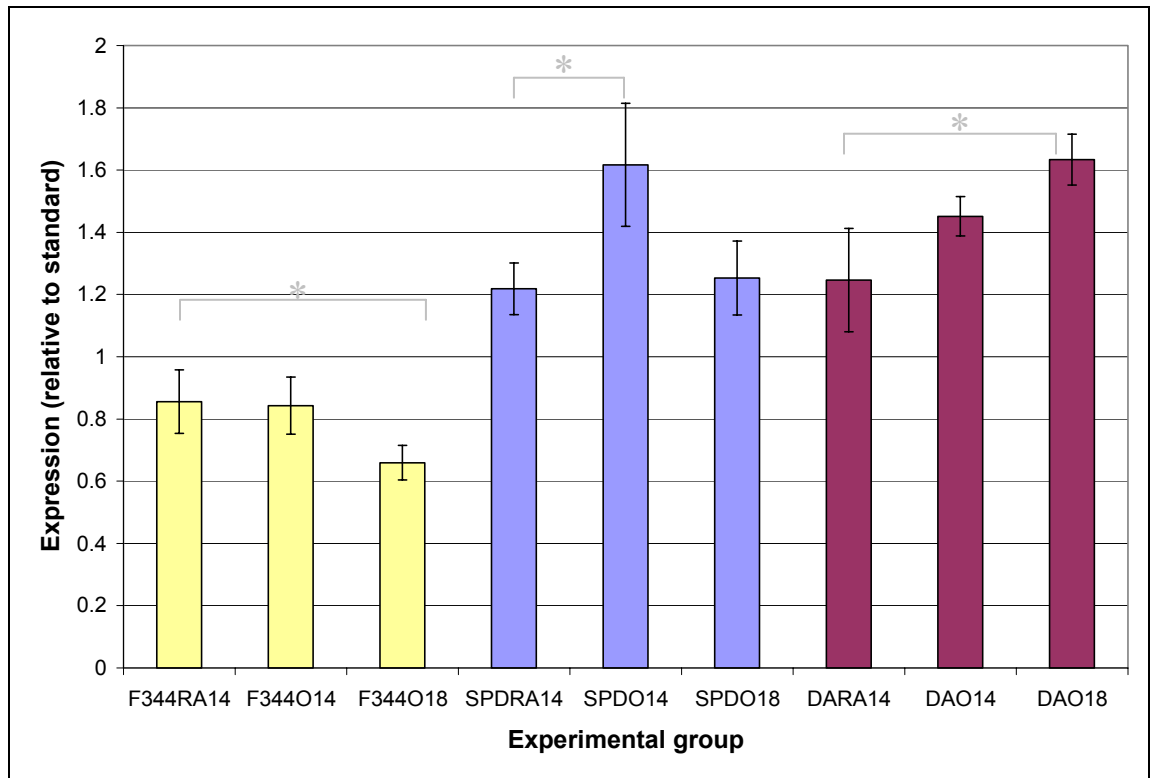
Figure 4.18 Retinal Ang2 mRNA expression in three rat strains – the influence of cyclic hyperoxia and relative hypoxia. * $p < 0.001$; *n*= 6 replicates per experimental group of three pooled rat retinae. Error bars: ± SD.

Key:

F344RA14: Fischer 344 room air day 14 (control)

F344O14: Fischer 344 cyclic hyperoxia day 14

F344O18: Fischer 344 day 18 (cyclic hyperoxia 14 days + 4 days room air)

SPDRA14: Sprague Dawley room air day 14 (control)

SPDO14: Sprague Dawley cyclic hyperoxia day 14

SPDO18: Sprague Dawley day 18 (cyclic hyperoxia 14 days + 4 days room air)

DARA14: Dark Agouti room air day 14 (control)

DAO14: Dark Agouti cyclic hyperoxia day 14

DAO18: Dark Agouti day 18 (cyclic hyperoxia 14 days + 4 days room air)

Comparison	Mean difference	95% C.I.	Significance
SPDO14>SPDRA14	33%	15-53%	p<0.001
DAO18>DARA14	31%	14-51%	p<0.001
F344O18< F344RA14	23%	11-33%	p<0.001
SPDRA14>F344RA14	42%	23-63%	p<0.001
DARA14>F344RA14	46%	27-68%	p<0.001
SPDRA14>F344RA14	72%	44-105%	p<0.001
DARA14>F344RA14	53%	28-83%	p<0.001
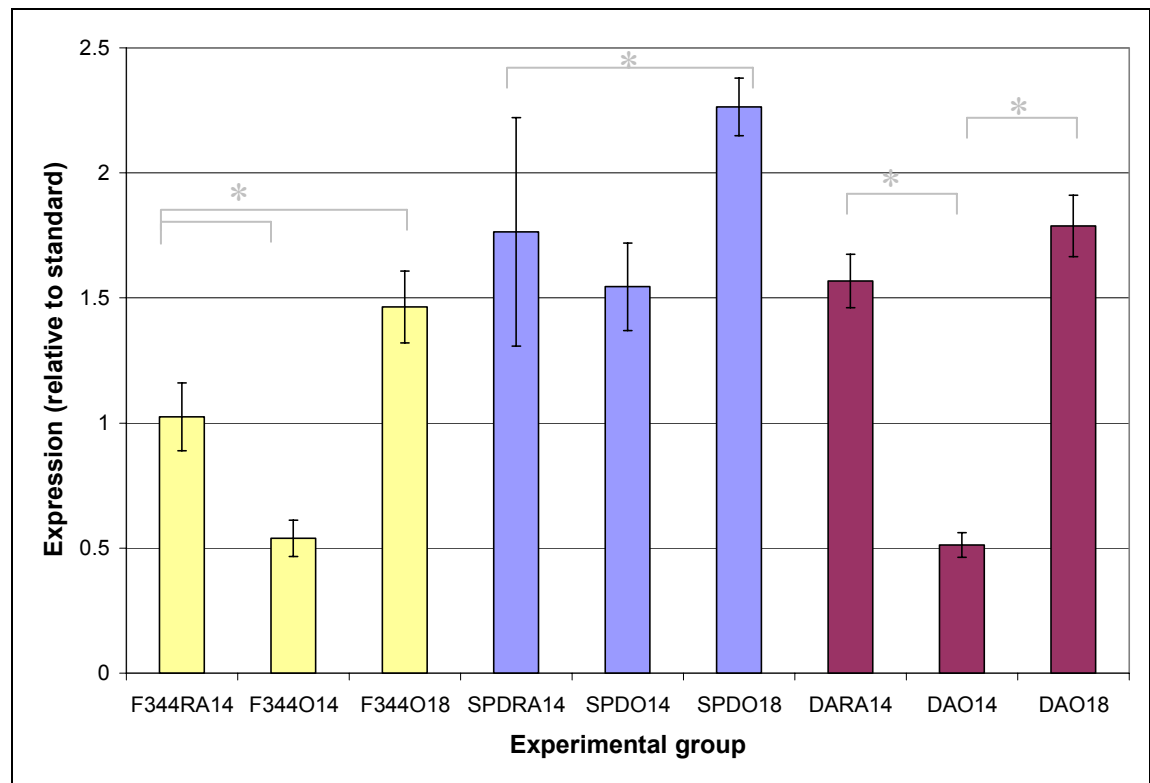
Figure 4.19 Retinal Tie2 mRNA expression in three rat strains – the influence of cyclic hyperoxia and relative hypoxia. * $p<0.001$; *n*= 6 replicates per experimental group of three pooled rat retinae. Error bars: ± SD.
Key:
F344RA14: Fischer 344 room air day 14 (control)
F344O14: Fischer 344 cyclic hyperoxia day 14
F344O18: Fischer 344 day 18 (cyclic hyperoxia 14 days + 4 days room air)
SPDRA14: Sprague Dawley room air day 14 (control)
SPDO14: Sprague Dawley cyclic hyperoxia day 14
SPDO18: Sprague Dawley day 18 (cyclic hyperoxia 14 days + 4 days room air)
DARA14: Dark Agouti room air day 14 (control)
DAO14: Dark Agouti cyclic hyperoxia day 14
DAO18: Dark Agouti day 18 (cyclic hyperoxia 14 days + 4 days room air)

Comparison	Mean difference	95% C.I.	Significance
F344O14<F344RA14	47%	37-56%	$p<0.001$
DAO14<DARA14	67%	61-73%	$p<0.001$
F344O18>F344RA14	43%	20-70%	$p<0.001$
SPDO18>SPDRA14	28%	108-153%	$p=0.001$

4.4.f.   The effect of cyclic hyperoxia and hypoxia on EPO mRNA expression

The pattern of retinal EPO expression closely resembled that of VEGF, however the relative changes were greater in magnitude for EPO (Figure 4.20). Oxygen exposure had a marked effect on EPO mRNA expression ($F_{(2,45)}$= 292.8; $p<0.001$) and the effect differed amongst rat strains ($F_{(4,45)}$=9.9; $p<0.001$). Following 14 days of cyclic hyperoxia, mean EPO expression was between 8.9-fold and 10.9-fold higher than in room air control groups. A statistically significant reduction in EPO expression was detected for the F344 ($p<0.001$) and SPD strains ($p=0.029$) after the relative hypoxia period (O18), however expression levels remained well above room air control levels. No statistically significant change in EPO expression was observed between the O14 and O18 time-points for the DA strain. The expression of EPO mRNA in room air control pools was uniformly low for all strains ($p=0.298$ for strain difference).

4.4.g.   The effect of cyclic hyperoxia and hypoxia on IGF-1 mRNA expression

Exposure to cyclic hyperoxia and relative hypoxia was associated with modest changes in retinal IGF-1 mRNA expression ($F_{(2,45)}$=54.3; $p<0.001$) that differed amongst strains (strain-treatment interaction: $F_{(4,45)}$=39.5; $p<0.001$) (Figure 4.21). Statistically significant differences were identified amongst strains in gene expression at the O14 time-point: in the SPD strain, IGF-1 mRNA was increased above room air levels; in the F344 it was decreased. IGF-1 mRNA levels were below room air control levels for all strains at the day 18 time-point. Room air control rats also differed in the extent of IGF-1 expression: expression was higher in the SPD strain than in the F344 and DA strains.

4.4.h.   The effect of cyclic hyperoxia and hypoxia on COX-2 mRNA expression

Rats exposed to the experimental oxygen protocol demonstrated small, but statistically significant differences in COX-2 mRNA expression from control rats raised in room air ($F_{(2,45)}$=27.5; $p<0.001$) (Figure 4.22). Changes in gene expression varied amongst strains (strain-treatment interaction: $F_{(4,45)}$=15.0; $p<0.001$). Following 14 days of cyclic hyperoxia, gene expression was comparable to matched room air control groups for the F344 and SPD strains, and reduced for the DA strain. By the day 18 time-point, COX-2 mRNA expression had increased in all strains – to room air control levels in the DA, and beyond in the F344 and SPD strains. In room air control groups, COX-2 mRNA

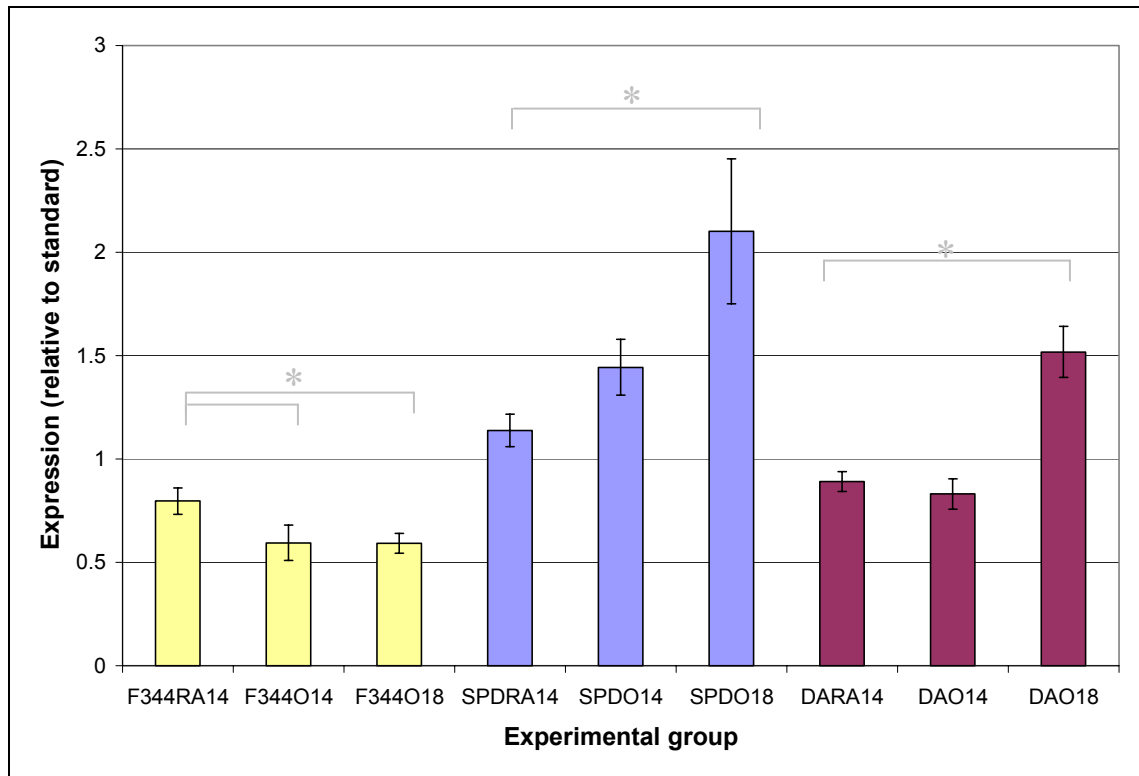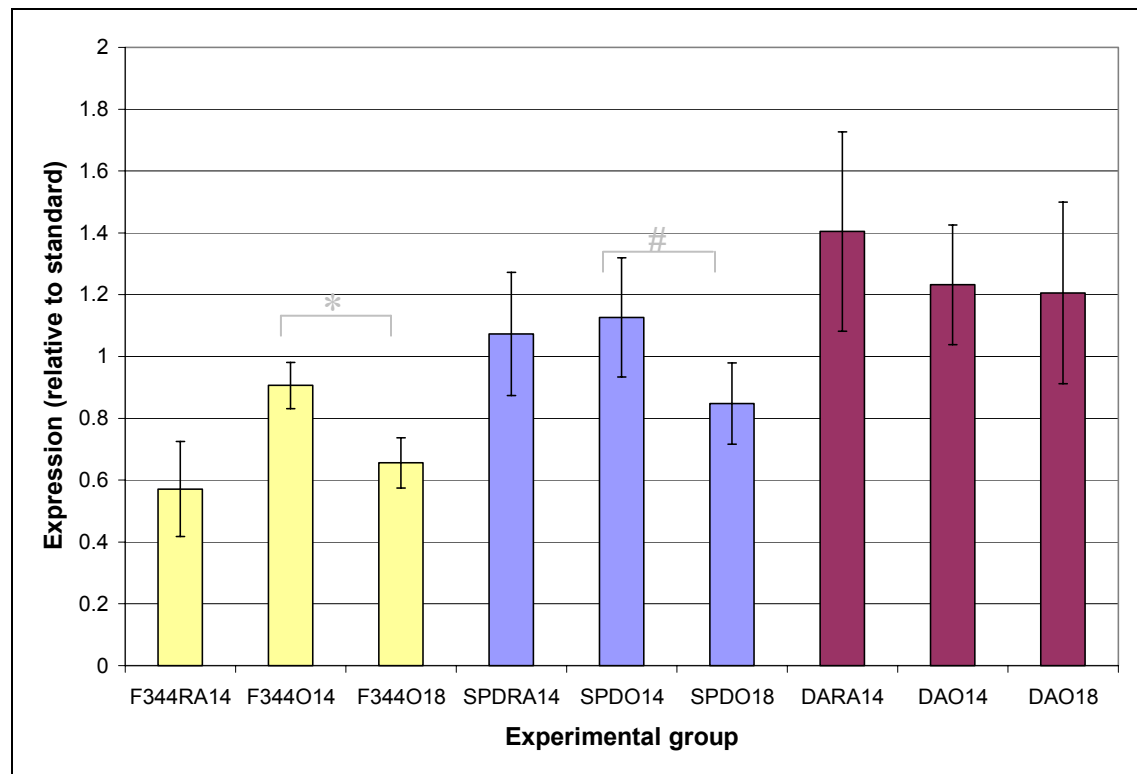expression was lower for the F344 strain than the SPD and DA strains.
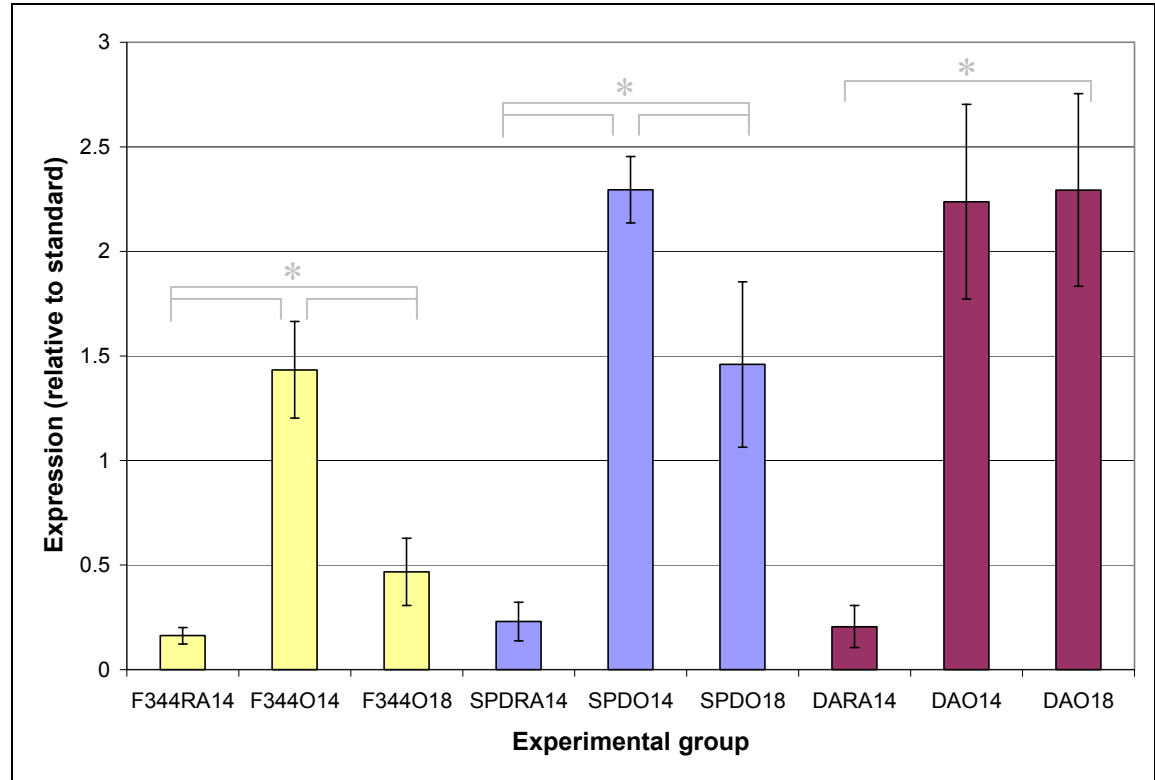
Figure 4.20 Retinal EPO mRNA expression in three rat strains – the influence of cyclic hyperoxia and relative hypoxia. * $p < 0.001$; *n*= 6 replicates per experimental group of three pooled rat retinae. Error bars: ± SD.
Key:
F344RA14: Fischer 344 room air day 14 (control)
F344O14: Fischer 344 cyclic hyperoxia day 14
F344O18: Fischer 344 day 18 (cyclic hyperoxia 14 days + 4 days room air)
SPDRA14: Sprague Dawley room air day 14 (control)
SPDO14: Sprague Dawley cyclic hyperoxia day 14
SPDO18: Sprague Dawley day 18 (cyclic hyperoxia 14 days + 4 days room air)
DARA14: Dark Agouti room air day 14 (control)
DAO14: Dark Agouti cyclic hyperoxia day 14
DAO18: Dark Agouti day 18 (cyclic hyperoxia 14 days + 4 days room air)

| Comparison	Mean difference	95% C.I.	Significance
SPDO14>SPDRA14	9-fold	5.4-14.5 fold	$p < 0.001$
F344O14>F344RA14	7.9-fold	4.7-12.7 fold	$p < 0.001$
DAO14>DARA14	9.9-fold	6.0-15.9 fold	$p < 0.001$
F344O18>F344RA14	1.9-fold	0.9-3.5 fold	$p < 0.001$
SPDO18>SPDRA14	5.3-fold	3.1-8.9 fold	$p < 0.001$
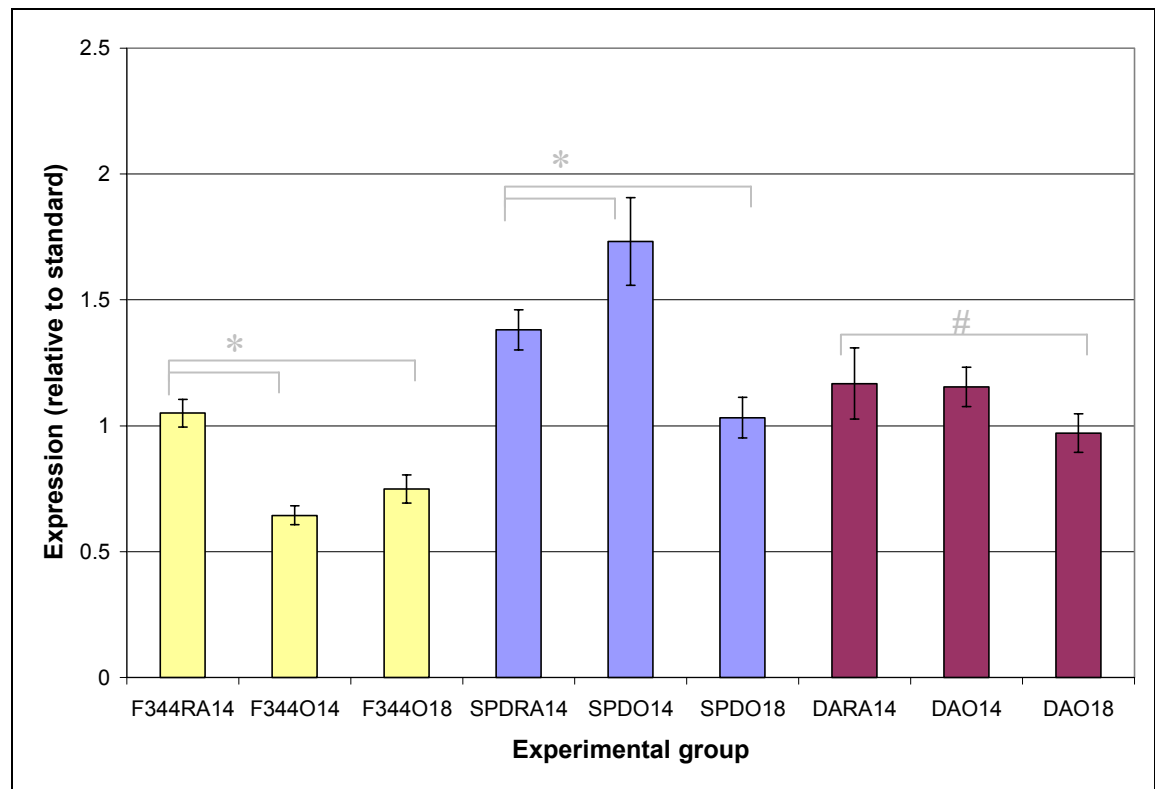
Figure 4.21 Retinal IGF-1 mRNA expression in three rat strains – the influence of cyclic hyperoxia and relative hypoxia. * $p<0.001$; # $p=0.001$; *n*= 6 replicates per experimental group of three pooled rat retinae. Error bars: ± SD.
Key:
F344RA14: Fischer 344 room air day 14 (control)
F344O14: Fischer 344 cyclic hyperoxia day 14
F344O18: Fischer 344 day 18 (cyclic hyperoxia 14 days + 4 days room air)
SPDRA14: Sprague Dawley room air day 14 (control)
SPDO14: Sprague Dawley cyclic hyperoxia day 14
SPDO18: Sprague Dawley day 18 (cyclic hyperoxia 14 days + 4 days room air)
DARA14: Dark Agouti room air day 14 (control)
DAO14: Dark Agouti cyclic hyperoxia day 14
DAO18: Dark Agouti day 18 (cyclic hyperoxia 14 days + 4 days room air)

| Comparison	Mean difference	95% C.I.	Significance
SPDO14>SPDRA14	25%	12-40%	$p<0.001$
F344O14>F344RA14	39%	31-45%	$p<0.001$
F344O18<F344RA14	29%	20-36%	$p<0.001$
SPDO18<SPDRA14	25%	16-34%	$p<0.001$
DAO18<DARA14	17%	7-26%	$p=0.001$
SPDRA14>F344RA14	32%	17-47%	$p<0.001$
SPDRA14>DARA14	18%	5-33%	$p=0.001$
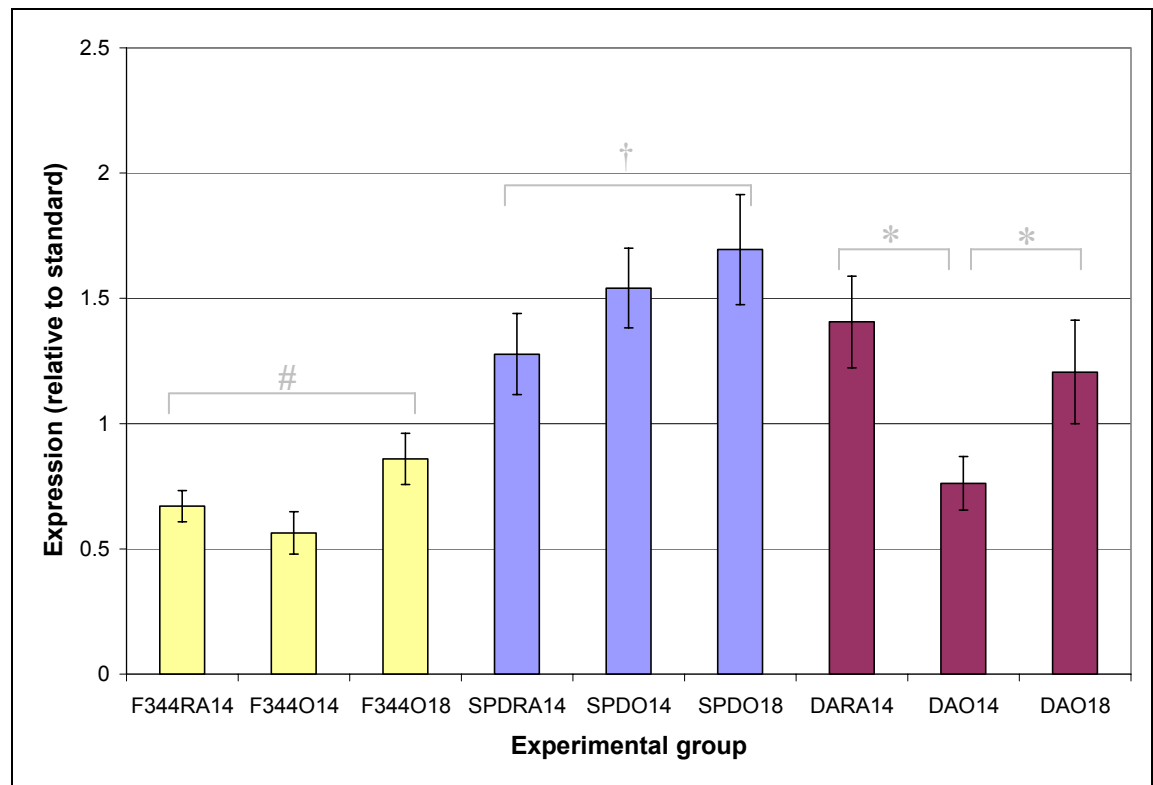
Figure 4.22 Retinal COX-2 mRNA expression in three rat strains – the influence of cyclic hyperoxia and relative hypoxia. * $p<0.001$; # $p=0.007$; † $p=0.002$; *n*= 6 replicates per experimental group of three pooled rat retinae. Error bars: ± SD.
Key:
F344RA14: Fischer 344 room air day 14 (control)
F344O14: Fischer 344 cyclic hyperoxia day 14
F344O18: Fischer 344 day 18 (cyclic hyperoxia 14 days + 4 days room air)
SPDRA14: Sprague Dawley room air day 14 (control)
SPDO14: Sprague Dawley cyclic hyperoxia day 14
SPDO18: Sprague Dawley day 18 (cyclic hyperoxia 14 days + 4 days room air)
DARA14: Dark Agouti room air day 14 (control)
DAO14: Dark Agouti cyclic hyperoxia day 14
DAO18: Dark Agouti day 18 (cyclic hyperoxia 14 days + 4 days room air)

Comparison	Mean difference	95% C.I.	Significance
DAO14<DARA14	39%	26-50%	p<0.001
F344O18>F344RA14	28%	6-55%	p=0.007
SPDO18>SPDRA14	33%	10-60%	p=0.002
SPDRA14>F344RA14	90%	57-130%	p<0.001
DARA14>F344RA14	110%	73-153%	p<0.001

4.4.i.   Interpretation of the observed changes in gene expression – correlation with strain differences in retinal vascular area.

The results of the real-time RT-PCR experiments demonstrated that room air control groups of the three strains differed significantly in the extent of angiogenic factor gene expression. These results are consistent with the finding that small, but statistically significant, differences existed in the extent of retinal vascularization amongst the strains following 14 days of life in room air conditions (section 3.2.a). One explanation for this difference in gene expression may be that the avascular peripheral retina exerted a hypoxic stimulus for angiogenesis in the SPD and DA strains – those strains with less developed vasculatures. Alternatively, the differences in gene expression may be intrinsic to the individual rat strains – reflecting differences in the set-points of the angiogenic balance in different strains. The ultimate objective of these studies is to identify those differences in gene expression amongst strains that are induced by the oxygen stimulus. Given the possibility of intrinsic strain differences, a conservative interpretation of oxygen-induced changes in gene expression should be informed by the observed strain differences in gene expression in room air. Accordingly, expression data for each gene, in each of the oxygen exposed groups, have been displayed as ratio quantities of expression levels of the same gene in matched room air control groups. Figure 4.23 demonstrates the retinal gene expression levels of rats exposed to 14 days of cyclic hyperoxia relative to room air control groups; Figure 4.24 shows the corresponding values for rats exposed to four days of relative hypoxia, after 14 days of cyclic hyperoxia.   Expression values above or below one represent increases or decreases in gene expression from the matched room air control group, respectively.

4.4.i.1   Strain differences in gene expression — exposure day 14

Following 14 days of cyclic hyperoxia, two distinct patterns of gene expression were apparent (Figure 4.23). The SPD and DA strains, both of which had large areas of avascular retina at this time-point, exhibited a pro-angiogenic pattern of gene expression: levels of the stimulatory factor, VEGF, were increased; while levels of the inhibitory factor, PEDF, were reduced. The modest increases in Ang2 have contributed to the pro-angiogenic milieu, as may have the rise in VEGFR-2 expression, evident in the SPD strain. In contrast, the F344 strain, which was relatively well vascularized at

this time-point, had a pattern of gene expression that was more closely aligned with the room air control group. The expression of VEGF was increased, but so too was the anti-angiogenic factor PEDF. The ratio of VEGF and PEDF protein expression – the VEGF/PEDF ratio – has been proposed as a surrogate marker of retinal angiogenic balance: the higher the ratio, the greater the stimulus for angiogenesis [334, 356, 419]. At day 14, the mRNA VEGF/PEDF ratio of oxygen exposed rats of the F344 strain was almost equal to that of room air exposed rats. In contrast, the mRNA VEGF/PEDF ratios of oxygen exposed SPD and DA rats were three times, and two times higher than those of room air controls, respectively. IGF-1 levels were marginally higher in the SPD and DA strains than in the F344 strain – this may have constituted an additional factor favouring angiogenesis in the former strains. Minor differences were noted amongst strains in the expression of COX-2 and Tie2, however these differences did not segregate with the differences in retinal vascular phenotype. EPO, which was expressed at very low levels in rats raised in room air, was markedly up-regulated in all strains following cyclic hyperoxia, and no significant strain differences were apparent at day 14.

4.4.i.2   *Strain differences in gene expression — exposure day 18*

The strain differences in angiogenic balance evident after 14 days of cyclic hyperoxia, persisted at day 18, after a four day period of relative hypoxia (Figure 4.24) – the balance was in favour of angiogenesis for the SPD and DA rats, and less so for F344 rats. When compared with the day 14 oxygen time-point, the expression of VEGF mRNA was increased in the DA strain, but was lower in the SPD and F344 strains. In F344 rats the VEGF/PEDF mRNA ratio remained unchanged; in the SPD and DA strains the ratios were two times, and three times higher than those of matched room air control rats, respectively. In the latter two strains, Ang2 remained marginally elevated, while VEGFR-2 expression was twice that of the room air control groups, compounding the drive for retinal angiogenesis. Differences amongst strains in the expression of COX-2, Tie2 and IGF-1 were small and not concordant with differences in retinal vascular extent. Relative EPO mRNA expression was substantially higher in the SPD and DA strains, than in the F344 strain.
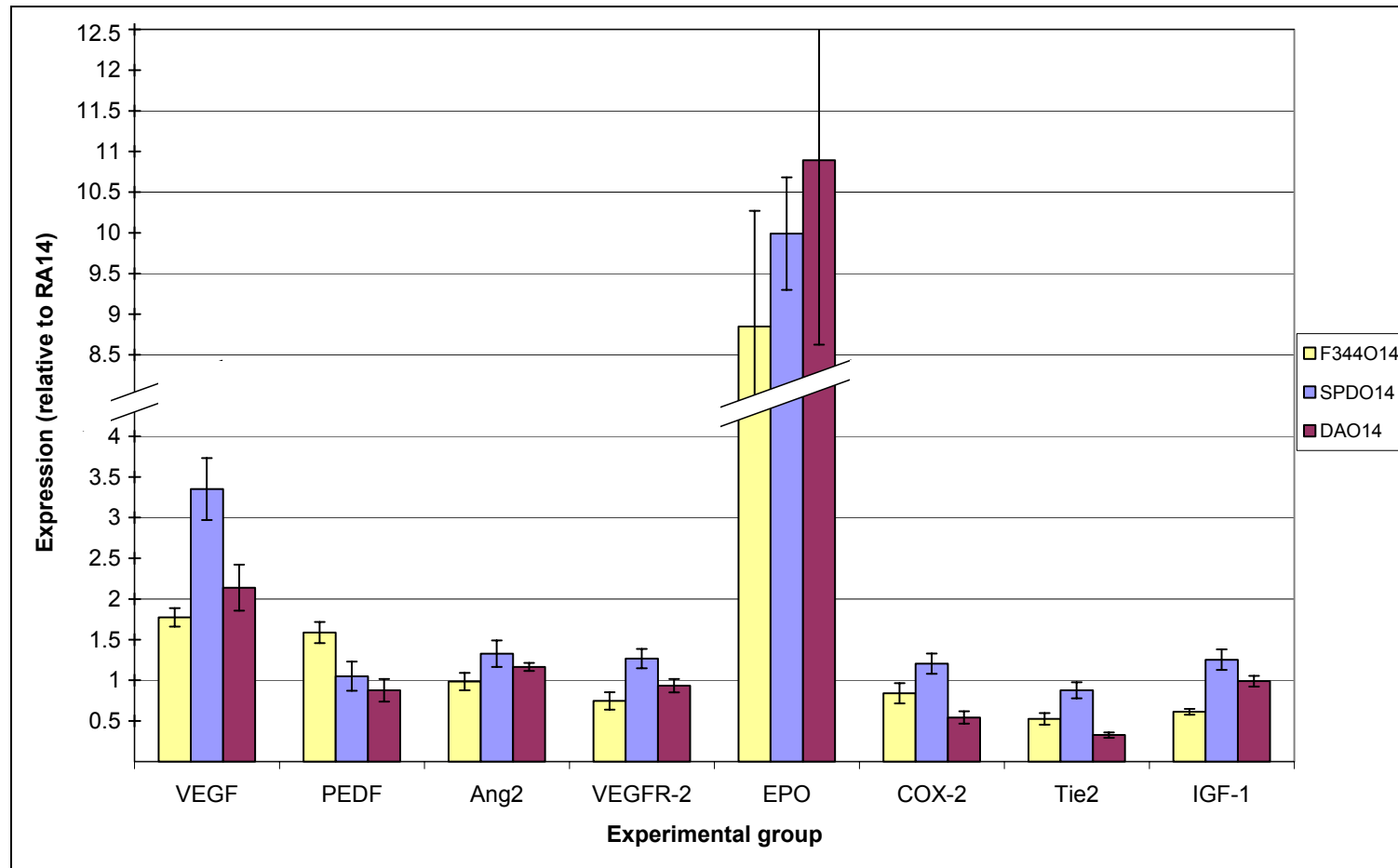
Figure 4.23 Angiogenic factor gene expression in the retinae of three rat strains following 14 days of cyclic hyperoxia (O14). Expression is relative to control groups of rats exposed to room air (RA14), matched by strain. *n*= pooled retinae of three rats per strain; 6 replicates per data point. Error bars: ± SD. Note broken y-axis. **Key:** F344O14= Fischer 344 cyclic hyperoxia day 14; SPDO14= Sprague Dawley cyclic hyperoxia day 14; DAO14= Dark Agouti cyclic hyperoxia day 14.
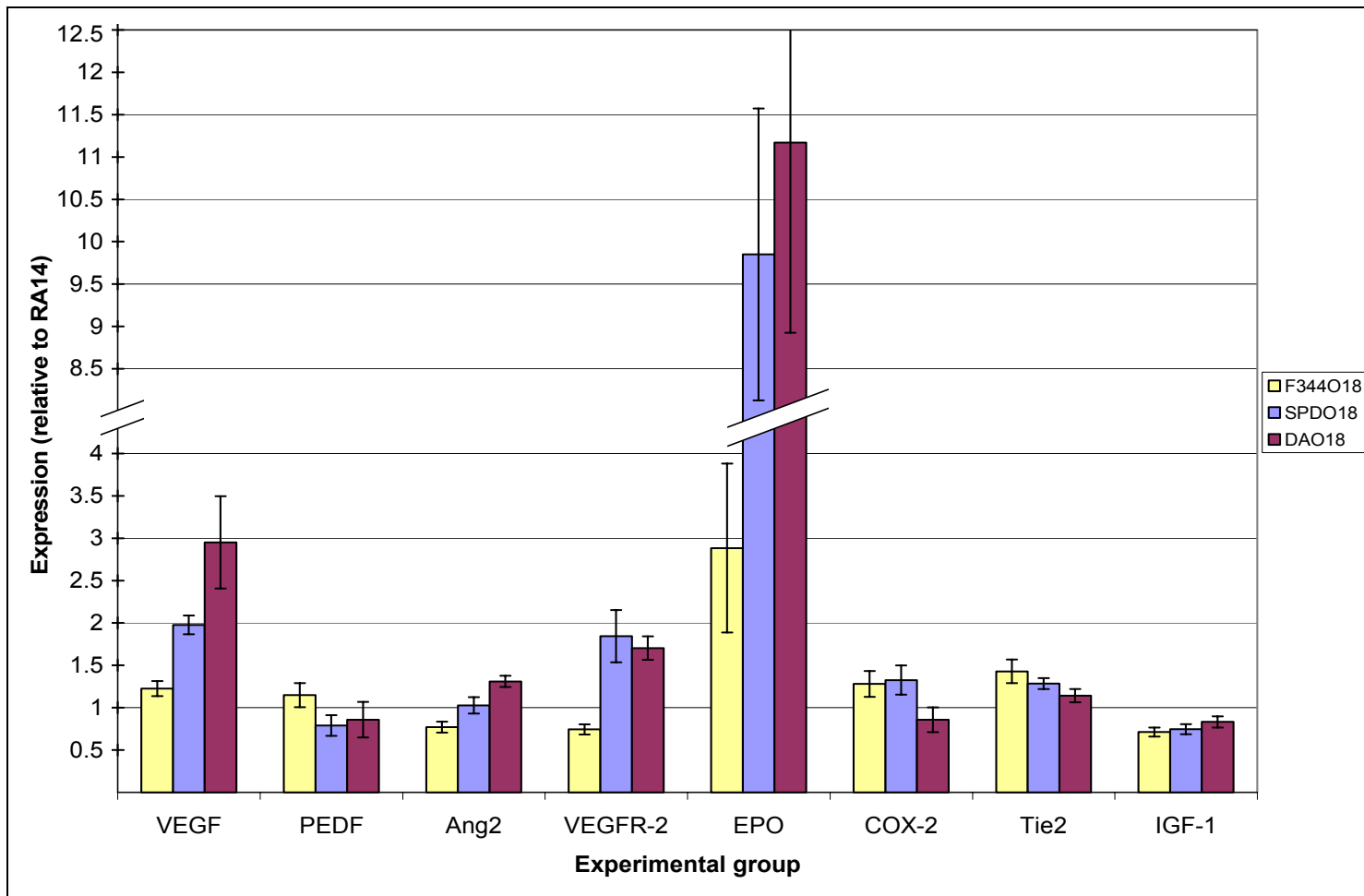
Figure 4.24 Angiogenic factor gene expression in the retinae of three rat strains following 14 days of cyclic hyperoxia and four days of relative hypoxia (O18). Expression is relative to control groups of rats exposed to room air (RA14), matched by strain. *n*= pooled retinae of three rats per strain; 6 replicates per data point. Error bars: ± SD. Note broken y-axis. **Key:** F344O18= Fischer 344 day 18; SPDO18= Sprague Dawley day 18; DAO18= Dark Agouti day 18.

In summary, quantitative real-time RT-PCR analyses of mRNA transcripts in the retinae of three strains of inbred rat have revealed significant differences in the expression of genes important in angiogenesis following exposure to cyclic hyperoxia and hypoxia. The F344 strain, which appears to be relatively resistant to the attenuating effects of cyclic hyperoxia on retinal vascularization, showed a modest level of pro-angiogenic factor gene expression at the day 14 and 18 time-points. This pattern of gene expression differed little from that seen in control rats reared in room air. In contrast, the SPD and DA strains showed marked attenuation in retinal vascularization, such that there were large avascular territories in the peripheral retina. At the day 14 and day 18 time-points, both strains demonstrated a pro-angiogenic transcriptome, with up-regulation of hypoxia-induced angiogenic factors. It remains to be determined why these strains fail to undergo functional retinal vascularization during the four day period of relative hypoxia, despite high levels of angiogenic gene expression. A comparative study of gene expression in the retinae of resistant and susceptible rat strains earlier in the period of cyclic hyperoxia was conducted with the aim of providing further insights into the underlying basis of the strain difference in susceptibility.

4.5.   STRAIN DIFFERENCES IN RETINAL GENE EXPRESSION DURING CYCLIC HYPEROXIA

4.5.a.   Experimental design

The expression of five angiogenic factor genes in the retinae of F344 and DA rat strains were compared at early time-points in the cyclic hyperoxia exposure, to identify factors that might contribute to the differences in retinal vascular extent that exist after the exposure. The SPD strain was not included in this analysis, as the patterns of gene expression observed in this strain at the day 14 and day 18 time-points were similar to those seen in the DA strain. Those genes that were shown to differ significantly amongst strains at the day 14 and day 18 time-points, and that segregated in a manner that was consistent with the difference in vascular extent – VEGF, PEDF, VEGFR-2, Ang2 and EPO – were selected for study at earlier exposure time-points. cDNA pools, derived from the retinae of three rats, were prepared for each analysis time-point, for of each of the two strains. Gene expression was examined by real-time RT-PCR, following the

protocol described previously (section 2.3.l). The time-points selected for transcript analysis were as follows: at the conclusion of exposure days 2 (O2) and 8 (O8), after 24 hour periods in room air; and at the ends of exposure days 3 (O3) and 9 (O9), following 24 hour periods of 80% oxygen (Figure 4.25). Thus gene expression was studied after periods of hyperoxia, and after periods of relative hypoxia (room air), to identify whether strain differences were the result of differential responses to one or other stimulus. The rats selected for gene expression studies at the hyperoxia time-points, days 3 and 9, were maintained in 80% oxygen until immediately before euthanasia and retinal harvesting, as hypoxia-induced changes in gene expression are known to commence soon after the onset of hypoxia [361, 362, 420].
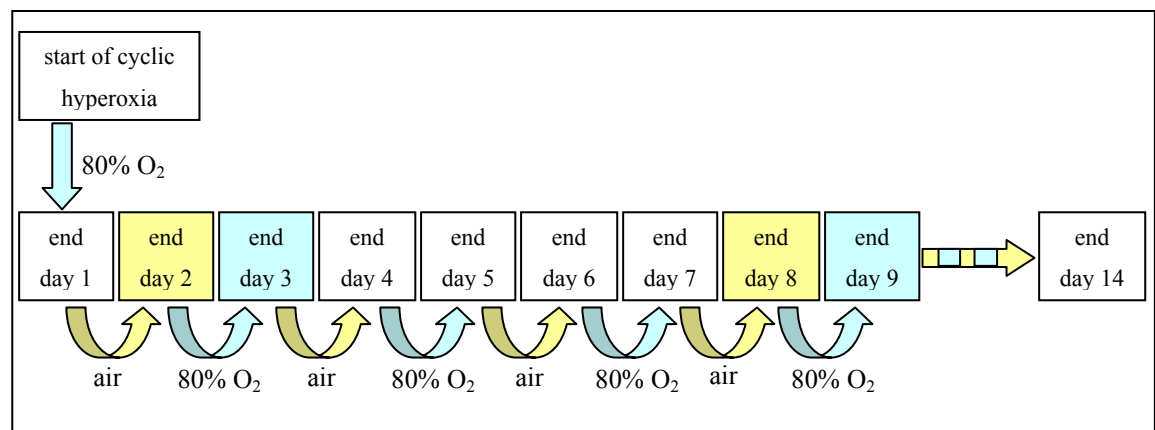
Figure 4.25 Cyclic hyperoxia protocol. Newborn rats were exposed to 24 hours of 80% oxygen (blue arrow) on the first day of postnatal life. The end of this initial cycle of hyperoxia marked the end of exposure day 1. During the subsequent 24 hour period, rats were exposed to room air (yellow arrow). Room air constituted relative hypoxia for the avascular retinae. In the conventional exposure protocol this alternating exposure to hyperoxia and room air continued for 14 days. Intermediate time-points were selected for gene expression analysis. Rat retinae were harvested at the ends of days 2, 3, 8 and 9. Days 2 and 8 constituted relative hypoxia time-points (yellow boxes); days 3 and 9 constituted hyperoxia time-points (blue boxes).

4.5.b. Strain differences in VEGF mRNA expression during cyclic hyperoxia

VEGF mRNA expression differed significantly between the exposure time-points ($F(3,40)=357.8$; $p<0.001$) and the extent of this difference varied between rat strains (strain-treatment interaction: $F(3,40)=5.2$; $p=0.004$) (Figure 4.26). Overall, VEGF expression in F344 retinae was between 70% and 163% higher than in DA retinae for all of the time-points examined (Table 4.4). In both strains, hyperoxia was associated with a

reduction in VEGF expression, while room air exposure (relative hypoxia) was associated with an increase in mRNA levels of the factor. The magnitudes of these changes were similar for both strains, however the absolute levels differed due to the higher baseline level of VEGF mRNA in F344 retinae at day 2 (FO2) (Figure 4.26). In F344 rats the expression of VEGF mRNA at day 2 (F344O2) was almost double that at day 3 (F344O3), and three and a half times higher at day 8 (F344O8), than at day 9 (F344O9). In the DA strain VEGF expression at day 2 (DAO2) was two and a half times higher than at day 3 (DAO3), and almost three times higher at day 8 (DAO8), than at day 9 (DAO9). In both strains there was an overall reduction in VEGF mRNA levels with time – levels were higher at day 2 than at day 8; and higher at day 3 than at day 9 (p<0.001 for all comparisons).

Table 4.4 Strain differences in VEGF mRNA expression during cyclic hyperoxia.

Comparison	Mean difference (%)	95% CI	p-value
FO2>DAO2	70	44-99	<0.001
FO3>DAO3	133	98-174	<0.001
FO8>DAO8	163	124-209	<0.001
FO9>DAO9	106	75-142	<0.001

4.5.c.   Strain differences in VEGFR-2 mRNA expression during cyclic hyperoxia

The expression of VEGFR-2 varied between the exposure time-points ($F_{(3,40)}$=587.8; p<0.001) and the extent of this variation differed between strains (strain-treatment interaction: $F_{(3,40)}$=38.0; p<0.001) (Figure 4.27). Mean VEGFR-2 expression was between 33% and 220% higher in the F344 strain than in the DA strain for all exposure time-points (p<0.001 for difference between strains at each time-point). Within strains, VEGFR-2 mRNA levels were similar at days 2 and 3. Expression levels fell significantly in both strains by day 8. In DA rats, mRNA levels at day 9 were almost double the levels detected at day 8, but they remained well below levels detected at days 2 and 3. In contrast to VEGF, changes in VEGFR-2 mRNA expression during cyclic hyperoxia were not concordant with fluctuations in oxygen tension. Overall there was decline in VEGFR-2 expression during the later stages of cyclic hyperoxia exposure.
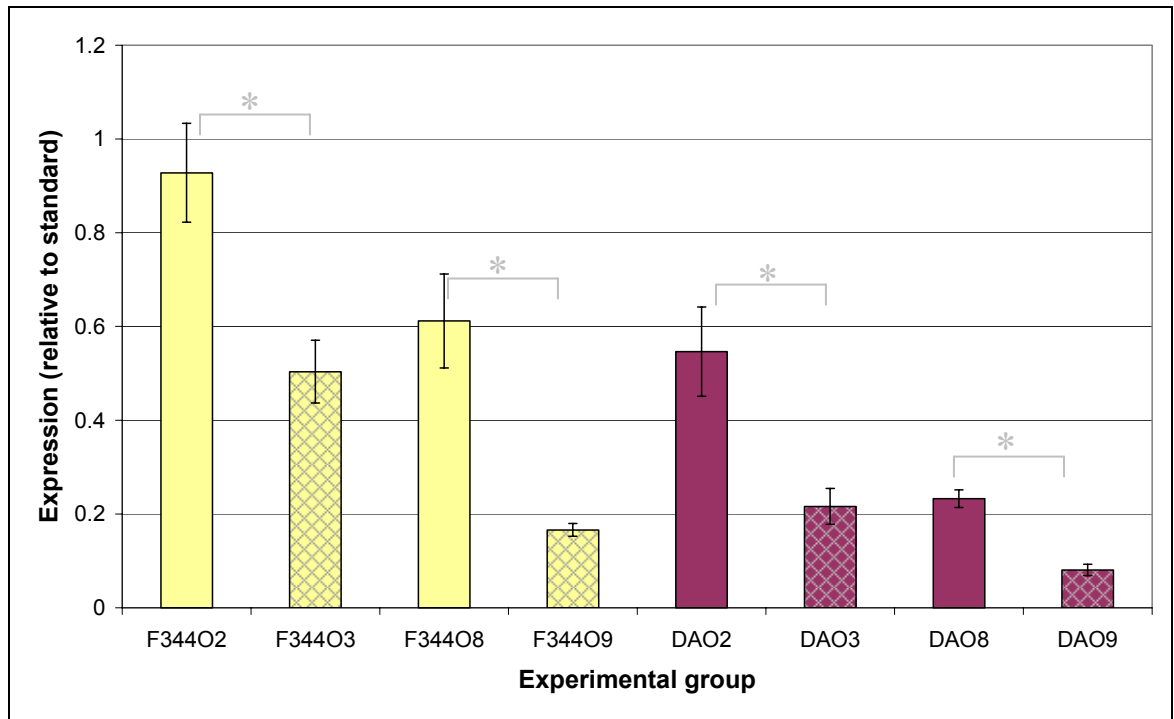
Figure 4.26 Strain differences in VEGF mRNA expression during cyclic hyperoxia.
VEGF mRNA expression was increased during cycles of relative hypoxia (plain bars) and reduced during cycles of hyperoxia (hatched bars). VEGF expression levels were significantly higher in retinae of the F344 strain than in those of the DA strain at each analysis time-point. * $p < 0.001$. Error bars: ± SD. *n*= 6 replicates per experimental group of three pooled rat retinae.
Key:
F344O2: Fischer 344 cyclic hyperoxia day 2 (room air time-point)
F344O3: Fischer 344 cyclic hyperoxia day 3 (80% oxygen time-point)
F344O8: Fischer 344 cyclic hyperoxia day 8 (room air time-point)
F344O9: Fischer 344 cyclic hyperoxia day 9 (80% oxygen time-point)
DAO2: Dark Agouti cyclic hyperoxia day 2 (room air time-point)
DAO3: Dark Agouti cyclic hyperoxia day 3 (80% oxygen time-point)
DAO8: Dark Agouti cyclic hyperoxia day 8 (room air time-point)
DAO9: Dark Agouti cyclic hyperoxia day 9 (80% oxygen time-point)

Comparison	Mean difference	95% C.I.	Significance
F344O2>F344O3	84%	48-130%	p<0.001
F344O8>F344O9	268%	196-360%	p<0.001
DAO2>DAO3	153%	103-215%	p<0.001
DAO8>DAO9	189%	132%-260%	p<0.001
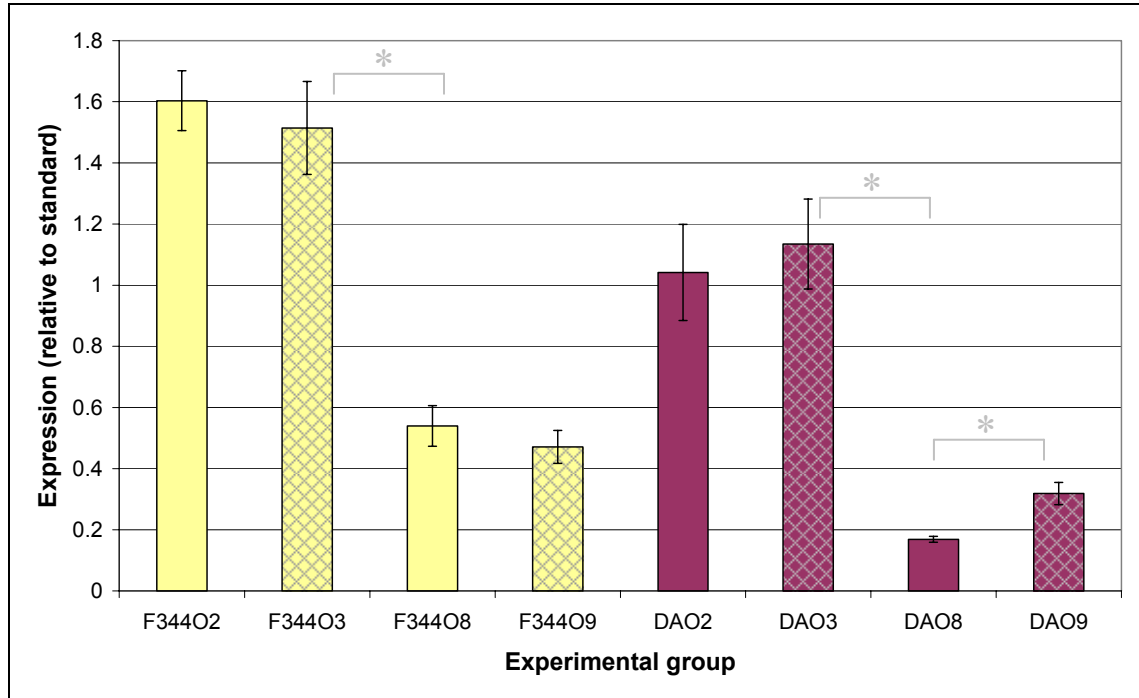
Figure 4.27 Strain differences in VEGFR-2 mRNA expression during cyclic hyperoxia. Higher levels of VEGFR-2 mRNA were expressed in the retinae of F344 rats than in DA rats at every time-point studied. In both strains mRNA levels declined significantly by exposure days 8 (FO8; DAO8) and 9 (FO9; DAO9). Hatched bars represent hyperoxia time-points (following 24 hours in 80% oxygen); plain bars represent room air time-points (relative-hypoxia). * p<0.001. Error bars: ± SD. *n*= 6 replicates per experimental group of three pooled rat retinae.

Key:

F344O2: Fischer 344 cyclic hyperoxia day 2 (room air time-point)
F344O3: Fischer 344 cyclic hyperoxia day 3 (80% oxygen time-point)
F344O8: Fischer 344 cyclic hyperoxia day 8 (room air time-point)
F344O9: Fischer 344 cyclic hyperoxia day 9 (80% oxygen time-point)
DAO2: Dark Agouti cyclic hyperoxia day 2 (room air time-point)
DAO3: Dark Agouti cyclic hyperoxia day 3 (80% oxygen time-point)
DAO8: Dark Agouti cyclic hyperoxia day 8 (room air time-point)
DAO9: Dark Agouti cyclic hyperoxia day 9 (80% oxygen time-point)

Comparison	Mean difference	95% C.I.	Significance
F344O8<F344O2	66%	60-72%	p<0.001
DAO8<DAO2	84%	81-86%	p<0.001
DAO9>DAO8	89%	58-125%	p<0.001

4.5.d. Strain differences in PEDF mRNA expression during cyclic hyperoxia

Overall, the expression of PEDF mRNA varied during the course of cyclic hyperoxia ($F_{(3,40)}$=38.8; $p<0.001$) and the extent of this variation did not differ between strains (strain-treatment interaction: $F_{(3,40)}$=2.5; $p=0.073$) (Figure 4.28). PEDF expression was maximal in F344 and DA rats at days 2 and 3 – no statistically significant differences were found either within, or between strains at these time-points. The expression of PEDF decreased significantly following 8 and 9 days of cyclic hyperoxia. In the F344 strain, mean PEDF transcript levels at days 8 and 9 were 40% and 64% respectively, of levels detected at day 2. In DA rats at exposure days 8 and 9, the mean level of PEDF mRNA was half the day 2 level. In contrast to VEGF, changes in PEDF gene expression were not concordant with the cyclic variation in oxygen tension – instead, there was a delayed and uniform reduction in gene expression in the retinae of both strains.

4.5.e. Strain differences in Ang2 mRNA expression during cyclic hyperoxia

There was an overall change in Ang2 mRNA expression during the course of 9 days of cyclic hyperoxia ($F(3,40)=9.4$; $p<0.001$) and the extent of this change differed between strains (strain-treatment interaction: $F(3,40)=5.7$; $p=0.002$) (Figure 4.29). Ang2 mRNA expression did not vary in the retinae of DA rats at any of the four intermediate time-points. In contrast, in F344 rats there was a statistically significant increase in Ang2 mRNA expression following 8 days of cyclic hyperoxia – transcript levels were 61% higher than at day 2. Retinal Ang2 mRNA levels were significantly higher ($p<0.001$) in the F344 strain than in the DA strain at days 3, 8 and 9 – at the day 8 time-point, mRNA expression in the F344 strain was almost twice that of the DA strain. In contrast to VEGF, the observed changes in Ang2 expression during cyclic hyperoxia were not concordant with the cyclic changes in oxygen tension.
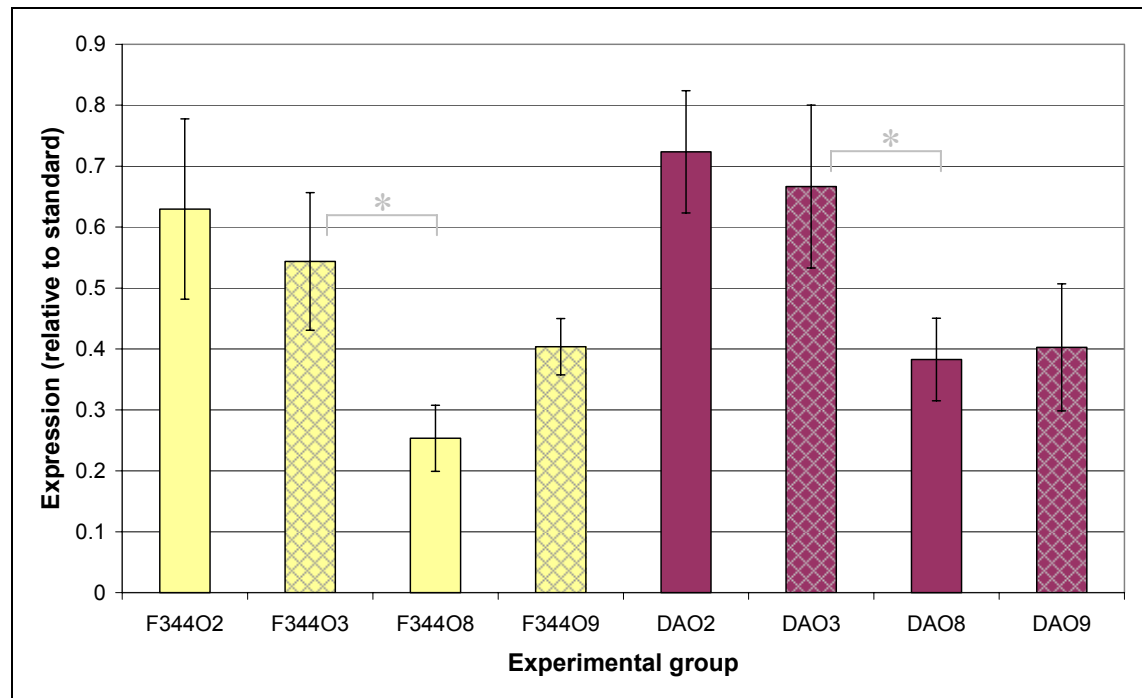
Figure 4.28 Strain differences in PEDF mRNA expression during cyclic hyperoxia.
PEDF mRNA expression was alike in the F344 and DA strains. mRNA levels declined significantly by exposure days 8 (FO8; DAO8) and 9 (FO9; DAO9). Hatched bars represent hyperoxia time-points (following 24 hours in 80% oxygen); plain bars represent room air time-points (relative-hypoxia). * $p < 0.001$. Error bars: ± SD. *n* = 6 replicates per experimental group of three pooled rat retinae.

Key:
F344O2: Fischer 344 cyclic hyperoxia day 2 (room air time-point)
F344O3: Fischer 344 cyclic hyperoxia day 3 (80% oxygen time-point)
F344O8: Fischer 344 cyclic hyperoxia day 8 (room air time-point)
F344O9: Fischer 344 cyclic hyperoxia day 9 (80% oxygen time-point)
DAO2: Dark Agouti cyclic hyperoxia day 2 (room air time-point)
DAO3: Dark Agouti cyclic hyperoxia day 3 (80% oxygen time-point)
DAO8: Dark Agouti cyclic hyperoxia day 8 (room air time-point)
DAO9: Dark Agouti cyclic hyperoxia day 9 (80% oxygen time-point)

Comparison	Mean difference	95% C.I.	Significance
F344O8<F344O2	60%	45-71%	p<0.001
F344O9<F344O2	36%	12-53%	p=0.004
DAO8<DAO2	46%	23-62%	p<0.001
DAO9<DAO2	46%	23-62%	p<0.001
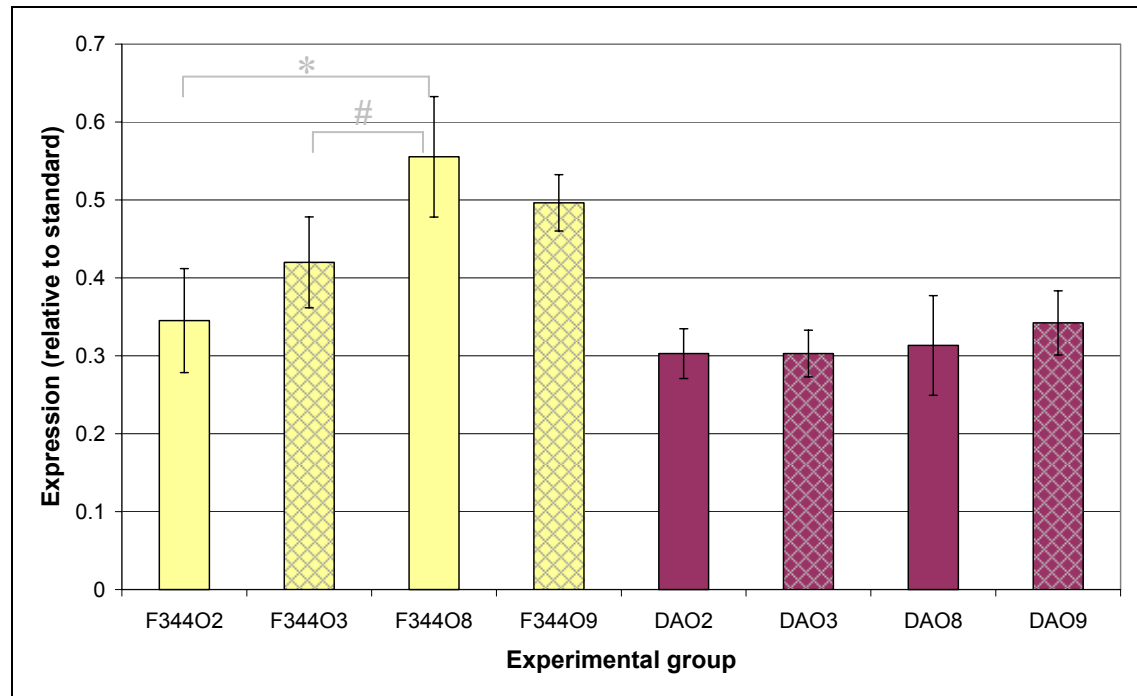
Figure 4.29 Strain differences in Ang2 mRNA expression during cyclic hyperoxia. Ang2 mRNA expression was greater in the F344 strain than the DA strain for all time-points beyond day 2. In F344 rat retinae mRNA levels increased significantly by exposure day 8 and remained elevated at day 9. In the DA strain there was no significant change in Ang2 transcript expression. Hatched bars represent hyperoxia time-points (following 24 hours in 80% oxygen); plain bars represent room air time-points (relative hypoxia). * $p < 0.001$; # $p = 0.007$. Error bars: ± SD. *n* = 6 replicates per experimental group of three pooled rat retinae.

Key:
F344O2: Fischer 344 cyclic hyperoxia day 2 (room air time-point)
F344O3: Fischer 344 cyclic hyperoxia day 3 (80% oxygen time-point)
F344O8: Fischer 344 cyclic hyperoxia day 8 (room air time-point)
F344O9: Fischer 344 cyclic hyperoxia day 9 (80% oxygen time-point)
DAO2: Dark Agouti cyclic hyperoxia day 2 (room air time-point)
DAO3: Dark Agouti cyclic hyperoxia day 3 (80% oxygen time-point)
DAO8: Dark Agouti cyclic hyperoxia day 8 (room air time-point)
DAO9: Dark Agouti cyclic hyperoxia day 9 (80% oxygen time-point)

Comparison	Mean difference	95% C.I.	Significance
F344O8>F344O2	61%	29-100%	p<0.001
F344O8>DAO8	78%	52-110%	p<0.001

4.5.f.   Strain differences in EPO mRNA expression during cyclic hyperoxia

During the early phases of cyclic hyperoxia retinal EPO expression was very low in both strains. Expression levels were close to the limits of detection and several replicates failed to amplify altogether. Even so, the expression of EPO mRNA in the retinae of F344 and DA rats did vary during the course of 9 days of cyclic hyperoxia ($F_{(3,31)}$=13.3; p<0.001) (Figure 4.30). However there was no overall difference in the extent of this variation between strains ($F_{(3,31)}$=0.97; p=0.42). In both strains the expression of EPO mRNA was substantially higher following room air exposures (days 2 and 8) than following exposure to 80% oxygen (days 3 and 9). In F344 rats, transcript levels were 3-fold higher at day 8 than at day 9; in DA rats, EPO mean mRNA levels at day 2 were 17-fold higher than at day 3. The cyclic variations in EPO gene expression were concordant with fluctuations in oxygen tension, similar to those of VEGF.

4.5.g.   Summary of strain differences in angiogenic factor gene expression during the course of cyclic hyperoxia

Several strain differences in retinal angiogenic gene expression were identified during the course of cyclic hyperoxia. Overall, pro-angiogenic gene expression was higher in the F344 strain than in the DA strain during the first 9 days of cyclic hyperoxia. This is consistent with the finding that rats of this strain exhibit more complete retinal vascularization following 14 days of cyclic hyperoxia than do rats of the DA strain. Moreover, this pattern of gene expression is the opposite of that observed after 14 days of cyclic hyperoxia, once substantial strain differences in retinal vascular extent (phenotype) impact on patterns of hypoxia-induced gene expression. At intermediate time-points in the two week exposure protocol – days 2, 3, 8 and 9 – strain differences in the expression of VEGF, VEGFR-2 and Ang2 were identified, with a predominance of these stimulatory factors in the F344 strain. In contrast to VEGFR-2 and Ang2, changes in VEGF expression in both strains closely parallelled the fluctuations in oxygen tension – mRNA expression was increased following periods of relative hypoxia and decreased following periods of hyperoxia. VEGF mRNA expression was significantly higher in the F344 strain, than the DA strain, at each of the early time-points. A similar pattern of cyclic variation in gene expression was identified for EPO, however significant strain differences were lacking. Ang2 and VEGFR-2 showed more
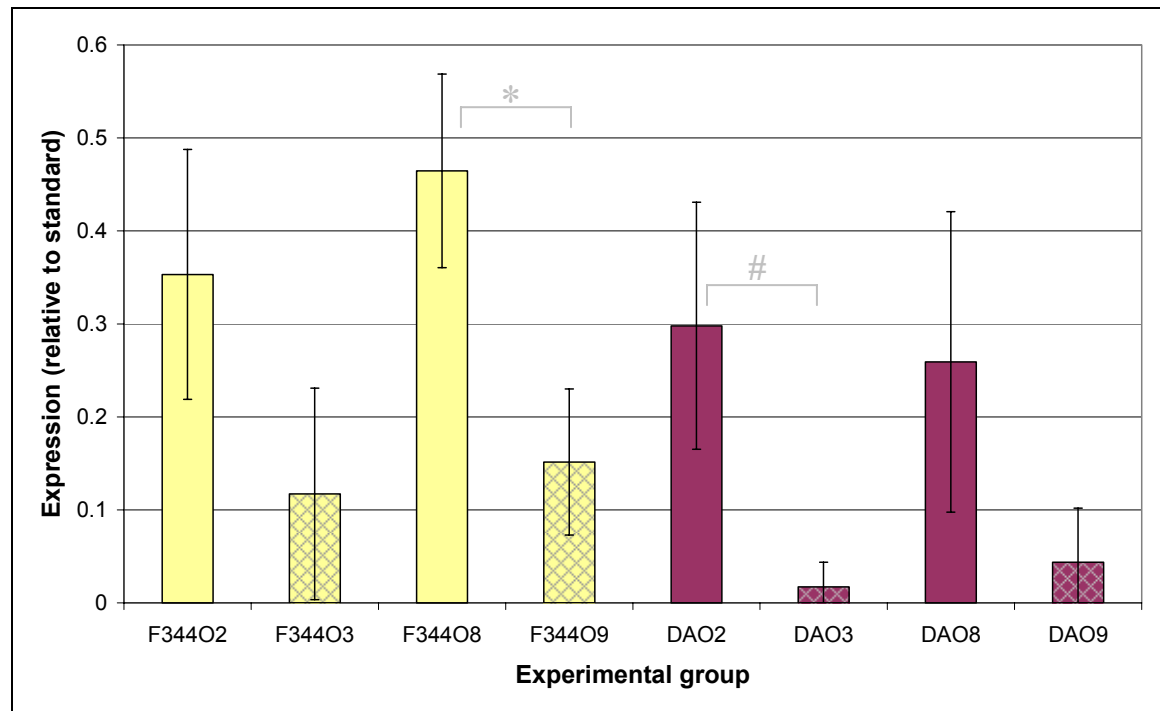
Figure 4.30 Strain differences in EPO mRNA expression during cyclic hyperoxia.
EPO mRNA expression was similar in the F344 and DA strains for all of the early time-points. In both strains, transcript levels were so low as to approach the limits of sensitivity of the PCR assay, hence the large standard deviations (error bars). EPO mRNA expression was increased following cycles of room air exposure (days 3 and 9) and decreased following hyperoxic periods. * p=0.002; # p=0.005. Error bars: ± SD. *n*= 6 replicates per experimental group of three pooled rat retinae.

Key:
F344O2: Fischer 344 cyclic hyperoxia day 2 (room air time-point)
F344O3: Fischer 344 cyclic hyperoxia day 3 (80% oxygen time-point)
F344O8: Fischer 344 cyclic hyperoxia day 8 (room air time-point)
F344O9: Fischer 344 cyclic hyperoxia day 9 (80% oxygen time-point)
DAO2: Dark Agouti cyclic hyperoxia day 2 (room air time-point)
DAO3: Dark Agouti cyclic hyperoxia day 3 (80% oxygen time-point)
DAO8: Dark Agouti cyclic hyperoxia day 8 (room air time-point)
DAO9: Dark Agouti cyclic hyperoxia day 9 (80% oxygen time-point)

Comparison	Mean difference	95% C.I.	Significance
F344O8>F344O9	200%	30-640%	p=0.002
DAO2>DAO3	1600%	400-5940%	p=0.005

delayed changes in gene expression – VEGFR-2 expression was decreased at later time-points (days 8 and 9) in both strains; while Ang2 mRNA increased modestly with time in the F344 strain alone. Expression of the anti-angiogenic factor PEDF was similar in both strains. Temporal changes in PEDF transcript levels closely mirrored those of VEGFR-2, with a reduction in expression between days 3 and 8. As VEGF expression was significantly higher for F344 rats than DA rats, and PEDF expression was similar for both strains, the ratio of VEGF to PEDF mRNA was greater for the F344 strain. It may be that this strain difference, coupled with higher levels of expression of VEGFR-2 and Ang2, is sufficient to account for the observed difference in retinal vascular extent between F344 and DA rats, following 14 days of cyclic hyperoxia.

4.6.   RETINAL GENE EXPRESSION IN THE BACKCROSS PROGENY OF DA AND F344 RAT STRAINS FOLLOWING CYCLIC HYPEROXIA

The heritability of strain differences in susceptibility to cyclic hyperoxia was studied in a series of cross-breeding experiments between F344 and DA rats, as described in section 3.2.e. The right retinae of several F1 progeny and all backcross offspring were collected following 14 days of cyclic hyperoxia, for vascular analysis. The offspring of the F1 X DA backcrosses had agouti coat pigmentation and brown eye colour, and all had retinal vascularization that was similar in extent to the DA parental strain. In contrast, offspring of the F1 X F344 backcrosses had a range of coat colours – white, hooded, agouti and black – and either red or brown eye colour. A cohort of 7 rats – four rats from one F1 X F344 backcross, and three from the other – incorporating the complete spectrum of coat and eye colours, was selected prospectively for retinal gene expression studies (Table 4.5). Following 14 days of cyclic hyperoxia the right retinae of selected rats were used for vascular analysis, while the left retinae were processed for RNA extraction as described previously (section 2.3.c). The retinal expression of five angiogenic genes was studied in accordance with the protocol described in section 2.3.l. The validity of using the left and right eyes of each rat for different analyses is supported by a study which demonstrated significant inter-eye correlation in retinal vascularization in a rat model of OIR [319]. A high level of inter-eye concordance in retinal vascular phenotype was also found in our own study population (data not shown).

Table 4.5 Characteristics of the backcross rat pups selected for gene expression studies. The progeny of two F1 X F344 backcrosses were exposed to 14 days of cyclic hyperoxia. Seven pups – designated 3.1-4.4 (prefix: backcross number; suffix: rat number) – were prospectively selected for angiogenic gene expression studies on the basis of coat and eye colour. At the end of cyclic hyperoxia, RNA was extracted from the left retina of each rat and reverse transcribed to yield cDNA for real-time RT-PCR analysis. A whole-mount preparation of the right retina of each rat was use to measure retinal vascular area.

Rat number	Coat colour	Eye colour	Retinal avascular area (% total)
3.1	Black	Dark brown	55.6
3.2	White	Red	37.5
3.3	Black hooded	Dark brown	86.4
4.1	White	Red	17.3
4.2	Black	Dark brown	78.3
4.3	Agouti	Dark brown	61.2
4.4	Black hooded	Dark brown	57.9

Prior to the analysis of gene expression, retinal cDNA samples were grouped according to the retinal avascular areas of fellow eyes. Pooling of samples was thought to be important in light of the inter-individual variation in retinal gene expression identified within an inbred rat population (section 4.1.a). Data derived from single subjects were therefore considered to be of limited value. The threshold for classification was arbitrarily assigned at 50%: rats with an avascular area of less than 50% of the total retinal area were deemed *resistant* (A); those with an area of greater than 50% were deemed *susceptible* (B) to the cyclic hyperoxic exposure. One albino rat from each backcross comprised the resistant group, whilst five pigmented rats made up the susceptible group. Mean avascular areas of the resistant and susceptible groups were 27.4% (17.3%; 37.5%) and 67.9 ± 13.7% (mean ± SD), respectively. Expression levels of five genes – VEGF, PEDF, Ang2, VEGFR-2 and EPO – were examined in the resistant and susceptible groups (Figure 4.31). While the differences between resistant and susceptible groups failed to achieve statistical significance for all genes, bar EPO ($p<0.001$)), the trend was for higher mean VEGF and EPO expression in the susceptible rats. The pattern of gene expression in the backcross pups was similar to that seen for the parental strains (Figure 4.23): resistant pups resembled the F344 strain, while susceptible

pups resembled the DA strain. Thus in parental strains and in backcross rats following 14 days of cyclic hyperoxia, the extent of avascular retina was associated with the extent of hypoxia-induced retinal gene expression (section 4.4.i.1).
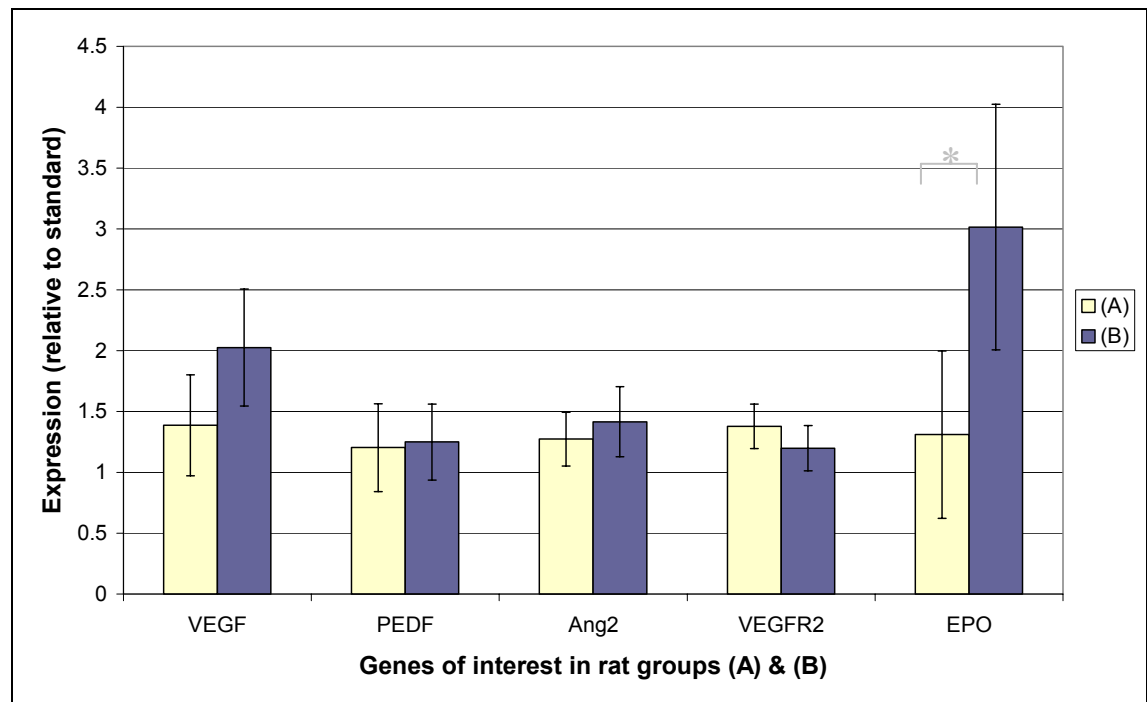
Figure 4.31 Angiogenic gene expression in F1 X F344 backcross rats following 14 days of cyclic hyperoxia – comparison between resistant and susceptible subgroups. Rats were divided into two subgroups – resistant (A), or susceptible (B) on the basis of retinal avascular area (threshold: 50% of total area) and gene expression was compared between subgroups. Two rats comprised the resistant group; five made up the susceptible group. 6 replicates per sample; error bars ± SD. * p<0.001.

In summary, patterns of angiogenic gene expression in pooled backcross rat retinae were similar to those seen in the parental rat strains following 14 days of cyclic hyperoxia – the expression of the hypoxia-induced transcripts, EPO and VEGF, appeared to be related to the extent of retinal avascular area. However the analysis of gene expression data in backcross retina was limited by small numbers of subjects.

4.7.   DISCUSSION

Inbred rat strains differed significantly in the retinal expression of angiogenic factor genes following two weeks of cyclic hyperoxia. At the day 14 and day 18 time-points, the balance of angiogenic factor gene expression was more in favour of angiogenesis in the SPD and DA strains, than in the F344 strain – there was higher relative expression of VEGF, VEGFR-2, Ang2 and EPO, and lower expression of the anti-angiogenic factor PEDF. The retinae of the SPD and DA strains were relatively poorly vascularized at these time-points. Therefore, it was expected that the drive for angiogenesis would be less marked in SPD and DA retinae, than in the more completely vascularized F344 retinae. The cause of the disparity between the expected and observed findings is most likely a consequence of the inter-relationship between retinal vascular extent and the hypoxic stimulus for further angiogenic gene expression (Figure 4.32). The day 14 and day 18 time-points followed periods of 24 hours and 4 days, respectively, of sustained room air exposure – exposures that constituted relative hypoxia for under-vascularized retinae. As retinal vascularization was more advanced in F344 rats at these time-points, it is likely that the retinae of these rats were less hypoxic than were those of the other two strains, and thus the drive for angiogenic factor gene expression was lower. Taken together, these observations suggested that the differences in angiogenic factor gene expression amongst strains at the day 14 and 18 time-points were the consequence of underlying differences in susceptibility to the vasoattenuating effects of cyclic hyperoxia, rather than their cause.

In order to identify the underlying basis for strain differences in the susceptibility to cyclic hyperoxia, it was necessary to examine gene expression at earlier time-points, when strain differences in retinal vascular extent were likely to be less marked. Accordingly, gene expression was examined after two, three, eight and nine days of cyclic hyperoxia in F344 and DA rats. Differences amongst strains in angiogenic gene expression identified at these early time-points are likely to have contributed to the differences in vascular extent observed at day 14. Strain differences were identified in the expression of VEGF, VEGFR-2 and Ang2, with significantly higher expression of these genes in F344 retinae, than in DA retinae. Differences were identified in the extent of gene expression between strains, but not in the pattern of gene expression across the

four time-points. No strain differences were found in the expression of PEDF or EPO. The likely contribution of each of the differentially expressed genes to the strain differences in retinal vascularization will be addressed in turn. The findings of related studies will be drawn upon to identify possible causes for the differences in gene expression.
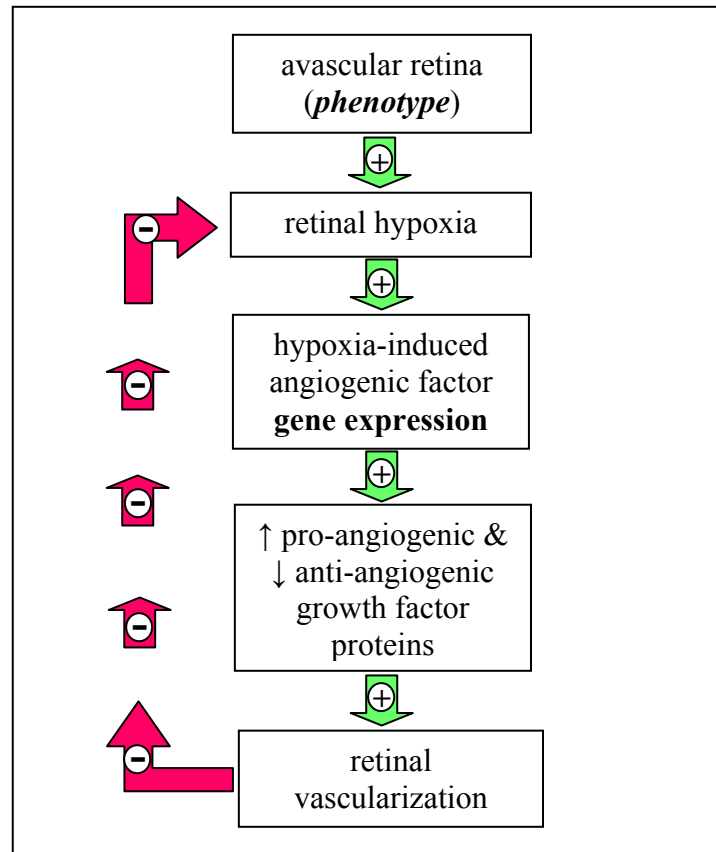
Figure 4.32 Retinal vascularization– the inter-relationship between phenotype and gene expression. During retinal vascularization, maturation of the neural retina leads to retinal hypoxia and hypoxia-induced angiogenic factor expression (green arrows). The resultant vascularization leads to a reduction in hypoxia and therefore in the stimulus for angiogenic factor expression (red arrows). Thus the extent of retinal vascularization and the drive for vascularization are linked. Retinae of the F344 strain are relatively well vascularized by the end of 14 days of cyclic hyperoxia, thus the hypoxic drive for further vascularization is relatively low. In contrast, the SPD and DA strains demonstrate relatively limited vascularization during 14 days of cyclic hyperoxia and thus hypoxic drive for angiogenic gene expression is relatively high.

4.7.a. Possible mechanisms for the observed strain differences in retinal gene expression between F344 and DA rats during cyclic hyperoxia

4.7.a.1 VEGF

Of the strain differences in retinal gene expression, those for VEGF were most marked. Overall VEGF transcript levels in F344 retinae were more than double those in DA retinae. Granted that the retinae of both strains were vascularized to similar extents at the early stages of cyclic hyperoxia, this difference in VEGF expression suggests that for a given degree of hypoxia, retinal VEGF expression was higher in F344 rats than in DA rats. The lack of a strain difference in the expression of EPO − an archetypal hypoxia-induced gene − supports the hypothesis that the retinae of both strains were subjected to equivalent degrees of hypoxia. VEGF expression was also higher in F344 rats than in DA rats, during hyperoxia. Differences in the regulation of VEGF gene expression are therefore likely to be central to the observed strain differences in rat retinal vascularization.

The induction of VEGF expression in hypoxia is largely due to an increase in gene transcription mediated by the hypoxia-inducible transcription factors (HIFs) [181]. HIF-1 is heterodimeric transcription factor comprised of alpha (HIF-1α) and beta (HIF-1β/aryl hydrocarbon receptor nuclear translocator [ARNT]) subunits (Figure 4.33) [344, 421, 422]. The HIF proteins are constitutively expressed, however the fate of HIF-1α is contingent upon intracellular oxygen tension (Figure 4.33). In the presence of oxygen, HIF-1α protein is hydroxylated, bound by the von Hippel-Lindau protein, and subsequently degraded via the ubiquitin-proteosome pathway. At least three prolyl-hydroxylases (prolyl-hydroxylases 1-3) and one asparaginyl-hydroxylase (factor inhibiting HIF [FIH]), have been implicated in this process [422]. The interaction of molecular oxygen with the oxygen-binding domains of the hydroxylases is an absolute requirement for enzyme activity [422]. Thus, under conditions of intracellular hypoxia, hydroxylase action is inhibited and HIF-1α protein accumulates. HIF-1α subsequently translocates to the nucleus where it associates with HIF-1β to form the dimeric transcription factor. HIF-1 binds to a six-base pair consensus sequence − the hypoxia-response element (HRE) − in the promoter regions of target genes, such as VEGF and EPO, driving their transcription. Given the central role of the HIF-system in the cellular

Figure 4.33 VEGF transcription and mRNA stabilisation (facing page). The transcription of VEGF is induced by the binding of the heterodimeric transcription factor HIF-1 to the hypoxia response element (HRE) in the promoter region of the gene. Abundance of the alpha- subunit of HIF (HIF-1α) is a key determinant of transcriptional activation of VEGF. Under normoxic or hyperoxic conditions HIF-1α is hydroxylated and degraded via the ubiquitin-proteosome pathway. During hypoxia, hydroxylation cannot occur and HIF-1α is able to translocate to the nucleus, where it associates with HIF-1β to drive VEGF transcription. Other transcription factors (AP-1, NFκB, AP-2, Sp-1) may modulate the transcriptional activity of the gene. The expression of these transcription factors may be regulated by cytokines and growth factors (insulin, IL-1, IGF-1, COX-2 and TNF). VEGF mRNA is inherently labile, due largely to sequences in the 3'-UTR. Stabilisation of VEGF mRNA is facilitated by several proteins induced by stress or hypoxia (HuR, hnPNPL, PAIP2). VEGF mRNA thus stabilised may be translated to yield VEGF protein.

Key:

(i) Symbols
Grey line: cell membrane
Pink oval: nucleus
Paired brown ovals: ribosomes
Purple cylinder: RNA polymerase
Grey bar: 5'-untranslated region (5'-UTR) of VEGF mRNA
Blue bar: 3'-untranslated region (3'-UTR) of VEGF mRNA
Red sphere: VEGF protein

(ii) Abbreviations
AP-1/2: activator protein-1/2
FIH: factor inhibiting HIF
HIF-1α/β: hypoxia-inducible factor-1 alpha/beta
hnRNPL: heterogenous nuclear ribonucleoprotein L
HRE: hypoxia-response element
HuR: Hu protein-R
IL-1: interleukin-1
NF-κB: nuclear factor-kappa B
PAIP2: poly(A)-binding protein-interacting protein p2
PHD 1-3: prolyl-hydroxylases 1-3
pVHL: von Hippel-Lindau protein
Sp-1: specificity protein-1
TNF: tumor necrosis factor
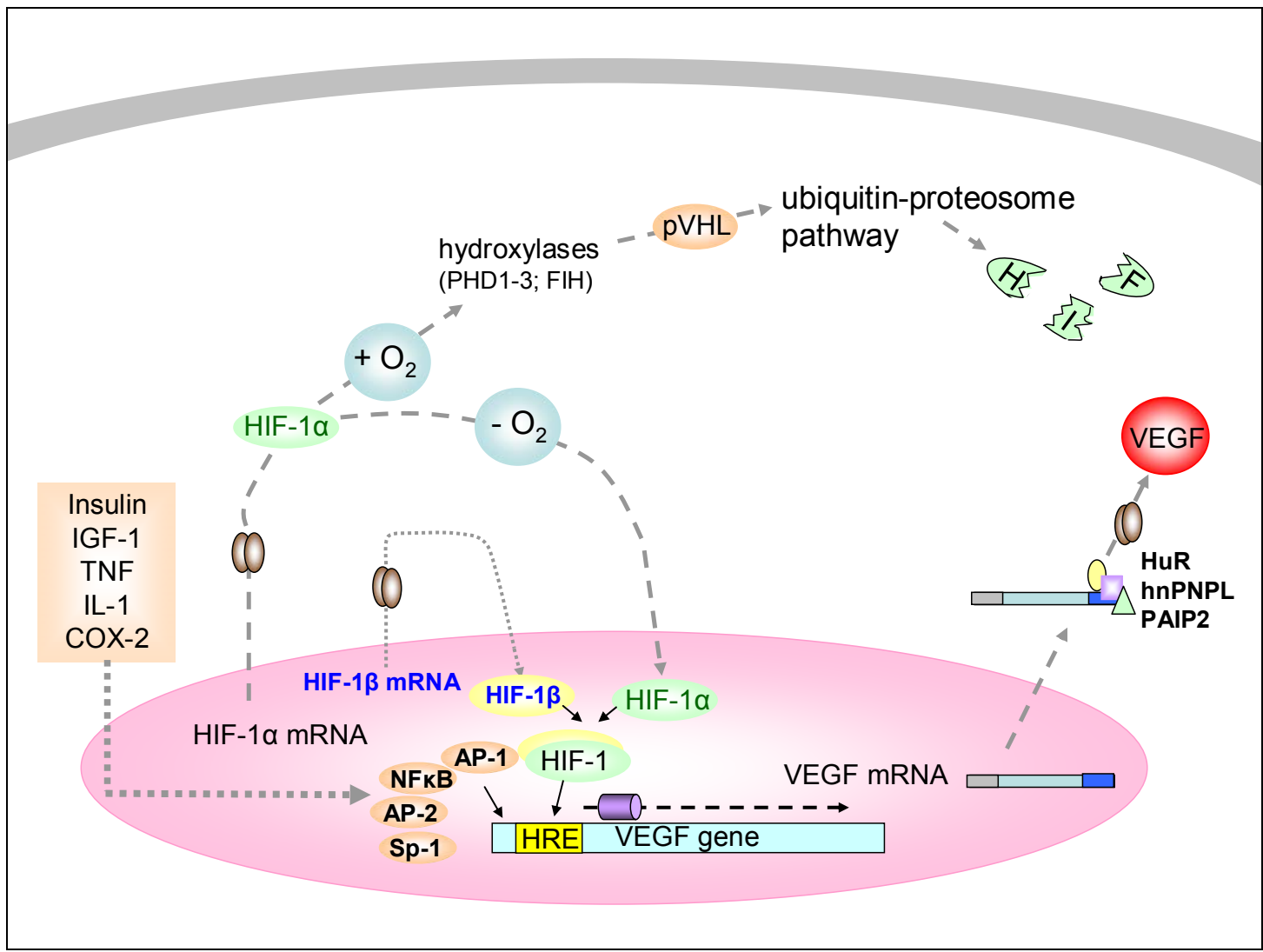
response to hypoxia, it is possible that strain differences in the regulation of this system may account for the observed differences in gene expression. Studies of HIF-1α expression in the rodent kidney point to marked differences in the oxygen threshold for HIF activation in different cell types – expression is potently induced cells in the proximal renal cortex by systemic hypoxia, but not in cells of the distal cortex, despite comparable levels of hypoxia [423]. Thus the set-point for HIF activation may differ between cell types [422]. It is possible that the strain differences in retinal gene expression and vascularization during cyclic hyperoxia may reflect differences in the set-points of the HIF-system between these strains. The mechanisms by which thresholds are set for the hypoxic regulation of HIF expression await elucidation.

Strain differences in the HIF-system may be attributable to polymorphisms in the HIF-1α gene. Several human HIF-1α polymorphisms are known. In a study of the genomic sequence of HIF-1α in patients with head and neck squamous cell carcinoma, two polymorphisms in exon 12 (1772 C→T; 1790 G→A) were found to be associated with increased transcriptional activity of the HIF-1 protein [424]. Tumours from patients who were heterozygous for one or other of the polymorphisms had significantly higher microvascular density than did tumours from patients who were homozygous for the wild type allele. *In vitro* reporter-gene studies demonstrated higher basal gene expression in polymorphic constructs than in wild-type constructs in normoxia [424]. Similar magnitudes of hypoxic-induction of gene expression from normoxic levels were found for both constructs. These differences in gene expression bear close resemblance to those observed for VEGF between F344 and DA rats during cyclic hyperoxia (Figure 4.26). The polymorphisms were not associated with increased HIF-1 protein stability and the mechanism of increased target gene transactivation remains to be determined – the authors speculate that the enhanced recruitment of transcriptional cofactors may play a role [424]. These polymorphisms were also found to be associated with the risk of renal cell carcinoma [425]. It is possible that HIF-1α polymorphisms may account for the strain difference in VEGF expression observed between F344 and DA rats during cyclic hyperoxia. Moreover, differences in the post-translational modification of HIF-1α or the hydroxylating enzymes could alter enzyme-substrate interactions [422], contributing to the observed differences between rat strains.

As levels of the HIF-hydroxylase enzymes are rate-limiting determinants of HIF-1α inactivation in normoxia and hyperoxia, it may be that the observed strain differences in gene expression are due to differences in hydroxylase abundance. Wide variations in the expression of the hydroxylating enzymes in different tissues are common, and several factors are known to modulate their expression including cytokines, growth factors and hormones [422]. The hypoxic induction of prolyl-hydroxylases-2 and -3 is even under the control of HIF-1. While strain differences in the regulation of one or more of the hydroxylase enzymes may account for differences in HIF-1-mediated gene expression in hyperoxia, it is not clear what effect this would have under hypoxic conditions.

It is apparent that there are multiple levels at which strain differences in the HIF-system could result in differences in gene expression. In addition to the aforementioned examples, strain differences in the expression of other factors, such as the von Hippel-Lindau protein, or the deubiqutinating enzymes, might be important [426]. Furthermore, the stability of HIF-1α protein is modulated by several other oxygen-regulated proteins including cAMP-response element binding protein (CREB)-binding protein, p300 and OS-9 [425, 427]. A hypoxia-induced HIF antagonist, inhibitory Per/Arnt/Sim domain protein (IPAS) – a product of alternative splicing of the HIF-3α mRNA – is expressed by cells of the inner nuclear layer and ganglion cell layer of the retina [428, 429]. Differences in the expression of any one of these HIF-regulatory factors could contribute to strain differences in retinal gene expression.

One fact that argues against the contribution of any of these differences in HIF-1 regulation to the observed rat strain differences is that HIF-1-target genes do not appear to be equally affected. A case in point is EPO – the hypoxia-inducible transcription factors are known to play central roles in the transcription of both VEGF and EPO in the retina [387]. Thus strain differences in the regulation of the HIF-system leading to higher HIF-mediated gene transcription in F344 rats, than in DA rats, would be expected to alter the expression levels of VEGF and EPO. This is not the case – while strain differences were identified for VEGF expression during cyclic hyperoxia, no significant differences were found for EPO. However, a recent study of murine OIR suggests that the retinal expression of VEGF and EPO may be independently regulated in hypoxia by HIF-1 and HIF-2, respectively [387]. In the retinae of transgenic mice deficient in

HIF-2, the hypoxic induction of EPO was inhibited relative to wild-type mice. However the retinal expression of 8 other hypoxia-inducible genes, including VEGF, was no different in wild-type and HIF-2-deficient mice, and HIF-1 expression was comparable in both groups [387]. These experiments suggest that in mice, the retinal expression of EPO in hypoxia is mediated by HIF-2, not by HIF-1. In contrast, VEGF expression appears to be independent of HIF-2. At present it is not known whether EPO and VEGF are independently regulated in the rat retina. Were this to be the case, the strain differences in VEGF expression identified in the present study might point to strain differences in HIF-1 expression or activity.

The regulation of VEGF and EPO gene expression is influenced by transcription factors other than the HIFs, such that the expression of these genes is not necessarily concordant [430, 431]. For instance, the transcription factors activator proteins-1 (AP-1) and -2 (AP-2), nuclear factor-κB (NF-κB) and specificity protein-1 (Sp-1) are all known to play roles in modulating the transcription of VEGF [374, 432]. The hypoxia-induced expression of NF-κB provides an important HIF-independent pathway for VEGF expression − NF-κB drives the transcription of COX-2, which in turn catalyses the production of PGE_2 a potent inducer of VEGF expression [374]. These transcription factors are in turn induced by numerous cytokines and growth factors, including interleukin-1, tumour necrosis factor, insulin and IGF-1 [374, 390]. The finding of strain differences in the retinal expression of VEGF, but not EPO, may be due to differences in the expression of transcription factors other than the HIFs. However, gene expression data for COX-2 and IGF-1 at the day 14 and day 18 time- points in the present study would suggest, at the mRNA level at least, that differential expression of these factors is not a key determinant of difference in VEGF expression between F344 and DA rats.

The observed strain differences in gene expression may not be related to the differential expression of transcription factors, but rather to differences in the VEGF gene. Several polymorphisms in the promoter region of the human VEGF gene are known to be associated with increased transcriptional activity (section 1.5.e) [294-297, 433]. Some of these polymorphisms are known to be associated with increased VEGF expression in hypoxia and in normoxia. It may be that similar polymorphisms account for the increased expression of VEGF mRNA seen in the F344 strain. Alternatively, rats of the

DA strain may have polymorphisms that are associated with reduced VEGF transcription.

Another possibility is that differences in mRNA stability may account for the strain difference in VEGF expression. VEGF mRNA is inherently labile, largely thanks to sequences in the 3'-untranslated region (3'-UTR) [434, 435], such as AU-rich elements, which are known to be associated with rapid mRNA turnover [436]. Strain differences in the 3'- region of the VEGF gene may account for differences in mRNA stability and therefore in mRNA abundance – VEGF lability may be greater in DA rats, than in F344 rats. Post-transcriptional regulation of VEGF mRNA is a major contributor to the accumulation of the factor in hypoxia. *In vitro* studies have demonstrated that VEGF mRNA half-life may be increased 2.5-fold by hypoxia [434]. The stabilisation of VEGF transcripts is facilitated by several hypoxia- and stress-inducible proteins, including Hu protein-R (HUR)[437], heterogenous nuclear ribonucleoprotein L (hnRNPL) [438] and poly(A)-binding protein-interacting protein p2 (PAIP2) [435] which interact with the 3'-UTR of VEGF mRNA. Differences in the expression of these proteins, or in their interaction with VEGF mRNA, may provide alternative explanations for the strain difference in VEGF levels. Polymorphisms of the VEGF 3'-UTR may account for differences in mRNA stability – at least one such polymorphism (936 C→T) has been identified in humans and has been associated with low plasma VEGF levels [439] and a lower risk of breast cancer in female carriers [440]. An observation that argues against strain differences in mRNA stability in the present study is the marked accumulation of VEGF mRNA that is evident following 14 days of cyclic hyperoxia in the SPD and DA strains.

In summary, there are numerous levels at which VEGF expression may differ between rat strains. Potential sources of this difference include polymorphisms in the VEGF gene, differences in HIF-1 regulation or transcriptional activity, differences in the expression of transcription factors other than HIFs, and differences in the stabilization of VEGF mRNA.

4.7.a.2   VEGFR-2

Differences in the retinal expression of VEGFR-2 between rats of the F344 and DA strains were identified during cyclic hyperoxia. Overall, expression levels were higher for rats of the F344 strain, than for rats of the DA strain. Both strains demonstrated similar patterns of gene expression – there was an overall reduction in VEGFR-2 expression in the later phases of cyclic hyperoxia, and changes in gene expression did not appear to be concordant with changes in oxygen tension. These findings argue for a less direct mechanism for the regulatory effects of oxygen on the expression of VEGFR-2 than of VEGF.

The delayed changes in VEGFR-2 expression induced by cyclic hyperoxia in this work are consistent with the findings of other studies of OIR. Werdich *et al.* compared VEGFR-2 protein levels in the retinae of rats exposed to room air with those of rats exposed to 14 days of alternating hyperoxia and hypoxia, using Western immunoblotting assays of whole retinal lysates [368]. At the end of this exposure VEGFR-2 levels were significantly lower than control levels. Expression of the receptor increased progressively during the period of relative hypoxia, reaching control levels by day 20. In another rat OIR model, retinal VEGFR-2 protein levels were increased after two days of relative hypoxia, and even more after 6 days [367]. The findings for VEGFR-2 protein expression match the changes in mRNA expression identified in this work. Thus cyclic hyperoxia appears to inhibit VEGFR-2 expression, while relative hypoxia is associated with delayed induction of VEGFR-2 expression.

Evidence for the direct transcriptional induction of VEGFR-2 in hypoxia is mixed [441]. In contrast to VEGF, the promoter of the VEGFR-2 gene lacks a classical hypoxia response element (HRE) – the binding site for HIF-1 – and VEGFR-2 expression does not appear to be regulated by HIF-1 [441]. However recent studies have identified a role for hypoxia-inducible factor-2 (HIF-2), a transcription factor in endothelial cells with a high degree of homology to HIF-1, in the induction VEGFR-2 expression in hypoxia [441, 442]. The alpha subunit of HIF-2, HIF-2α, accumulates in hypoxia, as does HIF-1α, interacting with HIF-1β to direct the expression of a repertoire of hypoxia induced genes. HIF-2 binds to modified HRE-related sequences in the VEGFR-2

promoter and synergises with Ets transcription factors to induce VEGFR-2 gene expression [441]. HIF-2 is also capable of binding to HRE and plays a role in the expression of other hypoxia induced genes in endothelial cells, including VEGF and EPO [442]. While HIF-2 is capable of up-regulating VEGRF-2 expression in endothelial cells *in vitro* and *in vivo,* its importance in angiogenesis awaits clarification [441].

In vitro studies have demonstrated that VEGF is an important autocrine and paracrine regulator of VEGFR-2 expression. Media conditioned by hypoxic myoblasts or tumour cells [363], known to contain VEGF, significantly up-regulated VEGFR-2 expression in endothelial cell cultures, and VEGF-neutralising receptor constructs inhibited this effect [443]. In other studies, exogenous VEGF was able to replicate the hypoxic induction of VEGFR-2 expression in cultured brain-slices [444]. VEGF induced a two-fold increase in VEGFR-2 expression in human umbilical vein endothelial cells (HUVEC) [445], as well as a three-fold increase in VEGFR-2 mRNA expression and a three to five-fold induction of VEGFR-2 protein in cultured bovine adrenal cortex endothelial cells [446]. Luciferase reporter gene studies confirmed that the effect of VEGF on VEGFR-2 expression was principally mediated at a transcriptional level. Additional experiments with VEGF receptor-binding mutants demonstrated that VEGFR-2 expression was dependent on the interaction of VEGF with VEGFR-2 [446]. Furthermore, selective inhibition of signalling pathways downstream of VEGFR-2 has implicated protein kinase-C, phospholipase C-γ and mitogen-activated protein kinase in the process. Together these findings provide strong evidence for a role of VEGF in VEGFR-2 induction and for a positive feedback mechanism for VEGF action [446].

While VEGFR-2 is known to be up-regulated within hours of hypoxia in several experimental models [361, 362], presumably under the control of hypoxia-induced transcription factors [442], several lines of evidence support a role for paracrine inducers of VEGFR-2 expression. Ray *et al.* demonstrated that the expression of VEGFR-2 mRNA in rat myocardium increased within an hour of ischaemia before returning to baseline by four hours, despite ongoing hypoxia and sustained VEGF expression [362]. Furthermore, in a model of chronic pulmonary hypoxia, increases in VEGFR-2 expression in the rat lung lagged behind acute increases in VEGF by up to four days [420]. The lack of sustained VEGFR-2 expression in acute hypoxia [362], coupled with

its delayed up-regulation in a model of chronic ischaemia [420], are consistent with the observations for retinal VEGFR-2 expression in this work. These findings collectively support the importance of paracrine regulation of VEGFR-2 expression.

It is possible that the delayed changes in VEGFR-2 expression observed in the context of cyclic hyperoxia in this work are due to paracrine regulation by VEGF. Despite intermittent spikes in VEGF, it is likely that the overall retinal expression of VEGF during 14 days of cyclic hyperoxia is less than that encountered in normal development, due to suppression of the factor during periods of hyperoxia. This notion is supported by the fact that retinal vascularization is impaired by cyclic hyperoxia, and that vasoattenuation can be reduced by the administration of exogenous VEGF [250]. Thus the decline in VEGFR-2 expression during the later stages of cyclic hyperoxia (days 8 and 9) may be due to an overall reduction in VEGF expression, coupled with direct suppression of VEGFR-2 transcription during hyperoxic periods. The higher expression of VEGF in the retinae of F344 rats than DA rats could therefore account for the strain differences that are apparent in VEGFR-2 expression.

At day 18, following four days of relative hypoxia in room air, the expression of VEGFR-2 is significantly up-regulated in the poorly vascularized retinae of the DA and SPD strains, in contrast to the well vascularized retinae of the F344 strain. The increased expression of VEGFR-2 at this time-point is likely to be a consequence of sustained elevation of VEGF expression and the accumulation of HIF-2α in the hypoxic retina. Increased stability of VEGFR-2 mRNA in hypoxia may also be important [447].

In summary, strain differences in VEGFR-2 expression may be secondary to differences in VEGF expression. During the early stages of cyclic hyperoxia VEGF expression is higher in the F344 strain, than in the DA strain. Accordingly, VEGFR-2 expression is higher in F344 rats than in DA rats. In keeping with the hypothesis of paracrine regulation by VEGF, changes in VEGFR-2 mRNA levels during cyclic hyperoxia are less concordant with fluctuations in oxygen tension than are those of VEGF. As VEGF mRNA expression is greater in DA rats than in F344 rats during the four days of relative hypoxia after 14 days of cyclic hyperoxia, so too is VEGFR-2 mRNA expression.

4.7.a.3　Ang2

Relatively modest differences were noted between F344 and DA rats for the retinal expression of Ang2 during cyclic hyperoxia. Ang2 mRNA levels were higher in F344 retinae than in DA retinae at three of the four early time-points. While there was no significant change in Ang2 expression in the DA strain between these time-points, there was a modest increase in mRNA levels in the F344 strain at later time-points. Following 14 days of cyclic hyperoxia, Ang2 mRNA levels were similar to room air control levels in both strains. Four days of relative hypoxia was associated with increased Ang2 expression in DA retinae and decreased expression in F344 retinae. Thus Ang2 expression appears to be higher in F344 rats than in DA rats during cyclic hyperoxia, and lower following cyclic hyperoxia. The overall pattern of Ang2 gene expression bears greater resemblance to that of VEGFR-2 than that of VEGF, with no concordance between cyclic fluctuations in oxygen tension and changes in gene expression. This may implicate an indirect mechanism for oxygen-mediated Ang2 gene regulation. While the differences in Ang2 expression between DA and F344 rats are relatively small, they may contribute in part to the observed strain difference in vascularization.

The hypoxic induction of Ang2 expression has been demonstrated in numerous *in vitro* and *in vivo* experiments. Ang2 mRNA expression was up-regulated within three hours of hypoxia in HUVEC and murine brain endothelial cells [448]. This was associated with a three-fold increase in Ang2 gene transcription and an increase in mRNA stability. The hypoxic-induction of Ang2 was not mediated by HIF – pharmacological HIF-inducers did not increase Ang2 expression, and hypoxic-induction of Ang2 was demonstrated in a cell line deficient in HIF-1β [448]. VEGF, signalling through VEGFR-2, is known to stimulate Ang2 expression [192, 449], and the inhibition of VEGF signalling was associated with a reduction in the hypoxic-induction of Ang2 in cultured endothelial cells [448]. Further experiments identified COX-2 and its prostanoid products, PGE$_2$ and PGI$_2$, as important mediators of increased Ang2 expression in hypoxia, with activities independent of their effects on VEGF expression [448]. Other studies have demonstrated that the regulation of endothelial cell Ang2 expression may vary between vascular beds – Ang2 expression was induced by VEGF in cultured bovine adrenal cortex microvascular endothelial cells, but not those of bovine retinal, aortic or pulmonary

artery origin [449].

Several studies have demonstrated the induction of Ang2 expression in rodent models of OIR [190-192, 450]. In murine OIR models, retinal Ang2 mRNA levels in mice exposed to five days of sustained hyperoxia were comparable to those of room air control animals, but significantly higher within 6 hours [190] and 12 hours [192] of relative hypoxia. Peak mRNA expression was coincident with the onset of maximal neovascularization (day five of relative hypoxia in the murine model) [190]. While the present study did not demonstrate such acute changes in Ang2 mRNA expression, the maximal up-regulation of mRNA in DA retinae at the day 18 time-point – the peak time for neovascularization – was similar to that seen in the murine model. Further evidence for the role of Ang2 in retinal neovascularization comes from Ang2-deficient mice – these mice fail to undergo hypoxia-induced angiogenesis [191].

It is possible that the differences observed in Ang2 mRNA expression between F344 and DA strains are related to differences in the expression of VEGF. Lower expression of VEGF in the DA strain during cyclic hyperoxia may have resulted in lower levels of VEGF-induced Ang2 expression and less extensive vascularization than was the case for the F344 strain. Furthermore, as Ang2 is known to potentiate the pro-angiogenic effect of VEGF, lower Ang2 expression may result in lower angiogenic activity at a given level of VEGF [190, 451, 452]. However differences in VEGF expression alone could not account for the patterns of Ang2 expression observed during cyclic hyperoxia – Ang2 levels remained stable, or increased slightly at days 8 and 9, despite reductions in VEGF mRNA. Given the importance of prostanoids in the regulation of Ang2 expression, it is possible that the strain differences in Ang2 mRNA levels were also influenced by the differences in COX-2 expression during cyclic hyperoxia. The present work did not examine COX-2 expression during cyclic hyperoxia. However, comparison of the expression levels of COX-2 and VEGF in F344 and DA rats at days 14 and 18 may explain the expression of Ang2 at these time-points (Figures 4.23 & 4.24). In the DA strain at day 14 COX-2 mRNA expression was almost half control levels, while VEGF expression was approximately double. Thus one stimulator of Ang2 expression was reduced and another was increased. Consistent with these findings, Ang2 expression at day 14 was near to control levels. At the day 18 time-point COX-2 expression had

increased to control levels, VEGF mRNA had increased further and accordingly, Ang2 expression was above control levels. In comparison, in F344 rats at day 14, VEGF mRNA was just above control levels, while COX-2 expression was just below and Ang2 expression was at control levels. At day 18, VEGF expression fell slightly, COX-2 expression increased by a similar extent and Ang2 expression decreased slightly. Together these observations suggest that the strain difference in Ang2 expression between F344 and DA rats may be due to the combined effects of differences in the expression of VEGF and COX-2. The importance of the contribution of COX-2 to strain differences in Ang2 expression remains in question, as expression data for COX-2 during cyclic hyperoxia are lacking.

4.7.b. Differences in retinal gene expression provide a basis for the strain differences in retinal vascularization in rat OIR

Taken together, the gene expression data provide a plausible basis for the differences in retinal vascularization between F344 and DA rats in the OIR model (Figure 4.34). Differences in the expression of VEGF appear to be central to the strain difference in vascularization. Cyclic hyperoxia inhibits VEGF mRNA expression to a lesser extent in F344 rats than in DA rats. Accordingly, the expression of VEGF-induced angiogenic factor genes, such as Ang2 and VEGFR-2 is impaired to a lesser extent in the F344 strain than in the DA strain. Although the overall drive for angiogenesis is reduced, pro-angiogenic stimuli are still sufficient to exceed the threshold for vascularization in the F344 strain. Thus F344 retinae are relatively well vascularized by the end of 14 days of cyclic hyperoxia and are subject to relatively modest hypoxia on room air exposure. The hypoxic drive for further angiogenic factor gene expression is low in these retinae. In contrast, the balance of pro-angiogenic stimuli in DA retinae fails to exceed the threshold for vascularization and retinae are poorly vascularized by the end of cyclic hyperoxia. Consequently, large territories of each DA retina are subject to hypoxia on room air exposure and the overall drive for angiogenic factor expression is marked, leading ultimately to aberrant retinal vascularization. These differences in gene expression may be more generally applicable – they may account for the observed hierarchy of susceptibility to OIR in the 6 rat strains studied.
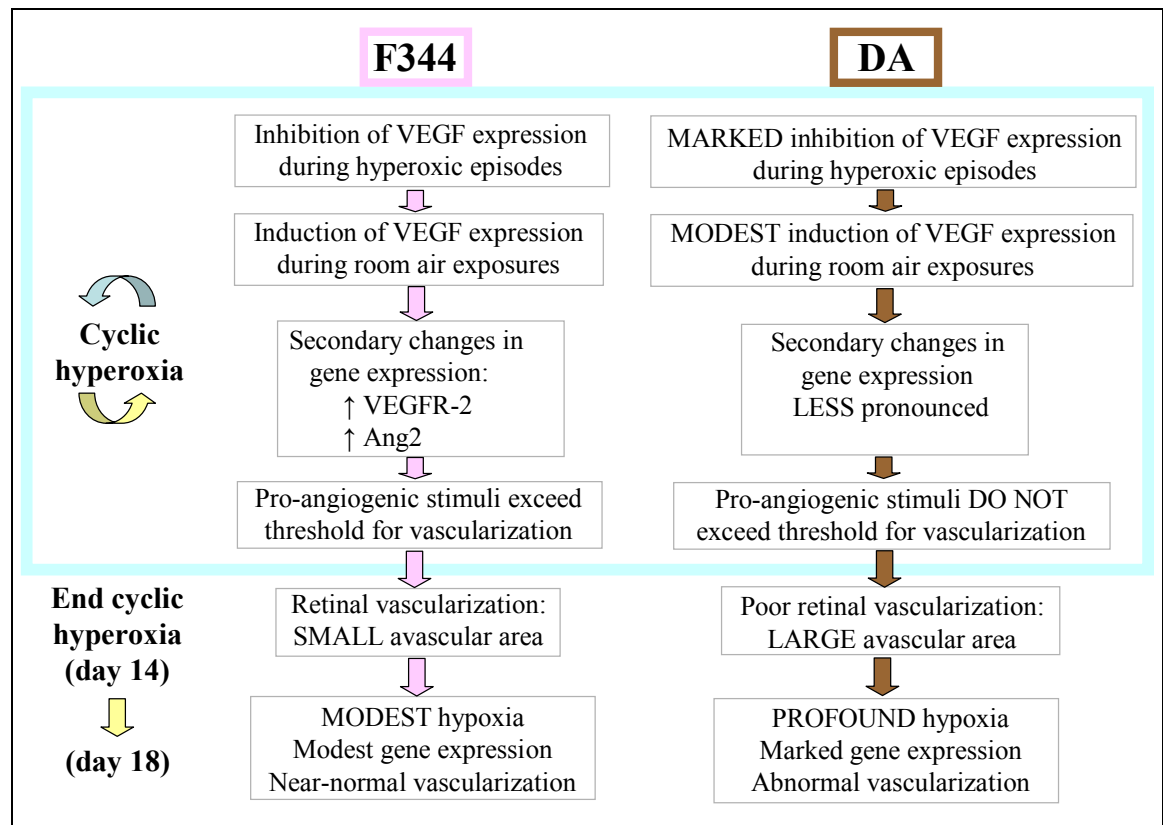
Figure 4.34 Strain differences in oxygen-induced retinopathy. Differences in the extent of VEGF expression appear to be central to differences in vascular extent.

4.7.c. Reconciling the lack of a strain difference in PEDF expression *during* cyclic hyperoxia with the difference evident *after* cyclic hyperoxia

The lack of a strain difference in PEDF expression between F344 and DA strains *during* cyclic hyperoxia is difficult to reconcile with the difference apparent *after* cyclic hyperoxia. Gao *et al*. demonstrated reciprocal regulation of PEDF and VEGF mRNA in rat OIR, using Northern blotting – PEDF expression was reduced and VEGF expression was increased during the period of relative hypoxia [356]. Reciprocal regulation of these factors was mediated in part by plasminogen kringle-5 [76]. Our study is in agreement with these findings, demonstrating reciprocity in the expression of PEDF and VEGF at the day 14 and 18 time-points: VEGF expression is higher, and PEDF expression is lower, in the DA strain than in the F344 strain (Figures 4.23 & 4.24). However, the same does not hold true for the early cyclic hyperoxia time-points – retinal VEGF expression is significantly higher in F344 rats than DA rats, yet PEDF expression is the same in both strains (Figures 4.26 & 4.28). Interestingly, Gao *et al.* did not examine the expression of either factor at early time-points, prior to the end of the hyperoxic

exposure [356]. Our results demonstrate that the reciprocal regulation of VEGF and PEDF is not manifest in the rat retina during the first 9 days of cyclic hyperoxia. It may be that plasminogen kringle-5 and other regulatory mediators are not expressed to a sufficient extent in the retina at this stage.

4.7.d.   The failure of retinal vascularization despite angiogenic factor expression

During the four days of room air exposure that followed 14 days of cyclic hyperoxia, vascularization of the peripheral retina was observed in rats of the F344 strain (section 3.2.b.1). The expression of the hypoxia-induced genes VEGF, EPO and Ang2 was lower at day 18, than at day 14 in these rats – presumably the result of a reduction in retinal hypoxia that accompanied vascularization (Figures 4.23 & 4.24). In contrast, there was no appreciable peripheral retinal vascularization in SPD or DA rats, despite relatively high levels of angiogenic gene expression (section 3.2.b.1; Figures 4.23 & 4.24). The basis for this difference is intriguing.

One explanation is that the profound retinal hypoxia experienced in SPD and DA rats adversely affected the capacity of retinal glial cells to provide the spatial cues required for directed progression of the nascent vascular network. Extensive astrocyte degeneration has been demonstrated during the proliferative phase of feline [253] and rat [453] OIR models. Astrocytes appear to be particularly susceptible to hypoxia in the developing retina, and their degeneration has been correlated with disruption of the normal retinal vascular architecture, and with the proliferation of vessels into the vitreous [453]. The apoptosis of astrocytes was less marked in those areas that were relatively well vascularized, than in those areas that were sparsely vascularized [453]. The source of ongoing hypoxia-induced VEGF expression in the face of astrocyte degeneration was found to be neurons of the ganglion cell layer [453]. As the retinae of SPD and DA rats are less extensively vascularized following 14 days of cyclic hyperoxia than are F344 rats, the hypoxia-induced apoptosis of astrocytes may occur to a greater extent in SPD and DA rats and account for the failure of peripheral vascularization despite angiogenic factor expression. This may also account for the more extensive vascular morphological abnormalities found in these strains, than in the F344 strain at day 18 (section 3.2.b.2). An alternative hypothesis, that the translation of mRNA into

functional angiogenic factor proteins may be impaired in the SPD and DA strains, seems unlikely, as dense central vascular proliferation occurs in both strains during the four day period in room air (section 3.2.b.1).

4.7.e. The implications of inter-animal variation in gene expression on the differences observed between pooled samples

A pilot experiment demonstrated significant variation in the extent of VEGF expression amongst individual SPD rats exposed to identical environmental conditions. This study highlighted that significant inter-animal variation in gene expression may occur, even within inbred populations. It follows that a proportion of the difference in gene expression observed between pooled samples may be due differences in the distribution of inter-animal variation within the pooled samples, rather than to true differences between the sample populations. As each cDNA pool studied in the strain-comparison of gene expression was derived from retinal RNA of three randomly selected rats, inter-animal variation should be randomly distributed amongst the pooled samples. The likely size of the effect of inter-animal variation on the differences observed between pooled samples can be gleaned by examining the expression data for VEGF in the F344 and DA strains during cyclic hyperoxia (Figure 4.26). These data are derived from 8 independent pooled samples. Similar changes in VEGF expression are seen in both strains with cyclic fluctuations in oxygen tension. Were differences due to randomly distributed inter-animal variation to comprise a significant proportion of the observed differences between these pools, one would not expect these patterns of gene expression to be so closely matched between strains. This observation makes it likely that the effect of inter-animal variation on the differences observed between pooled samples was small.

4.7.f.   Closing remarks

These studies have identified differences in retinal gene expression amongst inbred rat strains in a model of OIR that are concordant with the observed differences in retinal vascular extent and morphological abnormalities. The most significant difference amongst strains was the expression of VEGF during exposure to cyclic hyperoxia and hypoxia – resistance to the vascular attenuating effects of this exposure was associated with higher relative expression of VEGF mRNA. It is possible that the expression of other pro-angiogenic factor genes – Ang2 and VEGFR-2 – in the retinae of resistant rats was induced by VEGF. The basis for the underlying strain difference in VEGF gene expression remains to be established. Differences in the regulation of hypoxia-inducible transcription factors, or in their transcriptional activities, may be responsible. Alternatively, differences in VEGF mRNA stability; in VEGF gene polymorphisms; or in HIF-independent gene transcription may account for the strain difference. These findings are likely to have some relevance for human ROP. It may be that the extent of retinal VEGF expression in early postnatal life is a key determinant of the risk of retinopathy. Ultimately, the identification of genetic determinants of retinal VEGF expression may prove useful for the stratification of ROP risk or for therapeutic purposes, such as the augmentation of VEGF expression during the initial phase of vascular attenuation.

CHAPTER 5

DISCUSSION

5. CHAPTER 5: DISCUSSION

5.1.   INTRODUCTION

I have identified a hierarchy of susceptibility amongst neonatal rats of different strains to oxygen-induced retinopathy, a model of human retinopathy of prematurity. In addition, I have demonstrated a hereditary basis for the susceptibility trait and have identified strain differences in angiogenic factor gene expression that may account for the differences in retinal vascularization. The following discussion provides a synthesised account of the major findings of this study and seeks to establish the potential relevance of these observations to human ROP and to other disorders of angiogenesis.

5.2.   STUDY FINDINGS

5.2.a. Strain comparisons

This study is the first to identify differences in the susceptibilities of multiple inbred rat strains to OIR and to correlate these findings with angiogenic factor gene expression. The OIR model used in this work was biphasic – an initial exposure to alternating cycles of hyperoxia and relative hypoxia in room air was followed by a second phase of sustained room air exposure. I identified significant variation amongst rat strains in the retinal vascular response to the first exposure phase, which in turn led to heterogeneity in the response to the second phase. Specifically, neonatal rats of different strains varied significantly in the extent of retinal vascularization following 14 days of cyclic hyperoxia. F344, WF and LEW rats were relatively resistant to the attenuating effects of cyclic hyperoxia on retinal vascularization; SPD rats exhibited an intermediate level of susceptibility; while DA and HW rats were highly susceptible, with large avascular expanses. The extent of the avascular area in a given strain was positively associated with its risk of developing retinal vascular morphological abnormalities, including intravitreal neovascularization, following a four day period in the relative hypoxia of room air. Moreover, the effect of strain on the susceptibility to retinopathy was independent of postnatal weight gain, of litter size, and of differences in respiratory function.

5.2.b. The heritability of susceptibility to oxygen-induced retinopathy

Cross-breeding experiments between the relatively resistant F344 rats and the relatively susceptible DA rats demonstrated that susceptibility to OIR was a heritable trait. Backcross experiments confirmed this observation and were suggestive of an autosomal dominant pattern of inheritance of susceptibility to OIR. In addition, the breeding experiments identified a strong association between ocular pigmentation and the susceptibility to retinopathy – rats with ocular pigmentation were substantially more prone than albino rats to retinal vascular attenuation during the first phase of the model, as well as to aberrant vascularization during the second phase. Nevertheless, a hierarchy of susceptibility to OIR was also identified amongst the albino strains examined in this work – the avascular retinal areas of SPD rats were almost twice as extensive as those of F344 rats at the end of cyclic hyperoxia, and vascular morphological abnormalities were three times more common in SPD rats than in F344 rats after the period of relative hypoxia. These findings suggest that factors in addition to ocular pigmentation are of importance in the risk of retinopathy.

5.2.c. Quantitative retinal gene expression

I went on to identify quantitative differences in the expression of angiogenic factors in the retinae of different rat strains exposed to the same oxygen stimulus. These differences correlated well with the differences in the extent of retinal vascularization amongst the rat strains, suggesting that they may be of functional significance. Differences in the expression of at least three pro-angiogenic factor genes – VEGF, VEGFR-2 and Ang2 – may contribute to differences in the extent of retinal vascularization that occurs during the initial phase of the OIR model – the phase of cyclic hyperoxia. The disparity in the extent of retinal vascularization during cyclic hyperoxia is likely to account for strain differences in the degree of retinal hypoxia experienced during the second phase of the model, when rats are exposed to room air. As hypoxia induces the expression of a range of angiogenic factors, it is not surprising to find that rats with poorly developed retinal circulations express higher levels of these factors than those rats with more complete vascularization. If we were simply to compare angiogenic factor expression amongst rat strains during the period of relative hypoxia, in the second phase of the model, without consideration of differences in the

hypoxic drive for angiogenic factor expression, we might erroneously conclude that the differences observed reflect differences in the susceptibility to hypoxia. This is exactly what was done in the study by Gao *et al.* [334]. While this may seem to be a relatively minor oversight, it has a major bearing on the implications of the experimental findings. Our results suggest that the fundamental differences between rat strains in this model relate to the extent to which angiogenic factors are expressed in the developing retina during periods of cyclic hyperoxia. As hyperoxia and fluctuations between hyperoxia and hypoxia are thought to be major mediators of retinopathy in premature human infants, the identification of the basis of this difference in angiogenic factor expression in rats could be of importance for humans.

Of the eight candidate angiogenic factor genes examined in this work, VEGF played the most important role in the strain difference in susceptibility to cyclic hyperoxia. Higher levels of retinal expression of this gene during the period of cyclic hyperoxia were associated with more complete retinal vascularization. VEGF expression was higher in the relatively OIR-resistant F344 rats than in the more susceptible DA rats during both the hyperoxic cycles and the cycles of relative hypoxia in room air. This implicates a strain difference in the regulatory effect of oxygen on VEGF expression as a cause of the strain difference in retinal vascularization. The retinal expression of two other pro-angiogenic factor genes, VEGFR-2 and Ang2, were correlated with the expression of VEGF. This association may be more than coincidental, as VEGF is known to up-regulate the expression of both factors in a range of experimental contexts [192, 363, 444, 446, 449]. The basis for higher retinal VEGF expression in some strains than in others remains to be established, however the experimental observations point to several possible mechanisms.

Hypoxia-inducible transcription factors (HIFs) are central to the expression of a suite of genes in hypoxia, including VEGF (Figure 4.34). Accordingly strain differences in the expression or function of these transcription factors may be responsible for the observed differences in VEGF mRNA abundance. Our gene expression data demonstrated that the retinal expression of two HIF-regulated genes, VEGF and EPO, were concordant with cyclic fluctuations in oxygen tension in F344 and DA rats during the first phase of the model – expression was down-regulated during the hyperoxic cycles and up-regulated

during the hypoxic cycles. While no strain differences were found between F344 and DA rats for EPO expression during cyclic hyperoxia, marked differences were found for VEGF expression. This finding argues against strain differences in the HIF system, as we might expect to see similar strain differences in EPO expression if this were the case. However, if VEGF and EPO expression in the rata retina are independently regulated by HIF-1 and HIF-2, respectively, as appears to be the case in mice [387], this assumption may be incorrect. Thus it is possible that differences in the regulation of HIF-1, or differences in HIF-1 transcriptional activity could account for the strain difference in VEGF expression.

Other regulators of VEGF mRNA expression or stability may differ between the OIR-susceptible and OIR-resistant rat strains. In addition to HIFs, several accessory transcription factors such as AP-1, AP-2, NF-κB and Sp-1 modulate the expression of VEGF mRNA [374, 432] (Figure 4.34). These transcription factors are in turn regulated by a range of growth factors and cytokines [374, 390]. It is possible that differences in accessory VEGF transcription factors are implicated in the strain difference identified in this work. Alternatively, VEGF gene polymorphisms may be more important. As has already been discussed, polymorphisms upstream of the transcription start site of the VEGF gene are known to modulate VEGF mRNA expression in hypoxia [294-296]. Such polymorphisms might account for the strain difference in VEGF expression during the cycles of relative hypoxia, but not the difference seen during hyperoxia. Another hypothesis is that strain differences in retinal VEGF mRNA levels are attributable to differences in mRNA stability. VEGF mRNA is inherently unstable and sequences in the 3'-untranslated region (3'-UTR) are important in modulating message stability [434]. In hypoxia, stabilising proteins bind to the 3'-UTR of VEGF mRNA, prolonging its half-life [435, 437, 438]. Differences in the expression of these stabilising proteins or in their interaction with the 3'UTR of VEGF mRNA [439] may well account for the strain differences found in this study. A relative prolongation of VEGF mRNA stability in the OIR-resistant rat strains might account for the higher levels of VEGF mRNA detected in the retinae of these strains in hyperoxia and in hypoxia.

5.2.d. Differential vascularization of the central and peripheral retina

An important observation made in this work was that in comparison with F344, LEW and WF rats, vascularization of the peripheral retina was retarded in SPD, DA and HW rats during the four days of relative hypoxia that followed the period of cyclic hyperoxia in the experimental protocol. Central retinal vascularization occurred in all strains during this period, and particularly dense vasoproliferation was seen for SPD, DA and HW rats. Angiogenic factor gene expression was examined in the retinae of F344, SPD and DA rats at the beginning (day 14) and end (day 18) of the period of relative hypoxia in an attempt to account for the lack of peripheral vascularization in the latter two strains. Surprisingly, the retinal expression of the pro-angiogenic factors VEGF, VEGFR-2, Ang2 and EPO was higher in the SPD and DA rats than in F344 rats. Moreover, expression of the anti-angiogenic factor PEDF was lower in the SPD and DA strains than in the F344 strain. Thus, the overall balance of angiogenic factor expression was in favour of angiogenesis in SPD and DA rats, and less so in F344 rats.

These patterns of gene expression were the opposite of those identified during the first phase of the model, when pro-angiogenic factor mRNA levels were substantially higher in F344 rats than in DA rats. As has been discussed in the preceding section, DA rats, and presumably HW and SPD rats, appeared to be more prone to the inhibitory effects of cyclic hyperoxia on angiogenic factor gene expression than did F344 rats, and presumably WF and LEW rats. As a consequence, the retinae of DA, HW and SPD rats were less well vascularized than those of F344, LEW and WF rats by the end of the 14 day period of cyclic hyperoxia and thus exposed to more profound hypoxia during the sustained room air exposure period. The high levels of pro-angiogenic factor gene expression detected in the retinae of DA and SPD rats during the second phase of the model are likely to be the consequence of this profound hypoxia. Thus it appears that the retinae of DA, HW and SPD rats are capable of mounting a robust transcriptional response to sustained and pronounced hypoxia. The finding that pro-angiogenic factor gene expression was increased in the OIR-susceptible rats at day 14, but not at day 9 or earlier, suggests that there may be a transition point for hypoxia-induced gene expression in the retinae of these rats. In these strains it may be that hypoxia beyond a critical threshold level is sufficient to override the inhibitory effect of the preceding

hyperoxic cycle on pro-angiogenic factor gene expression.

Despite this pro-angiogenic milieu, less peripheral retinal vascularization was observed in SPD and DA rats than in F344 rats during the second phase of the model. The basis for the disparity between the stimulus for angiogenesis and the angiogenic response is intriguing. The fact that peripheral vascularization failed to occur despite a high level of pro-angiogenic factor expression, sufficient to bring about dense central vascularization, suggests that there may have been a loss of the normal guidance cues for directed angiogenesis in SPD and DA rats. Interactions between retinal astrocytes and vascular endothelial cells are essential for normal vascularization [51, 162, 343]. Stone and colleagues have demonstrated that retinal astrocytes undergo apoptosis in hypoxia, and that aberrant vascular proliferation is a frequent consequence [253, 453]. It seems likely that the peripheral avascular territories of those strains that were most susceptible to the vasoattenuating effects of cyclic hyperoxia – the SPD and DA strains – experienced more profound hypoxia during the period in room air. It follows that the hypoxic dysfunction and apoptosis of astrocytes would be more pronounced in the retinae of these rats than in those of more extensively vascularized strains, such as the F344. Although these hypotheses remain to be tested, they provide a cogent explanation for the vascular derangements seen in OIR and in ROP.

5.2.e. Study limitations

The limitations of this work warrant consideration. Our gene expression studies involved a focussed analysis of 8 angiogenic factor genes thought to be of importance in OIR. While these data have added to the collective understanding of OIR, they offer at best a fragmentary insight into the molecular events that occur in this complex process. The products of other genes are likely to play important roles in OIR and it is simplistic to attribute the strain differences in retinal vascularization in the OIR model to differences in the expression of a handful of selected genes. That differences in the expression or function of several gene products are likely to be important in the strain variation identified in this work is suggested by the phenotypic heterogeneity of backcross offspring. Another limitation of this work is that protein expression data are lacking. The regulation of protein expression is not just a function of mRNA expression – post-translational modification is also important. A case in point is PEDF. The

proteolytic degradation of PEDF is mediated in part by matrix metalloproteinases-2 and -9 (MMP-2 and MMP-9) [407]. As VEGF up-regulates the expression of MMP-2 and MMP-9, an inter-relationship may exist between VEGF and the anti-angiogenic factor PEDF that is not appreciable at the mRNA level [407]. Thus protein expression data for the genes examined in this study are likely to be of additional value in accounting for the strain differences that have been identified.

5.2.f.   Integration of study findings

The findings of the phenotypic studies can be integrated with the data for angiogenic factor gene expression to generate a unified hypothesis for the spectrum of strain differences in retinal vascularization identified in the OIR model. Rats that are relatively resistant to OIR exhibit more pronounced VEGF expression during the period of cyclic hyperoxia, than do more susceptible strains. VEGF in turn drives the expression of other pro-angiogenic factors – VEGFR-2 and Ang2. As a result, retinal vascularization proceeds in these rats, such that by the end of the period of cyclic hyperoxia only a relatively small proportion of the retina remains avascular. Modest hypoxia is experienced in these avascular territories during the four day period in room air, providing the stimulus for further angiogenic factor expression and vascularization. In contrast, more susceptible rat strains undergo relatively little vascularization during the cyclic hyperoxia period, owing to the marked suppression of VEGF expression. The large peripheral avascular territories in these retinae become profoundly hypoxic during the period of sustained room air exposure, as oxygen diffusion from the choroidal circulation is insufficient to meet retinal metabolic needs, and the retinal vasculature is rudimentary. Hypoxia is so profound in these territories as to impair astrocyte function and to induce their apoptosis. As a result, the guidance cues that ordinarily direct vascular endothelial cell migration into the retinal periphery are lost and peripheral vascularization is impaired. VEGF and other hypoxia-induced angiogenic factors are abundantly expressed by ganglion cells in the avascular regions [453]. The abundance of pro-angiogenic stimuli, coupled with a loss of guidance cues for angiogenesis, leads to aberrant vascular proliferation centrally, in the territories that were already vascularized by the end of the period of cyclic hyperoxia. Dense vascular proliferation occurs in these zones and some vessels breach the inner limiting membrane of the retina to proliferate in the vitreous humour.

Although many elements of this hypothesis are speculative at present, and while its applicability to human ROP remains to be established, it is likely to be of some value in guiding therapeutic strategies for ROP. Ultimately, the key to the prevention of ROP may lie in the discovery of the underlying driver of VEGF expression during cyclic hyperoxia in the relatively resistant strains. While the overall quantity of retinal VEGF expression may be important in determining the susceptibility to OIR, spatially appropriate expression of the factor may be just as important. Evidence for this assertion comes from the observation that vascularization of the peripheral retina fails to occur in SPD and DA rats during the period of relative hypoxia, despite high levels of VEGF expression. While the intraocular administration of exogenous VEGF during the initial phase of OIR may protect against some of the vascular attenuation that ordinarily occurs [52, 250], it is unlikely to facilitate normal vascularization, as spatial gradients of the factor that ordinarily mediate directed vascular proliferation will not be replicated. Furthermore, as VEGF is expressed in concert with a host of other angiogenic factors to facilitate functional vessel development, angiogenic *monotherapy* is likely to lead to vascular dysfunction. Moreover, while the inhibition of VEGF expression or VEGF signalling may inhibit aberrant vascular proliferation during the second phase of the model, it is equally likely to inhibit adaptive peripheral vascularization. A more appealing therapeutic strategy might involve the identification of the genetic basis for VEGF expression in resistant rat strains in cyclic hyperoxia, and the recapitulation of this mechanism in susceptible strains. The applicability of such an approach rests on the underlying basis of the difference in gene expression. Once vascular attenuation has occurred there may be a role for therapeutic measures aimed at minimising astrocyte injury, such as supplemental oxygen therapy to minimise hypoxia, or specific cytoprotective agents. As has been discussed, the evidence for a beneficial effect of supplemental oxygen therapy in OIR and in ROP is mixed [234, 270, 271], however this approach does seem to be mechanistically sound.

5.3. AN OVERVIEW OF RELATED STUDIES

This study has not been carried out in isolation. Other investigators have also identified differences amongst rodents of different strains in OIR, and in several other models of angiogenesis. The following discussion will draw parallels between the relevant studies and our own work. The aim of this discussion is to place our findings in the broader context of hereditary determinants of angiogenesis.

5.3.a. A comparison of the susceptibility of Brown Norway and Sprague Dawley rats to OIR

The pioneering work of Gao and colleagues identified differences in the susceptibilities of two different rat strains to OIR [334]. While this study has been discussed at length in Chapters 3 and 4, it is raised again here as it bears the closest resemblance to our own study and yet it arrives at very different conclusions. The basis for this disagreement will be reiterated.

In the study by Gao *et al.*, rats were exposed to five days of sustained hyperoxia (75% oxygen) between postnatal days 7 and 12, prior to a period of up to 10 days of relative hypoxia in room air [334]. Retinal vascular extent was examined on postnatal days 12, 14, 18 and 22, while retinal neovascularization was assessed on day 18 by the enumeration of intravitreal neovascular sprouts. Thus the methodology of this study differed from our own in several respects. A key point of difference was the use of sustained hyperoxia for the initial exposure phase, in contrast to the cyclic hyperoxia used in our study. Brown Norway (BN) rats were noted to have substantially larger avascular retinal areas than SPD rats at all time points from day 12 – the end of the hyperoxic exposure – to day 22 [334]. At day 18 the difference in vascular extent between the strains was more than five-fold. Intravitreal neovascular proliferation was substantially and significantly more common in BN rats than in SPD rats at day 18, as were vascular morphological abnormalities, such as vascular tortuosity and dilatation. In contrast, no strain differences were found in the extent of retinal vascularization in control animals raised in room air. Thus despite the methodological differences between this study and our own, the strain differences in susceptibility to OIR were remarkably similar. That is, the difference between DA rats and SPD rats identified in our study

parallels the difference between BN and SPD rats in the study by Gao *et al* [334].

The fundamental difference between the studies was in the interpretation of these observations. Gao and colleagues concluded that the BN strain was more susceptible to *hypoxia* than the SPD strain [334]. In arriving at this conclusion the investigators failed to take account of the significance of the strain differences in retinal vascular extent that followed the hyperoxic exposure period. As SPD retinae were more completely vascularized at the end of the hyperoxic exposure than those of BN rats, the extent of retinal hypoxia encountered by both strains was not equivalent. This difference would preclude any meaningful comparison of relative susceptibilities of the strains to hypoxia, as the stimulus for hypoxia-induced angiogenic factor expression would be less in SPD rats than in BN rats during the period in room air. A difference in the extent of retinal hypoxia accounts for the difference in VEGF expression between the strains that was detected at the day 18 time-point – VEGF was significantly lower in the retinae of SPD rats than BN rats. Our contention is that the strain difference observed by Gao and colleagues was not the result of a difference in susceptibility to *hypoxia*, but rather a difference in the susceptibility to *hyperoxia*. The difference in hypoxia-induced angiogenesis evident at the day 18 time-point was a consequence of the strain difference in susceptibility to vasoattenuation in hyperoxia.

The fact that BN and SPD rats differed in the extent of retinal vascularization after five days of sustained hyperoxia supports our hypothesis that a key difference between rat strains in the susceptibility to OIR relates to the extent of vascularization in hyperoxia. Relatively resistant rat strains undergo more extensive retinal vascularization during the period of hyperoxia, such that the retina is less prone to hypoxia on subsequent room air exposure. While we have not exposed neonatal rats to sustained hyperoxia, we predict that vascularization would be more pronounced in those strains found to be relatively resistant to cyclic hyperoxia – the F344, WF and LEW strains – than the more susceptible strains – SPD followed by the even more susceptible DA and HW strains. It is interesting to note that in our study the expression of VEGF was not the same in F344 and DA rats during the cycles of relative hypoxia in the period of cyclic hyperoxia – VEGF expression was higher in the relatively OIR-resistant F344 strain than in the relatively susceptible DA strain. This suggests that the difference between strains is not

merely limited to gene expression in hyperoxia, but in hypoxia as well. The relatively OIR-resistant F344 rat strain appears to be more 'susceptible' to hypoxia-induced VEGF expression than the DA rat strain during the first phase of our model. This observation turns the conclusion of Gao *et al.* upside down – while Gao suggested that susceptibility to hypoxia is greater in an OIR-susceptible rat strain [334], we have found the opposite: strains that are more capable of expressing VEGF in hypoxia are better equipped to mount an adaptive vascular response, preventing profound hypoxia on sustained room air exposure.

5.3.b. Rat strain differences in retinal vascular permeability in OIR and in diabetes

In a sequel to the studies comparing retinal vascularization in BN and SPD rats [334, 356], Zhang and colleagues sought to examine retinal vascular permeability in these strains [454]. An increase in vascular permeability is a well recognised antecedent of neovascularization and VEGF plays a central role in this process [85, 148, 149]. Retinal oedema, a consequence of vascular hyperpermeability, is a common early event in the proliferative retinopathies and is a major cause of vision loss in diabetic retinopathy and neovascular age-related macular degeneration [455, 456]. Retinal albumin extravasation was measured as a marker of retinal vascular hyperpermeability in neonatal BN and SPD rats during a period of relative hypoxia in room air that followed exposure to constant hyperoxia. Permeability was assessed at 7 time-points between postnatal days 12 – the end of the hyperoxic period – and 36 [454]. Retinal vascular permeability was substantially and significantly higher in hyperoxia-exposed BN rats than in age-matched control rats at each time-point, with the peak difference in permeability (8.7-fold higher)[454] coinciding with the timing of peak neovascularization [334]. In contrast, retinal vascular permeability in oxygen-exposed SPD rats was only above control levels for a brief period between days 14 and 16, and the peak difference (2.2-fold higher than control levels) was not as high as that seen in BN rats [454]. Thus retinal vascular hyperpermeability was substantially greater for a longer period in the BN strain than in the SPD strain. The strain difference in retinal vascular permeability was attributed to the differences in hypoxia-induced retinal VEGF expression detected in the earlier studies [334].

Zhang and colleagues also compared retinal vascular permeability in adult BN and SPD rats rendered diabetic with streptozotocin [454]. The diabetic rat is used to model human diabetic retinopathy as it exhibits the many of early retinal sequelae of diabetes such as vascular dilatation, blood-retinal barrier breakdown, pericyte dropout and microaneurysm formation [454, 457, 458]. BN rats exhibited increased retinal vascular permeability within one day of the onset of diabetes, and hyperpermeability was sustained for the 16 week duration of the study [454]. The mean increase in permeability above non-diabetic control rats was 1.9-fold. While diabetic SPD rats exhibited similar increases in vascular permeability as BN rats, the duration of hyperpermeability was substantially shorter, with a return to control levels within two weeks. Importantly the strain difference in retinal vascular permeability could not be attributed to differences in glycaemic status – average blood glucose levels of BN rats were similar to, or lower than, those of SPD rats at each time-point. Western blotting was used to compare retinal VEGF protein expression between diabetic BN and SPD rats. At each time-point, between 3 days and 16 weeks from the onset of diabetes, retinal VEGF appeared to be higher in BN rats than in SPD rats. However, as no quantitative data were provided, the magnitude of this strain difference in VEGF expression is not known.

In further experiments the retinal vascular responses of BN and SPD rats to the exogenous administration of IGF-1 and VEGF were assessed [454]. BN rats exhibited a significantly greater increase in vascular permeability than SPD rats following intravitreal injection of IGF-1. As IGF-1 is known to induce the expression of VEGF [390, 391, 459], the study authors hypothesised that the observed difference in retinal vascular permeability was attributable to differences in VEGF expression [454]. However as no comparison was made for VEGF expression in these rats, and as IGF-1 may have effects on vascular permeability that are independent of VEGF [459], this hypothesis remains somewhat speculative. Retinal vascular permeability was increased above control levels in both strains following VEGF administration and the increase was slightly but significantly higher in BN rats (0.4-fold, p=0.038). The study authors concluded that BN rats are more susceptible than SPD rats to "hypoxia-induced" retinal vascular hyperpermeability in the diabetes model and in the OIR model [454].

This conclusion may be incorrect on several grounds. As has already been discussed, the difference in the susceptibility of SPD and BN rats to OIR appears to stem from differences in the susceptibility to hyperoxia, not to hypoxia *per se*. Accordingly, differences in the extent of retinal vascularization between these strains at the end of the hyperoxic exposure are likely to account for the subsequent differences in VEGF expression and vascular permeability. Furthermore, while Zhang and colleagues [454] have demonstrated a significant effect of strain on retinal vascular permeability in diabetic rats, and while differences in retinal VEGF expression appear to be associated with this strain effect, differential susceptibility to hypoxia seems unlikely as a cause. The increase in retinal VEGF expression in diabetes is multifactorial in origin (reviewed by Brownlee [460]). Retinal hypoxia, a potent stimulus for VEGF expression, is associated with diabetes but is typically manifest in the context of chronic disease, once microvascular occlusion and retinal non-perfusion occur [461, 462]. Although retinal microvascular occlusion and vascular endothelial cell injury have been identified as early as one week after the onset of experimental diabetes in rats, it is unlikely that retinal hypoxia becomes significant until much later [458]. Therefore, in the acute setting, factors other than hypoxia are likely to be more important in driving VEGF expression in the diabetic retina. Hyperglycaemia leads to activation of a series of biochemical pathways that are known to induce VEGF expression [460]. Examples include the activation of protein kinase-C via diacylglycerol, via the polyol pathway, and via advanced glycation end products [460]. Protein kinase C is a potent mediator of VEGF expression. It is therefore possible that the strain differences in retinal vascular permeability and VEGF expression identified in the OIR and diabetic models are aetiologically distinct.

Accordingly it is very difficult to draw on these observations to speculate about how the strain differences identified in our study relate to diabetic retinopathy. While it is tempting to hypothesise that the rats strains that were susceptible to OIR in our study might also be susceptible to retinopathy in diabetes, there is insufficient evidence to do so with any confidence. In more general terms, the study of Zhang and colleagues provides insufficient evidence to conclude that the same genetic risk factors apply in OIR, as in diabetic retinopathy.

5.3.c. Lessons from the anterior segment: genetic factors may regulate sensitivity to VEGF and bFGF

Studies of corneal neovascularization in mice have identified strain-related differences in the response to the angiogenic factors VEGF and basic fibroblast growth factor (bFGF) [339, 340, 463]. The corneal implantation of angiogenic factor-impregnated pellets induced neovascularization that differed significantly amongst strains by up to an order of magnitude [339]. The response of a given strain to one factor was predictive of its response to the other. Further, this heterogeneity correlated with strain differences in the extent of vascularization of the corneoscleral limbus in untreated control mice – the strain with the most extensive limbal vasculature exhibited the greatest extent of corneal neovascularization induced by bFGF pellet implantation [340]. Interestingly, a correlation was identified between sensitivity to corneal angiogenesis and aortic vascular endothelial cell proliferation in an explant culture model [339]. This observation suggests that the identified strain differences in susceptibility to neovascularization are not unique to the cornea, but are indicative of systemic differences that may be of relevance to vascularization at other sites. While there was no clear association between ocular pigmentation and the susceptibility to corneal neovascularization in these studies, a striking association was apparent for iris neovascularization [339].

Iris neovascularization and hyphaema occurred frequently in 6 of 8 albino strains and in only one of 7 pigmented strains following corneal bFGF pellet implantation [339]. To further examine the influence of pigmentation on iris neovascularization, the investigators compared pigmented C57BL/6J mice with closely related albino C57BL/6J-Tyr^{c-2J} mice, which carry a mutation of the tyrosinase gene. Hyphaemas were identified in five of 9 eyes in the tyrosinase mutant group, compared with none of 70 eyes in the pigmented group following bFGF pellet implantation [339]. It is interesting to note that there was no significant difference in the extent of corneal neovascularization between these two groups of mice.

Another study identified strain-related differences in the extent of anterior segment neovascularization in mice following intravitreal injection of a viral vector encoding bFGF [463]. Neovascularization was frequent and severe in two albino strains (CD-1

and BALB/c) but not in a third (AKR), nor in a pigmented strain (C57BL/6J). The degree of corneal neovascularization in C57BL/6J-Tyr^{c-2J} mice was only marginally greater than C57BL/6J mice in this model, and iris neovascularization was not seen in either. Furthermore, over-expression of bFGF in the eyes of SPD rats failed to induce neovascularization of the cornea or iris [463]. No mention was made of strain-related differences in retinal neovascularization in this model. Taken together, these findings suggest that ocular pigmentation may have an inhibitory effect on bFGF- and VEGF-induced iris neovascularization. The basis for this protective effect and its relevance to retinal neovascularization remain to be established. Heterogeneity in the sensitivity to corneal neovascularization appears to be independent of pigmentary status and the risk of iris neovascularization. These data suggest that strain differences in the susceptibility to neovascularization may be vascular bed-specific. It is possible that differences in the set-point of the angiogenic balance in different vascular beds, such as the cornea and iris, renders them differentially susceptible to neovascularization and the set-point for a given tissue may differ amongst strains.

The genetic bases for strain differences in bFGF- and VEGF-induced corneal neovascularization in mice have been the subject of other studies. Two gene loci (quantitative trait loci) with highly significant linkage to the corneal angiogenic response to VEGF have been identified on chromosomes 2 and 10 [464]. Many genes known to play roles in angiogenesis map to these chromosomal regions, including genes encoding extracellular matrix components, matrix metalloproteinases, as well as angiogenic signalling molecules, such as thromboxane A2 receptor, ephrins and interleukin-1 receptor antagonist [464]. Of further note are several genes regulating serum IGF-1 concentration. In addition, four distinct quantitative trait loci with linkage to corneal bFGF responsiveness have been identified on chromosomes 4, 13, 15 and 18 [465]. Again numerous genes with known angiogenic activity map to these regions. It remains to be determined which of the genes at each locus make significant contributions to the observed differences in the angiogenic response.

In summary, there is compelling evidence for strain-related heterogeneity in the response to at least two angiogenic factors in mice. While the bulk of this evidence relates to anterior segment neovascularization, similar findings in an aortic explant

culture model point to a systemic effect. Ocular pigmentation appears to exert an inhibitory effect on VEGF- and bFGF-induced iris neovascularization that overrides the strain difference in sensitivity to these factors. The basis for this effect and its role in other pigmented tissues remain to be determined. Genetic studies point to complex polygenic bases for strain differences in the sensitivity to VEGF and to bFGF.

In contrast to these experiments, our studies have not sought to examine strain differences in the angiogenic response to a given quantity of an angiogenic *factor*, but rather quantitative differences in the expression of angiogenic factors amongst strains in response to a given *stimulus*. Our findings do not preclude the possibility that such differences in angiogenic factor responsiveness occur amongst the rat strains studied. However, as the strain differences in retinal vascular extent correlated well with the identified differences in angiogenic factor gene expression, we have no reason to suspect that strain differences in angiogenic factor responsiveness play an important role. The fact that strain differences may be operational at the level of angiogenic factor expression, and at the level of angiogenic factor responsiveness, attests to the complexity of the process of angiogenesis.

5.3.d. Strain differences in murine OIR

In a recent study, strain differences in retinal vascularization and angiogenic factor expression in a murine model of OIR were examined [466]. Five different strains of mice were exposed to constant hyperoxia from postnatal days five to 12, followed by five days in room air. In a departure from the established methods of quantifying retinal vascularization, the study authors measured total retinal vascular volume, using three-dimensional reconstructions of confocal microscopy images of fluorophore-perfused, flat-mounted retinae. The vascular volume measurement was expressed as an absolute quantity, rather than as a proportion of the total retinal volume. Retinal vascular volume was measured at a single time-point: at the end of the five day period in room air (day 17). In addition, the total surface area of intravitreal neovascular sprouts in histological sections was quantified for two strains – 129S3/SvIM and C57BL/6J – at the day 17 time-point. Strains differed by up to 2.2-fold in retinal vascular volume and 2.7-fold in intravitreal neovascularization. Retinal vascular volume and intravitreal

neovascularization were significantly higher in the 129S3/SvIM strain than in the C57BL/6J strain. Strain differences in retinal vascular volume were attributed to differences in the susceptibility to hypoxia-induced retinal vascularization. However, as no comparison was made amongst strains for retinal vascular volume at the end of the hyperoxic exposure period, this conclusion cannot be made with certainty. Moreover, as no measure was made of the extent of the avascular retinal area, the results of this study are very difficult to compare with our own. Importantly, vascular volume may not correlate with retinal vascular extent. To draw on an illustrative example from our study, it is possible that DA and HW rats would have similar vascular volumes to the F344 rats at the end of the relative hypoxia period (day 18) despite substantial differences in avascular retinal areas, due to the very dense central vascularization seen in the DA and HW strains. As angiogenic factor expression by avascular regions of the retina constitutes the major driver for ongoing vascularization, avascular retinal area is a more useful measure of retinal vascularization than absolute vascular volume, when used in isolation.

The expression levels of four angiogenic factors were compared between 129S3/SvIM and C57BL/6J mice at six time-points between 0 and 96 hours after the end of the hyperoxic period [466]. Granted that no comparison was made for the extent of retinal vascularization between these strains at the end of hyperoxic exposure (0 hour time-point), the significance of these data is difficult to interpret. Moreover, comparison of these data with our own is limited by the fact that gene expression was determined for posterior eyecups (retina, RPE, choroid and sclera) in the murine study, rather than for retinae alone. Nonetheless, in both mouse strains expression of the pro-angiogenic factors VEGF and Ang2 increased during the period of relative hypoxia in room air [466]. As was seen in our own study, the induction of Ang2 mRNA expression lagged behind the increase in VEGF expression, supporting the hypothesis that VEGF induces Ang2 expression (section 4.3.a.3). Small, but statistically significant differences were found in the expression levels of VEGF and Ang2 mRNA between the mouse strains at one of the six time-points: 48 hours after hyperoxic exposure, Ang2 and VEGF levels were 22% and approximately 70% higher, respectively, in 129S3/SvIM mice than in C57BL/6J mice [466].

Overall, the expression of the anti-angiogenic factors PEDF and thrombospondin-1 were higher in C57BL/6J mice than in 129S3/SvIM mice, but strain differences in the expression of these factors mirrored the differences seen in control animals [466]. The changes in PEDF and VEGF mRNA expression were concordant with changes in protein expression as measured by ELISA. In contrast with our findings in the rat, PEDF mRNA levels increased during the period of relative hypoxia in both mouse strains. However, as similar increases in PEDF expression were seen over the same period in control mice, and since no direct comparison was made between the mRNA expression levels of control and oxygen exposed mice, it is not possible to attribute the increase in PEDF expression to relative hypoxia. While these gene expression data need to be interpreted with caution, they are in broad agreement with our own – during the period of relative hypoxia, the expression of VEGF and Ang2 were higher in the strain that exhibited the most marked intravitreal neovascularization (incorporated in the vascular morphological abnormality measure in our study). While vascular volume data were collected for albino and pigmented mouse strains, measurements of gene expression data and intravitreal neovascularization were only collected for the pigmented C57BL/6J and 129S3/SvIM strains. Given the difficulties in interpreting the data for vascular volume, it is not possible to compare albino and pigmented strains in this model. However, the data for the C57BL/6J and 129S3/SvIM strains demonstrate differences in the susceptibilities of these two pigmented strains to OIR. This observation lends support to our own findings which demonstrate that factors in addition to ocular pigmentation are important in regulating susceptibility to OIR.

5.3.e. Parallels in tumour angiogenesis

Strain differences in tumour-associated angiogenesis have been identified between F344 and BN rats and the aetiology of this difference may be of relevance to the findings of the present study. F344 rats were highly susceptible to pituitary tumours (adenomas and adenocarcinomas) on chronic exposure to exogenous oestrogen, while BN rats were resistant, exhibiting very mild hyperplasia only [467-470]. SPD rats were also resistant to tumour development in this model [471]. A marked increase in tumour angiogenesis accompanied the neoplastic increase in pituitary mass in oestrogen-treated F344 rats [469]. These tumours were highly vascular with dense, tortuous and disorganised vessels

– angiogenesis was out of proportion with the increase in pituitary mass. Genetic mapping has identified 7 loci that contribute to the differences in pituitary tumour development between F344 and BN rats [472, 473]. Of these quantitative trait loci (QTLs), the Edpm5 (Estrogen-dependent pituitary mass on chromosome 5) locus has been linked with the difference in angiogenesis between BN and F344 rats in the pituitary tumour model [470]. Specifically, differences in the expression of the pro-angiogenic factors VEGF and matrix metalloproteinase-9 (MMP-9) have been strongly linked to the Edpm5 locus [474, 475].

A congenic rat strain carrying the BN Epdm5 allele on a F344 background was used to examine the effects of this QTL on angiogenesis [470]. Oestrogen-treated congenic rats developed pituitary tumours that were of similar size to those of F344 rats, but with significantly fewer blood vessels. Thus an uncoupling of the association between tumour growth and angiogenesis apparent in the F344 strain was observed in the congenic rats. In part, tumour angiogenesis is related to the hypoxia that accompanies tumour growth – the hypoxic-induction of angiogenic factors results in neovascularization and the amelioration of the hypoxia. Consequently, in the absence of sufficient angiogenesis, tumour growth in congenic rats was accompanied by extensive tumour necrosis [470]. These findings suggest that the Epdm5 QTL is important in regulating the switch to angiogenesis in oestrogen-induced tumours, while other QTLs regulate the susceptibility to neoplastic transformation. While the BN allele appeared to exert an inhibitory effect on tumour-associated angiogenesis, the F344 allele appeared to be permissive. The study authors speculated that F344 rats have mutations of one or more angiogenesis regulating genes in the chromosomal interval of the Edpm5 locus [470].

It is possible that the rat strain differences identified in the present study of OIR relate to differences at the Edpm5 locus. While the OIR and pituitary tumour models differ in many respects, a fundamental driver of angiogenesis in both models is hypoxia. F344 rats in the OIR model demonstrated higher VEGF expression than did DA rats when exposed to the same degree of hypoxia during the period of cyclic hyperoxia (days 2 and 8; Figure 4.27). Similarly, VEGF levels were substantially and significantly higher in the tumours of F344 rats than in those of F344 rats congenic for the BN Edpm5 locus [470]. Despite profound hypoxia in the tumours of the congenic strain – as reflected by the

extensive necrosis – the induction of VEGF expression was repressed. Therefore the BN Edpm5 locus appears to inhibit hypoxia-induced VEGF expression. As hypoxia ordinarily induces VEGF expression and angiogenesis, it is possible to extend the hypothesis proposed by Pandey *et al.* [470]: while the F344 Edpm5 locus is associated with exuberant angiogenesis in oestrogen-induced pituitary tumours, the BN Edpm5 allele appears to confer resistance to 'normal' hypoxia-induced angiogenesis. The rat strains identified as susceptible to OIR in the present study (SPD, DA and HW) may have Epdm5 alleles similar to that of the BN strain – accounting for the relatively low level of hypoxic VEGF expression – while the resistant strains (LEW and WF) may have alleles similar to the F344 strain – with a relatively high level of hypoxia-induced VEGF expression. One finding that argues against this hypothesis is the high level of VEGF expression in the retinae of susceptible rat strains during the period of relative hypoxia in OIR. Furthermore, as the Edpm5 locus is associated with oestrogen-induced angiogenesis it may be that the strain differences identified in this work were not due to differences at this locus, but rather the result of gender imbalances between the rat groups studied. However this seems unlikely as we found no association between gender and the susceptibility to retinopathy in any of the rat strains. Moreover, it is possible that the effect of the Edpm5 QTL on hypoxic angiogenic factor induction is dependent on high oestrogen levels, in which case differences at the locus would have no bearing on susceptibility to retinopathy in the OIR model. Finally, it is not known whether the Epdm5 locus can account for the strain differences in VEGF expression observed during periods of hyperoxia. Nonetheless, the possibility of an association between the strain differences in OIR and differences in genes at the Edpm5 locus is tantalising.

As the rat gene for VEGF is situated on chromosome 9, and the Epdm5 locus is on chromosome 5, the angiogenic differences identified between the F344 and BN strains in the tumour model must be independent of VEGF gene polymorphisms [470]. While several known angiogenesis genes map to the Edpm5 chromosomal interval, including Tie2, none of these genes are known to regulate VEGF expression, implicating a novel gene [470].

5.3.f. The broader implications of rat strain-related heterogeneity in the susceptibility to OIR

It is possible to speculate on the relevance of the strain differences identified in our study to angiogenesis in other contexts. Hypoxia is a major stimulus for neovascularization in a host of diseases including diabetic retinopathy, central retinal vein occlusion, tumour growth and ischaemic vascular disease, to name a few. A determinant of the susceptibility of rats to OIR appears to be the extent to which VEGF is expressed in cyclic hyperoxia. While the rat strains that are relatively susceptible to OIR exhibit low levels of VEGF expression during cycles of relative hypoxia early on in the OIR model, they do appear to be capable of mounting a robust response to more profound hypoxia encountered during the second phase of the model. It is possible then that the relative insensitivity of OIR-resistant strains to hypoxia evident at the early stages of the model is a developmental phenomenon that is lost with maturation. Alternatively it may be that these strains continue to exhibit muted responses to low grade hypoxia into later life, a finding that may be of significance for angiogenesis in other contexts. However, both of these suggestions are difficult to reconcile with the fact that normal vascularization ordinarily occurs in the retinae of these strains when they are raised in room air. Mild physiological hypoxia drives this process [176], suggesting that these rats are not intrinsically insensitive to hypoxia *per se*. Another, more likely hypothesis is that the cycles of relative hyperoxia inhibit the capacity for a transcriptional response to subsequent cycles of relative hypoxia. Thus we return to the hypothesis that the fundamental difference amongst rat strains in the OIR model stems from differences in gene expression during hyperoxia. Given that hyperoxia is only encountered in the context of oxygen therapy, the strain differences identified in this work may only be of relevance to OIR, and thus to ROP. Even if the rat strains studied in this work did exhibit differences in the susceptibility to hypoxia-induced retinal angiogenesis, it does not necessarily follow that these differences would translate to angiogenesis in other settings. This is so as the pattern of gene expression in the developing retina is likely to differ significantly from that in other tissues, including the adult retina.

5.3.g.   Bronchopulmonary dysplasia and ROP: more than meets the eye?

While the findings of this study may not be of direct relevance to disorders in which angiogenesis is induced by hypoxia, without antecedent hyperoxia, they may prove to be of value in diseases in which hyperoxia plays a pathogenic role. Bronchopulmonary dysplasia (BPD) is an important case in point. Like ROP, BPD is a condition unique to premature human infants, typically affecting the smallest and most premature babies [476, 477]. The disease is characterised by impaired lung development and is a major cause of neonatal mortality and morbidity, with long term cardiopulmonary disease common amongst survivors [477, 478]. BPD almost invariably follows mechanical ventilation and oxygen therapy for acute respiratory failure in premature neonates – barotrauma, volutrauma, regional pulmonary hyperoxia and comorbid infection are thought to be central to its pathogenesis [476, 477]. Key histological features of BPD include reductions in lung alveolarization and in microvascular density [479]. Alveolar development and angiogenesis appear to be tightly linked in pulmonary development – the expression of VEGF by the nascent respiratory epithelium provides a stimulus for angiogenesis, such that the two processes are closely coordinated [480]. VEGF expression is markedly reduced in the lungs on infants who die from BPD, implicating a lack of the factor in the pathogenesis of this disorder [481]. Recent experimental evidence provides strong support for this hypothesis [482-485].

Key features of BPD can be recapitulated in the neonatal rodent lung with ambient hyperoxia, as a large proportion of pulmonary development occurs *ex utero* in rodents [486-488]. For instance, the exposure of newborn rats to 95% oxygen for the first two weeks of life significantly impedes pulmonary vascularization and alveolar development [479]. Thébaud and colleagues induced similar changes in the lungs of neonatal rats reared in normoxia with the systemic administration of a VEGF antagonist [479]. The lungs of these rats were underdeveloped with striking hypoalveolarization and decreased microvascular density. Interestingly, VEGFR-2 protein expression was significantly lower in these lungs than in the lungs of untreated control rats. Similarly, VEGF and VEGFR-2 expression were reduced in the lungs of rats exposed to hyperoxia suggesting, as did our study of OIR, that VEGF may induce VEGFR-2 expression. The investigators demonstrated that overexpression of VEGF in the lungs of rats exposed to hyperoxia

prevented the occurrence of lung disease – intratracheal delivery of an adenoviral vector expressing VEGF, led to an increase in lung microvascular density and normal alveolarization [479]. Survival rates were significantly higher in hyperoxia exposed rats treated with the VEGF vector, than in untreated rats, or rats treated with a control vector. Vessels in the lungs of rats treated with VEGF gene therapy exhibited a fenestrated phenotype and were hyperpermeable, as demonstrated by a high wet-to-dry lung weight ratio. The use of a viral vector encoding both VEGF and angiopoietin-1, was equally effective at preventing lung disease in hyperoxia exposed rats, without the vascular hyperpermeablity evident in those rats treated with the VEGF vector alone [479].

ROP frequently occurs in the context of BPD, and BPD has been identified as an independent risk factor for the development of severe retinopathy [489, 490]. It has long been presumed that the need for oxygen supplementation in BPD, and particularly fluctuations in oxygen tension that are common in the disease, predispose to ROP. It is possible however that ROP and BPD may be linked at an even more fundamental level. We have identified that a key determinant of the risk of retinopathy in rats exposed to cyclic hyperoxia is the extent to which VEGF is expressed – strains with relatively poor VEGF gene expression are at greater risk of severe disease. Similarly, as is demonstrated by the study of Thébaud *et al*, the extent to which VEGF is expressed in hyperoxia in the developing lung is a key determinant of the risk of BPD. Strain differences in the susceptibility to hyperoxia-induced lung injury have been identified in rats and in mice, but no studies have compared the expression of VEGF amongst strains [341, 342, 491, 492]. Given that ROP and BPD commonly affect the same individuals, and given that VEGF expression is associated with the risk of both diseases, it is possible that the same genetic factors that predispose to retinopathy may also predispose to lung disease. Stated otherwise, premature infants may be predisposed to both ROP and BPD by virtue of genetic factors that regulate VEGF expression.

This hypothesis is speculative at present – it assumes that the same genetic risk factors apply in human ROP as in rat OIR, and that the susceptibility of a given rat strain to OIR is predictive of its susceptibility to hyperoxia-induced lung injury. The comparison of respiratory function between F344 and DA rats following cyclic hyperoxia in this work found no substantial strain differences in lung function. It is most likely that the oxygen

exposure protocol used in this study was insufficient to induce severe lung injury, and thus it is possible that differences in susceptibility to injury induced by this exposure would be subtle and unlikely to cause appreciable differences in respiratory function. Moreover we did not compare alveolar development and pulmonary vascularization in hyperoxia exposed F344 and DA rats. Further experiments are required to determine whether rat strain differences in susceptibility to OIR are predictive of the susceptibility to hyperoxia-induced lung disease. The identification of a shared genetic predisposition to BPD and ROP could have wide ranging implications for neonatal intensive care.

The finding that hyperoxic suppression of VEGF expression may play a role in the pathogenesis of ROP and BPD may have important therapeutic repercussions. A recent study has demonstrated a potential therapeutic role for an inhibitor of the hypoxia-inducible transcription factor (HIF)-regulating enzymes, the prolyl-hydroxylases, in hyperoxic lung injury [493]. As has been discussed, prolyl-hydroxylases catalyse the oxygen dependent degradation of the constitutively expressed transcription factors HIF-1α and HIF-2α (Figure 4.34) [422]. The enzymes are the major regulators of HIF abundance – the degradation of HIFs in normoxia and hyperoxia prevents the expression of a suite of hypoxia-inducible genes, including VEGF. Asikainen and colleagues found that HIF-1α and HIF-2α protein levels, as well as VEGF levels, were significantly higher in media conditioned by human lung microvascular endothelial cells treated with the prolyl-hyroxlase inhibitor, than in the media of untreated cells, following exposure to hyperoxia. Endothelial cells treated with the inhibitor demonstrated a substantial increase in branch formation – a marker of angiogenic activity. Similar changes in protein expression in hyperoxia were found in explant cultures of foetal baboon lungs treated with the prolyl-hydroxylase inhibitor. Thus the prolyl-hydroxylase inhibitor prevented the down-regulation of HIFs in hyperoxia, leading to increased expression of HIF target genes including VEGF. The authors of the study suggest that this therapy may offer hope for the prevention of BPD. Granted that hyperoxic-inhibition of HIF gene transcription is central to ROP, it is possible that prolyl-hydroxlase inhibitors may also be of value in preventing ROP.

5.4.   FUTURE DIRECTIONS

More work is required to identify the basis for the strain differences in susceptibility to OIR characterised in this study. Moreover, further experiments are required to establish the relevance of these findings to hyperoxia-induced lung injury in rats. Ultimately the relevance of these findings to human ROP and to BPD will need to be examined. It is clear that many questions remain unanswered. The molecular basis for the effect of ocular pigmentation on susceptibility to OIR is a case in point. Furthermore, the roles played by other factors implicated in the pathogenesis OIR warrant attention. For instance, although this study has demonstrated that retinal IGF-1 expression does not appear to make a significant contribution to the strain difference, evidence is emerging for a role of systemic IGF-1 in the risk of retinopathy [59, 395]. Other studies have implicated such factors as endothelial nitric oxide synthase activity [357] and the non-receptor tyrosine kinase c-*abl* in the pathogenesis of OIR [494]. Nunes *et al.* have demonstrated that mice deficient in c-*abl* failed to exhibit hyperoxia induced down-regulation of VEGF and were therefore resistant to OIR [494]. This suggests that c-*abl* may be important in the down-regulation of VEGF expression in hyperoxia. Further, experiments in a model of corneal neovascularization have demonstrated that c-*abl* deficient mice retain the capacity for robust VEGF-induced angiogenesis [494]. A mechanism for the effect of c-*abl* on VEGF expression remains elusive, however it is plausible that the factor may contribute to the strain difference identified in this work. The list of potential candidates for the strain difference is long and growing rapidly. Accordingly, there may be great virtue in embarking on broad-based gene expression studies, such as gene arrays, or proteomic analyses to identify factors that are differentially expressed in the retinae of susceptible and resistant strains. In addition, further cross-breeding studies and linkage analyses are likely to aid in the identification of genetic risk factors for susceptibility to retinopathy. While these studies may be time and resource intensive they are likely to be fruitful. This study has generated the impetus for such investigations to be undertaken.

5.5.   FINAL COMMENTS

This study has made several novel contributions to the understanding of oxygen-induced retinopathy. Foremost amongst these is the finding that the susceptibility to cyclic hyperoxia, rather than to hypoxia *per se,* is a key determinant of the risk of retinopathy. The study is the first to identify the significance of strain differences in the retinal response to hyperoxia and to correlate these with differences in angiogenic factor expression. The work adds to the body of evidence implicating ocular pigmentation in the risk of retinopathy, and establishes that factors independent of pigmentary status also make important contributions to the risk. Further, this is the first study to examine the association between the susceptibility to hyperoxic lung injury and the risk of oxygen-induced retinopathy. Strain differences in the susceptibility to lung injury did not account for differences in the susceptibility to retinopathy, indicating that the risk of retinopathy is related to differences in the regulatory effects of oxygen tension on retinal gene expression, rather than to differences in retinal oxygen supply. Significant lung injury was not induced by the oxygen exposure used in this study, however when the findings of this work are interpreted in light of other research, it is possible that the same genetic factors that govern the risk of oxygen-induced retinopathy may also contribute to the risk of hyperoxia-induced lung injury.

The findings of the retinal gene expression studies give important insights into the roles played by several angiogenic factor genes in OIR. The precision of these studies was ensured by the use of carefully validated controls and meticulous quantitative methods. A key determinant of the risk of retinopathy appears to be the extent to which VEGF is expressed during cyclic hyperoxia – higher levels of retinal VEGF expression are associated with more complete retinal vascularization and a lower risk of retinopathy. VEGF seems to up-regulate the expression of two other pro-angiogenic factors, VEGFR-2 and Ang2, which contribute to retinal vascular proliferation. This work has reproduced the findings of other studies in demonstrating that the extent of the avascular retinal area at the end of the cyclic hyperoxia period strongly correlates with the risk of aberrant vascular proliferation. However the study is unique in identifying quantitative differences in the extent of vascularization in central and peripheral retinal regions amongst strains. While central retinal vascularization occurred in all strains during the

period of relative hypoxia, significant peripheral vascularization was only seen in the retinae of relatively resistant strains. We hypothesise that the lack of peripheral vascularization despite high levels of pro-angiogenic factor expression in OIR-susceptible strains is due to hypoxia-induced astrocyte injury. This hypothesis remains to be tested.

In addition, this is the first study to demonstrate that the susceptibility to oxygen-induced retinopathy is a heritable trait. Cross-breeding experiments highlight that the susceptibility trait is dominantly inherited, however the phenotypic variation evident amongst backcross progeny is indicative of a polygenic mode of inheritance. It is hoped that further studies will lead to the identification of genetic risk factors for the susceptibility to OIR.

At the very least this study provides strong evidence for the effect of rat strain on retinopathy risk in the OIR model. This finding is of importance given that the model is widely used to test novel anti-angiogenic therapies. An understanding of differences in the susceptibilities of rat strains to retinopathy may have important implications for comparisons amongst these studies. In a broader context, this study may be of value for human retinopathy of prematurity. While the relevance of this work to the human disease remains to be established, it is possible that the same genetic determinants of retinopathy apply to rats and humans alike. Identification of the genetic risk factors for retinopathy may pave the way for genetic risk factor profiling of premature infants. When used in conjunction with conventional risk factor algorithms, genetic risk profiling may allow for more precise and timely stratification of risk, improving options for prophylactic therapy and minimising harm from unnecessary interventions. Ultimately, the characterisation of genetic determinants of the risk of ROP may facilitate the development of targeted therapeutic interventions. While this may sound like a distant possibility, the rapid pace of progress in angiogenesis research makes this a likely prospect. Research efforts such as this are central to minimising the burden of ROP and improving outcomes for premature infants.

APPENDIX 1

INBRED RAT STRAINS

APPENDIX 1: INBRED RAT STRAINS

A1.   INBRED RAT STRAINS

The rat strains used for scientific research today are almost exclusively derived from the Norway rat, which originated in the temperate regions of Asia and spread through Europe and the Americas during the 18th century. Rat domestication and breeding followed soon after [495]. In the early 20th century efforts were made to establish strains for scientific research. In 1906, under the stewardship of Drs Greenman and Donaldson, the Wistar Institute (Philadelphia, PA) established the first standardised laboratory animal, the WISTARAT, an outbred rat line [496]. It has been estimated that approximately half of all laboratory rats are derived from the original WISTARAT stock. The genealogy of Wistar lines has been documented by Lindsey [497]. Inbreeding was used to generate homogenous populations for genetic studies. A rat strain may be regarded as inbred if it is the product of more than 20 consecutive brother-sister matings, or more than 20 parent-offspring matings where the younger of the two parents is used for each successive mating.

The Wistar Furth strain, developed by J. Furth in 1945, and the Lewis strain, developed by M. Lewis in the early 1950's, are direct descendants of the WISTARAT line. The Sprague Dawley was originally developed in 1925 (Sprague Dawley Corporation, Wisconsin) as an outbred strain from a cross between a female WISTARAT and a hybrid male of unknown pedigree. The Sprague Dawley remains one of the most commonly used outbred rats today. Inbred Sprague Dawley populations were first developed in the 1970's [498]. The Fischer 344 strain, now the most widely used of all inbred rat strains, was first developed in 1920 by M.R. Curtis, of the Columbia Institute for Cancer Research (New York, NY) as the product of mating number 344, of rats acquired from a local rat breeder named Fischer. The DA rat strain, commonly referred to as the Dark Agouti, was originally named after its *d* blood group allele and its *a*gouti colour. The strain was developed by T. Odell Jr (Oak Ridge National Laboratory, TN) and inbreeding was completed in 1965 at the Wistar Institute. The sources of the rats used in this thesis are provided in Table 2.2 (Chapter 2), as is an account of their key characteristics. The sixth strain used in these experiments was the outbred Hooded Wistar strain – a locally outbred cross between a Wistar rat and a pigmented strain of unknown pedigree. Images of each of these strains are provided in Figure 3.1 (Chapter 3).

APPENDIX 2

REVERSE TRANSCRIPTION-PCR PRODUCT

SEQUENCING DATA

APPENDIX 2: PCR PRODUCT SEQUENCE DATA

A2. SEQUENCE DATA

The sequences of quantitative real-time reverse transcription-polymerase chain reaction products (amplicons) are provided below for each primer pair. Forward and reverse sequences were derived from the use of the forward and reverse primers in the sequencing reaction, respectively. Owing to the technical challenges of sequencing small PCR products, complete sequence could not be obtained for all amplicons. The predicted sequence (blue text) of each amplicon was determined from the published mRNA sequences of target genes (www.ncbi.nih.gov/BLAST/) – sequence accession numbers appear in parentheses. Reverse primed sequence is presented in black; forward primed sequence is in green. Sequence mismatches are in red. Numbers denote nucleotide positions in the rat mRNA sequence. The sequence for IGF-1 is provided in section A2.11. The key for the sequencing chromatograms is as follows:

red peak = thymine (T)

green peak = adenine (A)

blue peak = cytosine (C)

black peak = guanine (G)

A2.1. ARBP

766 (NM_022402.1)
*
```
AAAGGGTCCTGGCTTTGTCTGTGGAGACTGACTACACCTTCCCACTGGCT
AAAGGGTCCTGGCTTTGTCTGTGGAGACTGACTACACCTTCCCACTGGCT
                                      CCTTCCCT--GGCT
```

```
                                          856
                                          *
GAAAAGGTCAAGGCCTTCCTGGCCGATCCATCTGCATTTGC
-AAAAG-TCAAG
GA-AAGGTCAAGGCCTTCCTGGCCGATCCATCTGCATTTGC
```


ARBP forward

NCGGAGCTTGACTTTTCGCCGTGGGAAGGTGTAGTCAGTCTCCACAGACAAAGCCAGGACCCTTTAAGANN
      10   20   30   40   50   60   70
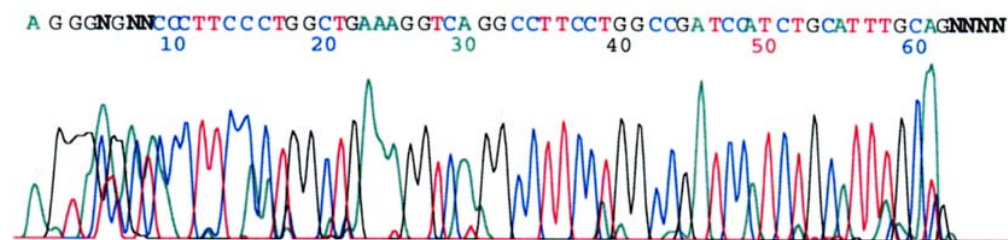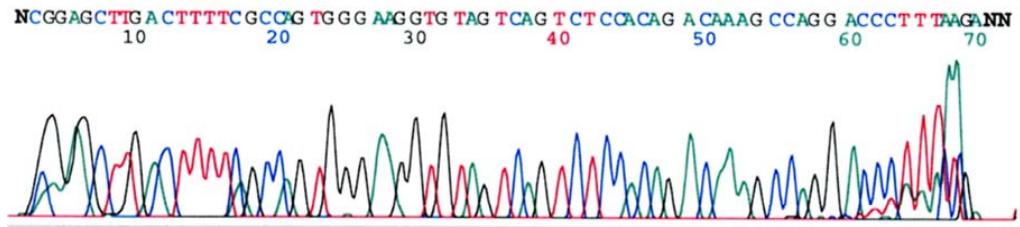
ARBP reverse

A2.2. Ang2

2244 (XM_344544.1)
*
CAGCTTGCTGACCATGATGTCATCGCCCGACTATAAGAGCTCTGTTGCTG
CAGCTTGCTGACCATGATGTCATCGCCCGACTATAAGAGCTCTGT
                                    TAAGAGCTCTGTTGCTG

                             2330
                             *
TCCCTAAAGAAGAGAAAACCACCTTCAGAGACTGTGC
TCCCTAAAGAAGAGAAAACCACCTTCAGAGACTGTGC

CGNTTAGAGCTCTGTTGCTGTCCCTAAAGAAGAGAAAACCACCTTCAGAGACTGTGCAN
     10   20   30   40   50

Ang2 forward

CTNTTAGGGNGCACAGAGCTCTTATAGTCGGGCGATGACATCATGGTCAGCAAGCTGAN
     10   20   30   40   50
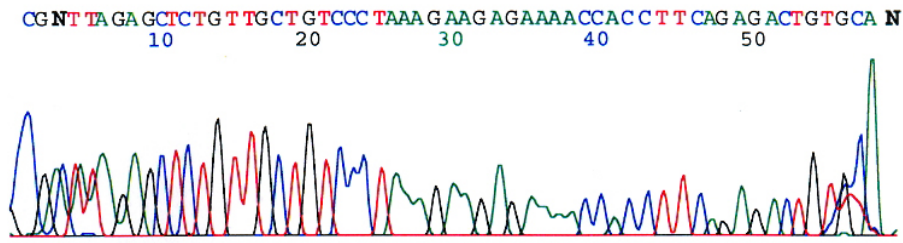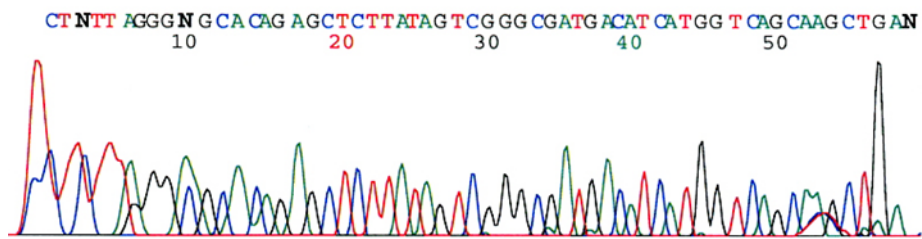
Ang2 reverse

A2.3. COX-2

1320 (AF_233596)
*
TCCTCCTTGAACACGGACTTGCTCACTTTGTTGAGTCATTCACCAGACAG
                GGACTTGCTCACTTTGTTGAGTCATTCACCAGACAG
                    CA-TTTGTTGAGTCATTCACCAGACAG

ATTGCTGGCCGGGTTGCTGGGGGAAGGAATGTTCCAATCGCTGTACAAGC
ATTGCTGGCCGGGTTGCTGGG--AA
ATTGCTGGCCGGGTTGCTGGGGGAAGGAATGTTCCAATCGCTGTACAAGC

  1421
  *
AG
AG
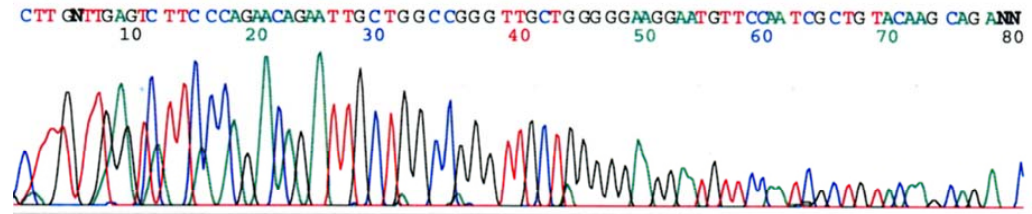
COX2 forward
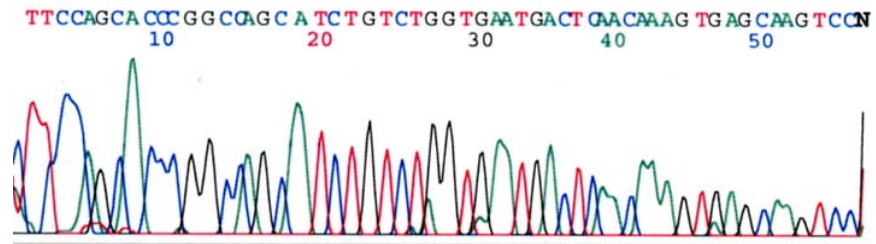
COX2 reverse

A2.4.   EPO

361 (NM_017001)
*
ACCAGAGAGTCTTCAGCTTCATATAGACAAAGCCATCAGTGGGCTACGTA
  CCAGAGAGTCTTCAGCTTCATATAGACAAAGCCATCAGTGGGCTACGTA
                          GACAAAGCCATCAGTGGGCTACGTA

GCCTCACTTCACTGCTTCGGGTGCTGGGAGCTCAGAAGGAATTGATGTCG
GCCTCACTTCACTGCTTCGGGTGCTG
GCCTCACTTCACTGCTTCGGGTGCTGGGAGCTCAGAAGGAATTGATGTCG

      464
       *
CCTC
CCTC
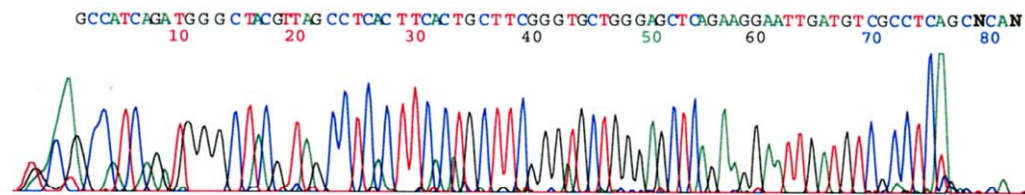
EPO forward
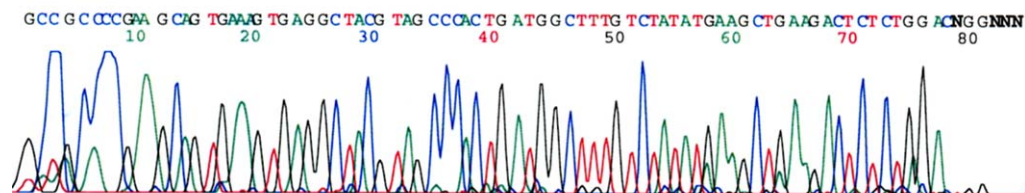
EPO reverse

A2.5.   HPRT

629 (NM_012583.2)
*
TTGTTGGATATGCCCTTGACTATAATGAGCACTTCAGGGATTTGAATCAT
TTGTTGGATATGCCCTTGACTATAATGAGCACTTCAGGGATTTGAATCAT
                          GTTTTTGAATCAT

GTTTGTGTCATCAGCGAAAGTGGAAAAGCCAAGTACAAAGCCTAAAAGA
GTTTGTGTCATCAGCGAAAGTG
GTTTGTGTCATCAGCGAAAGTGGAAAAGCCAAGTACAAAGCCTAAAAGA

      733
       *
CAGCGG
CAGCGG
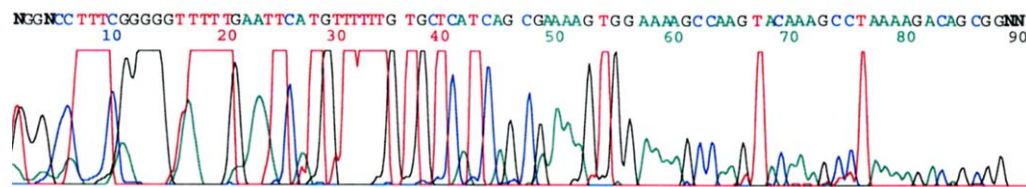
HPRT forward
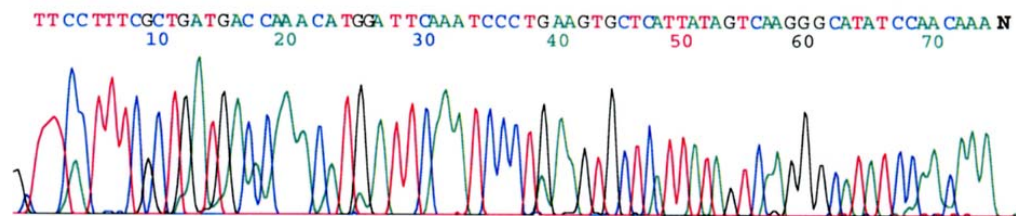
HPRT reverse

A2.6   PEDF

98 (NM_177927.2)
*
CAGCCAGAATGTCCCTGACAGCTCTCAGGATTCCCCAGCCCCTGACAGCA
CAGCCAGAATGTCCCTGACAGCTCTCAGGATTCCCCAGCCC-TGACAGCA
                                        CCAGCCC-TGACAGCA
                    176
                     *
CCGGGGAGCCCGTAGTGGAGGAGGATGAC
CC
CCGGGGAGCCCGTAGTGGAGGAGGATGAC
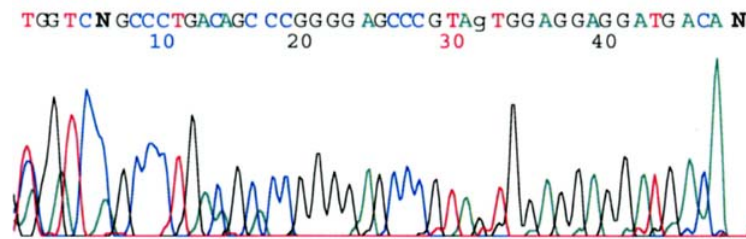
PEDF forward
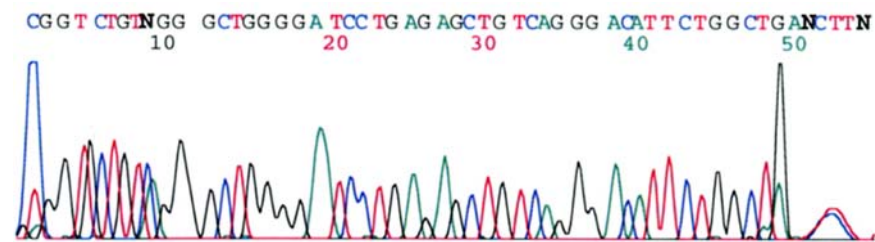
PEDF reverse

A2.7. RNAP2

4011 (XM_343922.2)
*

GTCCAATGACATCGTGGAGATCTTCACGGTACTGGGCATTGAGGCTGTGC
GTCCAATGACATCGTGGAGATCTTCACGGTACTGGGCATTGAGGCTGTGC
GGTACTGGGCATTGAGGCTGTGC

4106
*

GGAAGGCCCTGGAGCGAGAACTGTACCATGTCATCTCCTTTGATGG
GGAAGGCCCTGGAGCGAGAA
GGAAGGCCCTGGAGCGAGAACTGTACCATGTCATCTCCTTTGATGG
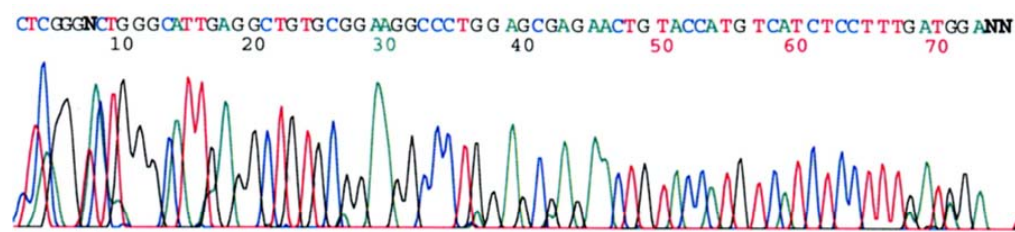
RNAP2 forward
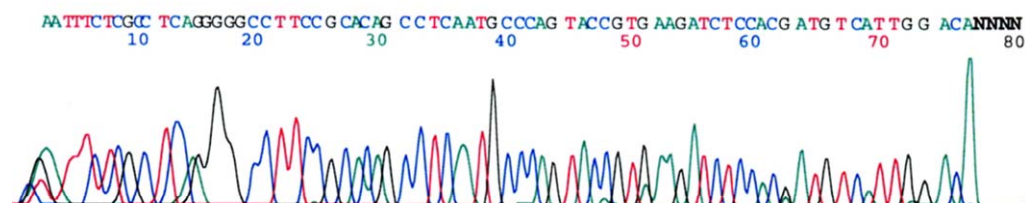
RNAP2 reverse

A2.8. Tie2

1680 (XM_342863.2)
*

TGGAGAAGGACATCCTGGACCTGTGAGAAGATTCACAACAGCGTCTATC
TGGAGAAGGACATCCTGGACCTGTGAGAAGATTCACAACAGCGTCTATC
CAACAGCGTCTATC

1778
*

GGACTCCCTCCTCCAAGAGGTCTCAGTCTCCTACCCAAAAGCCAGACAGC
GGACTCCCTCCTCCAAGAG
GGACTCCCTCCTCCAAGAGGTCTCAGTCTCCTACCCAAAAGCCAGACAGC

CG GGAGNTCCA CAG CG TCTATCG GACTCCC TCCTCC A GAGGTCTCAG TCTCCTACCCAAAAGCCAGACAG CANN
　　　　　10　　　　20　　　　30　　　　40　　　　50　　　　60　　　　70

Tie2 forward

ACNG AAC TCT TGG AGG AGG GAG TCCG A TAG ACG CTG TTG TGAATCTT CTCACAGG TCCAGG ATG TCCT T CTCCAAG N
　　　　10　　　　20　　　　30　　　　40　　　　50　　　　60　　　　70
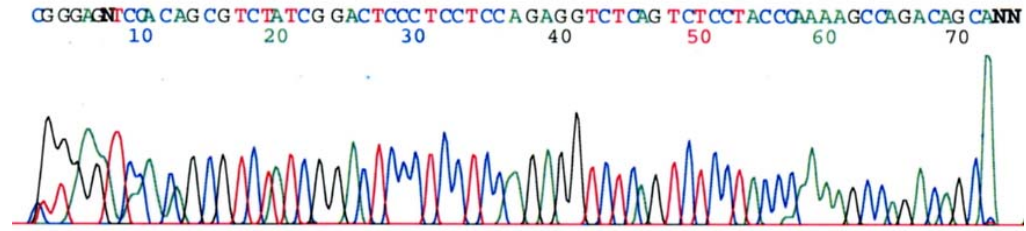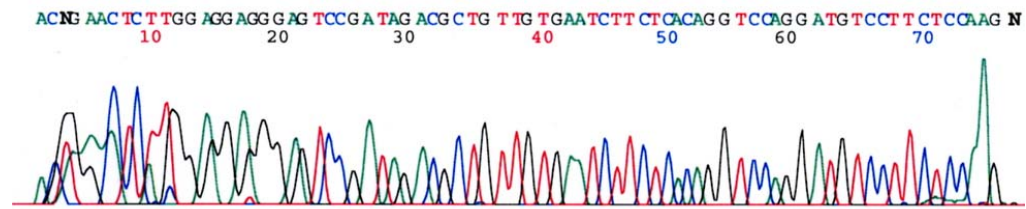
Tie2 reverse

A2.9.   VEGF

259 (NM_031836.1)
*

AATGATGAAGCCCTGGAGTGCGTGCCCACGTCGGAGAGCAACGTCACTA
AATGATGAAGCCCTGGAGTGCGTGCCCACGTCGGAGAGCAACGTCACTA
　　　　　　　　　　　　　　　　　　　　　　　ACGTCACTA

　　　　　　　　　　　　　　　　　　　348
　　　　　　　　　　　　　　　　　　　*
TGCAGATCATGCGGATCAAACCTCACCAAAGCCAGCACATA
TGCAGATCATGC
TGCAGATCATGCGGATCAAACCTCACCAAAGCCAGCACATA

NCCG TCG G AGAGCA CG TCAC TATG CAG ATCATG CG G ATCAAACC TCACCAAAGC CAG CaCAT AANN
　　　10　　　　20　　　　30　　　　40　　　　50　　　　60

VEGF forward

GC AGGATCTGCATAG TG ACGTTG CTC TCCG ACG TGG G CACG CAC TCCAGGG C TTCATCAT TA NN
　　　10　　　　20　　　　30　　　　40　　　　50　　　　60

VEGF reverse

A2.10. VEGFR-2

2588 (NM_013062.1)
*
TCTCGTACGGACCGTTAAGCGGGCCAATGAAGGGGAACTGAAGACAGGC
TCTCGTACGGACCGTTAAGCGGGCCAATGAAGGGGAACTGAAGACAGGC
                         TGAAGGGGAACTGAAGACAGGC

                                  2681
                                  *
TACTTGTCCATTGTCATGGATCCAGATGAACTGCCCTTGGATGAG
TACTTGTCCATT
TACTTGTCCATTGTCATGGATCCAGATGAACTGCCCTTGGATGAG

VEGFR2 forward

VEGFR2 reverse

A2.11. IGF-1 sequence

Alternative splicing yields two major species of rat IGF-1 mRNA. The predominant species, IGF-1A, is 99 bases in length and is 52 bases shorter than IGF-1B due to the splicing of a cassette exon, exon five [408-410]. The primers for IGF-1 used in this study were designed to detect both of the major splice variants. Accordingly, the forward and reverse primers were selected to hybridise with sequences encoded by exons four and six, respectively. Melting curve analyses and agarose gel electrophoresis photographs of IGF-1 PCR products confirmed the presence of two amplicons of the predicted sizes (Figure 4.3). The two IGF-1 PCR products were purified and sequenced – alignments with the predicted sequences are provided below. The sequence of the shorter product closely matched the published sequence

for IGF-1A. The sequence quality for the longer product was poor (refer to sequencing chromatogram). Nonetheless, there was a high degree of homology between the published IGF-1B sequence and those regions of the amplicon for which reliable sequence was attained. When the sequence analysis is considered in conjunction with the agarose gel electrophoresis, positive identification of the transcript as IGF-1B can be made with confidence.

IGF-1A

1091 (accession #: NM178866.2)
```
*
CACACTGACATGCCCAAGACTCAGAAGGAAGTACACTTGAAGAACACAA
CACACTGACATGCCCAAGACTCAGAAGGAAGTACACTTGAAGAACACAA
                                GGAAGTACACTTGAAGAACACAA

GTAGAGGAAGTGCAGGAAACAAGACCTACAGAATGTAGGAGGAGCCTCC
GTAGAGGAAGTGCAGGAAACAAG
GTAGAGGAAGTGCAGGAAACAAGACCTAC-GAATGTAGGAGGAGCCTCC
```

1189
```
*
C
C
```

IGF-1B

634 (accession #: X06107.1)
```
*
CACACTGACATGCCCAAGACTCAGAAGTCCCAGCCCCTATCGACACACA
CACACTGACATGCCCAAGACTCAGAAGTCCCAGCCCCTATCGACACACA

AGA-AA-AGGAAGCTGCAA-AGGAGA-AGGAAAGGAAGTACACTTGAA-
AGACAACAGGAAGCTGCAACAGGAGATAGGAAAGGAAGTACACTTGAA-
                                                AC

GAACACAAGTAGAGGAAGT---GCAGGA-AA-CA-AGA-C-CTAC-AGA
GAACACAAGTAGAGGAAGT---GCAGGA-AA-CA-AG
GAACACAAGTAGAGGAAGTGTCGC-GGAGAAGCAGAGAGCGCTACGAGA
```

784
```
                         *
ATGTAGG-A-GGAGCCTCCC
ATGTAGGTATGGAGCCTCCC
```

G AG TCC T TG AAGA C CA G TAGA G GAAGTGCAGG AAAC A G ACCT ACNG AATG TAG G AGG AG CCT CCCANA
          10   20   30   40   50   60

IGF-1A forward

GC TG TTTCTGCAC TTCCTC TAC T TG TG TTCT TC A G TG TACT TCCT T CTNAG TCTTGG GCATG TCAG TG TG AN A
          10   20   30   40   50   60   70

IGF-1A reverse

CANCC NTNTC GAC CNCAA GTAAAAG G AAG TGT G CNG AG GCAN N AGGCT ACG G AA TG T A CG AGG AG CCT CCCANC
          10   20   30   40   50   60   70

IGF-1B forward

G NTG TTTC TGCC T TCC TCTAC T TG TG TTCT TCANG TG TACT T CCT TNCN AT CCCC GT TGCA GCTNCC GTGT CTTG TG TGTCN ATAG GGG CTG GG ACTTCTG AG TCTTGG G CATG T CAG
          10   20   30   40   50   60   70   80   90   100   110   120

TG TG A

IGF-1B reverse

APPENDIX 3

REAL-TIME RT-PCR MATHEMATICS

APPENDIX 3: REAL-TIME RT-PCR MATHEMATICS

A3. MATHEMATICAL CONSIDERATIONS IN REAL-TIME RT-PCR

A3.1. PCR amplification kinetics

Quantification in real-time RT-PCR rests on several fundamental mathematical principles. These principles have been described in several review papers [411, 413, 499]. The following is a direct quotation from the paper by Meijerink *et al*. [411]:

"During PCR amplification, the number of molecules that is synthesised (X_n) depends on the number of template molecules present at the beginning of the reaction (X_O), the reaction efficiency (E) and the number of amplification cycles (n). In real-time PCR sample positivity is defined as the cycle number at which emitted fluorescence exceeds…[a threshold value], called the threshold cycle (Ct). The number of molecules synthesised at the threshold cycle (X_{Ct}) is specific, but constant (C) for each reaction type".

$$X_n = X_O * (1+E)^n <=> X_{Ct} = X_O * (1+E)^{Ct} <=> \mathbf{X_O = C * (1+E)^{-Ct}}$$ [411, 413]

A3.1.a Using PCR kinetics for relative quantification: the delta-delta Ct method

The following is an adaptation of the method outlined by Livak and Schmittgen [413]:

The number of copies of a gene of interest in a given sample (sample A) at its threshold cycle (X_{CtA}) can be expressed as:

$$X_{CtA} = X_{OA} * (1+E_A)^{CtA}$$

just as the number of copies of an internal control (reference) gene in the same sample, at is threshold cycle (X_{CtR}) can be expressed as:

$$X_{CtR} = X_{OR} * (1+E_R)^{CtR}$$

Therefore the expression of the gene of interest relative to the reference gene can be determined in the following manner:

$$X_{CtA}/X_{CtR} = [X_{OA} * (1+E_A)^{CtA}] / [X_{OR} * (1+E_R)^{CtR}]$$

Assuming equal amplification efficiencies for the gene of interest and the reference gene ($E_A = E_R$) and giving X_{CtA}/X_{CtR} the value of X the equation can be rearranged as follows:

$$X = X_{OA}/X_{OR} * (1+E)^{CtA-CtR}$$

As X_{OA}/X_{OR} is equal to the amount of the gene of interest normalised to the reference

gene it can be substituted for the value X_N

$$X = X_N * (1+E)^{CtA-CtR}$$

$$X = X_N * (1+E)^{\Delta Ct}$$

where ΔCt= the difference between threshold cycles for the gene of interest and the reference gene. Rearranging:

$$X_N = X * (1+E)^{-\Delta Ct}$$

The final step – the calibration step – is to divide the normalised relative expression value for the gene of interest in sample A by the normalised value for the same gene in a standard sample (S) :

$$X_{NA}/ X_{Ns} = [X * (1+E)^{-\Delta CtA}]/ [X * (1+E)^{-\Delta CtS}]$$

$$X_{NA}/ X_{Ns} = (1+E)^{-\Delta\Delta Ct}$$

where: $-\Delta\Delta Ct = -(\Delta CtA - \Delta CtS)$

Thus normalised relative gene expression $= (1+E)^{-\Delta\Delta Ct}$ [413]

A3.1.b. The delta Ct method of quantification

The quantification algorithm recommended by the GeNorm software application utilizes a modification of the delta-delta Ct method, known as the delta Ct method. Quantification of gene expression in a sample of interest (A) is still performed relative to a standard sample (S), however normalisation of the relative expression value is not incorporated in the calculation. Normalisation may be undertaken as a separate step. The separation of relative quantification and normalisation may be advantageous in that it simplifies the process of normalising gene expression with more than one reference gene. It also allows for differences in the amplification efficiencies of the gene of interest and the reference genes. The derivation of the delta Ct equation is as follows [413]:

$$X_{Ct} = X_O * (1+E)^{Ct}$$

Equation (1) above can be rearranged to represent the expression of the gene of interest in sample A (X_{OA}) as follows:

$$X_{Ct} = X_{OA} * (1+E)^{CtA}$$

$$X_{OA} = X_{Ct} * (1+E)^{-CtA}$$

The relationship between the expression of the gene of interest in sample A and the expression of the same gene in a standard sample (s) is described by the equation:

$$X_{OA}/ X_{OS} = [X_{Ct} * (1+E)^{-CtA}]/ [X_{Ct} * (1+E)^{-CtS}]$$

$$X_{OA}/ X_{OS} = (1+E)^{-CtA}/(1+E)^{-CtS}$$

$$X_{OA}/ X_{OS} = (1+E)^{-(CtA-CtS)}$$

$$X_{OA}/ X_{OS} = (1+E)^{(CtS-CtA)}$$

As X_{OA}/ X_{OS} describes non-normalised expression of the gene of interest in sample A relative to the standard sample (Q):

$$Q=(1+E)^{(CtS-CtA)}$$

or

$$Q=(1+E)^{-\Delta Ct} \text{ where } \Delta Ct = CtA\text{-}CtS$$

Normalisation is subsequently achieved by dividing the relative expression value (Q) by an appropriate normalisation factor as described in Chapter 4 (4.2.c.2).

A3.2. PCR efficiency calculation

The standard curve was generated by plotting the Ct values of a serially diluted sample against the logarithm of the cDNA concentration. The linear function of the standard curve was described by: y= mx + c

where:

y was the Ct value;

x was the logarithm of the cDNA concentration ($\log X_o$);

m was the gradient;

and c was the y-intercept.

Rearranging the equation $X_{Ct}=X_o*(1+E)^{Ct}$ for the standard curve:

$$Log X_{Ct}=Log[X_o*(1+E)^{Ct}]$$

$$Log X_{Ct}= Log\ X_o + Log(1+E)*Ct$$

$$Ct*Log(1+E)=Log X_{Ct} - Log X_o$$

$$Ct = (LogX_{Ct} - LogX_o)/Log(1+E)$$

$$Ct = (-LogX_o + LogX_{Ct}) * 1/Log(1+E)$$

$$Ct = -1/Log(1+E)*LogX_o + 1/Log(1+E)*LogX_{Ct}$$

Thus the gradient of the standard curve (g) was $-1/Log\,(1+E)$

Rearranging for E:

$$1/g = -log(1+E) <=> 10^{-(1/g)} = 1+E <=> \mathbf{E = 10^{-(1/g)} - 1}.$$

In support of this derivation, Meijerink *et al.* and Nigro *et al.* also reported a value of $-1/Log(1+E)$ for the slope of the standard curve [411, 500].

Important note:

Not all standard curves for real-time PCR data are plotted in this fashion. For cases where the absolute quantity of template in the cDNA sample is known, the linear function of the standard curve $y=mx + c$ has the values $LogX_o$ for y and Ct for x. In this case the efficiency value is calculated as follows [418]:

$$X_{Ct} = X_o * (1+E)^{Ct}$$

$$X_o = X_{Ct}/(1+E)^{Ct}$$

$$LogX_o = Log[X_{Ct}/(1+E)^{Ct}]$$

$$LogX_o = LogX_{Ct} - Log(1+E)*Ct$$

$$LogX_o = -Log(1+E)*Ct + LogX_{Ct}$$

Thus the value for slope is:

$$s = -Log(1+E)$$

and efficiency is:

$$E = 10^{-S} - 1$$

APPENDIX 4

NORMALISATION OF GENE EXPRESSION DATA

APPENDIX 4: NORMALISATION OF GENE EXPRESSION DATA

A4.1. Background

The use of reference genes, otherwise known as *internal control genes*, in relative real-time RT-PCR is indispensable in controlling for variation in sample loading, ensuring the comparability of test samples. Although all of the RNA samples used in this work were quantified by spectrophotometry and subjected to qualitative appraisal (2.3.e), minor variations in RNA quantity or quality may have had considerable bearing on cDNA yield following reverse transcription (RT). Furthermore, it has been demonstrated that RT efficiency may differ substantially between samples, leading to significant variations in cDNA yield [301, 501]. In order to control for this variation, the relative quantity value of each gene, in each sample, was normalised to the relative expression level of the reference genes.

Constitutively expressed genes, serving "housekeeping" functions in fundamental cellular processes, or playing structural roles, are commonly used as reference genes. A reference gene need not be a housekeeping gene however – stably expressed tissue-restricted genes may serve as reference genes for the normalisation of samples derived from the same tissue. As studies of numerous reference genes have shown, housekeeping genes are usually regulated to some extent [301, 414, 501, 502]. In fact, the transcription of even the most stably expressed gene is subject to variation with fluctuations the cell cycle and in oxygen and nutrient status [502]. The characteristics of an ideal reference gene are summarised in Table A4.1. In short, the optimal reference gene should be expressed equally in all cells, at all times, under all experimental conditions – it should reflect the overall rate of mRNA synthesis [502]. Unfortunately, no single reference gene is ideal [301, 414].

Table A4.1 Characteristics of an ideal reference gene.

Attribute	References
Stable expression in samples from different subjects	[301, 503]
Stable expression under different experimental conditions	[301, 503]
Expressed to a similar extent as the gene of interest	[504]
Expression should reflect overall mRNA transcription levels	[414, 502]
If multiple reference genes are to be used, they should have independent functions in cellular maintenance	[501]
No pseudogenes – increased likelihood of amplification of contaminating genomic DNA	[505]

A4.2. Selection of candidate reference genes

A review of the real-time RT-PCR literature was conducted to identify the most appropriate candidate reference genes for the present study (Table A4.2). It is apparent that the expression stability of reference genes may vary significantly in different tissues [414], and thus a key focus of the literature review was the identification of reference genes used in studies of retinal gene expression. As has been mentioned, hypoxia has a profound influence on gene expression – with the exception of a relatively small number of hypoxia-induced genes, transcription is significantly reduced. As fluctuations in oxygen tension are central to the induction of retinopathy in OIR, a key criterion for the selection of candidate reference genes was expression stability under varying oxygen tensions. Interestingly, many studies examining the effects of hypoxia on gene expression have utilised GAPDH as a reference gene, despite the fact that its expression is upregulated by HIF-1 in hypoxia [506-508]. As the present study involves comparisons of gene expression between rats of different ages, reference genes that have been demonstrated to have stable expression during retinal development were also considered for inclusion. 18S and 28S ribosomal RNA were not considered as candidate reference genes, as the expression ratios of rRNA and mRNA may vary considerably [414]. Moreover, 18S and 28S rRNA are expressed to a far greater extent than are most other genes, making them inappropriate as reference genes for most applications [414, 502].

Table A4.2 Reference genes used in other studies

Gene/genes	Study context	Expression stability	Reference
ARBP	Murine retinal development	ARBP expression stable during development, minor variation in expression between earliest time-points (day 1 and day 3)	[509]
ARBP	Rat OIR	ARBP (36B4): expression stability not assessed	[394]
ARBP	Mouse retina and brain: RNA from mice of mixed ages and genotypes	ARBP: expression stability not assessed	[510]
ARBP; 28S rRNA; cyclophilin; GAPDH	Murine OIR: measurement of gene expression at the end of hyperoxia and during relative hypoxia	ARBP expression stable at all time-points; 28S expression decreased at 12 hours of relative hypoxia; expression stability of other genes not stated	[511]
β-actin; GAPDH; HPRT; SDHA	Cultured rat cortical neurons: response to ischaemia with or without IGF-1 or bFGF	Expression stability of individual reference genes not stated: used geometric mean of all four genes for normalisation	[512]
β-actin; HPRT; GAPDH	Retinal ischaemia (Wistar rat): elevated intraocular pressure	HPRT and GAPD: stable expression; β-actin: significant upregulation in ischaemia	[513]
β-actin; CYCA; GAPDH; 28S rRNA	Direct comparison of reference gene expression stability in 4 different cultured cell lines in normoxia and hypoxia	28 S rRNA stably expressed in all cell lines irrespective of oxygen tension; GAPDH expression induced – identified as putative HIF-1 induced gene; variation in basal expression and hypoxic regulation of other genes between cell lines	[507]

Table A4.2 (continued) Reference genes used in other studies

Gene/genes	Study context	Expression stability	Reference
β-actin; CYCA; GAPDH	Focal cerebral ischaemia in rats (Sprague Dawley)	Significant down-regulation of CYCA and GAPDH with ischaemia; β-actin increased	[514]
CYCA	Murine OIR: gene expression measured at 10 time-points between day 3 and 33	CYCA expression stable during retinal development; expression stability during and after hyperoxia not stated	[515]
GAPDH; 18S rRNA	Neonatal rat pups (Sprague Dawley) exposed to hypoxia (8% O_2) and variable periods of reoxygenation	No mention of reference gene expression stability – similar results attained with normalisation using either gene	[516]
GAPDH	Rat ischaemia reperfusion	GAPDH: expression stability not assessed	[517]
RNAPII	Comparison of 13 reference genes in 16 different tissues	RNAPII stable expression in all tissues; little change in expression in cultured T cell line following mitogenic stimulation	[502]

Key:

ARBP: acidic ribosomal phosphoprotein
CYCA: cyclophilin A
GAPDH: glyceraldehyde-3-phosphate dehydrogenase
HPRT: hypoxanthine guanine phosphoribosyltransferase
RNAPII: RNA polymerase II
SDHA: succinate dehydrogenase complex, subunit A

A4.3. Reference gene expression stability and normalisation using multiple reference genes

Several methods have been proposed to circumvent the limitations of reference genes for accurate normalisation of gene expression in test samples. An approach that is gaining increasing acceptance is the use of several reference genes, in place of one, for normalisation [414, 514, 518, 519]. In a study of 10 housekeeping genes, Vandesompele *et al.* demonstrated that reliance on a single housekeeping gene for normalisation may lead to 3.0-fold and 6.4-fold differences in target gene quantification in 25% and 10% of cases, respectively [414]. In sporadic cases variation was greater than 20-fold [414]. The authors of this study proposed a method of assessing the expression stability of candidate reference genes based on comparisons between gene pairs. The method is centred on the assumption that the expression ratio of two ideal control genes should be the same in different samples [301]. The average (arithmetic mean) pair-wise variation between the expression of a given reference gene and all other candidate reference genes is used as a marker of expression-stability. Accordingly reference genes can be ranked according to the stability of their expression. GeNorm, a public-domain software application (accessible at: http://medgen.ugent.be/~jvdesomp/genorm/), provides a convenient means for testing the expression stability of reference genes. GeNorm was used to guide the selection of reference genes in the present study.

A4.3.a. GeNorm internal gene-stability measurement

As per Vandesompele *et al*. [414]:

"For every combination of two internal control genes j and k, an array A_{jk} of m elements is calculated which consist of $\log_2$-transformed expression ratios a_{ij}/a_{ik} (equation 1). We define the pairwise variation V_{jk} for the control genes j and k as the standard deviation of the A_{jk} elements (equation 2). The gene-stability measure M_j for control gene j is the arithmetic mean of all pairwise variations in V_{jk} (equation 3)":

$(\forall j,k \in [1,n]$ and $j \neq k)$:

$$A_{jk} = \left\{ \log_2\left(\frac{a_{1j}}{a_{1k}}\right), \log_2\left(\frac{a_{2j}}{a_{2k}}\right), ..., \log_2\left(\frac{a_{mj}}{a_{mk}}\right) \right\} = \left\{ \log_2\left(\frac{aij}{aik}\right) \right\}_{i=1 \to m} \quad (1)$$

$$V_{jk} = std.dev(A_{jk}) \quad\quad\quad\quad (2)$$

$$M_j = \frac{\sum_{k=1}^{n} V_{jk}}{n-1} \quad\quad\quad\quad (3)$$

BIBLIOGRAPHY

1. *Wolff's anatomy of the eye and orbit.* 8th ed, ed. A.J. Bron, R.C. Tripathi, and B.J. Tripathi. 1997, London: Chapman & Hall.
2. Provis, J.M., *Development of the primate retinal vasculature.* Prog Retin Eye Res, 2001. **20**(6): p. 799-821.
3. Kanski, J.J., *Clinical Ophthalmology: A Systematic Approach.* Fifth ed. 2003, London: Butterworth Heinemann.
4. Burkitt, H.G., B. Young, and J.W. Heath, *Wheater's Functional Histology: A Text and Colour Atlas.* Third ed. 1993, Edinburgh: Churchill Livingstone.
5. Cunha-Vaz, J., *The blood-ocular barriers.* Surv Ophthalmol, 1979. **23**(5): p. 279-96.
6. Alm, A. and A. Bill, *Ocular and optic nerve blood flow at normal and increased intraocular pressures in monkeys (Macaca irus): a study with radioactively labelled microspheres including flow determinations in brain and some other tissues.* Exp Eye Res, 1973. **15**(1): p. 15-29.
7. Tornquist, P. and A. Alm, *Retinal and choroidal contribution to retinal metabolism in vivo. A study in pigs.* Acta Physiol Scand, 1979. **106**(3): p. 351-7.
8. Laties, A.M., *Central retinal artery innervation. Absence of adrenergic innervation to the intraocular branches.* Arch Ophthalmol, 1967. **77**(3): p. 405-9.
9. Ferrari-Dileo, G., E.B. Davis, and D.R. Anderson, *Biochemical evidence for cholinergic activity in retinal blood vessels.* Invest Ophthalmol Vis Sci, 1989. **30**(3): p. 473-7.
10. Ye, X.D., A.M. Laties, and R.A. Stone, *Peptidergic innervation of the retinal vasculature and optic nerve head.* Invest Ophthalmol Vis Sci, 1990. **31**(9): p. 1731-7.
11. Bill, A., *Autonomic nervous control of uveal blood flow.* Acta Physiol Scand, 1962. **56**: p. 70-81.
12. Alm, A. and A. Bill, *The oxygen supply to the retina. II. Effects of high intraocular pressure and of increased arterial carbon dioxide tension on uveal and retinal blood flow in cats. A study with radioactively labelled microspheres including flow determinations in brain and some other tissues.* Acta Physiol Scand, 1972. **84**(3): p. 306-19.
13. Robinson, F., et al., *Retinal blood flow autoregulation in response to an acute increase in blood pressure.* Invest Ophthalmol Vis Sci, 1986. **27**(5): p. 722-6.
14. Friedman, E. and S.R. Chandra, *Choroidal blood flow. 3. Effects of oxygen and carbon dioxide.* Arch Ophthalmol, 1972. **87**(1): p. 70-1.
15. Michaelson, I.C. and A.C. Campbell, *Anatomy of the finer retinal vessels.* Trans Ophthalmol Soc UK, 1940. **60**: p. 71-112.
16. Hayreh, S.S., *The choriocapillaris.* Albrecht Von Graefes Arch Klin Exp Ophthalmol, 1974. **192**(3): p. 165-79.
17. Johnson, P.C., *Review of Previous Studies and Current Theories of Autoregulation.* Circ Res, 1964. **15**: p. SUPPL:2-9.
18. Gariano, R.F., M.L. Iruela-Arispe, and A.E. Hendrickson, *Vascular development in primate retina: comparison of laminar plexus formation in monkey and human.* Invest Ophthalmol Vis Sci, 1994. **35**(9): p. 3442-55.
19. Ishikawa, T., *Fine structure of retinal vessels in man and the macaque monkey.* Invest Ophthalmol, 1963. **2**: p. 1-15.
20. Cunha-Vaz, J.G., M. Shakib, and N. Ashton, *Studies on the permeability of the*

blood-retinal barrier. I. On the existence, development, and site of a blood-retinal barrier. Br J Ophthalmol, 1966. **50**(8): p. 441-53.

21.   Penfold, P.L., et al., *Angiogenesis in normal human retinal development: the involvement of astrocytes and macrophages.* Graefes Arch Clin Exp Ophthalmol, 1990. **228**(3): p. 255-63.

22.   Tout, S., et al., *The role of Muller cells in the formation of the blood-retinal barrier.* Neuroscience, 1993. **55**(1): p. 291-301.

23.   Janzer, R.C. and M.C. Raff, *Astrocytes induce blood-brain barrier properties in endothelial cells.* Nature, 1987. **325**(6101): p. 253-7.

24.   Bill, A., P. Tornquist, and A. Alm, *Permeability of the intraocular blood vessels.* Trans Ophthalmol Soc U K, 1980. **100**(3): p. 332-6.

25.   Anderson, B., Jr. and H.A. Saltzman, *Retinal Oxygen Utilization Measured by Hyperbaric Blackout.* Arch Ophthalmol, 1964. **72**: p. 792-5.

26.   Ames, A., 3rd, *Energy requirements of CNS cells as related to their function and to their vulnerability to ischemia: a commentary based on studies on retina.* Can J Physiol Pharmacol, 1992. **70 Suppl**: p. S158-64.

27.   Hogeboom van Buggenum, I.M., et al., *Ocular oxygen measurement.* Br J Ophthalmol, 1996. **80**(6): p. 567-73.

28.   Yu, D.Y. and S.J. Cringle, *Oxygen distribution and consumption within the retina in vascularised and avascular retinas and in animal models of retinal disease.* Prog Retin Eye Res, 2001. **20**(2): p. 175-208.

29.   Wangsa-Wirawan, N.D. and R.A. Linsenmeier, *Retinal oxygen: fundamental and clinical aspects.* Arch Ophthalmol, 2003. **121**(4): p. 547-57.

30.   Haugh, L.M., R.A. Linsenmeier, and T.K. Goldstick, *Mathematical models of the spatial distribution of retinal oxygen tension and consumption, including changes upon illumination.* Ann Biomed Eng, 1990. **18**(1): p. 19-36.

31.   Folkow, B. and E. Neil, *Circulation.* 1971, New York: Oxford University Press.

32.   Alm, A., A. Bill, and F.A. Young, *The effects of pilocarpine and neostigmine on the blood flow through the anterior uvea in monkeys. A study with radioactively labelled microspheres.* Exp Eye Res, 1973. **15**(1): p. 31-6.

33.   Linsenmeier, R.A. and R.D. Braun, *Oxygen distribution and consumption in the cat retina during normoxia and hypoxemia.* J Gen Physiol, 1992. **99**(2): p. 177-97.

34.   Braun, R.D., R.A. Linsenmeier, and T.K. Goldstick, *Oxygen consumption in the inner and outer retina of the cat.* Invest Ophthalmol Vis Sci, 1995. **36**(3): p. 542-54.

35.   Ahmed, J., M.K. Pulfer, and R.A. Linsenmeier, *Measurement of blood flow through the retinal circulation of the cat during normoxia and hypoxemia using fluorescent microspheres.* Microvasc Res, 2001. **62**(2): p. 143-53.

36.   Pournaras, C.J., et al., *Diffusion of O2 in the retina of anesthetized miniature pigs in normoxia and hyperoxia.* Exp Eye Res, 1989. **49**(3): p. 347-60.

37.   Linsenmeier, R.A. and C.M. Yancey, *Effects of hyperoxia on the oxygen distribution in the intact cat retina.* Invest Ophthalmol Vis Sci, 1989. **30**(4): p. 612-8.

38.   Cleaver, O. and D.A. Melton, *Endothelial signaling during development.* Nat Med, 2003. **9**(6): p. 661-8.

39.   Saladin, K.S., *Anatomy and Physiology: the unity of form and function.* 2004, New York: McGraw-Hill.

40.   Carmeliet, P., *Angiogenesis in health and disease.* Nat Med, 2003. **9**(6): p. 653-

60.

41. Risau, W. and I. Flamme, *Vasculogenesis.* Annu Rev Cell Dev Biol, 1995. **11**: p. 73-91.

42. Risau, W., *Mechanisms of angiogenesis.* Nature, 1997. **386**(6626): p. 671-4.

43. Pardanaud, L., F. Yassine, and F. Dieterlen-Lievre, *Relationship between vasculogenesis, angiogenesis and haemopoiesis during avian ontogeny.* Development, 1989. **105**(3): p. 473-85.

44. Henkind, P. and L.F. De Oliveira, *Development of retinal vessels in the rat.* Invest Ophthalmol, 1967. **6**(5): p. 520-30.

45. Asahara, T., et al., *Isolation of putative progenitor endothelial cells for angiogenesis.* Science, 1997. **275**(5302): p. 964-7.

46. Grant, M.B., et al., *Adult hematopoietic stem cells provide functional hemangioblast activity during retinal neovascularization.* Nat Med, 2002. **8**(6): p. 607-12.

47. Otani, A., et al., *Bone marrow-derived stem cells target retinal astrocytes and can promote or inhibit retinal angiogenesis.* Nat Med, 2002. **8**(9): p. 1004-10.

48. Asahara, T. and A. Kawamoto, *Endothelial progenitor cells for postnatal vasculogenesis.* Am J Physiol Cell Physiol, 2004. **287**(3): p. C572-9.

49. Folkman, J., et al., *Induction of angiogenesis during the transition from hyperplasia to neoplasia.* Nature, 1989. **339**(6219): p. 58-61.

50. Kandel, J., et al., *Neovascularization is associated with a switch to the export of bFGF in the multistep development of fibrosarcoma.* Cell, 1991. **66**(6): p. 1095-104.

51. Stone, J., et al., *Development of retinal vasculature is mediated by hypoxia-induced vascular endothelial growth factor (VEGF) expression by neuroglia.* J Neurosci, 1995. **15**(7 Pt 1): p. 4738-47.

52. Alon, T., et al., *Vascular endothelial growth factor acts as a survival factor for newly formed retinal vessels and has implications for retinopathy of prematurity.* Nat Med, 1995. **1**(10): p. 1024-8.

53. Pierce, E.A., et al., *Vascular endothelial growth factor/vascular permeability factor expression in a mouse model of retinal neovascularization.* Proc Natl Acad Sci U S A, 1995. **92**(3): p. 905-9.

54. Hanneken, A., et al., *Altered distribution of basic fibroblast growth factor in diabetic retinopathy.* Arch Ophthalmol, 1991. **109**(7): p. 1005-11.

55. Khaliq, A., et al., *Increased expression of placenta growth factor in proliferative diabetic retinopathy.* Lab Invest, 1998. **78**(1): p. 109-16.

56. Nagineni, C.N., et al., *Transforming growth factor-beta induces expression of vascular endothelial growth factor in human retinal pigment epithelial cells: involvement of mitogen-activated protein kinases.* J Cell Physiol, 2003. **197**(3): p. 453-62.

57. Friedlander, M., et al., *Involvement of integrins alpha v beta 3 and alpha v beta 5 in ocular neovascular diseases.* Proc Natl Acad Sci USA, 1996. **93**(18): p. 9764-9.

58. Smith, L.E., et al., *Regulation of vascular endothelial growth factor-dependent retinal neovascularization by insulin-like growth factor-1 receptor.* Nat Med, 1999. **5**(12): p. 1390-5.

59. Hellstrom, A., et al., *Low IGF-I suppresses VEGF-survival signaling in retinal endothelial cells: direct correlation with clinical retinopathy of prematurity.* Proc Natl Acad Sci U S A, 2001. **98**(10): p. 5804-8.

60.   Fruttiger, M., et al., *PDGF mediates a neuron-astrocyte interaction in the developing retina.* Neuron, 1996. **17**(6): p. 1117-31.

61.   Steen, B., et al., *Matrix metalloproteinases and metalloproteinase inhibitors in choroidal neovascular membranes.* Invest Ophthalmol Vis Sci, 1998. **39**(11): p. 2194-200.

62.   Ozaki, H., H. Hayashi, and K. Oshima, *Angiogenin levels in the vitreous from patients with proliferative diabetic retinopathy.* Ophthalmic Res, 1996. **28**(6): p. 356-60.

63.   Xin, X., et al., *Hepatocyte growth factor enhances vascular endothelial growth factor-induced angiogenesis in vitro and in vivo.* Am J Pathol, 2001. **158**(3): p. 1111-20.

64.   Gardiner, T.A., et al., *Inhibition of tumor necrosis factor-alpha improves physiological angiogenesis and reduces pathological neovascularization in ischemic retinopathy.* Am J Pathol, 2005. **166**(2): p. 637-44.

65.   He, S., et al., *A role for connective tissue growth factor in the pathogenesis of choroidal neovascularization.* Arch Ophthalmol, 2003. **121**(9): p. 1283-8.

66.   Yoshida, A., et al., *Role of NF-kappaB-mediated interleukin-8 expression in intraocular neovascularization.* Invest Ophthalmol Vis Sci, 1998. **39**(7): p. 1097-106.

67.   Yoshida, S., et al., *Role of MCP-1 and MIP-1alpha in retinal neovascularization during postischemic inflammation in a mouse model of retinal neovascularization.* J Leukoc Biol, 2003. **73**(1): p. 137-44.

68.   Hurskainen, M., et al., *Abnormal maturation of the retinal vasculature in type XVIII collagen/endostatin deficient mice and changes in retinal glial cells due to lack of collagen types XV and XVIII.* Faseb J, 2005. **19**(11): p. 1564-6.

69.   Spranger, J., et al., *Release of the angiogenesis inhibitor angiostatin in patients with proliferative diabetic retinopathy: association with retinal photocoagulation.* Diabetologia, 2000. **43**(11): p. 1404-7.

70.   Aranda, J., et al., *Prolactins are natural inhibitors of angiogenesis in the retina.* Invest Ophthalmol Vis Sci, 2005. **46**(8): p. 2947-53.

71.   Ye, H.Q., et al., *Differential expression of MT1-MMP (MMP-14) and collagenase III (MMP-13) genes in normal and wounded rat corneas.* Invest Ophthalmol Vis Sci, 2000. **41**(10): p. 2894-9.

72.   Auricchio, A., et al., *Inhibition of retinal neovascularization by intraocular viral-mediated delivery of anti-angiogenic agents.* Mol Ther, 2002. **6**(4): p. 490-4.

73.   Spranger, J., et al., *Deficient activation and different expression of transforming growth factor-beta isoforms in active proliferative diabetic retinopathy and neovascular eye disease.* Exp Clin Endocrinol Diabetes, 1999. **107**(1): p. 21-8.

74.   Suzuma, K., et al., *Expression of thrombospondin-1 in ischemia-induced retinal neovascularization.* Am J Pathol, 1999. **154**(2): p. 343-54.

75.   Dawson, D.W., et al., *Pigment epithelium-derived factor: a potent inhibitor of angiogenesis.* Science, 1999. **285**(5425): p. 245-8.

76.   Gao, G., et al., *Down-regulation of vascular endothelial growth factor and up-regulation of pigment epithelium-derived factor: a possible mechanism for the anti-angiogenic activity of plasminogen kringle 5.* J Biol Chem, 2002. **277**(11): p. 9492-7.

77.   Carmeliet, P. and R.K. Jain, *Angiogenesis in cancer and other diseases.* Nature, 2000. **407**(6801): p. 249-57.

78.   Kim, I., et al., *Angiopoietin-1 reduces VEGF-stimulated leukocyte adhesion to*

endothelial cells by reducing ICAM-1, VCAM-1, and E-selectin expression. Circ Res, 2001. **89**(6): p. 477-9.

79.   Amano, S., et al., *Requirement for vascular endothelial growth factor in wound- and inflammation-related corneal neovascularization.* Invest Ophthalmol Vis Sci, 1998. **39**(1): p. 18-22.

80.   Maisonpierre, P.C., et al., *Angiopoietin-2, a natural antagonist for Tie2 that disrupts in vivo angiogenesis.* Science, 1997. **277**(5322): p. 55-60.

81.   Davis, S. and G.D. Yancopoulos, *The angiopoietins: Yin and Yang in angiogenesis.* Curr Top Microbiol Immunol, 1999. **237**: p. 173-85.

82.   Pepper, M.S., *Role of the matrix metalloproteinase and plasminogen activator- plasmin systems in angiogenesis.* Arterioscler Thromb Vasc Biol, 2001. **27**(7): p. 1104-1117.

83.   Zhang, H., C. Li, and P.C. Baciu, *Expression of integrins and MMPs during alkaline-burn-induced corneal angiogenesis.* Invest Ophthalmol Vis Sci, 2002. **43**(4): p. 955-962.

84.   Dvorak, H.F., *Tumors: wounds that do not heal. Similarities between tumor stroma generation and wound healing.* N Engl J Med, 1986. **315**(26): p. 1650-9.

85.   Dvorak, H.F., et al., *Vascular permeability factor/vascular endothelial growth factor, microvascular hyperpermeability, and angiogenesis.* Am J Pathol, 1995. **146**(5): p. 1029-39.

86.   Houck, K.A., et al., *Dual regulation of vascular endothelial growth factor bioavailability by genetic and proteolytic mechanisms.* J Biol Chem, 1992. **267**(36): p. 26031-7.

87.   Sholley, M.M., et al., *Mechanisms of neovascularization: vascular sprouting can occur without proliferation of endothelial cells.* Lab Invest, 1984. **51**(6): p. 624-634.

88.   Helmlinger, G., et al., *Formation of endothelial cell networks.* Nature, 2000. **405**(6783): p. 139-41.

89.   Philipp, W., L. Speicher, and C. Humpel, *Expression of vascular endothelial growth factor and its receptors in inflamed and vascularized human corneas.* Invest Ophthalmol Vis Sci, 2000. **41**(9): p. 2514-22.

90.   Gale, N.W. and G.D. Yancopoulos, *Growth factors acting via endothelial cell- specific receptor tyrosine kinases: VEGFs, angiopoietins, and ephrins in vascular development.* Genes Dev, 1999. **13**(9): p. 1055-66.

91.   Burger, P.C., D.B. Chandler, and G.K. Klintworth, *Corneal neovascularization studied by electron microscopy of vascular casts.* Lab Invest, 1983. **48**(2): p. 169-180.

92.   Edelman, J.L., M.R. Castro, and Y. Wen, *Correlation of VEGF expression by leukocytes with the growth and regression of blood vessels in the rat cornea.* Invest Ophthalmol Vis Sci, 1999. **40**(6): p. 1112-23.

93.   Gale, N.W., et al., *Ephrin-B2 selectively marks arterial vessels and neovascularization sites in the adult, with expression in both endothelial and smooth-muscle cells.* Dev Biol, 2001. **230**(2): p. 151-60.

94.   Dumont, D.J., et al., *Dominant-negative and targeted null mutations in the endothelial receptor tyrosine kinase, tek, reveal a critical role in vasculogenesis of the embryo.* Genes Dev, 1994. **8**(16): p. 1897-909.

95.   Suri, C., et al., *Requisite role of angiopoietin-1, a ligand for the TIE2 receptor, during embryonic angiogenesis.* Cell, 1996. **87**(7): p. 1171-80.

96.   Gale, N.W., et al., *Angiopoietin-2 is required for postnatal angiogenesis and*

lymphatic patterning, and only the latter role is rescued by Angiopoietin-1. Dev Cell, 2002. **3**(3): p. 411-23.

97.   Stalmans, I., et al., *Arteriolar and venular patterning in retinas of mice selectively expressing VEGF isoforms.* J Clin Invest, 2002. **109**(3): p. 327-36.

98.   Carmeliet, P., et al., *Impaired myocardial angiogenesis and ischemic cardiomyopathy in mice lacking the vascular endothelial growth factor isoforms VEGF164 and VEGF188.* Nat Med, 1999. **5**(5): p. 495-502.

99.   Benjamin, L.E., I. Hemo, and E. Keshet, *A plasticity window for blood vessel remodelling is defined by pericyte cover of the preformed endothelial network and is regulated by PDGF-B and VEGF.* Development, 1998. **125**: p. 1591-1598.

100.   Hirschi, K.K., et al., *Endothelial cells modulate the proliferation of mural cell precursors via platelet-derived growth factor-BB and heterotypic cell contact.* Circ Res, 1999. **84**(3): p. 298-305.

101.   Song, S., et al., *PDGFRbeta(+) perivascular progenitor cells in tumours regulate pericyte differentiation and vascular survival.* Nat Cell Biol, 2005. **7**(9): p. 870-879.

102.   Carmeliet, P., *Mechanisms of angiogenesis and arteriogenesis.* Nat Med, 2000. **6**(4): p. 389-95.

103.   Garmy-Susini, B., et al., *Integrin alpha4beta1-VCAM-1-mediated adhesion between endothelial and mural cells is required for blood vessel maturation.* J Clin Invest, 2005. **115**(6): p. 1542-51.

104.   Joussen, A.M., et al., *VEGF-dependent conjuctivalization of the corneal surface.* Invest Ophthalmol Vis Sci, 2003. **44**(1): p. 117-123.

105.   RayChaudhury, A. and P.A. D'Amore, *Endothelial cell regulation by transforming growth factor-beta.* J Cell Biochem, 1991. **47**(3): p. 224-9.

106.   Chang, J.H., et al., *Corneal neovascularization.* Curr Opin Ophthalmol, 2001. **12**(4): p. 242-9.

107.   Ambati, B.K., et al., *Angiostatin inhibits and regresses corneal neovascularization.* Am J Ophthalmol, 2002. **120**(8): p. 1063-1068.

108.   Lobov, I.B., P.C. Brooks, and R.A. Lang, *Angiopoietin-2 displays VEGF-dependent modulation of capillary structure and endothelial cell survival in vivo.* Proc Natl Acad Sci U S A, 2002. **99**(17): p. 11205-10.

109.   Oshima, Y., et al., *Different effects of angiopoietin-2 in different vascular beds: new vessels are most sensitive.* Faseb J, 2005. **19**(8): p. 963-5.

110.   Tsiamis, A.C., et al., *Vascular endothelial growth factor modulates the Tie-2:Tie-1 receptor complex.* Microvasc Res, 2002. **63**(2): p. 149-58.

111.   Ohno-Matsui, K., et al., *Vascular endothelial growth factor upregulates pigment epithelium-derived factor expression via VEGFR-1 in human retinal pigment epithelial cells.* Biochem Biophys Res Commun, 2003. **303**(3): p. 962-7.

112.   Miyagishi, D., et al., *Regulation of the expression of pigment epithelium-derived factor, an anti-angiogenic factor in human oral squamous cell carcinoma cell lines.* Cancer Lett, 2003. **196**(1): p. 77-85.

113.   Ferrara, N., *Role of vascular endothelial growth factor in regulation of physiological angiogenesis.* Am J Physiol - Cell Physiol, 2001. **280**(6): p. C1358-66.

114.   Rees, M., et al., *Regulation of endometrial angiogenesis.* Climacteric, 1999. **2**(1): p. 52-8.

115.   Stouffer, R.L., et al., *Regulation and action of angiogenic factors in the primate ovary.* Arch Med Res, 2001. **32**(6): p. 567-75.

116. Zygmunt, M., et al., *Angiogenesis and vasculogenesis in pregnancy.* Eur J Obstet Gynecol Reprod Biol, 2003. **110 Suppl 1**: p. S10-8.

117. Gerber, H.P. and N. Ferrara, *The role of VEGF in normal and neoplastic hematopoiesis.* J Mol Med, 2003. **81**(1): p. 20-31.

118. Frank, S., et al., *Regulation of vascular endothelial growth factor expression in cultured keratinocytes. Implications for normal and impaired wound healing.* J Biol Chem, 1995. **270**(21): p. 12607-13.

119. Aiello, L.P., *Vascular endothelial growth factor. 20th-century mechanisms, 21st-century therapies.* Invest Ophthalmol Vis Sci, 1997. **38**(9): p. 1647-52.

120. Jacquemin, P., et al., *Transcription factor hepatocyte nuclear factor 6 regulates pancreatic endocrine cell differentiation and controls expression of the proendocrine gene ngn3.* Mol & Cell Biol, 2000. **20**(12): p. 4445-54.

121. Clavel, G., N. Bessis, and M.C. Boissier, *Recent data on the role for angiogenesis in rheumatoid arthritis.* Joint Bone Spine, 2003. **70**(5): p. 321-6.

122. Detmar, M., *Evidence for vascular endothelial growth factor (VEGF) as a modifier gene in psoriasis.* J Invest Dermatol, 2004. **122**(1): p. xiv-xv.

123. Celletti, F.L., et al., *Vascular endothelial growth factor enhances atherosclerotic plaque progression.* Nat Med, 2001. **7**(4): p. 425-9.

124. Sano, T. and H. Horiguchi, *Von Hippel-Lindau disease.* Microsc Res Tech, 2003. **60**(2): p. 159-64.

125. Carmeliet, P., et al., *Abnormal blood vessel development and lethality in embryos lacking a single VEGF allele.* Nature, 1996. **380**(6573): p. 435-9.

126. Ferrara, N., et al., *Heterozygous embryonic lethality induced by targeted inactivation of the VEGF gene.* Nature, 1996. **380**(6573): p. 439-42.

127. Carmeliet, P. and D. Collen, *Role of vascular endothelial growth factor and vascular endothelial growth factor receptors in vascular development.* Curr Top Microbiol Immunol, 1999. **237**: p. 133-58.

128. Hughes, S., H. Yang, and T. Chan-Ling, *Vascularization of the human fetal retina: roles of vasculogenesis and angiogenesis.* Invest Ophthalmol Vis Sci, 2000. **41**(5): p. 1217-28.

129. Keck, P.J., et al., *Vascular permeability factor, an endothelial cell mitogen related to PDGF.* Science, 1989. **246**: p. 1309-1312.

130. Leung, D.W., et al., *Vascular endothelial growth factor is a secreted angiogenic mitogen.* Science, 1989. **246**(4935): p. 1306-9.

131. Gospodarowicz, D., J.A. Abraham, and J. Schilling, *Isolation and characterization of a vascular endothelial cell mitogen produced by pituitary-derived folliculo stellate cells.* Proc Natl Acad Sci U S A, 1989. **86**(19): p. 7311-5.

132. Plouet, J., J. Schilling, and D. Gospodarowicz, *Isolation and characterization of a newly identified endothelial cell mitogen produced by AtT-20 cells.* Embo J, 1989. **8**(12): p. 3801-6.

133. Tischer, E., et al., *Vascular endothelial growth factor: a new member of the platelet-derived growth factor gene family.* Biochem Biophys Res Commun, 1989. **165**(3): p. 1198-206.

134. Praloran, V., et al., *Mitogenic activity of vasculotropin for peripheral human lymphocytes.* C R Acad Sci III, 1991. **313**: p. 21-26.

135. Guerrin, M., et al., *Vasculotropin/vascular endothelial growth factor is an autocrine growth factor for human retinal pigment epithelial cells cultured in vitro.* J Cell Physiol, 1995. **164**: p. 385-394.

136. Yourney, P.A., S. Gohari, and R.F. Alderson, *Vascular endothelial cell growth factors promote the in vitro development of rat photoreceptor cells.* J Neurosci, 2000. **20**(18): p. 6781-8.

137. Sondell, M., G. Lundborg, and M. Kanje, *Vascular endothelial growth factor has neurotrophic activity and stimulates axonal outgrowth, enhancing cell survival and Schwann cell proliferation in the peripheral nervous system.* J Neurosci, 1999. **19**: p. 5731-5740.

138. Bagnard, D., et al., *Semaphorin 3A-vascular endothelial growth factor-165 balance mediates migration and apoptosis of neural progenitor cells by the recruitmet of shared receptor.* J Neurosci, 2001. **21**: p. 3332-3341.

139. Hofman, P., et al., *Endothelial cell hypertrophy induced by vascular endothelial growth factor in the retina: new insights into the pathogenesis of capillary nonperfusion.* Arch Ophthalmol, 2001. **119**(6): p. 861-6.

140. Gerber, H.P., et al., *Vascular endothelial growth factor regulates endothelial cell survival through the phosphatidylinositol 3'-kinase/Akt signal transduction pathway. Requirement for Flk-1/KDR activation.* J Biol Chem, 1998. **273**(46): p. 30336-43.

141. Gerber, H.P., V. Dixit, and N. Ferrara, *Vascular endothelial growth factor induces expression of the antiapoptotic proteins Bcl-2 and A1 in vascular endothelial cells.* J Biol Chem, 1998. **273**(21): p. 13313-6.

142. Pidgeon, G.P., et al., *Vascular endothelial growth factor (VEGF) upregulates BCL-2 and inhibits apoptosis in human and murine mammary adenocarcinoma cells.* Br J Cancer, 2001. **85**(2): p. 273-278.

143. Katoh, O., et al., *Vascular endothelial growth factor inhibits apoptotic death in haematopoietic cells after exposure to chemotherapeutic drugs by inducing MCL1 acting as an antiapoptotic factor.* Cancer Res, 1998. **58**(23): p. 5565-5569.

144. Joussen, A.M., et al., *Retinal vascular endothelial growth factor induces intercellular adhesion molecule-1 and endothelial nitric oxide synthase expression and initiates early diabetic retinal leukocyte adhesion in vivo.* Am J Pathol, 2002. **160**(2): p. 501-9.

145. Hernandez, C., et al., *Vitreous levels of vascular cell adhesion molecule and vascular endothelial growth factor in patients with proliferative diabetic retinopathy: a case-control study.* Diabetes Care, 2001. **24**(3): p. 516-21.

146. Wang, H. and J.A. Keiser, *Vascular endothelial growth factor upregulates the expression of matrix metalloproteinases in vascular smooth muscle cells. Role of flt-1.* Circ Res, 1998. **83**: p. 832-840.

147. Unemori, E.N., et al., *Vascular endothelial growth factor induces interstitial collagenase expression in human endothelial cells.* J Cell Physiol, 1992. **153**(3): p. 557-62.

148. Senger, D.R., et al., *Tumor cells secrete a vascular permeability factor that promotes accumulation of ascites fluid.* Science, 1983. **219**(4587): p. 983-5.

149. Roberts, W.G. and G.E. Palade, *Increased microvascular permeability and endothelial fenestration induced by vascular endothelial growth factor.* J Cell Sci, 1995. **108**: p. 2369-2379.

150. Waltenberger, J., et al., *Different signal transduction properties of KDR and Flt1, two receptors for vascular endothelial growth factor.* J Biol Chem, 1994. **269**(43): p. 26988-95.

151. Gille, H., et al., *A repressor sequence in the juxtamembrane domain of Flt-1*

(VEGFR-1) constitutively inhibits vascular endothelial growth factor-dependent phosphatidylinositol 3'-kinase activation and endothelial cell migration. EMBO J, 2000. **19**(15): p. 4064-73.

152. Cleaver, O. and P.A. Krieg, *VEGF mediates angioblast migration during development of the dorsal aorta in Xenopus.* Development, 1998. **125**(19): p. 3905-14.

153. Clauss, M., et al., *Vascular permeability factor: a tumor-derived polypeptide that induces endothelial cell and monocyte procoagulant activity, and promotes monocyte migration.* J Exp Med, 1990. **172**(6): p. 1535-45.

154. Ku, D.D., et al., *Vascular endothelial growth factor induces EDRF-dependent relaxation in coronary arteries.* Am J Physiol, 1993. **265**: p. H586-H592.

155. Gabrilovich, D.I., et al., *Production of vascular endothelial growth factor by human tumors inhibits the functional maturation of dendritic cells.* Nat Med, 1996. **2**: p. 1096-1103.

156. Pekala, P., et al., *Regulation of hexose transport in aortic endothelial cells by vascular permeability factor and tumour necrosis factor, but not insulin.* J Biol Chem, 1990. **265**: p. 18051-18054.

157. Sone, H., B.K. Deo, and A.K. Kumagai, *Enhancement of glucose transport by vascular endothelial growth factor in retinal endothelial cells.* Invest Ophthalmol Vis Sci, 2000. **41**(7): p. 1876-1884.

158. Saint-Geniez, M. and P.A. D'Amore, *Development and pathology of the hyaloid, choroidal and retinal vasculature.* Int J Dev Biol, 2004. **48**(8-9): p. 1045-58.

159. Ko, M.K., J.G. Chi, and B.L. Chang, *Hyaloid vascular pattern in the human fetus.* J Pediatr Ophthalmol Strabismus, 1985. **22**(5): p. 188-93.

160. Michaelson, I.C., *The mode of development of the vascular system of the retina, with some observations on its significance for certain retinal diseases.* Trans Ophthalmol Soc U K, 1948. **68**: p. 137-81.

161. Ashton, N., *Retinal angiogenesis in the human embryo.* Br Med Bull, 1970. **26**(2): p. 103-6.

162. Provis, J.M., et al., *Development of the human retinal vasculature: cellular relations and VEGF expression.* Exp Eye Res, 1997. **65**(4): p. 555-68.

163. Chan-Ling, T., et al., *Astrocyte-endothelial cell relationships during human retinal vascular development.* Invest Ophthalmol Vis Sci, 2004. **45**(6): p. 2020-32.

164. Ling, T.L. and J. Stone, *The development of astrocytes in the cat retina: evidence of migration from the optic nerve.* Brain Res Dev Brain Res, 1988. **44**(1): p. 73-85.

165. Ling, T.L., J. Mitrofanis, and J. Stone, *Origin of retinal astrocytes in the rat: evidence of migration from the optic nerve.* J Comp Neurol, 1989. **286**(3): p. 345-52.

166. Campbell, F.W., *The influence of a low atmospheric pressure on the development of the retinal vessels in the rat.* Trans Ophthalmol Soc U K, 1951. **71**: p. 287-300.

167. Byerly, T., *Studies in growth: I. Suffocation effects in the chick embryo.* Anat Record, 1926. **32**(4): p. 249-270.

168. Ashton, N., B. Ward, and G. Serpell, *Role of oxygen in the genesis of retrolental fibroplasia.* Br J Ophthalmol, 1953. **37**: p. 513-520.

169. Cogan, D.G., *Development and Senescence of the Human Retinal Vasculature.* Trans Ophthalmol Soc U K, 1963. **83**: p. 465-89.

170. Ashton, N., *Oxygen and the growth and development of retinal vessels. In vivo and in vitro studies. The XX Francis I. Proctor Lecture.* Am J Ophthalmol, 1966. **62**(3): p. 412-35.

171. Chan-Ling, T.L., P. Halasz, and J. Stone, *Development of retinal vasculature in the cat: processes and mechanisms.* Curr Eye Res, 1990. **9**(5): p. 459-78.

172. Flower, R.W., et al., *Postnatal retinal vascular development of the puppy.* Invest Ophthalmol Vis Sci, 1985. **26**(7): p. 957-68.

173. Fruttiger, M., *Development of the mouse retinal vasculature: angiogenesis versus vasculogenesis.* Invest Ophthalmol Vis Sci, 2002. **43**(2): p. 522-7.

174. McLeod, D.S., et al., *Visualization of a developing vasculature.* Microvasc Res, 1987. **33**(2): p. 257-69.

175. Lutty, G.A., C. Merges, and D.S. McLeod, *5' nucleotidase and adenosine during retinal vasculogenesis and oxygen-induced retinopathy.* Invest Ophthalmol Vis Sci, 2000. **41**(1): p. 218-29.

176. Chan-Ling, T. and J. Stone, *Retinopathy of prematurity: its origins in the architecture of the retina.* Prog Ret Res, 1993. **12**: p. 155-178.

177. Gogat, K., et al., *VEGF and KDR gene expression during human embryonic and fetal eye development.* Invest Ophthalmol Vis Sci, 2004. **45**(1): p. 7-14.

178. Plate, K.H., et al., *Vascular endothelial growth factor is a potential tumour angiogenesis factor in human gliomas in vivo.* Nature, 1992. **359**(6398): p. 845-8.

179. Shweiki, D., et al., *Vascular endothelial growth factor induced by hypoxia may mediate hypoxia-initiated angiogenesis.* Nature, 1992. **359**(6398): p. 843-5.

180. Liu, Y., et al., *Hypoxia regulates vascular endothelial growth factor gene expression in endothelial cells. Identification of a 5' enhancer.* Circ Res, 1995. **77**(3): p. 638-43.

181. Forsythe, J.A., et al., *Activation of vascular endothelial growth factor gene transcription by hypoxia-inducible factor 1.* Mol Cell Biol, 1996. **16**(9): p. 4604-4613.

182. Rapaport, D.H. and J. Stone, *The site of commencement of maturation in mammalian retina: observations in the cat.* Brain Res, 1982. **281**(3): p. 273-9.

183. Weiter, J.J., R. Zuckerman, and C.L. Schepens, *A model for the pathogenesis of retrolental fibroplasia based on the metabolic control of blood vessel development.* Ophthalmic Surg, 1982. **13**(12): p. 1013-7.

184. Provis, J.M., et al., *Development of the human retina: patterns of cell distribution and redistribution in the ganglion cell layer.* J Comp Neurol, 1985. **233**(4): p. 429-51.

185. Dreher, B. and S.R. Robinson, *Development of the retinofugal pathway in birds and mammals: evidence for a common 'timetable'.* Brain Behav Evol, 1988. **31**(6): p. 369-90.

186. Okamoto, N., et al., *Transgenic mice with increased expression of vascular endothelial growth factor in the retina: a new model of intraretinal and subretinal neovascularization.* Am J Pathol, 1997. **151**(1): p. 281-91.

187. Tobe, T., et al., *Evolution of neovascularization in mice with overexpression of vascular endothelial growth factor in photoreceptors.* Invest Ophthalmol Vis Sci, 1998. **39**(1): p. 180-8.

188. Gerhardt, H., et al., *VEGF guides angiogenic sprouting utilizing endothelial tip cell filopodia.* J Cell Biol, 2003. **161**(6): p. 1163-77.

189. Meister, M., et al., *Synchronous bursts of action potentials in ganglion cells of*

the developing mammalian retina. Science, 1991. **252**(5008): p. 939-43.

190. Hackett, S.F., et al., *Angiopoietin 2 expression in the retina: upregulation during physiologic and pathologic neovascularization.* J Cell Physiol, 2000. **184**(3): p. 275-84.

191. Hackett, S.F., et al., *Angiopoietin-2 plays an important role in retinal angiogenesis.* J Cell Physiol, 2002. **192**(2): p. 182-7.

192. Oh, H., et al., *Hypoxia and vascular endothelial growth factor selectively up-regulate angiopoietin-2 in bovine microvascular endothelial cells.* J Biol Chem, 1999. **274**(22): p. 15732-9.

193. Park, Y.S., N.H. Kim, and I. Jo, *Hypoxia and vascular endothelial growth factor acutely up-regulate angiopoietin-1 and Tie2 mRNA in bovine retinal pericytes.* Microvasc Res, 2003. **65**(2): p. 125-31.

194. Zamora, D.O., et al., *Soluble forms of EphrinB2 and EphB4 reduce retinal neovascularization in a model of proliferative retinopathy.* Invest Ophthalmol Vis Sci, 2005. **46**(6): p. 2175-82.

195. Hellstrom, A., et al., *IGF-I is critical for normal vascularization of the human retina.* J Clin Endocrinol Metab, 2002. **87**(7): p. 3413-6.

196. Dorrell, M.I., E. Aguilar, and M. Friedlander, *Retinal vascular development is mediated by endothelial filopodia, a preexisting astrocytic template and specific R-cadherin adhesion.* Invest Ophthalmol Vis Sci, 2002. **43**(11): p. 3500-10.

197. Luhmann, U.F., et al., *Role of the Norrie Disease Pseudoglioma Gene in Sprouting Angiogenesis during Development of the Retinal Vasculature.* Invest Ophthalmol Vis Sci, 2005. **46**(9): p. 3372-82.

198. Yoon, H.Z., et al., *Neuropeptide Y expression in a mouse model of oxygen-induced retinopathy.* Clin Experiment Ophthalmol, 2002. **30**(6): p. 424-9.

199. Majka, S., et al., *The balance between proteinases and inhibitors in a murine model of proliferative retinopathy.* Invest Ophthalmol Vis Sci, 2001. **42**(1): p. 210-5.

200. Behling, K.C., E.M. Surace, and J. Bennett, *Pigment epithelium-derived factor expression in the developing mouse eye.* Mol Vis, 2002. **8**: p. 449-54.

201. West, H., W.D. Richardson, and M. Fruttiger, *Stabilization of the retinal vascular network by reciprocal feedback between blood vessels and astrocytes.* Development, 2005. **132**(8): p. 1855-62.

202. Mi, H., H. Haeberle, and B.A. Barres, *Induction of astrocyte differentiation by endothelial cells.* J Neurosci, 2001. **21**(5): p. 1538-47.

203. Terry, T.L., *Extreme prematurity and fibroblastic overgrowth of persistent vascular sheath behind each crystalline lens.* Am J Ophthalmol, 1942. **25**: p. 203-204.

204. Ryan, H., *Retrolental fibroplasia. A clinicopathologic study.* Am J Ophthalmol, 1952. **35**: p. 329-342.

205. *An international classification of retinopathy of prematurity. II. The classification of retinal detachment. The International Committee for the Classification of the Late Stages of Retinopathy of Prematurity.* Arch Ophthalmol, 1987. **105**(7): p. 906-12.

206. *An international classification of retinopathy of prematurity. The Committee for the Classification of Retinopathy of Prematurity.* Arch Ophthalmol, 1984. **102**(8): p. 1130-4.

207. *The International Classification of Retinopathy of Prematurity revisited.* Arch Ophthalmol, 2005. **123**(7): p. 991-9.

208.   Schaffer, D.B., et al., *Prognostic factors in the natural course of retinopathy of prematurity. The Cryotherapy for Retinopathy of Prematurity Cooperative Group.* Ophthalmology, 1993. **100**(2): p. 230-7.

209.   Early Treatment For Retinopathy Of Prematurity Cooperative, G., *Revised indications for the treatment of retinopathy of prematurity: results of the early treatment for retinopathy of prematurity randomized trial.* Arch Ophthalmol, 2003. **121**(12): p. 1684-94.

210.   Hertle, R.W., D.B. Schaffer, and J.A. Foster, *Pediatric Eye Disease: color atlas and synopsis.* 2002, U.S.A: McGraw-Hill.

211.   Steinkuller, P.G., et al., *Childhood blindness.* J Aapos, 1999. **3**(1): p. 26-32.

212.   Wheatley, C.M., et al., *Retinopathy of prematurity: recent advances in our understanding.* Br J Ophthalmol, 2002. **86**(6): p. 696-700.

213.   Darlow, B.A., et al., *Prenatal risk factors for severe retinopathy of prematurity among very preterm infants of the Australian and New Zealand Neonatal Network.* Pediatrics, 2005. **115**(4): p. 990-6.

214.   Palmer, E.A., et al., *Incidence and early course of retinopathy of prematurity. The Cryotherapy for Retinopathy of Prematurity Cooperative Group.* Ophthalmology, 1991. **98**(11): p. 1628-40.

215.   Engle, W.A., *Age terminology during the perinatal period.* Pediatrics, 2004. **114**(5): p. 1362-4.

216.   *Multicenter trial of cryotherapy for retinopathy of prematurity. Three-month outcome. Cryotherapy for Retinopathy of Prematurity Cooperative Group.* Arch Ophthalmol, 1990. **108**(2): p. 195-204.

217.   Good, W.V., et al., *The incidence and course of retinopathy of prematurity: findings from the early treatment for retinopathy of prematurity study.* Pediatrics, 2005. **116**(1): p. 15-23.

218.   Palmer, E.A., et al., *15-year outcomes following threshold retinopathy of prematurity: final results from the multicentre trial of cryotherapy for retinopathy of prematurity.* Arch Ophthalmol, 2005. **123**(3): p. 311-8.

219.   Recsan, Z., R. Vamos, and G. Salacz, *Laser treatment of zone I prethreshold and stage 3 threshold retinopathy of prematurity.* J Pediatr Ophthalmol Strabismus, 2003. **40**(4): p. 204-7.

220.   Vander, J.F., et al., *Revised indications for early treatment of retinopathy of prematurity.* Arch Ophthalmol, 2005. **123**(3): p. 406-7; discussion 409-10.

221.   Jalali, S., V.A. Essuman, and R. Thomas, *Clinical application of the revised indications for the treatment of retinopathy of prematurity.* Arch Ophthalmol, 2005. **123**(3): p. 407-8; discussion 409-10.

222.   Coats, D. and R. Saunders, *The dilemma of exercising clinical judgment in the treatment of retinopathy of prematurity.* Arch Ophthalmol, 2005. **123**(3): p. 408-9; discussion 409-10.

223.   Vohr, B.R., et al., *Neurodevelopmental and functional outcomes of extremely low birth weight infants in the National Institute of Child Health and Human Development Neonatal Research Network, 1993-1994.* Pediatrics, 2000. **105**(6): p. 1216-26.

224.   Quinn, G.E., et al., *Health-related quality of life at age 10 years in very low-birth-weight children with and without threshold retinopathy of prematurity.* Arch Ophthalmol, 2004. **122**(11): p. 1659-66.

225.   Campbell, K., *Intensive oxygen therapy as a possible cause of retrolental fibroplasia: A clinical approach.* Med J Aust, 1951. **2**: p. 48-50.

226. Ashton, N., B. Ward, and G. Serpell, *Effect of oxygen on developing retinal vessels with particular reference to the problem of retrolental fibroplasia.* Br J Ophthalmol, 1954. **38**: p. 397-432.

227. Kinsey, V.E., J.T. Jacobus, and F.M. Hemphill, *Cooperative study of retrolental fibroplasia and the use of oxygen.* Arch Ophthalmol, 1956. **56**: p. 481-529.

228. Zacharias, L., *Retrolental fibroplasia: A survey.* Am J Ophthalmol, 1952. **35**: p. 1426-1454.

229. Ingalls, T.H., *Congenital encephalo-ophthalmic dysplasia; epidemiologic implications.* Pediatrics, 1948. **1**: p. 315-325.

230. Szewczyk, T.S., *Retrolental fibroplasia: Etiology and prophylaxis. A preliminary report.* Am J Ophthalmol, 1951. **34**(12): p. 1649-1650.

231. Bembridge, B.A., et al., *Retrolental fibroplasia. A problem of prematurity.* Br Med J, 1952. **4760**: p. 675-680.

232. Szewczyk, T.S., *Retrolental fibroplasia: Etiology and prophylaxis.* Am J Ophthalmol, 1952. **35**(3): p. 301-310.

233. Patz, A., *Studies on the effect of high oxygen administration in retrolental fibroplasia: I. Nursery observations.* Am J Ophthalmol, 1952. **35**: p. 1248-1253.

234. *Supplemental Therapeutic Oxygen for Prethreshold Retinopathy Of Prematurity (STOP-ROP), a randomized, controlled trial. I: primary outcomes.* Pediatrics, 2000. **105**(2): p. 295-310.

235. Patz, A., *Oxygen studies in retrolental fibroplasia: II. The production of microscopic changes of retrolental fibroplasia in experimental animals.* Am J Ophthalmol, 1953. **36**: p. 1511-1522.

236. Gyllensten, L.J. and B.E. Hellstrom, *Experimental approach to the pathogenesis of retrolental fibroplasia: II. The influence of the developmental maturity on oxygen-induced changes in the mouse eye.* Am J Ophthalmol, 1955. **39**(4): p. 475-488.

237. Owens, W.C. and E.U. Owens, *Retrolental fibroplasia in premature infants.* Am J Ophthalmol, 1949. **32**(1): p. 1-21.

238. Patz, A., *The role of oxygen in retrolental fibroplasia.* Pediatrics, 1957. **19**: p. 504-524.

239. Silverman, W.A., *A cautionary tale about supplemental oxygen: the albatross of neonatal medicine.* Pediatrics, 2004. **113**(2): p. 394-6.

240. Cunningham, S., et al., *Transcutaneous oxygen levels in retinopathy of prematurity.* Lancet, 1995. **346**(8988): p. 1464-5.

241. Avery, M.E., *Recent increase in mortality from hyaline membrane disease.* J Pediatr, 1960. **57**: p. 553-9.

242. McDonald, A., *Neurological and ophthalmic disorders in children of very low birth weight.* Br Med J, 1962. **1**: p. 895-900.

243. Bolton, D.P. and K.W. Cross, *Further observations on cost of preventing retrolental fibroplasia.* Lancet, 1974. **1**(7855): p. 445-8.

244. Askie, L.M. and D.J. Henderson-Smart, *Restricted versus liberal oxygen exposure for preventing morbidity and mortality in preterm or low birth weight infants.* Cochrane Database Syst Rev, 2001(4): p. CD001077.

245. Phelps, D.L., *Retinopathy of prematurity: an estimate of vision loss in the United States--1979.* Pediatrics, 1981. **67**(6): p. 924-5.

246. Gibson, D.L., et al., *Retinopathy of prematurity: a new epidemic?* Pediatrics, 1989. **83**(4): p. 486-92.

247. Simons, B.D. and J.T. Flynn, *Retinopathy of prematurity and associated factors.*

Int Ophthalmol Clin, 1999. **39**(2): p. 29-48.

248. Kinsey, V.E., et al., *PaO2 levels and retrolental fibroplasia: a report of the cooperative study.* Pediatrics, 1977. **60**(5): p. 665-668.

249. Lucey, J.F. and B. Dangman, *A reexamination of the role of oxygen in retrolental fibroplasia.* Pediatrics, 1984. **73**(1): p. 82-96.

250. Pierce, E.A., E.D. Foley, and L.E. Smith, *Regulation of vascular endothelial growth factor by oxygen in a model of retinopathy of prematurity.* Arch Ophthalmol, 1996. **114**(10): p. 1219-28.

251. Dorey, C.K., et al., *Correlation of vascular permeability factor/vascular endothelial growth factor with extraretinal neovascularization in the rat.* Arch Ophthalmol, 1996. **114**(10): p. 1210-7.

252. Cunningham, S., et al., *A novel model of retinopathy of prematurity simulating preterm oxygen variability in the rat.* Invest Ophthalmol Vis Sci, 2000. **41**(13): p. 4275-4280.

253. Stone, J., et al., *Roles of vascular endothelial growth factor and astrocyte degeneration in the genesis of retinopathy of prematurity.* Invest Ophthalmol Vis Sci, 1996. **37**(2): p. 290-9.

254. Aiello, L.P., et al., *Suppression of retinal neovascularization in vivo by inhibition of vascular endothelial growth factor (VEGF) using soluble VEGF-receptor chimeric proteins.* Proc Natl Acad Sci U S A, 1995. **92**(23): p. 10457-61.

255. Robinson, G.S., et al., *Oligodeoxynucleotides inhibit retinal neovascularization in a murine model of proliferative retinopathy.* Proc Natl Acad Sci U S A, 1996. **93**: p. 4851-4856.

256. Sone, H., et al., *Effects of intraocular or systemic administration of neutralizing antibody against vascular endothelial growth factor on the murine experimental model of retinopathy.* Life Sci, 1999. **65**(24): p. 2573-80.

257. Ozaki, H., et al., *Blockade of vascular endothelial cell growth factor receptor signalling is sufficient to completely prevent retinal neovascularization.* Am J Pathol, 2000. **156**(2): p. 697-707.

258. Rota, R., et al., *Marked inhibition of retinal neovascularization in rats following soluble-flt-1 gene transfer.* J Gene Med, 2004. **6**: p. 992-1002.

259. Eyetech Study Group, *Preclinical and phase 1a clinical evaluation of an anti-VEGF pegylated aptamer (EYE001) for the treatment of exudative age-related macular degeneration.* Retina, 2002. **22**(2): p. 143-152.

260. Bainbridge, J.W., et al., *A peptide encoded by exon 6 of VEGF (EG3306) inhibits VEGF-induced angiogenesis in vitro and ischaemic retinal neovascularisation in vivo.* Biochem Biophys Res Commun, 2003. **302**(4): p. 793-9.

261. Young, T.L., et al., *Histopathology and vascular endothelial growth factor in untreated and diode laser-treated retinopathy of prematurity.* J Aapos, 1997. **1**(2): p. 105-10.

262. Pournaras, C.J., et al., *Scatter photocoagulation restores tissue hypoxia in experimental vasoproliferative microangiopathy in miniature pigs.* Ophthalmology, 1990. **97**(10): p. 1329-33.

263. Banach, M.J. and D.M. Berinstein, *Laser therapy for retinopathy of prematurity.* Curr Opin Ophthalmol, 2001. **12**(3): p. 164-70.

264. Wilson, A.S., et al., *Argon laser photocoagulation-induced modification of gene expression in the retina.* Invest Ophthalmol Vis Sci, 2003. **44**(4): p. 1426-34.

265. Umeda, N., et al., *Colocalization of Tie2, angiopoietin 2 and vascular endothelial growth factor in fibrovascular membrane from patients with*

retinopathy of prematurity. Ophthalmic Res, 2003. **35**(4): p. 217-23.

266.   Bedrossian, R.H., P. Carmichael, and J.A. Ritter, *Effect of oxygen weaning in retrolental fibroplasia.* AMA Arch Ophthalmol, 1954. **53**(4): p. 514-8.

267.   Ashton, N., *Experimental retrolental fibroplasia.* Annu Rev Med, 1957. **8**: p. 441-54.

268.   Patz, A. and A.B. Eastham, *Oxygen studies in retrolental fibroplasia. V. The effect of rapid vs. gradual withdrawal from oxygen on the mouse eye.* AMA Arch Ophthalmol, 1957. **57**(5): p. 724-9.

269.   Phelps, D.L. and A.L. Rosenbaum, *Effects of marginal hypoxemia on recovery from oxygen-induced retinopathy in the kitten model.* Pediatrics, 1984. **73**(1): p. 1-6.

270.   Chan-Ling, T., B. Gock, and J. Stone, *Supplemental Oxygen Therapy. Basis for non-invasive treatment of retinopathy of prematurity.* Invest Ophthalmol Vis Sci, 1995. **36**(7): p. 1215-1230.

271.   Lloyd, J., et al., *Supplemental oxygen for the treatment of prethreshold retinopathy of prematurity.* Cochrane Database Syst Rev, 2003(2): p. CD003482.

272.   Anderson, C.G., W.E. Benitz, and A. Madan, *Retinopathy of prematurity and pulse oximetry: a national survey of recent practices.* J Perinatol, 2004. **24**(3): p. 164-8.

273.   Cole, C.H., et al., *Resolving our uncertainty about oxygen therapy.* Pediatrics, 2003. **112**(6 Pt 1): p. 1415-9.

274.   Chow, L.C., K.W. Wright, and A. Sola, *Can changes in clinical practice decrease the incidence of severe retinopathy of prematurity in very low birth weight infants?* Pediatrics, 2003. **111**(2): p. 339-45.

275.   Tin, W., et al., *Pulse oximetry, severe retinopathy, and outcome at one year in babies of less than 28 weeks gestation.* Arch Dis Child Fetal Neonatal Ed, 2001. **84**(2): p. F106-10.

276.   Askie, L.M., et al., *Oxygen-saturation targets and outcomes in extremely preterm infants.* N Engl J Med, 2003. **349**(10): p. 959-67.

277.   *Benefits of Oxygen Saturation Targeting, trial II (BOOST II).* 2005, NHMRC Clinical Trials Centre. http://www.ctc.usyd.edu.au/trials/other_trials/boost.htm. Access date: Nov 15, 2005.

278.   Ng, Y.K., et al., *Epidemiology of retinopathy of prematurity.* Lancet, 1988. **2**(8622): p. 1235-8.

279.   Saunders, R.A., et al., *Racial variation in retinopathy of prematurity. The Cryotherapy for Retinopathy of Prematurity Cooperative Group.* Arch Ophthalmol, 1997. **115**(5): p. 604-8.

280.   Rapp, L.M. and T.P. Williams, *The role of ocular pigmentation in protecting against retinal light damage.* Vision Res, 1980. **20**(12): p. 1127-31.

281.   Ricci, B., et al., *Effect of light on oxygen-induced retinopathy in the rat model. Light and OIR in the rat.* Doc Ophthalmol, 1990. **74**(4): p. 287-301.

282.   Wesolowski, E. and L.E. Smith, *Effect of light on oxygen-induced retinopathy in the mouse.* Invest Ophthalmol Vis Sci, 1994. **35**(1): p. 112-9.

283.   Reynolds, J.D., et al., *Lack of efficacy of light reduction in preventing retinopathy of prematurity. Light Reduction in Retinopathy of Prematurity (LIGHT-ROP) Cooperative Group.* N Engl J Med, 1998. **338**(22): p. 1572-6.

284.   Tadesse, M., et al., *Race, Candida sepsis, and retinopathy of prematurity.* Biol Neonate, 2002. **81**(2): p. 86-90.

285.   Lang, D.M., J. Blackledge, and R.W. Arnold, *Is Pacific race a retinopathy of*

prematurity risk factor? Arch Pediatr Adolesc Med, 2005. **159**(8): p. 771-3.

286.   Xu, Q., et al., *Vascular development in the retina and inner ear: control by Norrin and Frizzled-4, a high-affinity ligand-receptor pair.* Cell, 2004. **116**(6): p. 883-95.

287.   Robitaille, J., et al., *Mutant frizzled-4 disrupts retinal angiogenesis in familial exudative vitreoretinopathy.* Nat Genet, 2002. **32**(2): p. 326-30.

288.   Toomes, C., et al., *Mutations in LRP5 or FZD4 underlie the common familial exudative vitreoretinopathy locus on chromosome 11q.* Am J Hum Genet, 2004. **74**(4): p. 721-30.

289.   Hiraoka, M., et al., *Insertion and deletion mutations in the dinucleotide repeat region of the Norrie disease gene in patients with advanced retinopathy of prematurity.* J Hum Genet, 2001. **46**(4): p. 178-81.

290.   Toomes, C., et al., *Further evidence of genetic heterogeneity in familial exudative vitreoretinopathy; exclusion of EVR1, EVR3, and EVR4 in a large autosomal dominant pedigree.* Br J Ophthalmol, 2005. **89**(2): p. 194-7.

291.   Mechoulam, H. and E.A. Pierce, *Retinopathy of prematurity: molecular pathology and therapeutic strategies.* Am J Pharmacogenomics, 2003. **3**(4): p. 261-77.

292.   Hutcheson, K.A., et al., *Norrie disease gene sequence variants in an ethnically diverse population with retinopathy of prematurity.* Mol Vis, 2005. **11**: p. 501-8.

293.   Haider, M.Z., et al., *A C597-->A polymorphism in the Norrie disease gene is associated with advanced retinopathy of prematurity in premature Kuwaiti infants.* J Biomed Sci, 2002. **9**(4): p. 365-70.

294.   Vannay, A., et al., *Association of genetic polymorphisms of vascular endothelial growth factor and risk for proliferative retinopathy of prematurity.* Pediatr Res, 2005. **57**(3): p. 396-8.

295.   Watson, C.J., et al., *Identification of polymorphisms within the vascular endothelial growth factor (VEGF) gene: correlation with variation in VEGF protein production.* Cytokine, 2000. **12**(8): p. 1232-5.

296.   Cooke, R.W., et al., *Genetic polymorphisms and retinopathy of prematurity.* Invest Ophthalmol Vis Sci, 2004. **45**(6): p. 1712-5.

297.   Awata, T., et al., *Functional VEGF C-634G polymorphism is associated with development of diabetic macular edema and correlated with macular retinal thickness in type 2 diabetes.* Biochem Biophys Res Commun, 2005. **333**(3): p. 679-85.

298.   Awata, T., et al., *A common polymorphism in the 5'-untranslated region of the VEGF gene is associated with diabetic retinopathy in type 2 diabetes.* Diabetes, 2002. **51**(5): p. 1635-9.

299.   *Statement for the Use of Animals in Ophthalmic and Visual Research*, The Association for Research in Vision and Ophthalmology. http://www.arvo.org/AboutARVO/animalst.asp. Access date: Aug 29, 2005.

300.   *Australian code of practice for the care and use of animals for scientific purposes.* 2004, The National Health and Medical Research Council of Australia. http://www7.health.gov.au/nhmrc/publications/synopses/ea16syn.htm. Access date: Aug 29, 2005.

301.   Bustin, S.A., *Absolute quantification of mRNA using real-time reverse transcription polymerase chain reaction assays.* J Mol Endocrinol, 2000. **25**(2): p. 169-93.

302.   Morrison, T.B., J.J. Weis, and C.T. Wittwer, *Quantification of low-copy*

transcripts by continuous SYBR Green I monitoring during amplification. Biotechniques, 1998. **24**(6): p. 954-8, 960, 962.

303. Ririe, K.M., R.P. Rasmussen, and C.T. Wittwer, *Product differentiation by analysis of DNA melting curves during the polymerase chain reaction.* Anal Biochem, 1997. **245**(2): p. 154-60.

304. Peterson, R.A., et al., *Ink perfusion for displaying capillaries in the chicken.* Stain Technology, 1965. **40**(6): p. 351-6.

305. Tompsett, D., *Anatomical Techniques.* 2nd ed. 1970, Great Britain: E&S Livingstone.

306. Jee, W.S. and J.S. Arnold, *India ink-gelatin vascular injection of skeletal tissues.* Stain Technology, 1960. **35**(2): p. 59-65.

307. West, W., *Injection of the arterial system of the mouse.* Stain Technology, 1962. **37**(2): p. 99-103.

308. Filep, J.G., A. Delalandre, and M. Beauchamp, *Dual role for nitric oxide in the regulation of plasma volume and albumin escape during endotoxin shock in conscious rats.* Circ Res, 1997. **81**(5): p. 840-7.

309. Filep, J.G., *Endogenous endothelin modulates blood pressure, plasma volume, and albumin escape after systemic nitric oxide blockade.* Hypertension., 1997. **30**(1 Pt 1): p. 22-8.

310. Ventresca, M.R., J.R. Gonder, and A.K. Tanswell, *Oxygen-induced proliferative retinopathy in the newborn rat.* Can J Ophthalmol, 1990. **25**(4): p. 186-9.

311. Penn, J.S., B.L. Tolman, and L.A. Lowery, *Variable oxygen exposure causes preretinal neovascularization in the newborn rat.* Invest Ophthalmol Vis Sci, 1993. **34**(3): p. 576-85.

312. Reynaud, X. and C.K. Dorey, *Extraretinal neovascularization induced by hypoxic episodes in the neonatal rat.* Invest Ophthalmol Vis Sci, 1994. **35**(8): p. 3169-77.

313. Penn, J.S., B.L. Tolman, and M.M. Henry, *Oxygen-induced retinopathy in the rat: relationship of retinal nonperfusion to subsequent neovascularization.* Invest Ophthalmol Vis Sci, 1994. **35**(9): p. 3429-35.

314. Penn, J.S., et al., *The range of PaO2 variation determines the severity of oxygen-induced retinopathy in newborn rats.* Invest Ophthalmol Vis Sci, 1995. **36**(10): p. 2063-70.

315. Stone, J., *The whole mount handbook: a guide to the preparation of retinal whole mounts.* 1981, Sydney: Maitland Publications.

316. Chan-Ling, T., *Glial, vascular, and neuronal cytogenesis in whole-mounted cat retina.* Microsc Res Tech, 1997. **36**(1): p. 1-16.

317. Hayes, C.E. and I.J. Goldstein, *An α-D-Galactosyl-binding Lectin from Bandeiraea simplicifolia Seeds. Isolation by affinity chromatography and characterization.* J Biol Chem, 1974. **249**(6): p. 1904-14.

318. Holmes, J.M. and L.A. Duffner, *The effect of postnatal growth retardation on abnormal neovascularization in the oxygen exposed neonatal rat.* Curr Eye Res, 1996. **15**(4): p. 403-9.

319. Zhang, S., D.A. Leske, and J.M. Holmes, *Neovascularization grading methods in a rat model of retinopathy of prematurity.* Invest Ophthalmol Vis Sci, 2000. **41**(3): p. 887-91.

320. Martinez, F., et al., *Mechanical ventilation effect on surfactant content, function, and lung compliance in the newborn rat.* Pediatr Res, 2004. **56**(1): p. 19-25.

321.   Sokal, R.R. and F.J. Rohlf, *Biometry: The principles and practice of statistics in biological research.* 3rd ed. 1995, New York: Freeman. 887.

322.   Madan, A. and J.S. Penn, *Animal models of oxygen-induced retinopathy.* Front Biosci, 2003. **8**: p. 1030-43.

323.   Patz, A., *Oxygen studies in retrolental fibroplasia: IV. Clinical and experimental observations.* Am J Ophthalmol, 1954. **38**(3): p. 291-308.

324.   Ashton, N. and R. Blach, *Studies on developing retinal vessels VIII. Effect of oxygen on the retinal vessels of the ratling.* Br J Ophthalmol, 1961. **45**: p. 321-340.

325.   Patz, A., *The role of oxygen in retrolental fibroplasia.* Trans Am Ophthalmol Soc, 1968. **66**: p. 940-85.

326.   Gole, G., *Animal Models of Retinopathy of prematurity*, in *Retinopathy of prematurity*, W.A. Silverman and J.T. Flynn, Editors. 1985, Blackwell Scientific: M.A. p. 53-95.

327.   McLeod, D.S., S.A. D'Anna, and G.A. Lutty, *Clinical and histopathologic features of canine oxygen-induced proliferative retinopathy.* Invest Ophthalmol Vis Sci, 1998. **39**(10): p. 1918-32.

328.   Smith, L.E., et al., *Oxygen-induced retinopathy in the mouse.* Invest Ophthalmol Vis Sci, 1994. **35**(1): p. 101-11.

329.   Holmes, J.M., et al., *Metabolic acidosis-induced retinopathy in the neonatal rat.* Invest Ophthalmol Vis Sci, 1999. **40**(3): p. 804-9.

330.   Holmes, J.M., L.A. Duffner, and J.C. Kappil, *The effect of raised inspired carbon dioxide on developing rat retinal vasculature exposed to elevated oxygen.* Curr Eye Res, 1994. **13**(10): p. 779-82.

331.   Holmes, J.M., D.A. Leske, and S. Zhang, *The effect of raised inspired carbon dioxide on normal retinal vascular development in the neonatal rat.* Curr Eye Res, 1997. **16**(1): p. 78-81.

332.   Holmes, J.M., et al., *Carbon dioxide-induced retinopathy in the neonatal rat.* Curr Eye Res, 1998. **17**(6): p. 608-16.

333.   Zhang, S., et al., *Postnatal growth retardation exacerbates acidosis-induced retinopathy in the neonatal rat.* Curr Eye Res, 2001. **22**(2): p. 133-9.

334.   Gao, G., et al., *Difference in ischemic regulation of vascular endothelial growth factor and pigment epithelium-derived factor in brown norway and sprague dawley rats contributing to different susceptibilities to retinal neovascularization.* Diabetes, 2002. **51**(4): p. 1218-25.

335.   Csaky, K., et al., *Strain specific phenotype variation in VEGF-induced choroidal neovascularization in the rat (Abstract).* Invest Ophthalmol Vis Sci, 2001. **42**(S227).

336.   Safa, R. and N.N. Osborne, *Retinas from albino rats are more susceptible to ischaemic damage than age-matched pigmented animals.* Brain Res, 2000. **862**(1-2): p. 36-42.

337.   Engelmann, R., et al., *A different retinal glia response to optic nerve injury/lipopolysaccharide administration in hooded and albino rats.* Brain Res, 2001. **889**(1-2): p. 251-5.

338.   Kitzmann, A., et al., *Incidence and severity of neovascularization in oxygen- and metabolic acidosis-induced retinopathy depend on rat source.* Curr Eye Res, 2002. **25**(4): p. 215-20.

339.   Rohan, R.M., et al., *Genetic heterogeneity of angiogenesis in mice.* Faseb J, 2000. **14**(7): p. 871-6.

340. Chan, C.K., et al., *Mouse strain-dependent heterogeneity of resting limbal vasculature.* Invest Ophthalmol Vis Sci, 2004. **45**(2): p. 441-7.

341. Stenzel, J.D., et al., *Hyperoxic lung injury in Fischer-344 and Sprague-Dawley rats in vivo.* Free Radic Biol Med, 1993. **14**(5): p. 531-9.

342. Knight, S.A., C.V. Smith, and S.E. Welty, *Iron and oxidized beta-casein in the lavages of hyperoxic Fischer-344 rats.* Life Sci, 1998. **62**(2): p. 165-76.

343. Chan-Ling, T. and J. Stone, *Degeneration of astrocytes in feline retinopathy of prematurity causes failure of the blood-retinal barrier.* Invest Ophthalmol Vis Sci, 1992. **33**(7): p. 2148-59.

344. Semenza, G.L., *HIF-1: mediator of physiological and pathophysiological responses to hypoxia.* J Appl Physiol, 2000. **88**(4): p. 1474-80.

345. Strohl, K.P., et al., *Ventilation and metabolism among rat strains.* J Appl Physiol, 1997. **82**(1): p. 317-23.

346. Golder, F.J., et al., *Differences in time-dependent hypoxic phrenic responses among inbred rat strains.* J Appl Physiol, 2005. **98**(3): p. 838-44.

347. Allegaert, K., et al., *Perinatal growth characteristics and associated risk of developing threshold retinopathy of prematurity.* J Aapos, 2003. **7**(1): p. 34-7.

348. Holmes, J.M. and L.A. Duffner, *The effect of litter size on normal retinal vascular development in the neonatal rat.* Curr Eye Res, 1995. **14**(8): p. 737-40.

349. Oetting, W.S., *Albinism.* Curr Opin Pediatr, 1999. **11**(6): p. 565-71.

350. Blaszczyk, W.M., et al., *A Tyrosinase missense mutation causes albinism in the Wistar rat.* Pigment Cell Res, 2005. **18**(2): p. 144-5.

351. Akeo, K., D.B. Ebenstein, and C.K. Dorey, *Dopa and oxygen inhibit proliferation of retinal pigment epithelial cells, fibroblasts and endothelial cells in vitro.* Exp Eye Res, 1989. **49**(3): p. 335-46.

352. Akeo, K., Y. Tanaka, and S. Okisaka, *A comparison between melanotic and amelanotic retinal pigment epithelial cells in vitro concerning the effects of L-dopa and oxygen on cell cycle.* Pigment Cell Res, 1994. **7**(3): p. 145-51.

353. Ilia, M. and G. Jeffery, *Retinal mitosis is regulated by dopa, a melanin precursor that may influence the time at which cells exit the cell cycle: analysis of patterns of cell production in pigmented and albino retinae.* J Comp Neurol, 1999. **405**(3): p. 394-405.

354. Blaszczyk, W.M., H. Straub, and C. Distler, *GABA content in the retina of pigmented and albino rats.* Neuroreport, 2004. **15**(7): p. 1141-4.

355. Tombran-Tink, J. and L.V. Johnson, *Neuronal differentiation of retinoblastoma cells induced by medium conditioned by human RPE cells.* Invest Ophthalmol Vis Sci, 1989. **30**(8): p. 1700-7.

356. Gao, G., et al., *Unbalanced expression of VEGF and PEDF in ischemia-induced retinal neovascularization.* FEBS Lett, 2001. **489**(2-3): p. 270-6.

357. Brooks, S.E., et al., *Reduced severity of oxygen-induced retinopathy in eNOS-deficient mice.* Invest Ophthalmol Vis Sci, 2001. **42**(1): p. 222-8.

358. Zhang, D., et al., *Intravitreal injection of plasminogen kringle 5, an endogenous angiogenic inhibitor, arrests retinal neovascularization in rats.* Diabetologia, 2001. **44**(6): p. 757-65.

359. Pfaffl, M.W., *Quantification strategies in real-time PCR*, in *A-Z of quantitative PCR*, S. Bustin, Editor. 2004, International University Line: La Jolla, CA.

360. Petrova, T.V., T. Makinen, and K. Alitalo, *Signaling via vascular endothelial growth factor receptors.* Exp Cell Res, 1999. **253**(1): p. 117-30.

361. Li, J., et al., *VEGF, flk-1, and flt-1 expression in a rat myocardial infarction*

model of angiogenesis. Am J Physiol, 1996. **270**(5 Pt 2): p. H1803-11.

362.   Ray, P.S., et al., *Early effects of hypoxia/reoxygenation on VEGF, ang-1, ang-2 and their receptors in the rat myocardium: implications for myocardial angiogenesis.* Mol Cell Biochem, 2000. **213**(1-2): p. 145-53.

363.   Brogi, E., et al., *Hypoxia-induced paracrine regulation of vascular endothelial growth factor receptor expression.* J Clin Invest, 1996. **97**(2): p. 469-76.

364.   Suzuma, K., et al., *Increased expression of KDR/Flk-1 (VEGFR-2) in murine model of ischemia-induced retinal neovascularization.* Microvasc Res, 1998. **56**(3): p. 183-91.

365.   McLeod, D.S., et al., *Localization of VEGF receptor-2 (KDR/Flk-1) and effects of blocking it in oxygen-induced retinopathy.* Invest Ophthalmol Vis Sci, 2002. **43**(2): p. 474-82.

366.   Wilkinson-Berka, J.L., et al., *Inhibition of platelet-derived growth factor promotes pericyte loss and angiogenesis in ischemic retinopathy.* Am J Pathol, 2004. **164**(4): p. 1263-73.

367.   Robbins, S.G., V.S. Rajaratnam, and J.S. Penn, *Evidence for upregulation and redistribution of vascular endothelial growth factor (VEGF) receptors flt-1 and flk-1 in the oxygen-injured rat retina.* Growth Factors, 1998. **16**(1): p. 1-9.

368.   Werdich, X.Q., et al., *Variable oxygen and retinal VEGF levels: correlation with incidence and severity of pathology in a rat model of oxygen-induced retinopathy.* Exp Eye Res, 2004. **79**(5): p. 623-30.

369.   Zachary, I., *VEGF signalling: integration and multi-tasking in endothelial cell biology.* Biochem Soc Trans, 2003. **31**(Pt 6): p. 1171-7.

370.   Teichert-Kuliszewska, K., et al., *Biological action of angiopoietin-2 in a fibrin matrix model of angiogenesis is associated with activation of Tie2.* Cardiovasc Res, 2001. **49**(3): p. 659-70.

371.   Holash, J., et al., *Vessel cooption, regression, and growth in tumors mediated by angiopoietins and VEGF.* Science, 1999. **284**(5422): p. 1994-8.

372.   Loughna, S. and T.N. Sato, *Angiopoietin and Tie signaling pathways in vascular development.* Matrix Biol, 2001. **20**(5-6): p. 319-25.

373.   Tian, H., S.L. McKnight, and D.W. Russell, *Endothelial PAS domain protein 1 (EPAS1), a transcription factor selectively expressed in endothelial cells.* Genes Dev, 1997. **11**(1): p. 72-82.

374.   Lukiw, W.J., et al., *Coordinate activation of HIF-1 and NF-kappaB DNA binding and COX-2 and VEGF expression in retinal cells by hypoxia.* Invest Ophthalmol Vis Sci, 2003. **44**(10): p. 4163-70.

375.   Wilkinson-Berka, J.L., et al., *COX-2 inhibition and retinal angiogenesis in a mouse model of retinopathy of prematurity.* Invest Ophthalmol Vis Sci, 2003. **44**(3): p. 974-9.

376.   Bonazzi, A., et al., *Regulation of cyclooxygenase-2 by hypoxia and peroxisome proliferators in the corneal epithelium.* J Biol Chem, 2000. **275**(4): p. 2837-44.

377.   Schmedtje, J.F., Jr., et al., *Hypoxia induces cyclooxygenase-2 via the NF-kappaB p65 transcription factor in human vascular endothelial cells.* J Biol Chem, 1997. **272**(1): p. 601-8.

378.   Tsujii, M., et al., *Cyclooxygenase regulates angiogenesis induced by colon cancer cells.* Cell, 1998. **93**(5): p. 705-16.

379.   Williams, C.S., et al., *Host cyclooxygenase-2 modulates carcinoma growth.* J Clin Invest, 2000. **105**(11): p. 1589-94.

380.   Bazan, N.G. and W.J. Lukiw, *Cyclooxygenase-2 and presenilin-1 gene*

expression induced by interleukin-1beta and amyloid beta 42 peptide is potentiated by hypoxia in primary human neural cells. J Biol Chem, 2002. **277**(33): p. 30359-67.

381.   Sennlaub, F., et al., *Cyclooxygenase-2 in human and experimental ischemic proliferative retinopathy.* Circulation, 2003. **108**(2): p. 198-204.

382.   Wang, G.L. and G.L. Semenza, *General involvement of hypoxia-inducible factor 1 in transcriptional response to hypoxia.* Proc Natl Acad Sci U S A, 1993. **90**(9): p. 4304-8.

383.   Anagnostou, A., et al., *Erythropoietin has a mitogenic and positive chemotactic effect on endothelial cells.* Proc Natl Acad Sci U S A, 1990. **87**(15): p. 5978-82.

384.   Ribatti, D., et al., *Human erythropoietin induces a pro-angiogenic phenotype in cultured endothelial cells and stimulates neovascularization in vivo.* Blood, 1999. **93**(8): p. 2627-36.

385.   Anagnostou, A., et al., *Erythropoietin receptor mRNA expression in human endothelial cells.* Proc Natl Acad Sci U S A, 1994. **91**(9): p. 3974-8.

386.   Carlini, R.G., A.A. Reyes, and M. Rothstein, *Recombinant human erythropoietin stimulates angiogenesis in vitro.* Kidney Int, 1995. **47**(3): p. 740-5.

387.   Morita, M., et al., *HLF/HIF-2alpha is a key factor in retinopathy of prematurity in association with erythropoietin.* Embo J, 2003. **22**(5): p. 1134-46.

388.   King, G.L., et al., *Receptors and growth-promoting effects of insulin and insulinlike growth factors on cells from bovine retinal capillaries and aorta.* J Clin Invest, 1985. **75**(3): p. 1028-36.

389.   Grant, M.B., S. Caballero, and W.J. Millard, *Inhibition of IGF-I and b-FGF stimulated growth of human retinal endothelial cells by the somatostatin analogue, octreotide: a potential treatment for ocular neovascularization.* Regul Pept, 1993. **48**(1-2): p. 267-78.

390.   Treins, C., et al., *Regulation of hypoxia-inducible factor (HIF)-1 activity and expression of HIF hydroxylases in response to insulin-like growth factor I.* Mol Endocrinol, 2005. **19**(5): p. 1304-17.

391.   Poulaki, V., et al., *Insulin-like growth factor-I plays a pathogenetic role in diabetic retinopathy.* Am J Pathol, 2004. **165**(2): p. 457-69.

392.   Smith, L.E., et al., *Essential role of growth hormone in ischemia-induced retinal neovascularization.* Science, 1997. **276**(5319): p. 1706-9.

393.   Kondo, T., et al., *Knockout of insulin and IGF-1 receptors on vascular endothelial cells protects against retinal neovascularization.* J Clin Invest, 2003. **111**(12): p. 1835-42.

394.   Leske, D.A., et al., *The role of VEGF and IGF-1 in a hypercarbic oxygen-induced retinopathy rat model of ROP.* Mol Vis, 2004. **10**: p. 43-50.

395.   Spranger, J., et al., *Systemic levels contribute significantly to increased intraocular IGF-I, IGF-II and IGF-BP3 [correction of IFG-BP3] in proliferative diabetic retinopathy.* Horm Metab Res, 2000. **32**(5): p. 196-200.

396.   Steele, F.R., et al., *Pigment epithelium-derived factor: neurotrophic activity and identification as a member of the serine protease inhibitor gene family.* Proc Natl Acad Sci U S A, 1993. **90**(4): p. 1526-30.

397.   Becerra, S.P., et al., *Pigment epithelium-derived factor behaves like a noninhibitory serpin. Neurotrophic activity does not require the serpin reactive loop.* J Biol Chem, 1995. **270**(43): p. 25992-9.

398.   Simonovic, M., P.G. Gettins, and K. Volz, *Crystal structure of human PEDF, a potent anti-angiogenic and neurite growth-promoting factor.* Proc Natl Acad Sci

U S A, 2001. **98**(20): p. 11131-5.

399. Volpert, O.V., et al., *Inducer-stimulated Fas targets activated endothelium for destruction by anti-angiogenic thrombospondin-1 and pigment epithelium-derived factor.* Nat Med, 2002. **8**(4): p. 349-57.

400. Aymerich, M.S., et al., *Evidence for pigment epithelium-derived factor receptors in the neural retina.* Invest Ophthalmol Vis Sci, 2001. **42**(13): p. 3287-93.

401. Bilak, M.M., et al., *Identification of the neuroprotective molecular region of pigment epithelium-derived factor and its binding sites on motor neurons.* J Neurosci, 2002. **22**(21): p. 9378-86.

402. Ogata, N., et al., *Expression of pigment epithelium-derived factor in normal adult rat eye and experimental choroidal neovascularization.* Invest Ophthalmol Vis Sci, 2002. **43**(4): p. 1168-75.

403. Eichler, W., et al., *PEDF derived from glial Muller cells: a possible regulator of retinal angiogenesis.* Exp Cell Res, 2004. **299**(1): p. 68-78.

404. Spranger, J., et al., *Loss of the antiangiogenic pigment epithelium-derived factor in patients with angiogenic eye disease.* Diabetes, 2001. **50**(12): p. 2641-5.

405. Ogata, N., et al., *Pigment epithelium-derived factor in the vitreous is low in diabetic retinopathy and high in rhegmatogenous retinal detachment.* Am J Ophthalmol, 2001. **132**(3): p. 378-82.

406. Mori, K., et al., *Pigment epithelium-derived factor inhibits retinal and choroidal neovascularization.* J Cell Physiol, 2001. **188**(2): p. 253-63.

407. Notari, L., et al., *Pigment epithelium-derived factor is a substrate for matrix metalloproteinase type 2 and type 9: implications for downregulation in hypoxia.* Invest Ophthalmol Vis Sci, 2005. **46**(8): p. 2736-47.

408. Lowe, W.L., et al., *Distribution and regulation of rat insulin-like growth factor-1 messenger ribonucleic acids encoding alternative carboxyterminal E-peptides: evidence for differential processing and regulation in liver.* Mol Endocrinol, 1988. **2**: p. 528-35.

409. Bach, M.A., et al., *Alternative splicing produces messenger RNAs encoding insulin-like growth factor-1 prohormones that are differentially glycosylated in vitro.* Mol Endocrinol, 1990. **4**: p. 899-904.

410. Zhang, J., R.E. Whitehead, and L.E. Underwood, *Effect of fasting on insulin-like growth factor (IGF)-1A and IGF-1B messenger ribonucleic acids and prehormones in rat liver.* Endocrinology, 1997. **138**(8): p. 3112-18.

411. Meijerink, J., et al., *A novel method to compensate for different amplification efficiencies between patient DNA samples in quantitative real-time PCR.* J Mol Diagn, 2001. **3**(2): p. 55-61.

412. Pfaffl, M.W., *A new mathematical model for relative quantification in real-time RT-PCR.* Nucleic Acids Res, 2001. **29**(9): p. e45.

413. Livak, K.J. and T.D. Schmittgen, *Analysis of relative gene expression data using real-time quantitative PCR and the 2(-Delta Delta C(T)) Method.* Methods, 2001. **25**(4): p. 402-8.

414. Vandesompele, J., et al., *Accurate normalization of real-time quantitative RT-PCR data by geometric averaging of multiple internal control genes.* Genome Biol, 2002. **3**(7): p. RESEARCH0034.

415. Haendler, B. and E. Hofer, *Characterization of the human cyclophilin gene and of related processed pseudogenes.* Eur J Biochem, 1990. **190**(3): p. 477-82.

416. Zhang, Z., et al., *Millions of years of evolution preserved: a comprehensive catalog of the processed pseudogenes in the human genome.* Genome Res, 2003.

13(12): p. 2541-58.

417.   Mutimer, H., et al., *Pitfalls of processed pseudogenes in RT-PCR.* Biotechniques, 1998. **24**(4): p. 585-8.

418.   Rutledge, R.G. and C. Cote, *Mathematics of quantitative kinetic PCR and the application of standard curves.* Nucleic Acids Res, 2003. **31**(16): p. e93.

419.   Kim, S.Y., et al., *Expression of pigment epithelium-derived factor (PEDF) and vascular endothelial growth factor (VEGF) in sickle cell retina and choroid.* Exp Eye Res, 2003. **77**(4): p. 433-45.

420.   Tuder, R.M., B.E. Flook, and N.F. Voelkel, *Increased gene expression for VEGF and the VEGF receptors KDR/Flk and Flt in lungs exposed to acute or to chronic hypoxia. Modulation of gene expression by nitric oxide.* J Clin Invest, 1995. **95**(4): p. 1798-807.

421.   Pugh, C.W. and P.J. Ratcliffe, *Regulation of angiogenesis by hypoxia: role of the HIF system.* Nat Med, 2003. **9**(6): p. 677-84.

422.   Schofield, C.J. and P.J. Ratcliffe, *Oxygen sensing by HIF hydroxylases.* Nat Rev Mol Cell Biol, 2004. **5**(5): p. 343-54.

423.   Rosenberger, C., et al., *Expression of hypoxia-inducible factor-1alpha and -2alpha in hypoxic and ischemic rat kidneys.* J Am Soc Nephrol, 2002. **13**(7): p. 1721-32.

424.   Tanimoto, K., et al., *Hypoxia-inducible factor-1alpha polymorphisms associated with enhanced transactivation capacity, implying clinical significance.* Carcinogenesis, 2003. **24**(11): p. 1779-83.

425.   Ollerenshaw, M., et al., *Polymorphisms in the hypoxia inducible factor-1alpha gene (HIF1A) are associated with the renal cell carcinoma phenotype.* Cancer Genet Cytogenet, 2004. **153**(2): p. 122-6.

426.   Li, Z., et al., *VHL protein-interacting deubiquitinating enzyme 2 deubiquitinates and stabilizes HIF-1alpha.* EMBO Rep, 2005. **6**(4): p. 373-8.

427.   Baek, J.H., et al., *OS-9 interacts with hypoxia-inducible factor 1alpha and prolyl hydroxylases to promote oxygen-dependent degradation of HIF-1alpha.* Mol Cell, 2005. **17**(4): p. 503-12.

428.   Makino, Y., et al., *Inhibitory PAS domain protein is a negative regulator of hypoxia-inducible gene expression.* Nature, 2001. **414**(6863): p. 550-4.

429.   Makino, Y., et al., *Inhibitory PAS domain protein (IPAS) is a hypoxia-inducible splicing variant of the hypoxia-inducible factor-3alpha locus.* J Biol Chem, 2002. **277**(36): p. 32405-8.

430.   Sandner, P., et al., *Divergent regulation of vascular endothelial growth factor and of erythropoietin gene expression in vivo.* Pflugers Arch, 1996. **431**(6): p. 905-12.

431.   Gess, B., P. Sandner, and A. Kurtz, *Differential effects of kinase inhibitors on erythropoietin and vascular endothelial growth factor gene expression in rat hepatocytes.* Pflugers Arch, 1996. **432**(3): p. 426-32.

432.   Tischer, E., et al., *The human gene for vascular endothelial growth factor. Multiple protein forms are encoded through alternative exon splicing.* J Biol Chem, 1991. **266**(18): p. 11947-54.

433.   Lambrechts, D., et al., *VEGF is a modifier of amyotrophic lateral sclerosis in mice and humans and protects motoneurons against ischemic death.* Nat Genet, 2003. **34**(4): p. 383-94.

434.   Levy, A.P., N.S. Levy, and M.A. Goldberg, *Post-transcriptional regulation of vascular endothelial growth factor by hypoxia.* J Biol Chem, 1996. **271**(5): p.

2746-2753.

435. Onesto, C., et al., *Poly(A)-binding protein-interacting protein 2, a strong regulator of vascular endothelial growth factor mRNA.* J Biol Chem, 2004. **279**(33): p. 34217-26.

436. Chen, C.Y. and A.B. Shyu, *AU-rich elements: characterization and importance in mRNA degradation.* Trends Biochem Sci, 1995. **20**(11): p. 465-70.

437. Levy, N.S., et al., *Hypoxic stabilization of vascular endothelial growth factor mRNA by the RNA-binding protein HuR.* J Biol Chem, 1998. **273**(11): p. 6417-23.

438. Shih, S.C. and K.P. Claffey, *Regulation of human vascular endothelial growth factor mRNA stability in hypoxia by heterogeneous nuclear ribonucleoprotein L.* J Biol Chem, 1999. **274**(3): p. 1359-65.

439. Renner, W., et al., *A common 936 C/T mutation in the gene for vascular endothelial growth factor is associated with vascular endothelial growth factor plasma levels.* J Vasc Res, 2000. **37**(6): p. 443-8.

440. Krippl, P., et al., *A common 936 C/T gene polymorphism of vascular endothelial growth factor is associated with decreased breast cancer risk.* Int J Cancer, 2003. **106**(4): p. 468-71.

441. Elvert, G., et al., *Cooperative interaction of hypoxia-inducible factor-2alpha (HIF-2alpha) and Ets-1 in the transcriptional activation of vascular endothelial growth factor receptor-2 (Flk-1).* J Biol Chem, 2003. **278**(9): p. 7520-30.

442. Takeda, N., et al., *Endothelial PAS domain protein 1 gene promotes angiogenesis through the transactivation of both vascular endothelial growth factor and its receptor, Flt-1.* Circ Res, 2004. **95**(2): p. 146-53.

443. Barleon, B., et al., *Vascular endothelial growth factor up-regulates its receptor fms-like tyrosine kinase 1 (FLT-1) and a soluble variant of FLT-1 in human vascular endothelial cells.* Cancer Res, 1997. **57**(23): p. 5421-5.

444. Kremer, C., et al., *Up-regulation of flk-1/vascular endothelial growth factor receptor 2 by its ligand in a cerebral slice culture system.* Cancer Res, 1997. **57**(17): p. 3852-9.

445. Herve, M.A., et al., *VEGF189 stimulates endothelial cells proliferation and migration in vitro and up-regulates the expression of Flk-1/KDR mRNA.* Exp Cell Res, 2005. **309**(1): p. 24-31.

446. Shen, B.Q., et al., *Homologous up-regulation of KDR/Flk-1 receptor expression by vascular endothelial growth factor in vitro.* J Biol Chem, 1998. **273**(45): p. 29979-85.

447. Waltenberger, J., et al., *Functional upregulation of the vascular endothelial growth factor receptor KDR by hypoxia.* Circulation, 1996. **94**(7): p. 1647-54.

448. Pichiule, P., J.C. Chavez, and J.C. LaManna, *Hypoxic regulation of angiopoietin-2 expression in endothelial cells.* J Biol Chem, 2004. **279**(13): p. 12171-80.

449. Mandriota, S.J. and M.S. Pepper, *Regulation of angiopoietin-2 mRNA levels in bovine microvascular endothelial cells by cytokines and hypoxia.* Circ Res, 1998. **83**(8): p. 852-9.

450. Das, A., et al., *Angiopoietin/Tek interactions regulate mmp-9 expression and retinal neovascularization.* Lab Invest, 2003. **83**(11): p. 1637-45.

451. Asahara, T., et al., *Tie2 receptor ligands, angiopoietin-1 and angiopoietin-2, modulate VEGF-induced postnatal neovascularization.* Circ Res, 1998. **83**(3): p. 233-40.

452. Oshima, Y., et al., *Angiopoietin-2 enhances retinal vessel sensitivity to vascular*

endothelial growth factor. J Cell Physiol, 2004. **199**(3): p. 412-7.

453.   Zhang, Y. and J. Stone, *Role of astrocytes in the control of developing retinal vessels.* Invest Ophthalmol Vis Sci, 1997. **38**(9): p. 1653-66.

454.   Zhang, S.X., et al., *Genetic difference in susceptibility to the blood-retina barrier breakdown in diabetes and oxygen-induced retinopathy.* Am J Pathol, 2005. **166**(1): p. 313-21.

455.   Moss, S.E., R. Klein, and B.E. Klein, *The 14-year incidence of visual loss in a diabetic population.* Ophthalmology, 1998. **105**(6): p. 998-1003.

456.   Congdon, N., et al., *Causes and prevalence of visual impairment among adults in the United States.* Arch Ophthalmol, 2004. **122**(4): p. 477-85.

457.   Yu, D.Y., et al., *Pathogenesis and intervention strategies in diabetic retinopathy.* Clin Experiment Ophthalmol, 2001. **29**(3): p. 164-6.

458.   Joussen, A.M., et al., *Leukocyte-mediated endothelial cell injury and death in the diabetic retina.* Am J Pathol, 2001. **158**(1): p. 147-52.

459.   Brausewetter, F., et al., *Microvascular permeability is increased in both types of diabetes and correlates differentially with serum levels of insulin-like growth factor I (IGF-I) and vascular endothelial growth factor (VEGF).* Horm Metab Res, 2001. **33**(12): p. 713-20.

460.   Brownlee, M., *Biochemistry and molecular cell biology of diabetic complications.* Nature, 2001. **414**(6865): p. 813-20.

461.   Ben-Nun, J., V.A. Alder, and I.J. Constable, *Retinal microvascular patency in the diabetic rat.* Int Ophthalmol, 2004. **25**(4): p. 187-92.

462.   Kohner, E.M., *The problems of retinal blood flow in diabetes.* Diabetes, 1976. **25**(2 SUPPL): p. 839-44.

463.   Gupta, A.R., et al., *Strain-dependent anterior segment neovascularization following intravitreal gene transfer of basic fibroblast growth factor (bFGF).* J Gene Med, 2001. **3**(3): p. 252-9.

464.   Rogers, M.S., et al., *Genetic loci that control vascular endothelial growth factor-induced angiogenesis.* Faseb J, 2003. **17**(14): p. 2112-4.

465.   Rogers, M.S., et al., *Genetic loci that control the angiogenic response to basic fibroblast growth factor.* Faseb J, 2004. **18**(10): p. 1050-9.

466.   Chan, C.K., et al., *Differential expression of pro- and antiangiogenic factors in mouse strain-dependent hypoxia-induced retinal neovascularization.* Lab Invest, 2005. **85**(6): p. 721-33.

467.   Wiklund, J., J. Rutledge, and J. Gorski, *A genetic model for the inheritance of pituitary tumor susceptibility in F344 rats.* Endocrinology, 1981. **109**(5): p. 1708-14.

468.   Wendell, D.L., A. Herman, and J. Gorski, *Genetic separation of tumor growth and hemorrhagic phenotypes in an estrogen-induced tumor.* Proc Natl Acad Sci U S A, 1996. **93**(15): p. 8112-6.

469.   Pandey, J., et al., *Strain differences and inheritance of angiogenic versus angiostatic activity in oestrogen-induced rat pituitary tumours.* Angiogenesis, 2002. **5**(1-2): p. 53-66.

470.   Pandey, J., A. Bannout, and D.L. Wendell, *The Edpm5 locus prevents the 'angiogenic switch' in an estrogen-induced rat pituitary tumor.* Carcinogenesis, 2004. **25**(10): p. 1829-38.

471.   Elias, K.A. and R.I. Weiner, *Direct arterial vascularization of estrogen-induced prolactin-secreting anterior pituitary tumors.* Proc Natl Acad Sci U S A, 1984. **81**(14): p. 4549-53.

472. Wendell, D.L. and J. Gorski, *Quantitative trait loci for estrogen-dependent pituitary tumor growth in the rat.* Mamm Genome, 1997. **8**(11): p. 823-9.

473. Wendell, D.L., et al., *Different functions of QTL for estrogen-dependent tumor growth of the rat pituitary.* Mamm Genome, 2000. **11**(10): p. 855-61.

474. Sclafani, R.V. and D.L. Wendell, *Suppression of estrogen-dependent MMP-9 expression by Edpm5, a genetic locus for pituitary tumor growth in rat.* Mol Cell Endocrinol, 2001. **176**(1-2): p. 145-53.

475. Cracchiolo, D., et al., *Estrogen-dependent growth of a rat pituitary tumor involves, but does not require, a high level of vascular endothelial growth factor.* Exp Biol Med (Maywood), 2002. **227**(7): p. 492-9.

476. Northway, W.H., Jr., R.C. Rosan, and D.Y. Porter, *Pulmonary disease following respirator therapy of hyaline-membrane disease. Bronchopulmonary dysplasia.* N Engl J Med, 1967. **276**(7): p. 357-68.

477. Stenmark, K.R. and V. Balasubramaniam, *Angiogenic therapy for bronchopulmonary dysplasia: rationale and promise.* Circulation, 2005. **112**(16): p. 2383-5.

478. Jobe, A.J., *The new BPD: an arrest of lung development.* Pediatr Res, 1999. **46**(6): p. 641-3.

479. Thebaud, B., et al., *Vascular endothelial growth factor gene therapy increases survival, promotes lung angiogenesis, and prevents alveolar damage in hyperoxia-induced lung injury: evidence that angiogenesis participates in alveolarization.* Circulation, 2005. **112**(16): p. 2477-86.

480. Maniscalco, W.M., et al., *Hyperoxic injury decreases alveolar epithelial cell expression of vascular endothelial growth factor (VEGF) in neonatal rabbit lung.* Am J Respir Cell Mol Biol, 1997. **16**(5): p. 557-67.

481. Bhatt, A.J., et al., *Disrupted pulmonary vasculature and decreased vascular endothelial growth factor, Flt-1, and TIE-2 in human infants dying with bronchopulmonary dysplasia.* Am J Respir Crit Care Med, 2001. **164**(10 Pt 1): p. 1971-80.

482. Klekamp, J.G., K. Jarzecka, and E.A. Perkett, *Exposure to hyperoxia decreases the expression of vascular endothelial growth factor and its receptors in adult rat lungs.* Am J Pathol, 1999. **154**(3): p. 823-31.

483. Hosford, G.E. and D.M. Olson, *Effects of hyperoxia on VEGF, its receptors, and HIF-2alpha in the newborn rat lung.* Am J Physiol Lung Cell Mol Physiol, 2003. **285**(1): p. L161-8.

484. Lin, Y.J., et al., *Inhaled nitric oxide enhances distal lung growth after exposure to hyperoxia in neonatal rats.* Pediatr Res, 2005. **58**(1): p. 22-9.

485. Kunig, A.M., et al., *Recombinant human VEGF treatment enhances alveolarization after hyperoxic lung injury in neonatal rats.* Am J Physiol Lung Cell Mol Physiol, 2005. **289**(4): p. L529-35.

486. Wilson, W.L., et al., *Hyperoxia-induced pulmonary vascular and lung abnormalities in young rats and potential for recovery.* Pediatr Res, 1985. **19**(10): p. 1059-67.

487. Shaffer, S.G., et al., *Chronic vascular pulmonary dysplasia associated with neonatal hyperoxia exposure in the rat.* Pediatr Res, 1987. **21**(1): p. 14-20.

488. Randell, S.H., R.R. Mercer, and S.L. Young, *Neonatal hyperoxia alters the pulmonary alveolar and capillary structure of 40-day-old rats.* Am J Pathol, 1990. **136**(6): p. 1259-66.

489. Brown, D.R., A.W. Biglan, and M.M. Stretavsky, *Retinopathy of prematurity:*

the relationship with intraventricular hemorrhage and bronchopulmonary dysplasia. J Pediatr Ophthalmol Strabismus, 1990. **27**(5): p. 268-71.

490. Holmstrom, G., U. Broberger, and P. Thomassen, *Neonatal risk factors for retinopathy of prematurity--a population-based study.* Acta Ophthalmol Scand, 1998. **76**(2): p. 204-7.

491. Hudak, B.B., L.Y. Zhang, and S.R. Kleeberger, *Inter-strain variation in susceptibility to hyperoxic injury of murine airways.* Pharmacogenetics, 1993. **3**(3): p. 135-43.

492. Cho, H.Y., et al., *Linkage analysis of susceptibility to hyperoxia. Nrf2 is a candidate gene.* Am J Respir Cell Mol Biol, 2002. **26**(1): p. 42-51.

493. Asikainen, T.M., et al., *Activation of hypoxia-inducible factors in hyperoxia through prolyl 4-hydroxylase blockade in cells and explants of primate lung.* Proc Natl Acad Sci U S A, 2005. **102**(29): p. 10212-7.

494. Nunes, I., et al., *c-abl is required for the development of hyperoxia-induced retinopathy.* J Exp Med, 2001. **193**(12): p. 1383-91.

495. Pass, D. and G. Freeth, *The Rat.* 1993, ANZCCART. http://www.adelaide.edu.au/ANZCCART/publications/FS_TheRat.pdf. Access date: Jul 18, 2004.

496. de Vries, C., et al., *The fms-like tyrosine kinase, a receptor for vascular endothelial growth factor.* Science, 1992. **255**(5047): p. 989-91.

497. *The Laboratory Rat*, ed. H.J. Baker, J.R. Lindsey, and S.H. Weisbroth. Vol. v1 Biology and Diseases. 1979, New York: Academic Press.

498. Festing, M.F.W., *Inbred Strains of Rats. Index of Major Rat Strains.* 1998, Mouse Genome Informatics. http://www.informatics.jax.org/external/festing/rat/STRAINS.shtml. Access date: Oct 15, 2005.

499. Ginzinger, D.G., *Gene quantification using real-time quantitative PCR: an emerging technology hits the mainstream.* Exp Hematol, 2002. **30**(6): p. 503-12.

500. Nigro, J.M., et al., *Detection of 1p and 19q loss in oligodendroglioma by quantitative microsatellite analysis, a real-time quantitative polymerase chain reaction assay.* Am J Pathol, 2001. **158**(4): p. 1253-62.

501. de Kok, J.B., et al., *Normalization of gene expression measurements in tumor tissues: comparison of 13 endogenous control genes.* Lab Invest, 2005. **85**(1): p. 154-9.

502. Radonic, A., et al., *Guideline to reference gene selection for quantitative real-time PCR.* Biochem Biophys Res Commun, 2004. **313**(4): p. 856-62.

503. Lion, T., *Current recommendations for positive controls in RT-PCR assays.* Leukemia, 2001. **15**(7): p. 1033-7.

504. Kidd, V. and T. Lion, *Debate round-table. Appropriate controls for RT-PCR.* Leukemia, 1997. **11**(6): p. 871-81.

505. Peters, I.R., et al., *Real-time RT-PCR: considerations for efficient and sensitive assay design.* J Immunol Methods, 2004. **286**(1-2): p. 203-17.

506. Graven, K.K., et al., *Regulation of endothelial cell glyceraldehyde-3-phosphate dehydrogenase expression by hypoxia.* J Biol Chem, 1994. **269**(39): p. 24446-53.

507. Zhong, H. and J.W. Simons, *Direct comparison of GAPDH, beta-actin, cyclophilin, and 28S rRNA as internal standards for quantifying RNA levels under hypoxia.* Biochem Biophys Res Commun, 1999. **259**(3): p. 523-6.

508. Tricarico, C., et al., *Quantitative real-time reverse transcription polymerase chain reaction: normalization to rRNA or single housekeeping genes is*

inappropriate for human tissue biopsies. Anal Biochem, 2002. **309**(2): p. 293-300.

509. Feeney, S.A., et al., *Role of vascular endothelial growth factor and placental growth factors during retinal vascular development and hyaloid regression.* Invest Ophthalmol Vis Sci, 2003. **44**(2): p. 839-47.

510. Hackam, A.S., et al., *Comparative gene expression analysis of murine retina and brain.* Mol Vis, 2004. **10**: p. 637-49.

511. Simpson, D.A., et al., *Retinal VEGF mRNA measured by SYBR green I fluorescence: A versatile approach to quantitative PCR.* Mol Vis, 2000. **6**: p. 178-83.

512. Yoshida, E., T.G. Atkinson, and B. Chakravarthy, *Neuroprotective gene expression profiles in ischemic cortical cultures preconditioned with IGF-1 or bFGF.* Brain Res Mol Brain Res, 2004. **131**(1-2): p. 33-50.

513. Dijk, F., E. Kraal-Muller, and W. Kamphuis, *Ischemia-induced changes of AMPA-type glutamate receptor subunit expression pattern in the rat retina: a real-time quantitative PCR study.* Invest Ophthalmol Vis Sci, 2004. **45**(1): p. 330-41.

514. Bond, B.C., et al., *The quantification of gene expression in an animal model of brain ischaemia using TaqMan real-time RT-PCR.* Brain Res Mol Brain Res, 2002. **106**(1-2): p. 101-16.

515. Shih, S.C., et al., *Selective stimulation of VEGFR-1 prevents oxygen-induced retinal vascular degeneration in retinopathy of prematurity.* J Clin Invest, 2003. **112**(1): p. 50-7.

516. Bernaudin, M., et al., *Brain genomic response following hypoxia and re-oxygenation in the neonatal rat. Identification of genes that might contribute to hypoxia-induced ischemic tolerance.* J Biol Chem, 2002. **277**(42): p. 39728-38.

517. Arai-Gaun, S., et al., *Heme oxygenase-1 induced in muller cells plays a protective role in retinal ischemia-reperfusion injury in rats.* Invest Ophthalmol Vis Sci, 2004. **45**(11): p. 4226-32.

518. Bustin, S.A., *Quantification of mRNA using real-time reverse transcription PCR (RT-PCR): trends and problems.* J Mol Endocrinol, 2002. **29**(1): p. 23-39.

519. Szabo, A., et al., *Statistical modeling for selecting housekeeper genes.* Genome Biol, 2004. **5**(8): p. R59.